REACTIVE POLYMER COATINGS: A ROBUST PLATFORM TOWARDS SOPHISTICATED SURFACE ENGINEERING FOR BIOTECHNOLOGY

by

Hsien-Yeh Chen

A dissertation submitted in partial fulfillment
of the requirements for the degree of
Doctor of Philosophy
(Chemical Engineering)
in The University of Michigan
2008

Doctoral Committee:

Assistant Professor Joerg Lahann, Chair
Professor Erdogan Gulari
Professor Ronald Larson
Associate Professor Shuichi Takayama

My mother and my deceased father

ACKNOWLEDGEMENTS

I would like to take this opportunity to express my sincere appreciation to all the people who have provided encouragement, support, and friendship during my Ph.D.

First of all, I would like to thank Professor Joerg Lahann for his inspirations and for his professional guidance. Both directly and by example, he has taught me so much about how to creatively approach research problems, and resiliently to overcome difficulties and challenges. He has also helped me greatly in improving my writing and presentation skills. Working with him has been a valuable and rewarding experience, and it is with his support and help that I could have achieved this far in my Ph.D. research.

I would also like to express my special thanks to my committee members, Professor Erdogan Gulari, Professor Ronald Larson, and Professor Shuichi Takayama, for their advices and for their efforts in reviewing my thesis.

I am grateful to many collaborators outside of my department, who have helped me in many ways. I would like to thank Professor Francesco Stellacci and Sarah Thévenet from MIT for their coolaboration on the work of SuSN, Professor Henry Hess and Ashutosh Agarwal from University of Florida for their collaboration on protein-resistant modifications, Professor Zhan Chen and Arthur McClelland from Chemistry Department at the University of Michigan for their asisstance in Sum Frequency Generation (SFG) characterizations.

Moreover, I would like to thank Dr. Jean-Marie Rouillard for his assistance with the projection lithography technology and his insightful suggestions. I also would like to thank Dr. Onnop Srivannavit, who has helped me to initiate at the beginning of my Ph.D. work and his continuous support on fabrication process in cleanroom.

Special thank should also be given to my current group members for their friendship

and technical supports: David Peng, Kyung Ho Roh, Dr. Xuwei Jiang, Dr. Mutsumi Yoshida, Dr. Aiwu Sun, Dr. Abbass Kazemi, Yaseen Elkasabi, Himabindu Nandivada, Allen Ahang Ahmadi, Allison Bourke, Srijanani Bhaskar, Agusti Panades Llorens, Marc Aluma Lopez, Sridhar Valluri, Sohyun Ahn, Yuan Ma, Kelley Pollack, and Laura Chang. And also the support from our former group members: Dr. Lidija Bondarenko, Jason Wu, Sonsoles de Olano, Gemma Galvan, and Dave Alberts.

I am truly fortunate to have acquainted many friends during my Ph.D. in the University of Michigan. These friends have made my school life enjoyable and fun. I would like to thank Pei-Jie (Penny) Chen, Yu-Chieh Wu, Ling-Yu (Josie) Huang, Kay Chen, Heidi Chang, Hsien-Chang Lin, Ji-Ying (Jessica) Wu, Ares Chen, Chih-Wei (Joe) Chou, Jim Chang, Peichin Chang, Erica Ke, Danial Hohne, Peter Ho, Edward Jan, Ayse Bilge Ozel, Dr. Andre Taylor, Dr. Chang Hwan Kim, Dr. Xiaoyin Chen, Deshpremy Mukhija, Khamir Mehta, Paul Podsiadlo, Bongsup Shim, Wen-Lung Huang, Yolanda Lin, Katherine Lin, Ji hoon Kim, Weixian Shi, and many others.

I would like to thank the staff in the Electron Microbeam Analysis Laboratory (EMAL) for their hard works and efforts in keeping the facilities running smoothly and in maintaining the equipments. I would also like to thank the administrative staff from the Chemical Engineering department for their helps.

Acknowledgement should also be given to the financial support by the NSF in the form of a CAREER grant (DMR-0449462) and the funding from the NSF under MRI program (DMR 0420785).

Finally, with tremendous gratitude, I want to acknowledge my mother and my deceased father for their love, patience, and support. After learning what it takes to raise a child from my friends with children, I realized what sacrifices they have made in raising me, and I am really grateful for their unlimited love and devotion.

TABLE OF CONTENTS

LIST OF FIGURES

LIST OF TABLES

ABSTRACT

Functionalized poly(*p*-xylylenes) or so-called *reactive polymers* can be synthesized via chemical vapor deposition (CVD) polymerization. The resulting ultra-thin coatings are pinhole-free and can be conformally deposited to a wide range of substrates and materials. More importantly, the equipped functional groups can served as anchoring sites for tailoring the surface properties, making these reactive coatings a robust platform that can deal with sophisticated challenges faced in biointerfaces.

In this work presented herein, surface coatings presenting various functional groups were prepared by CVD process. Such surfaces include aldehyde-functionalized coating to precisely immobilize saccharide molecules onto well-defined areas and alkyne-functionalized coating to click azide-modified molecules via Huisgen 1,3-dipolar cycloaddition reaction. Moreover, CVD copolymerization has been conducted to prepare multifunctional coatings and their specific functions were demonstrated by the immobilization of biotin and NHS-ester molecules.

By using a photodefinable coating, polyethylene oxides were immobilized onto a wide range of substrates through photo-immobilization. Spatially controlled protein resistant properties were characterized by selective adsorption of fibrinogen and bovine serum albumin as model systems. Alternatively, surface initiator coatings were used for polymer graftings of poly(ethylene glycol) methyl ether methacrylate, and the resultant protein- and cell- resistant properties were characterized by adsorption of kinesin motor proteins, fibrinogen, and murine fibroblasts (NIH3T3).

Accessibility of reactive coatings within confined microgeometries was systematically studied, and the preparation of homogeneous polymer thin films within the inner surface of microchannels was demonstrated. Moreover, these advanced coatings

were applied to develop a dry adhesion process for microfluidic devices. This process provides (i) excellent bonding strength, (ii) extended storage time prior to bonding, and (iii) well-defined surface functionalities for subsequent surface modifications. Finally, we have also prepared surface microstructures and surface patterns using reactive coatings via photopatterning, projection lithography, supramolecular nanostamping (SuNS), and vapor-assisted micropatterning in replica structures (VAMPIR). These patterning techniques can be complimentarily used and provide access to precisely confined microenvironments on flat and curved geometries.

Reactive coatings provide a technology platform that creates active, long-term control and may lead to improved mimicry of biological systems for effective bio-functional modifications.

CHAPTER 1

INTRODUCTION

Reactions and interactions occur on surfaces, and the composition and structure of a surface are usually quite different from those of the bulk material.[1] It has long been researched that the observed biological response to materials is initiated by interactions with material residing in the same thin surface region.[2,3] The impact of biomedical surface science has revolutionized the developments of biotechnology in the field of chemistry, biology, medicine, materials, and engineering. The advancements in surface science instrumentation that have occurred in the past quarter of a century have significantly increased our ability to characterize the surface composition and molecular structure of biomaterials. Similar advancements have occurred in material science and molecular biology. The combination of these advances have allowed the development of the biological model for surface science, where the ultimate goal is to gain a detailed understanding of how the surface properties of a material control the biological reactivity of a cell interacting with that surface. Numerous advances have showed that the surface properties of a material are directly related to *in vitro* biological performance such as protein adsorption and cell growth.[4] Future directions and opportunities for surface scientists working in biomedical research include exploiting biological knowledge, biomimetics, precision immobilization, self-assembly, nanofabrication, smart surfaces, and control of non-specific reactions.[4]

1.1 Surface Engineering of Biointerfaces

Latest advancements in biomaterials aim to control biological responses. The

surfaces of such biomaterials, the biointerfaces, are critical in many aspects, and have recently begun to attract the attention they deserve as a unique interdisciplinary research area.[5] The critical criteria for designing biointerfaces require controlled properties of biomolecules, non-fouling (or low nonspecific protein adsorption), compatibility with microfabrication, accessible within microgeometries, applicability on three dimensional objects, defined microstructures (surface patterns), biodegradability, and surface gradient. Defined and stable surface properties along with the capability to immobilize active biomolecules onto a surface are key features for the development of miniaturized biodevices, such as micro total analysis systems (μTAS),[6] microfabricated cell sorters,[7] microseparators for DNA[8] and proteins,[9,10] cell-based assays,[11] and embryonic patterning networks.[12] In such miniaturized high-tech systems, very large surface-to-volume ratios are typically encountered creating a situation where slight inhomogeneities in the surface chemistry will cause device malfunction.[13]

Intensive researches have been conducted to achieve the design of such criteria. For instance, researchers have directed covalent immobilization[14,15] of the molecules to a surface. Various silanization procedures have also been reported on glass or silicon surfaces.[16-20] Alternatively, photoactivable linkers allow the immobilization on various materials in a homogeneous layer.[21,22] A stable immobilization on gold surface has also been reported through self-assembled monolayers (SAMs) formed by alkanethiol endowed with a negatively charged end group protect the surface from non-specific binding and additionally provide a functional group for a coupling of antibody molecules,[22-24] chelators for histidine-tagged protein binding[25] or artificial recognition molecules.[26] Binding of streptavidin molecules to SAM provides a molecular anchor for any biotinylated molecule. Supported phospholipid bilayers (SPBs) has also been used to study cell-cell interactions, protein-lipid interactions, protein crystallization, as well as membrane properties in general. On the other hand, the unique feature of the streptavidin-biotin system has been utilized bioanalysis[27] and is suitable for electrochemical[28,29] and optical biosensors.[30] Another approach is to create a thin polymer layer on a sensor in order to increase the surface density of the signaling molecules. Moreover, conducting polymers[31] such as polyvinylpyridin functionalized with Os-complexes,[32] polypyrrole,[33] polytyramine,[34] polythiophen,[35]

PEG-vinylferrocene,[36] crosslinked avidin–biotin-enzyme[37] or silk fibroin[38] create wired networks and are suitable as matrices for redox enzymes. Techniques by using polymer grafting is also a widely applied; typical pretreatment methods include chemical modification,[38,39] plasma,[40] UV,[41,42] UV/ozone,[43,44] ion beam,[45] excimer, and laser activation of preadsorbed photoinitiators.[46,47] Other techniques such as Langmuir-Blodgett deposition[17] and layer-by-layer (LBL)[48,49] adsorption have also been the focus of intense research.

1.2 Vapor-Based Modifications

Solvent-based methods have been widely adapted for biologically-tailored (biomimetic) modifications as discussed in section 1.2; however, associated problems such as by-products, harmful chemical, solvents, catalysts, and initiators can lead to the malfunction of end products and devices, making these methods insufficient for more sophisticated, miniaturized, and sensitive biological applications. With this respect, biologically oriented surface modification *via* vapor-based methods has also drawn enormous attentions in recent years. These methods generally have the advantages of being easy to process compared to solvent-based modification, free of solvents, catalysts or initiators, and usually can be prepared at a relatively low temperature.[13,50] Many researchers have exploited the use of chemical vapor deposition (CVD) polymerization to develop surface modification protocols for a wide range of different substrate materials. For instance, Gleason et al. used hot filament[51] and plasma polymerization to create functional materials coatings, while Dygert et al. have successfully deposit a polyimide film using resonant infrared laser ablation (RIR-LA).[52] The preparation of an insoluble conjugated polymer in various shapes by the chemical vapor deposition polymerization of 2,5-bis(chloromethyl)thiophene was also reported by Lee and Jin et al.[53] Moreover, Cao and Ratner et al. reported the use of plasma deposited tetraethylene glycol dimethyl ether (tetraglyme) coatings that exhibit ultralow fibrinogen adsorption to reduce blood activation.[54] Lee and Frank have report that vapor deposition can be used to synthesize surface-grafted polypeptides from a wide range of a-amino acids.[55] Chang et al. used

free-radical polymerization of vinyl monomers resulting in polystyrene, polyacrylamide, or poly(N-isopropylacrylamide) by covalently attached initiators.[56] On the other hand, Gu and Xu et al. used polyacetylene (HOPA) films as a precursor and applied a combination of soft lithography and solventless polymerization to synthesize ultra-hard microstructures on the surface.[57]

1.3 Commercial Poly-*para*-xylylene Polymer Coatings

Among these vapor-based methods to deposit polymers, poly-*para*-xylylenes prepared *via* chemical vapor deposition, is known to be one of the best established system. These polymers were prepared *via* the mechanism of the CVD polymerization of [2.2]paracyclophanes and was originally developed by Gorham[58] and has since been utilized under the Parylene brand in a wide range of applications.[59,60] The name can be varied as parylene N, parylene C, or parylene D, etc.[61] according to different halogen substitution at *para* position on the benzene rings; nevertheless, they are collectively used as non-functional and inert coatings. Parylenes (or non-functionalized poly-*p*-xylylene) coatings have been used for more than 20 years as conformal coatings for various medical and electronic devices due to their biocompatible/biostable properties and being excellent moisture, chemical and dielectric barrier protection.[60] On the other hand, the CVD polymerization is a conformal and pinhole-free coating process, and is applicable to a wide range of substrates and materials. The coatings can be prepared on devices with complex geometries in high fidelity and is usually at room temperature or less, which is pleasant for most of the biological applications. More importantly, the Food and Drug Administration (FDA) has approved their uses as coatings in some of the medical implants.[59,60]

1.4 Functionalized Poly-*para*-xylylenes *via* CVD Polymerization Process

While commercialization of parylene coatings have significantly advanced in applications such as stents, cardic pacemakers and defibrillators, neuronal probes, orthodentic devices, or for bio-MEMS applications, these parylene coatings are non-functionalized and lack anchor groups for further modification, hence unsuitable as effective linkers for biomolecules.[13] Researchers have exploited methods to prepare functional groups that act as anchor groups in further modification procedures. Several approaches have been recently developed to modify the surface properties of poly-*p*-xylylene coatings, such as plasma etching[62] or wet-chemical modification.[63] For instance, Ishaque et al.[64] reported a two-step CVD process using the Gilch route[65] and synthesized 10 different functional poly(*p*-xylylenes), and found that the surface energy can be decreased most significantly by fluoro-substituents. Using an alternative approach, Herrera-Alonso and McCarthy have reported wet chemical modification on poly(*p*-xylylene) coatings via sulfonation, aminomethylation, or amidomethylation,[65] while Senkevich et al. have reported that ultrathin oligomeric *para*-xylylene films which contain unterminating chain-endings can then be functionalized with wet or dry chemistry.[66] On the other hand, Lahann and Langer have successfully refined the Gorham process to prepare functionalized poly-*p*-xylylenes (*reactive polymers*)[67] from substituted [2.2]paracyclophanes. These polymers possess all the advantages of their commercial siblings, but in addition, provide versatile anchor groups for sophisticated surface modifications. These *reactive polymers* can be deposited via chemical vapor deposition (CVD) polymerization to generate ultra thin (20-100nm) films as conformal coatings and, due to the pre-defined chemical functionalities, provide a flexible solution to surface engineering challenges as they decouple surface design from bulk properties. Hence, the technology comprises essentially a one-step coating procedure to generate functionalized surfaces without requiring any kind of post-treatment once the films are deposited. The CVD-based polymer films can be generically applied to a wide variety of substrates and establish a reactive interface that allows for further modification. More importantly, the resulting functionalized poly-*p*-xylylenes establish interfaces equipped with chemically reactive groups that can be selected from a variety of different chemical species, including amines,[68,69] alcohols,[67,70,71] aldehydes,[72] activated ester,[73,74] alkynes,[75] and anhydrides,[76] which can be selected depending on the specific needs of a

given application. The simplicity in providing a wide range of functional groups, the excellent adhesion to various substrates, and its applicability to devices with three-dimensional geometries are key advantages when compared to polymers deposited by solvent-based methods. In principle, these polymers are well suited as a platform for biomedical applications.

1.5 Hypothesis and Specific Aims

Based on the previous success on CVD polymerization of functionalized [2.2]paracyclophanes to deposit *reactive polymers* and the excellent properties possessed by these polymers as potential tools to deal with the critical challenges of biointerfaces, these reactive polymers can be used to develop general protocols of surface engineering for biotechnology. This is how this thesis was motivated and how the research was directed, aiming to using these *reactive polymers* to (1) perform controlled immobilization of biomolecules, (2) develop non-fouling surfaces that inhibit protein adsorption and cell adhesion, (3) investigate the feasibility of CVD polymerization within confined geometries, (4) develop an alternate strategy for adhesive bonding, and (5) develop a clean process for designable surface patterns. The herein reported materials in this thesis will discuss the challenges associated with these aims, the techniques used to address these challenges and also the characterization methods applied to prove the concepts. The materials used are either have been processed for submission or have been previously reported in *Macromolecular Rapid Communications*,[72] *Angewandte Chemie-International Edition*,[75] *Advanced Materials*,[77-79] *Analytical Chemistry*,[80] *Advanced Functional Materials*,[81] *Journal of the American Chemical Society*,[82] and *Proceedings of the National Academy of Sciences of the United States of America*,[83] and have been slight modified.

1.6 Overview

Research on poly(*p*-xylylenes) and its derivatives is gaining significance due to the interesting property profile of this class of aromatic polymers. Poly(*p*-xylylenes) have been successfully established in many applications, among those are protective coatings, insulating coatings, interlayer dielectrics, biomaterials, precursors for electroluminescent polymers and sensors, just to name a few of them. The synthesis of new derivatives of poly(*p*-xylylenes) is, however, necessary in order to fully exploit the promising property profile of poly(*p*-xylylenes). In addition, CVD polymerization establishes a general but simple protocol for the preparation of these polymer coatings. The resulting reactive coatings are applicable to various substrates such as polymers, metals, or composites, generates a fairly universal plateform without relying on board chemical alternation of the balk material. Development of such polymer coatings may be explored in various applications including nano-printing technology, dry adhesive bonding in bio-MEMS, fabrication of polymer composites, micro-/nano-fluidics, and study of cell behavior.

References

[1] Castner, D. G., Surface science - View from the edge. *Nature* **2003,** 422, (6928), 129.

[2] Vogler, E. A., Structure and reactivity of water at biomaterial surfaces. *Advances in Colloid and Interface Science* **1998,** 74, 69.

[3] Ratner, B. D.; Bryant, S. J., Biomaterials: Where we have been and where we are going. *Annual Review of Biomedical Engineering* **2004,** 6, 41.

[4] Castner, D. G.; Ratner, B. D., Biomedical surface science: Foundations to frontiers. *Surface Science* **2002,** 500, (1-3), 28.

[5] Chilkoti, A.; Hubbell, J. A., Biointerface science. *Mrs Bulletin* **2005,** 30, (3), 175.

[6] Berg, A.; Olthius, W.; Bergveld, P., *Micro Total Analysis Systems 2000*. 1st ed.; Springer: 2000.

[7] Fu, A. Y.; Spence, C.; Scherer, A.; Arnold, F. H.; Quake, S. R., A microfabricated fluorescence-activated cell sorter. *Nature Biotechnology* **1999,** 17, (11), 1109.

[8] Effenhauser, C. S.; Bruin, G. J. M.; Paulus, A.; Ehrat, M., Integrated Capillary Electrophoresis on Flexible Silicone Microdevices: Analysis of DNA Restriction Fragments and Detection of Single DNA Molecules on Microchips. *Analytical Chemistry* **1997,** 69, (17), 3451.

[9] Chen, S. H.; Sung, W. C.; Lee, G. B.; Lin, Z. Y.; Chen, P. W.; Liao, P. C., A disposable poly(methylmethacrylate)-based microfluidic module for protein identification by nanoelectrospray ionization-tandem mass spectrometry. *Electrophoresis* **2001,** 22, (18), 3972.

[10] Mao, H.; Yang, T.; Cremer, P. S., Design and characterization of immobilized enzymes in microfluidic systems. *Analytical Chemistry* **2002,** 74, (2), 379.

[11] Li, P. C. H.; Harrison, D. J., Transport, manipulation, and reaction of biological cells on-chip using electrokinetic effects. *Analytical Chemistry* **1997,** 69, (8), 1564.

[12] Lucchetta, E. M.; Lee, J. H.; Fu, L. A.; Patel, N. H.; Ismagilov, R. F., Dynamics of Drosophila embryonic patterning network perturbed in space and time using microfluidics. *Nature* **2005,** 434, (7037), 1134.

[13] Lahann, J., Vapor-based polymer coatings for potential biomedical applications. *Polymer International* **2006,** 55, (12), 1361.

[14] Scouten, W. H.; Luong, J. H. T.; Brown, R. S., Enzyme or Protein Immobilization Techniques for Applications in Biosensor Design. *Trends in Biotechnology* **1995,** 13, (5), 178.

[15] Kallury, K. M. R.; Lee, W. E.; Thompson, M., Enhanced Stability of Urease Immobilized onto Phospholipid Covalently Bound to Silica, Tungsten, and Fluoropolymer Surfaces. *Analytical Chemistry* **1993,** 65, (18), 2459.

[16] Bhatia, S. K.; Cooney, M. J.; Shriverlake, L. C.; Fare, T. L.; Ligler, F. S., Immobilization of Acetylcholinesterase on Solid-Surfaces - Chemistry and Activity Studies. *Sensors and Actuators B-Chemical* **1991,** 3, (4), 311.

[17] Elender, G.; Kuhner, M.; Sackmann, E., Functionalisation of Si/SiO2 and glass surfaces with ultrathin dextran films and deposition of lipid bilayers. *Biosensors & Bioelectronics* **1996,** 11, (6-7), 565.

[18] Flounders, A. W.; Brandon, D. L.; Bates, A. H., Patterning of immobilized antibody layers via photolithography and oxygen plasma exposure. *Biosensors & Bioelectronics* **1997,** 12, (6), 447.
[19] Matveev, S. V., Controlled Modification of the Quartz Surface by Amino-Groups. *Biosensors & Bioelectronics* **1994,** 9, (4-5), 333.
[20] Vandenberg, E. T.; Bertilsson, L.; Liedberg, B.; Uvdal, K.; Erlandsson, R.; Elwing, H.; Lundstrom, I., Structure of 3-Aminopropyl Triethoxy Silane on Silicon-Oxide. *Journal of Colloid and Interface Science* **1991,** 147, (1), 103.
[21] Collioud, A.; Clemence, J. F.; Sanger, M.; Sigrist, H., Oriented and Covalent Immobilization of Target Molecules to Solid Supports - Synthesis and Application of a Light-Activatable and Thiol-Reactive Cross-Linking Reagent. *Bioconjugate Chemistry* **1993,** 4, (6), 528.
[22] Delamarche, E.; Sundarababu, G.; Biebuyck, H.; Michel, B.; Gerber, C.; Sigrist, H.; Wolf, H.; Ringsdorf, H.; Xanthopoulos, N.; Mathieu, H. J., Immobilization of Antibodies on a Photoactive Self-Assembled Monolayer on Gold. *Langmuir* **1996,** 12, (8), 1997.
[23] Duschl, C.; Sevin-Landais, A.-F.; Vogel, H., Surface engineering: optimization of antigen presentation in self-assembled monolayers. *Biophysical Journal* **1996,** 70, (4), 1985.
[24] Lu, B.; Xie, J.; Lu, C.; Wu, C.; Wei, Y., Oriented Immobilization of Fab' Fragments on Silica Surfaces. *Analytical Chemistry* **1995,** 67, (1), 83.
[25] Keller, T. A.; Duschi, C.; Kroeger, D.; Sevin-Landais, A.-F.; Vogel, H.; Cervigni, S. E.; Dumy, P., Reversible oriented immobilization of histidine-tagged proteins on gold surfaces using a chelator thioalkane. *Supramolecular Science* **1996,** 2, (3-4), 155.
[26] Rickert, J.; Weiss, T.; Gopel, W., Self-assembled monolayers for chemical sensors: Molecular recognition by immobilized supramolecular structures. *Sensors and Actuators B-Chemical* **1996,** 31, (1-2), 45.
[27] Gosling, J. P., A decade of development in immunoassay methodology. *Clinical Chemistry (Washington, DC, United States)* **1990,** 36, (8, Pt. 1), 1408.
[28] Kossek, S.; Padeste, C.; Tiefenauer, L., Immobilization of streptavidin for immunosensors on nanostructured surfaces. *Journal of Molecular Recognition* **1996,** 9, (5/6), 485.
[29] Vreeke, M. S.; Rocca, P., Biosensors based on crosslinking of biotinylated glucose oxidase by avidin. *Electroanalysis* **1996,** 8, (1), 55.
[30] Narang, U.; Anderson, G. P.; King, K. D.; Liss, H. S.; Ligler, F. S., Enhanced biosensor performance using an avidin-biotin bridge for antibody immobilization. *Proceedings of SPIE-The International Society for Optical Engineering* **1997,** 2980, (Advances in Fluorescence Sensing Technology III), 187.
[31] Cosnier, S., Biomolecule immobilization on electrode surfaces by entrapment or attachment to electrochemically polymerized films. A review. *Biosensors & Bioelectronics* **1999,** 14, (5), 443.
[32] Linke, B.; Kerner, W.; Kiwit, M.; Pishko, M.; Heller, A., Amperometric biosensor for in vivo glucose sensing based on glucose oxidase immobilized in a redox hydrogel. *Biosensors & Bioelectronics* **1994,** 9, (2), 151.

[33] Yon-Hin, B. F. Y.; Smolander, M.; Crompton, T.; Lowe, C. R., Covalent electropolymerization of glucose oxidase in polypyrrole. Evaluation of methods of pyrrole attachment to glucose oxidase on the performance of electropolymerized glucose sensors. *Analytical Chemistry* **1993,** 65, (15), 2067.
[34] Cooper, J. C.; Schubert, F., A Biosensor for L-Amino-Acids Using Polytyramine for Enzyme Immobilization. *Electroanalysis* **1994,** 6, (11-12), 957.
[35] Hiller, M.; Kranz, C.; Huber, J.; Baeuerle, P.; Schuhmann, W., Amperometric biosensors produced by immobilization of redox enzymes at polythiophene-modified electrode surfaces. *Advanced Materials* **1996,** 8, (3), 219.
[36] Sirkar, K.; Pishko, M. V., Amperometric Biosensors Based on Oxidoreductases Immobilized in Photopolymerized Poly(ethylene glycol) Redox Polymer Hydrogels. *Analytical Chemistry* **1998,** 70, (14), 2888.
[37] Qian, J.; Liu, Y.; Liu, H.; Yu, T.; Deng, J., Immobilization of horseradish peroxidase with a regenerated silk fibroin membrane and its application to a tetrathiafulvalene-mediating H2O2 sensor. *Biosensors & Bioelectronics* **1997,** 12, (12), 1213.
[38] Xiao, D. Q.; Wirth, M. J., Kinetics of surface-initiated atom transfer radical polymerization of acrylamide on silica. *Macromolecules* **2002,** 35, (8), 2919.
[39] Bergbreiter, D. E.; Xu, G. F.; Zapata, C., Heterogeneous Grafting Chemistry Using Residual Unsaturation as a Graft Site Precursor. *Macromolecules* **1994,** 27, (6), 1597.
[40] Chen, H.; Belfort, G., Surface modification of poly(ether sulfone) ultrafiltration membranes by low-temperature plasma-induced graft polymerization. *Journal of Applied Polymer Science* **1999,** 72, (13), 1699.
[41] Hu, S. W.; Ren, X. Q.; Bachman, M.; Sims, C. E.; Li, G. P.; Allbritton, N. L., Surface-directed, graft polymerization within microfluidic channels. *Analytical Chemistry* **2004,** 76, (7), 1865.
[42] Hu, S. W.; Ren, X. Q.; Bachman, M.; Sims, C. E.; Li, G. P.; Allbritton, N., Surface modification of poly(dimethylsiloxane) microfluidic devices by ultraviolet polymer grafting. *Analytical Chemistry* **2002,** 74, (16), 4117.
[43] Loh, F. C.; Tan, K. L.; Kang, E. T.; Neoh, K. G.; Pun, M. Y., Near-Uv Radiation-Induced Surface Graft-Copolymerization of Some O-3-Pretreated Conventional Polymer-Films. *European Polymer Journal* **1995,** 31, (5), 481.
[44] Genzer, J.; Fischer, D. A.; Efimenko, K., Fabricating two-dimensional molecular gradients via asymmetric deformation of uniformly-coated elastomer sheets. *Advanced Materials* **2003,** 15, (18), 1545.
[45] Corelli, J. C.; Steckl, A. J.; Pulver, D.; Randall, J. N., Ultralow Dose Effects in Ion-Beam Induced Grafting of Polymethylmethacrylate (Pmma). *Nuclear Instruments & Methods in Physics Research Section B-Beam Interactions with Materials and Atoms* **1987,** 19-2, 1009.
[46] Srinivasan, R.; Maynebanton, V., Self-Developing Photoetching of Poly(Ethylene-Terephthalate) Films by Far Ultraviolet Excimer Laser-Radiation. *Applied Physics Letters* **1982,** 41, (6), 576.
[47] Rohr, T.; Ogletree, D. F.; Svec, F.; Frechet, J. M. J., Surface functionalization of thermoplastic polymers for the fabrication of microfluidic devices by photoinitiated grafting. *Advanced Functional Materials* **2003,** 13, (4), 264.

[48] Decher, G., Fuzzy nanoassemblies: Toward layered polymeric multicomposites. *Science* **1997,** 277, (5330), 1232.
[49] Shevchenko, E. V.; Talapin, D. V.; Kotov, N. A.; O'Brien, S.; Murray, C. B., Structural diversity in binary nanoparticle superlattices. *Nature* **2006,** 439, (7072), 55.
[50] Lahann, J., Reactive polymer coatings for biomimetic surface engineering. *Chemical Engineering Communications* **2006,** 193, (11), 1457.
[51] Murthy, S. K.; Olsen, B. D.; Gleason, K. K., Effect of filament temperature on the chemical vapor deposition of fluorocarbon-organosilicon copolymers. *Journal of Applied Polymer Science* **2004,** 91, (4), 2176.
[52] Dygert, N. L.; Gies, A. P.; Schriver, K. E.; Haglund, R. F., Deposition of polyimide precursor by resonant infrared laser ablation. *Applied Physics a-Materials Science & Processing* **2007,** 89, (2), 481.
[53] Lee, K. R.; Yu, Y. J.; Joo, S. H.; Lee, C. Y.; Choi, D. H.; Joo, J. S.; Park, Y. S.; Jin, J. I., Poly(2,5-thienylene vinylene) in nano shapes by CVD polymerization. *Macromolecular Rapid Communications* **2007,** 28, (9), 1057.
[54] Cao, L.; Chang, M.; Lee, C. Y.; Castnet, D. G.; Sukavaneshvar, S.; Ratner, B. D.; Horbett, T. A., Plasma-deposited tetraglyme surfaces greatly reduce total blood protein adsorption, contact activation, platelet adhesion, platelet procoagulant activity, and in vitro thrombus deposition. *Journal of Biomedical Materials Research Part A* **2007,** 81A, (4), 827.
[55] Lee, N. H.; Frank, C. W., Surface-initiated vapor polymerization of various alpha-amino acids. *Langmuir* **2003,** 19, (4), 1295.
[56] Rhee, S. W.; Taylor, A. M.; Tu, C. H.; Cribbs, D. H.; Cotman, C. W.; Jeon, N. L., Patterned cell culture inside microfluidic devices. *Lab on a Chip* **2005,** 5, (1), 102.
[57] Gu, H. W.; Zheng, R. K.; Zhang, X. X.; Xu, B., Using soft lithography to pattern highly oriented polyacetylene (HOPA) films via solventless polymerization. *Advanced Materials* **2004,** 16, (15), 1356.
[58] Gorham, W. F., A new general synthetic method for the preparation of linear poly-p-xylylenes. *Journal of Polymer Science, Polymer Chemistry Edition* **1966,** 4, (12), 3027.
[59] Grzybowski, B. A.; Haag, R.; Bowden, N.; Whitesides, G. M., Generation of Micrometer-Sized Patterns for Microanalytical Applications Using a Laser Direct-Write Method and Microcontact Printing. *Analytical Chemistry* **1998,** 70, (22), 4645.
[60] Duffy, D. C.; McDonald, J. C.; Schueller, O. J. A.; Whitesides, G. M., Rapid Prototyping of Microfluidic Systems in Poly(dimethylsiloxane). *Analytical Chemistry* **1998,** 70, (23), 4974.
[61] Senkevich, J. J.; Mitchell, C. J.; Vijayaraghavan, A.; Barnat, E. V.; McDonald, J. F.; Lu, T. M., Unique structure/properties of chemical vapor deposited parylene E. *Journal of Vacuum Science & Technology a-Vacuum Surfaces and Films* **2002,** 20, (4), 1445.
[62] Nowlin, T. E.; Smith, D. F., Surface Characterization of Plasma-Treated Poly-P-Xylylene Films. *Journal of Applied Polymer Science* **1980,** 25, (8), 1619.
[63] Herrera-Alonso, M.; McCarthy, T. J., Chemical surface modification of poly(p-xylylene) thin films. *Langmuir* **2004,** 20, (21), 9184.

[64] Ishaque, M.; Agarwal, S.; Greiner, A., Synthesis and properties of novel poly(p-xylylene)s with aliphatic substituents. *E-Polymers* **2002**.
[65] Gilch, H. G.; Wheelwri.Wl, Polymerization of Alpha-Halogenated P-Xylenes with Base. *Journal of Polymer Science Part a-1-Polymer Chemistry* **1966,** 4, (6Pa1), 1337.
[66] Senkevich, J. J.; Yang, G. R.; Lu, T. M., The facile surface modification of poly(p-xylylene) ultrathin films. *Colloids and Surfaces a-Physicochemical and Engineering Aspects* **2003,** 216, (1-3), 167.
[67] Lahann, J.; Langer, R., Novel Poly(p-xylylenes): Thin Films with Tailored Chemical and Optical Properties. *Macromolecules* **2002,** 35, (11), 4380.
[68] Lahann, J.; Hocker, H.; Langer, R., Synthesis of amino[2.2]paracyclophanes - Beneficial monomers for bioactive coating of medical implant materials. *Angewandte Chemie-International Edition* **2001,** 40, (4), 726.
[69] Lahann, J.; Klee, D.; Hocker, H., Chemical vapour deposition polymerization of substituted [2.2]paracyclophanes. *Macromolecular Rapid Communications* **1998,** 19, (9), 441.
[70] Lahann, J.; Langer, R., Surface-initiated ring-opening polymerization of epsilon-caprolactone from a patterned poly(hydroxymethyl-p-xylylene). *Macromolecular Rapid Communications* **2001,** 22, (12), 968.
[71] Lahann, J.; Langer, R., Surface-initiated ring-opening polymerization of e-caprolactone from a patterned poly(hydroxymethyl-p-xylylene). *Macromolecular Rapid Communications* **2001,** 22, (12), 968.
[72]Schurmann, K.; Lahann, J.; Niggemann, P.; Klosterhalfen, B.; Meyer, J.; Kulisch, A.; Klee, D.; Gunther, R. W.; Vorwerk, D., Biologic response to polymer-coated stents: In vitro analysis and results in an iliac artery sheep model. *Radiology* **2004,** 230, (1), 151.
[72] Nandivada, H.; Chen, H. Y.; Lahann, J., Vapor-based synthesis of poly [(4-formyl-p-xylylene)-co-(p-xylylene)] and its use for biomimetic surface modifications. *Macromolecular Rapid Communications* **2005,** 26, (22), 1794.
[73] Lahann, J.; Balcells, M.; Lu, H.; Rodon, T.; Jensen, K. F.; Langer, R., Reactive polymer coatings: A first step toward surface engineering of microfluidic devices. *Analytical Chemistry* **2003,** 75, (9), 2117.
[74] Lahann, J.; Choi, I. S.; Lee, J.; Jenson, K. F.; Langer, R., A new method toward microengineered surfaces based on reactive coating. *Angewandte Chemie-International Edition* **2001,** 40, (17), 3166.
[75] Nandivada, H.; Chen, H. Y.; Bondarenko, L.; Lahann, J., Reactive polymer coatings that "click"". *Angewandte Chemie-International Edition* **2006,** 45, (20), 3360.
[76] Lahann, J.; Balcells, M.; Rodon, T.; Lee, J.; Choi, I. S.; Jensen, K. F.; Langer, R., Reactive polymer coatings: A platform for patterning proteins and mammalian cells onto a broad range of materials. *Langmuir* **2002,** 18, (9), 3632.
[77] Elkasabi, Y.; Chen, H. Y.; Lahann, J., Multipotent polymer coatings based on chemical vapor deposition copolymerization. *Advanced Materials* **2006,** 18, (12), 1521.
[78] Katira, P.; Agarwal, A.; Fischer, T.; Chen, H. Y.; Jiang, X.; Lahann, J.; Hess, H., Quantitative analysis of ultra-low protein coverages on protein-resisting surfaces using surface-bound kinesin motor proteins. *Advanced Materials* **2007**, accepted.

[79] Thévenet, S.; Chen, H. Y.; Stellacci, F.; Lahann, J., A generic approach towards nanostructured surfaces based on supramolecular nanostamping on reactive polymer coatings. *Advanced Materials* **2007**, accepted.
[80] Chen, H. Y.; Lahann, J., Fabrication of discontinuous surface patterns within microfluidic channels using photodefinable vapor-based polymer coatings. *Analytical Chemistry* **2005,** 77, (21), 6909.
[81] Jiang, X.; Chen, H. Y.; Galvan, G.; Yoshida, M.; Lahann, J., Vapor-based initiator coatings for atom transfer radical polymerization. *Advanced Functional Materials* **2007**, accepted.
[82] Chen, H. Y.; Elkasabi, Y.; Lahann, J., Surface modification of confined microgeometries via vapor-deposited polymer coatings. *Journal of the American Chemical Society* **2006,** 128, (1), 374.
[83] Chen, H. Y.; Rouillard, J. M.; Gulari, E.; Lahann, J., Colloids with high-definition surface structures. *Proceedings of the National Academy of Sciences of the United States of America* **2007,** 104, (27), 11173.

CHAPTER 2

CONTROLLED IMMOBOLIZATION OF BIOMOLECULES BY USING REACTIVE POLYMER COATINGS

Defined and stable surface properties are essential characteristics of many future biodevices, such as high-density protein and DNA arrays,[1,2] micro total analysis systems (μTAS),[3] microfabricated cell sorting and detection devices,[4] or miniaturized networks for cell isolation and culturing.[5,6] Because of the high surface-to-volume ratios typically encountered in miniaturized biodevices, even minor variations in the surface chemistry can reduce device performance. As a consequence, development of well-defined biointerfaces, which combine the biological functionality of naturally derived support matrices with the versatility and robustness of synthetic polymers will be increasingly important for a large number of biotechnological applications. Engineering of material surfaces has therefore emerged as a critical challenge in the development of a variety of biomedical devices.[7] In general, covalent linkage of biomolecules to a surface requires suitable chemical groups on the substrate that support chemoselective coupling reactions. Since most substrates of interest in the biomedical field do not bear reactive groups of appropriate types and densities, they must be introduced either in a proper surface-functionalization step or via the deposition of functionalized thin-film coatings. Recently, we established a surface modification technique based on the chemical vapor deposition (CVD) polymerization of substituted [2,2]paracyclophanes, to prepare a diverse class of functionalized poly-*p*-xylylenes with a wide variety of functional groups such as amines, esters and alcohols, which can be used for covalent binding of biomolecules.[8,9] Advantages of the CVD technique include control of the composition and architecture of the films, high accuracy, solvent-free environments, and excellent adhesion. This technique fulfills the need for a simple and broadly applicable surface modification system that creates stable platforms for the increasing needs of biointerface

modifications in biotechnology.

As a consequence, development of well-defined biointerfaces, which combine the biological functionality of naturally derived support matrices with the versatility and robustness of synthetic polymers will be increasingly important for a large number of biotechnological applications.

2.1 Biomimetic Surface Modification by Using a Formyl Functionalized Polymer Coating

The materials in this section are adapted from previously reported data in "Vapor-Based Synthesis of Poly[(4-formyl-p-xylylene)-co-(p-xylylene)] and Its Use for Biomimetic Surface Modifications, *Macromolecular Rapid Communications* (2005) 26, 1794", by H. Nandivada, H.-Y. Chen, and J. Lahann; and have been slightly modified.

The aldehyde group is a suitable candidate for surface modification because of its high specificity towards functional groups such as hydrazide, hydroxylamino, and thiosemicarbazide groups.[10,11] Aldehyde groups have already been generated on glass, silicon and metal surfaces using the multi-step silanization process or plasma polymerization of aldehyde-containing monomers.[1,12] However, these protocols result in poorly defined polymers or may involve the use of organic solvents and other chemicals. These features could potentially reduce the biological applicability of the aldehyde-modified surfaces. In addition, these methods are often substrate-specific. Therefore a substrate-independent procedure, such as CVD polymerization, is highly attractive for the preparation of aldehyde functionalized surfaces. In this section, we report the CVD polymerization of 4-formyl-[2,2]paracyclophane to yield an aldehyde functionalized poly-*p*-xylylene, poly(4-formyl-*p*-xylylene-*co*-*p*-xylylene), which is suitable for the immobilization of polysaccharides. The chemical composition of the resulting polymer thin films was confirmed by infrared spectroscopy (IR) and X-ray photoelectron spectroscopy (XPS). Furthermore, we established the availability of the aldehyde groups on the surface of the polymer films via chemical conversion with

hydrazides to yield hydrazone linkages and by tethering model sugars to the reactive surfaces.

The precursor 4-formyl[2,2]paracyclophane (**1**) can be synthesized either using the two-step synthesis from [2.2]paracyclophane or via the oxidation of 4-hydroxy[2,2] paracyclophane.[13,14] The resulting dimmer (**1**) was CVD polymerized to yield poly(4-formyl-*p*-xylylene-*co*-*p*-xylylene) (**2**). For CVD polymerization (Figure 2.1), **1** was sublimed in the sublimation chamber under a reduced pressure of 0.54 mbar at a temperature of 100-120 ^{o}C. The vaporized dimer was then transported by an inert carrier gas (argon) into the pyrolysis zone, at a temperature of 670 ^{o}C, where the methylene bridges were homolytically cleaved and quinodimethanes were formed. These monomers were then adsorbed onto the substrate at a temperature of 10 ^{o}C. Under these conditions, the monomers underwent spontaneous polymerization on the substrate.

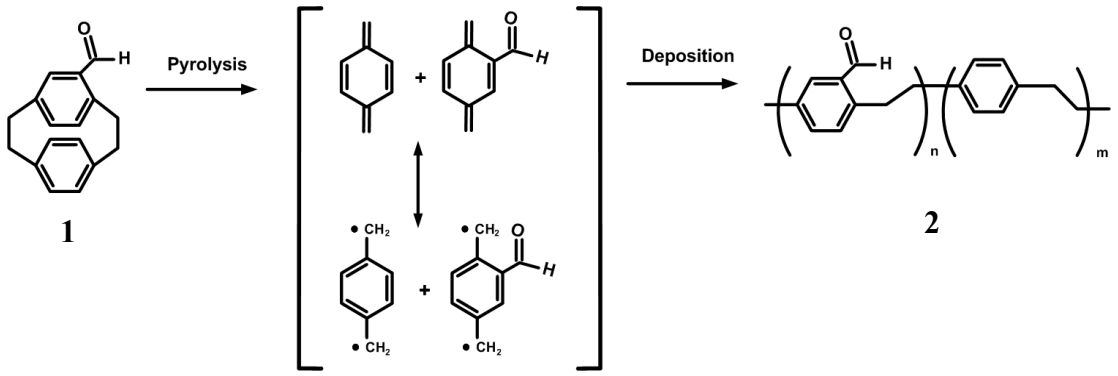

Figure 2.1: CVD polymerization of 4-formyl[2,2]paracyclophane (**1**) to yield poly(4-formyl-*p*-xylylene-*co*-*p*-xylylene) (**2**).

X-ray photoelectron spectroscopy (XPS) was used to determine the elemental composition of polymer **2** (Table 2.1). From the XPS survey spectrum and the high-resolution spectra, a value of 92.5 % for carbon and 7.5 % for oxygen was found, in close accordance with the theoretical composition of 94.4 % for carbon and 5.6 % for oxygen. The high resolution C_{1s} spectrum of polymer **2** (Figure 2.2) showed that the ratio between the α-carbon of the formyl group (C-C=O) and the carbonyl carbon (C=O) is 0.88, as compared to the calculated value of 1. The signal at 291.2 eV indicated π->π* transitions which are a characteristic feature of aromatic polymers and have been previously reported for poly-*p*-xylylenes.[15] The symmetric O_{1s} signal at 533.2 eV can be attributed to a single energy state for all the oxygen atoms in the polymer. Thus the XPS data confirmed the chemical structure of polymer **2** shown in Figure 2.1. The strong carbonyl stretch at 1688 cm^{-1} in the infrared spectrum (IR) also confirmed the presence of the aldehyde group in polymer **2** after CVD polymerization. Further evidence of the aldehyde group was provided by the characteristic band for aldehyde C-H stretching vibrations at 2734 cm^{-1}. Polymer **2** exhibited good adhesion to a wide variety of substrates such as gold, silica, glass and poly(dimethylsiloxane) (PDMS). The adhesion of polymer **2** was analyzed by pressing scotch tape onto the polymer coating and then peeling it off. Visual examination showed the intactness of the film and IR spectrum confirmed the presence of the film. Polymer **2** was insoluble in aqueous solutions as well as in a variety of standard organic solvents such as ethanol, acetone, methanol, dichloromethane, chloroform, dimethyl-formamide (DMF) and toluene.

TABLE 2.1
XPS ANALYSIS OF POLY(4-FORMYL-*P*-XYLYLENE-*CO*-*P*-XYLYLENE).

	C-C	**C**-C=O	**C**=O	**π-π***
BE (eV)	285.19	286.78	287.86	291.15
Calculated (%)	88.2	5.9	5.9	-
Experimental (%)	87.7	4.4	5.0	2.9

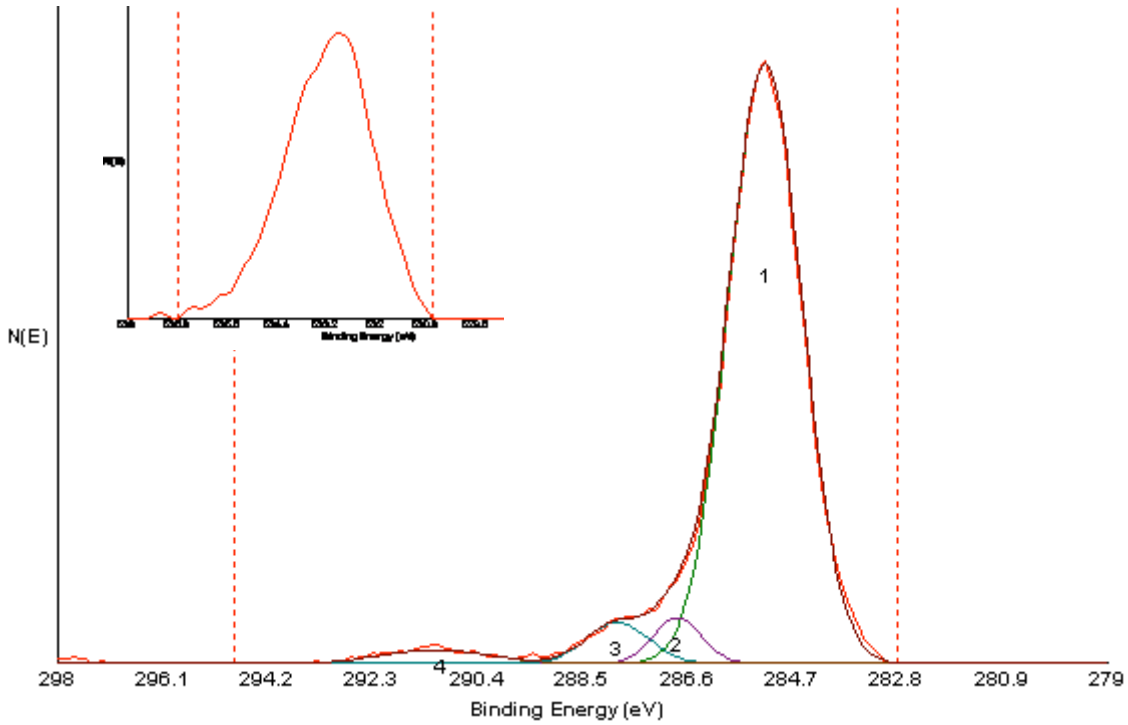

Figure 2.2: High resolution C1s and O1s (inset) XPS spectra of polymer **2**. Binding energies (eV) with the corresponding bonds are as follows: 285.19 (C-C), 286.78 (C-C=O), 287.86 (C=O), 291.15 (π-π*).

The ability to support chemical reactions on the surface of a substrate or a device is a highly desirable property for the functionalized coatings. The availability and reactivity of the aldehyde groups on polymer **2** was studied using hydrazone formation. Hydrazones are formed via the conversion of aldehydes with hydrazines or hydrazides and is a widely used immobilization strategy.[15] Using microcontact printing, the condensation reaction between the aldehyde groups on the surface and a biotinyl hydrazide was performed (at pH 5-6). For microcontact printing, biotinamidocaproyl hydrazide (3) was inked onto an oxidized PDMS stamp and stamped onto the aldehyde substrate creating a pattern. We chose **3** as our prototype ligand owing to the strong non-covalent interaction between biotin and streptavidin and streptavidin's ability to be used as a universal platform for further binding of biotinylated biomolecules.[15] After the immobilization of the biotin ligand **3**, the biotin-binding was examined by utilizing rhodamine-labeled streptavidin (**4**) as the binding partner. The rhodamine-labeled streptavidin specifically bound to the biotin-based patterns (Figure 2.3) creating homogeneous and reproducible patterns on the reactive coating, thus showing that the aldehyde groups on the surface are reactive and can be used as anchoring sites.

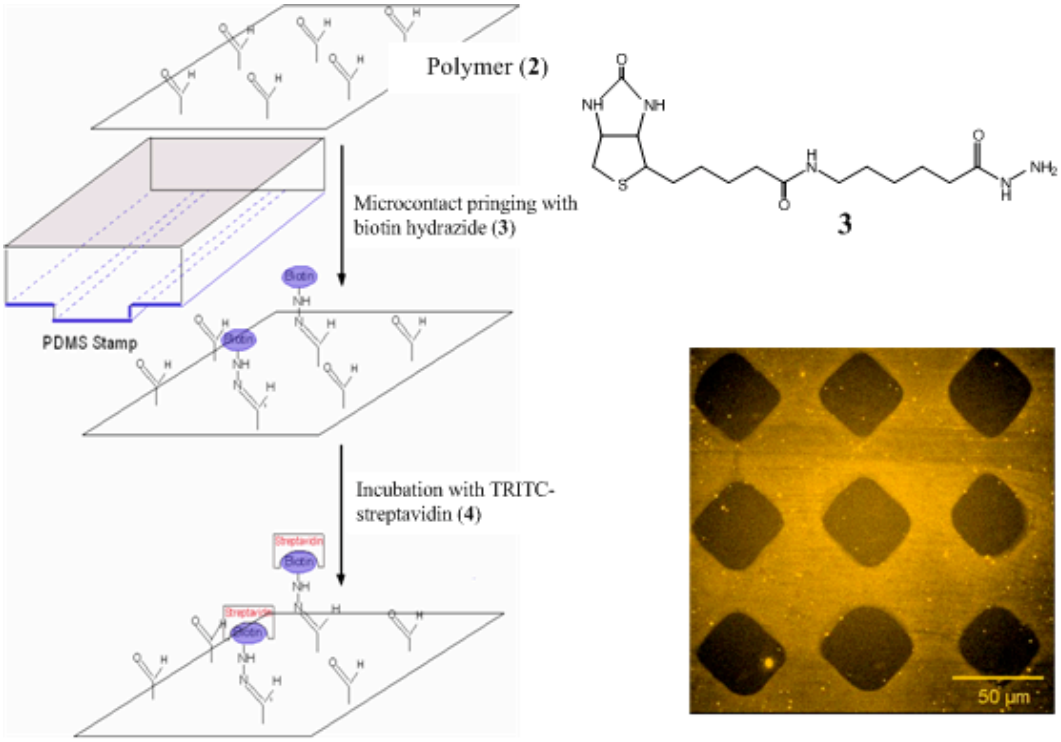

Figure 2.3: (a) Scheme for surface modification of polymer **2** using microcontact printing; (b) a typical fluorescence micrograph of **4** bound to ligand **3**, which was patterned onto polymer **2**.

The specificity of hydrazides and hydrazines towards aldehydes and ketones also makes them superb binding agents for the immobilization of saccharides.[10] Carbonyl-containing surfaces can be modified using dihydrazide homobifunctional linkers, to form hydrazone bonds on one side and yielding alkyl hydrazide spacers on the other side, suitable for subsequent reaction with formyl-containing groups available in saccharides.[10] Adipic acid dihydrazide (**5**) was chosen as the linker due to its intermediate length spacer arm, which leads to accessible reactive sites for further reaction. Using microcontact printing, substrate coated with polymer **2** was patterned with linker **5**, thus creating hydrazide-activated surfaces suitable for targeting saccharides. To prove this, the hydrazide-modified polymer surface was reacted with a disaccharide, 2-α mannobiose (**6**). One mannose group reacted with the hydrazide while leaving the other saccharide group free. This saccharide binding was investigated by applying a solution of rhodamine-labeled concanavalin A (**7**), a mannose specific lectin, that recognized the free mannose unit.[16] The patterned substrates were visualized using fluorescence microscopy (Figure 2.4). The rhodamine-labeled lectin specifically bound to the disaccharide-presenting surface, which in turn was immobilized onto a substrate coated with polymer **2** and patterned with 25 μm stripes of linker **5**.

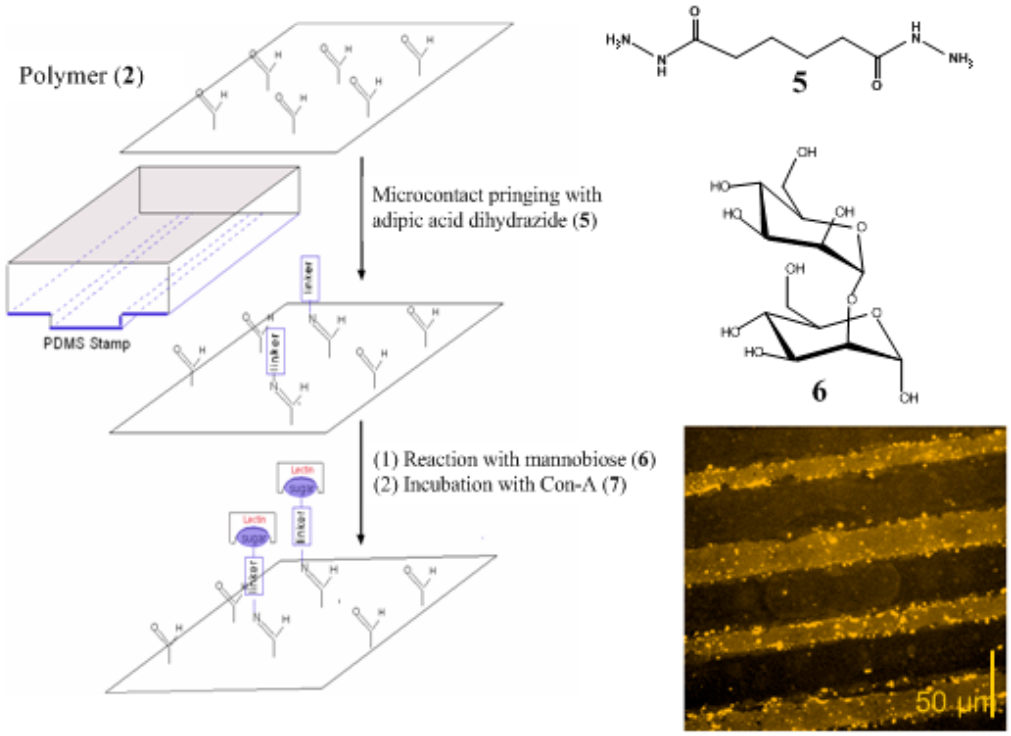

Figure 2.4: (a) Scheme showing the immobilization of oligosaccharides; (b) the corresponding fluorescence micrograph of **7** bound to **6** which is covalently linked to surfaces patterned with linker **6**; line profile with a line width of 25 µm.

2.2 Surface Modification via Click Chemistry by Using an Alkyne Functionalized Polymer Coating

The materials in this section are adapted from previously reported data in "Reactive Polymer Coatings that Click, *Angewandte Chemie International Edition* (2006) 45, 20, 3360", by H. Nandivada, H.-Y. Chen, L. Bondarenko, J. Lahann; and have been slightly modified.

A new type of biofunctional surface based on alkyne-containing vapor-based polymer coatings has also been prepared. These reactive coatings are applicable to a wide range of substrates and can be modified by subsequent spatially-directed 'click

chemistry'. Click chemistry represents a family of powerful and efficient chemical reactions, which are modular, wide in scope, insensitive to solvents and pH, and give stereoselective conversions with high to very high yields.[17] The most widely used click reaction is the Huisgen 1,3-dipolar cycloaddition between azides and terminal alkynes.[18] This coupling reaction has been employed for drug discovery applications[19] and for the target-guided synthesis of enzyme-inhibitors.[20,21] Moreover, Huisgen 1,3-dipolar cycloadditions of azide and alkyne functionalized SAMs have been used as a versatile tool for tailoring surface functionalities.[15,22-24] Bioorthogonality, dependence on enforced proximity, and the enforcement of proper alignment of the reactants make click reactions promising candidates for biointerface design.[25] However, further use is currently hampered by the availability of reactive polymer coatings that are compatible with dipolar cycloadditions.

In this section, we report the synthesis of alkyne-containing polymers via CVD polymerization of diethynyl[2,2]paracyclophane (**8a**) and 4-ethynyl[2,2]paracyclophane (**8b**) (Figurr 2.5) and their subsequent use for spatially-directed Huisgen 1,3-dipolar cycloaddition.

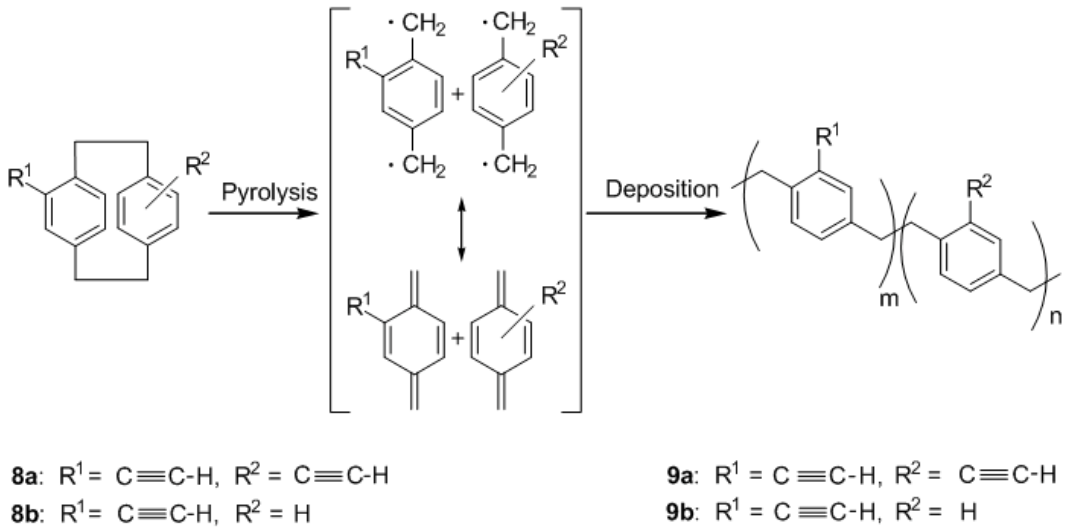

8a: R^1 = C≡C-H, R^2 = C≡C-H
8b: R^1 = C≡C-H, R^2 = H

9a: R^1 = C≡C-H, R^2 = C≡C-H
9b: R^1 = C≡C-H, R^2 = H

Figure 2.5: Synthesis of alkyne-containing polymers via CVD polymerization of diethynyl-[2,2] paracyclophane (**8a**) and 4-ethynyl-[2,2]paracyclophane (**8b**).

Prior to CVD polymerization, the starting materials **8a** and **8b** were prepared from the commercially available [2.2]paracyclophane (**1**), which was first converted to the respective di- and mono- formyl derivatives followed by Bestmann's acetylene synthesis, which yielded the corresponding alkyne functionalized compounds **8a** and **8b**.[26] Under the conditions of the dialkyne synthesis, pseudo-ortho and pseudo-meta derivatives have been reported as the major isomers.[26]

First, we attempted the CVD polymerization of the di-alkyne **8a**, which was expected to yield poly(diethynyl-*p*-xylylene) (**9a**). For this purpose, **8a** was sublimed at 90-110 ^{o}C and a reduced pressure of 0.5 mbar. The reactants were then transported into pyrolysis chamber (650 ºC) and deposition chamber (15 ºC), where the spontaneous formation of a polymer film was observed. However, the FTIR spectrum of polymer films formed under these conditions did not show a C-H stretch around 3200 cm^{-1} in indicating the absence of alkyne groups. Instead, several side products were formed, which were not further characterized, but could potentially be due to an alkyne-vinylidine rearrangement.[27] Alteration of process conditions, (e.g., pyrolysis temperatures below 550 ^{o}C), resulted in alkyne-functionalized polymers, with typical ellipsometric

thicknesses of about 50 nm (for 50 mg of the precursor polymerized). Nevertheless, these polymer films showed little reactivity and had poor stability towards organic solvents, so they were not pursued further.

Instead, we shifted our focus to the CVD polymerization of the mono-alkyne **8b**. In clear contrast to the di-alkyne containing polymer **9a**, poly(4-ethynyl-*p*-xylylene-co-*p*-xylylene) (**9b**) could be prepared without appreciable side reactions, even under very typical CVD conditions[15] (pressure of 0.5 mbar, sublimation, pyrolysis and substrate temperatures of 90-110 ^{o}C, 680 ^{o}C and 15 ^{o}C, respectively). Moreover, the FTIR spectrum of **9b** revealed a strong alkyne C-H stretch at 3286 cm^{-1} and a signal at 2100 cm^{-1} which is the characteristic C-C stretch for the triple bond. Evidence from the FTIR data was reaffirmed by X-ray photoelectron spectroscopy (XPS), which was used to quantify the surface elemental composition of **9b**. Polymer **9b** consists of about 98.7% carbon and only traces of oxygen are observed. These data compared well with the theoretical composition of **9b**. Moreover, the high resolution C1s spectrum of **9b** further revealed a symmetric and narrow peak centered at 285.6 eV with a full width at half maximum (FWHM) of 1.13 eV. This can be associated with the presence of a single type of carbon, i.e. carbon that is bound to carbon or hydrogen.[28] The C1s peak spectrum further showed a smaller signal centered at 291.7 eV, which can be attributed to π-π^{*} shake-up signal characteristic of aromatic π electrons. This signal has been observed for similar polymer systems in the past.[15] Polymer **9b** was found to have an ellipsometric thickness of 91.81±0.03 nm (for 50 mg of precursor) and was stable in aqueous solutions and organic solvents such as acetone, ethanol, methanol and chloroform. Probing the adhesiveness of **9b** using the scotch tape test[29] showed that the film had good adhesion to a wide variety of substrates such as glass, poly(dimethylsiloxane) (PDMS), silicon and gold.

To assess whether the reactive coating **9b** can be used for heterogeneous click reactions, its reactivity against azides was studied. Specifically, the Huisgen 1,3-dipolar cycloaddition between **9b** and an azide-containing biotin-based ligand (**4**) in the presence of copper(II) sulfate and sodium ascorbate was examined (Figure 2.6). As described for solvent-based systems, this irreversible exergonic fusion reaction occurs in the presence

of a copper(I) catalyst yielding five-membered heterocyclic triazoles.[30] Sodium ascorbate acts as a reductant, generating Cu^{I} ions *in situ* from $CuSO_4$, which functions as the active catalyst of the cycloaddition.[30] Compound **4** was chosen as the representative ligand in this study, because biotin undergoes a strong non-covalent interaction with streptavidin, which in turn has been widely used for binding of a wide range of biotinylated biomolecules.[13]

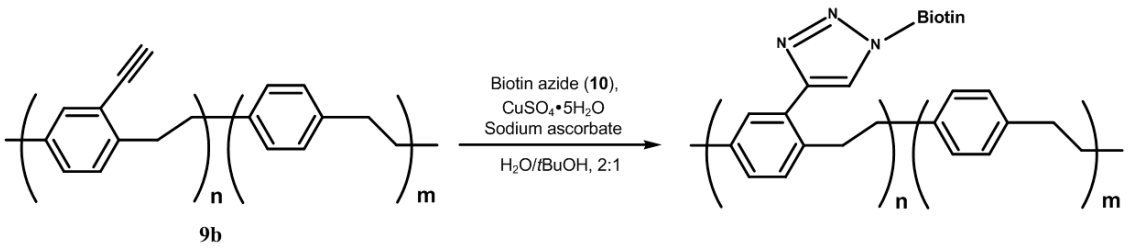

Figure 2.6: Huisgen 1,3-dipolar cycloaddition between biotin-based azide-ligand (**10**) and the poly(4-ethynyl-*p*-xylylene-*co*-*p*-xylylene) (**9b**).

To ensure spatial control over the cycloaddition reaction, a microcontact printing (μCP) approach was chosen. For this approach to be successful, Cu^{I} catalyst and azide reactant **10** had to be decoupled. This was achieved by microcontact printing only the Cu^{I} catalyst onto a preadsorbed film of ligand **10**. In this two-step process illustrated in Figure 2.7, a thin layer of **10** and sodium ascorbate was spread onto **9b** and the solvent was dried using N_2. Next, a patterned PDMS stamp was inked with a solution of $CuSO_4$ and kept in contact with the substrate for 12-18 hours. After rinsing, the patterned substrate was incubated with an aqueous solution of rhodamine-labeled streptavidin. Fluorescence microscopy was used to assess the spatially-directed immobilization of **10** onto polymer **9b**. The fluorescence micrographs shown in Figures 2.8a and 2.8c confirmed selective protein coupling in the regions where the $CuSO_4$ solution was microcontact printed, thus proving the binding of **10** to polymer **9b**. This supports the conclusion that the alkyne groups on the polymer surface are reactive and can be effectively used as anchoring sites for surface modifications. The two-step approach

(preadsorption + microcontact printing of the catalyst) was found to be superior to the concurrent microcontact printing of catalyst and azide. Furthermore, our study revealed the catalytic activity of Cu^{I} ions to be essential for the heterogeneous click reaction. Regions without Cu^{I} catalyst did not show fluorescence due to a lack of azide binding in the absence of the catalyst. To complement the fluorescence study, patterned surfaces were further analyzed by imaging ellipsometry in the mapping mode. The ellipsometric images shown in Figures 2.8b and 2.8d reveal protein patterns, which are inline with the corresponding fluorescence patterns. The observed thickness differences of about 1-2 nm between the biotinylated regions with streptavidin and the non-biotinylated polymer regions are comparable with literature-reported thicknesses of protein monolayers.

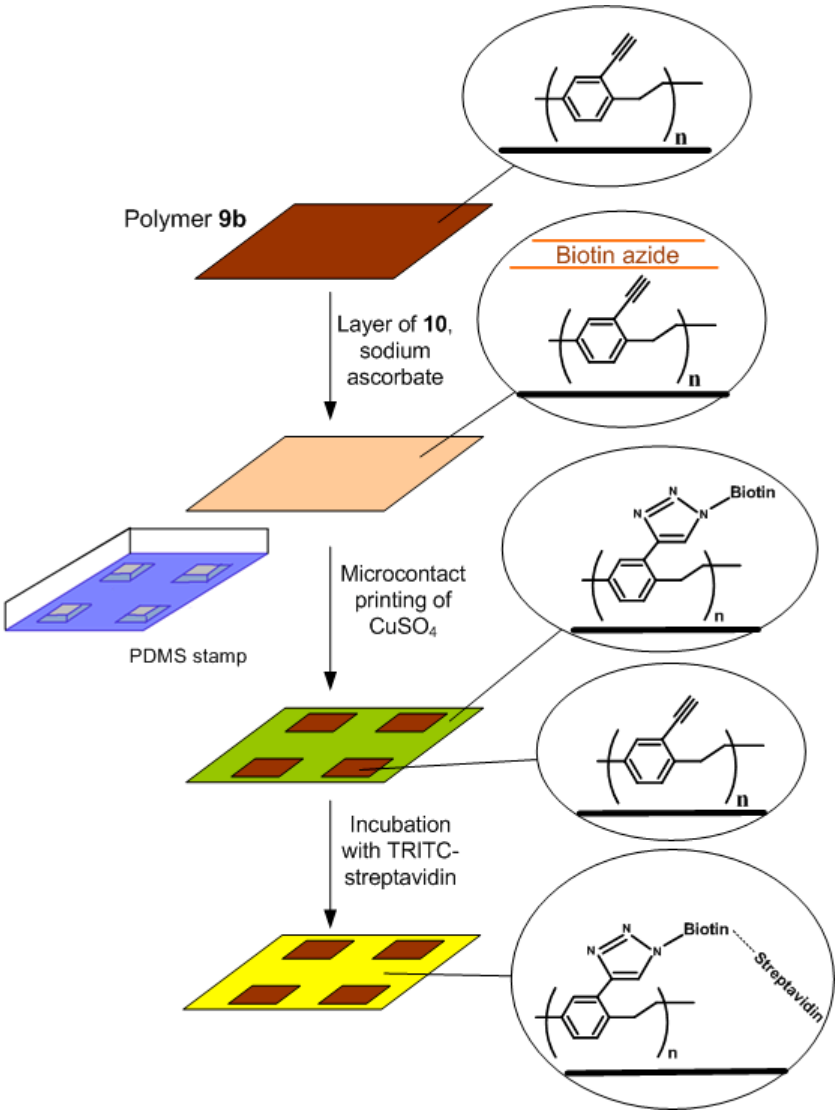

Figure 2.7: Immobilization of azide-containing ligand on the reactive polymer coating. The CuI catalyst is microcontact printed on a preadsorbed layer of biotin-based azide-ligand (**10**) on the reactive polymer **9b**.

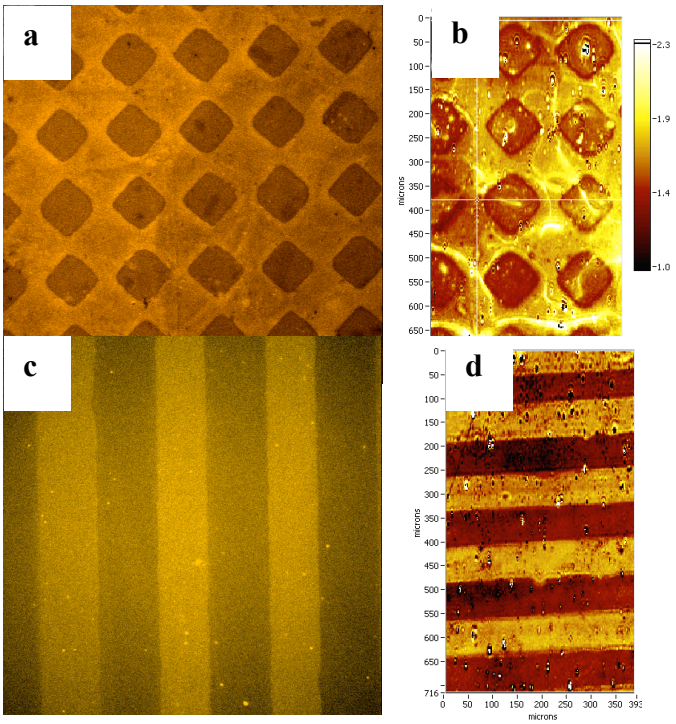

Figure 2.8: Fluorescence micrographs (a) and (c) showing the binding of TRITC-streptavidin to patterns of biotin azide formed by μCP. (b) and (d) are showing corresponding imaging ellipsometric image.

2.3 Multi-Functional Surface Modification by CVD Copolymerization

The materials in this section are adapted from previously reported data in "Multipotent Polymer Coatings Based on Chemical Vapor Deposition Copolymerization, *Advanced Materials* (2006) 18, 1521", by Y. Elkasabi, H.-Y. Chen, J. Lahann; and have been slightly modified.

In a significant extension of our previous work, we now report on the use of CVD copolymerization to fabricate multipotent and modular coatings. The term "multipotent coating" in this context, refers to a reactive coating that is compatible with the simultaneous presentation of multiple biomolecules in controllable ratios.

Prior to CVD copolymerization, 4-trifluoroacetyl-[2.2]paracyclophane (**1**) and 4-aminomethyl-[2.2]paracyclophane (**2**) were synthesized from commercially available [2.2]paracyclophane following established synthetic routes.[31,32] CVD copolymerization of **1** and **2** was then conducted and resulted in a vacuum-deposited film of copolymer **3** on the substrate (Figure 2.9). For CVD copolymerization, mixtures of carefully purified dimers **1** and **2** were initially sublimated under a reduced pressure of 56 Pa at 90–100 °C. The sublimation temperatures of **1** and **2** were sufficiently similar, and so to ensure that the compounds were exposed to comparable sublimation conditions they were placed near each other within the CVD system. Sublimated **1** and **2** were then transferred to the pyrolysis zone, which was heated to 670 °C to ensure cleavage of the aliphatic C–C bonds, resulting in the corresponding quinodimethanes (monomers). In the last step, monomers were adsorbed on the substrate at approximately 10 °C and spontaneously polymerized. CVD copolymerization of **1** and **2** resulted in transparent and topologically uniform polymer films with thicknesses between 50 and 200 nm. The film thickness is mainly determined by the total amount of [2.2]paracyclophanes used for polymerization. For instance, the thickness of a film produced by the deposition of 20 mg of equimolar amounts of **1** and **2** was determined by means of imaging ellipsometry to be 115 ± 15 nm. Moreover, the multifunctional coatings showed excellent chemical stability in a dry-air environment. No significant change in composition or chemical behavior was found for samples stored in a dry-air atmosphere for several weeks compared to freshly prepared samples. All copolymers as well as the two homopolymers **4** and **5** remained intact after rinsing with standard solvents such as water, chloroform, acetone, and ethanol.

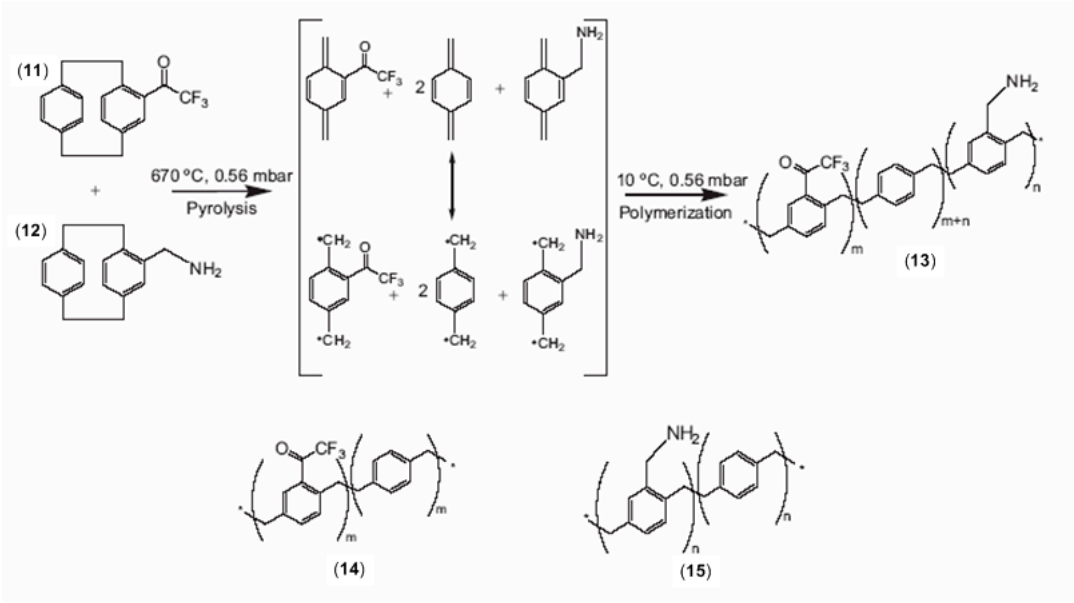

Figure 2.9: The multifunctional polymer (**13**) accessible by CVD copolymerization of [2.2]paracyclophanes **11** and **12**; the structures of the individual polymers **14** and **15** are shown for comparison.

The elemental composition of the copolymer poly[4-aminomethyl-*p*-xylylene-*co*-4-trifluoroacetyl-*p*-xylylene-*co*-*p*-xylylene] (**13**) was studied by X-ray photoelectron spectroscopy (XPS). XPS is capable of detecting atomic composition within a depth of about 10 nm.[31] Copolymer **13** was compared to the individual polymers, poly[4-trifluoroacetyl-*p*-xylylene-*co*-*p*xylylene] (**14**) and poly[4-aminomethyl-*p*-xylylene -*co*-*p*-xylylene] (**15**, see Table 2.2). Characteristic chemical elements detected for the individual polymers **14** and **15**, such as oxygen (polymer **14**), fluorine (polymer **14**), and nitrogen (polymer **15**), were simultaneously detected in the copolymer, indicating the presence of both functional groups on the surface. Because nitrogen is only present in the aminomethyl group of polymer **15**, while fluorine is present in only the ketone function of polymer **14**, the ratio of the elemental composition of nitrogen and fluorine is a good indicator of the chemical quality of the copolymer films. Using XPS, we found a N/F ratio of 0.332, which is in good accordance with the theoretically expected ratio of 0.333. Accordingly, side reactions, such as decomposition of the functional groups, were

negligible when pyrolysis temperatures under 670 °C and working pressures between 40 and 60 Pa were chosen. Furthermore, XPS revealed no signs of cross-reaction of the aminomethyl and ketone groups under the conditions of CVD polymerization. Table 2.2 shows the experimental results of the high-resolution C1s XPS for the 1:1 copolymer to be in good agreement with theoretical values.[15,33]

TABLE 2.2
POLY[(4-AMINOMETHYL-*P*-XYLYLENE)-*CO*-(4-TRIFLUOROACETYL-*P*-XYLYLENE)-*CO*-*P*-XYLYLENE] (**13**) PREPARED WITH A 1:1 FEED RATIO, COMPARED TO THE INDIVIDUAL POLYMERS **14** AND **15**.

Polymer		C–C	C–N	C=O	$\pi \rightarrow \pi^*$	C–F
	BE [eV]	285.0	286.8	288.4	291.2	292.9
13	Calculated [%]	89.2	3.6	3.6	–	3.6
	Experimental [%] [a]	89.5	3.1	3.3	4.3 [b]	4.1
14	Calculated [%]	81.48	0	9.26	–	9.26
	Experimental [%]	80.17	0	9.29	4.2	10.54
15	Calculated [%]	94.12	5.88	0	–	0
	Experimental [%]	94.27	5.73	0	5.8	0

[a] Percentage of total without $\pi \rightleftharpoons \pi^*$ applies to all experimental values.
[b] Actual value obtained; applies to all $\pi \rightleftharpoons \pi^*$ values.

To further support the XPS data, we used grazing-angle Fourier-transform IR (FTIR) spectroscopy to assess the structure of copolymers deposited onto a gold substrate. Figure 2.10 displays IR spectra of polymer films made by copolymerization of **11** and **12** using varying feed ratios. The spectra range from 100% of compound **12** (trace a) to 100% of compound **11** (trace g). All spectra were normalized based on the C–H band intensity (2926.1 cm^{-1}), because the C–H group is present in each polymer. As the feed ratio changed, the peak intensities of side groups changed accordingly. Due to potential differences in film thickness, we restrained ourselves to qualitative analysis only. The carbonyl stretches at 1716 cm^{-1}, characteristic of the COCF3 groups, were compared to the C–H band at 2926.1 cm^{-1}. The carbonyl stretch at 1716 cm^{-1} is absent in spectrum a. For spectra b–g, the carbonyl stretch grows until maximum intensity is attained in

spectrum g. The same trend can be observed for the C–F stretches at 1227, 1202, and 1152 cm^{-1}. Similarly, the signal at 977 cm^{-1} increases as the contribution of the ketone increases, to become a strong signal in the spectrum of pure polymer **14**. This band has been previously reported for similar polymers.[34]

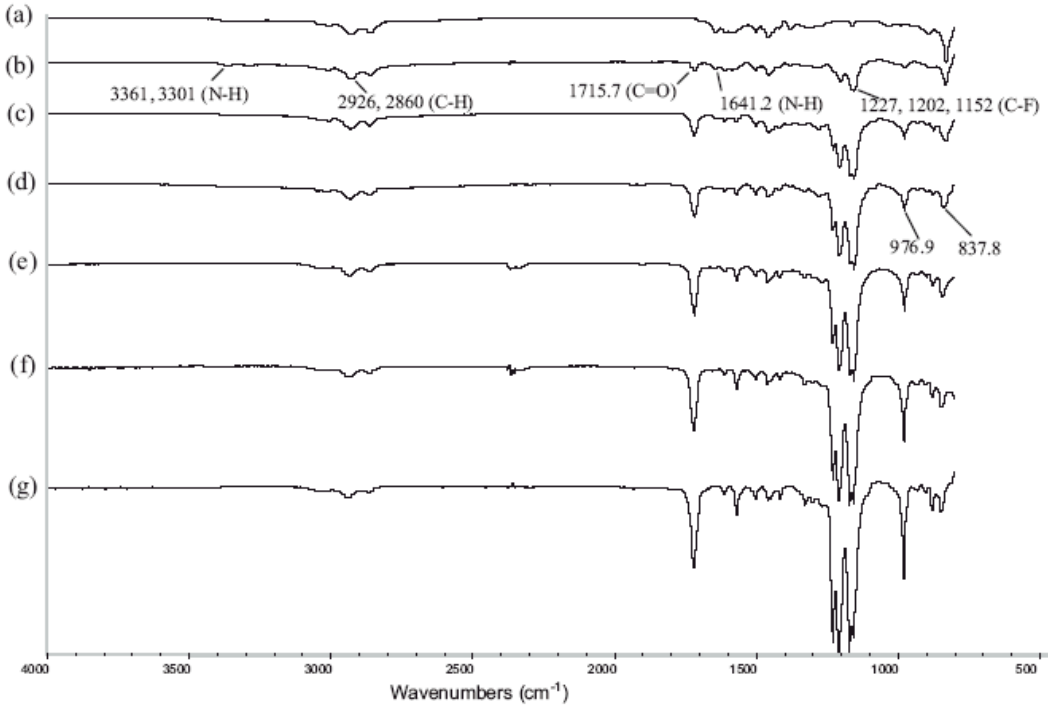

Figure 2.10:FTIR spectra of **13**, obtained from varying molar feed ratios of **11:12**. a) 100% **12**, b) 1:5 **11:12**, c) 1:2, d) 1:1, e) 2:1, f) 5:1, g) 100% **11**.

Once the fundamental concept of CVD copolymerization of [2.2]paracyclophanes containing different functional groups was established, the structural properties of the resulting copolymers needed to be elucidated in further detail. In principle, CVD copolymerization could result in a true copolymer— with properties distinct from individual polymers **14** and **15**—or in a layered blend of the two polymers.

We used X-ray diffraction (XRD) measurements of thin CVD films before and after annealing to address this question.[35] This approach takes advantage of the fact that

poly(*p*xylylenes) are often semicrystalline polymers with characteristic features in the XRD spectra.[36] Since XRD data for polymers **14** and **15** have not yet been reported, we studied the individual CVD polymers first. Prior to annealing, no diffraction patterns were obtained for either **14** or **15**, indicating that both films were largely amor- phous in the as-deposited state. However, after annealing for 14 h at 120 °C, the trifluoroacetyl-functionalized polymer **14** showed characteristic diffraction patterns, which likely correspond to (020) and (110) planes, and a *d*-spacing greater than that reported for the monoclinic poly(*p*-xylylene).[37] In contrast, the aminomethyl functionalized polymer **15** remained amorphous. Figure 2.11 compares diffraction patterns before and after annealing for the individual polymers **14** and **15** and the copolymers. Exposing the films to a high-temperature environment allows for realignment of functional groups to form crystalline domains.[31] Next, we assessed the structural properties of polymer **13** made by copolymerization of an equimolar feed ratio of **11** and **12**. Based on the FTIR study, we expected this copolymer to contain both components in about the same ratio. If the copolymerization results in a layered blend of individual polymers **14** and **15**, the resulting diffraction pattern should essentially be the superposition of the diffraction patterns of the individual polymers. If, however, the CVD copolymerization results in a true copolymer, a new polymer with a distinct, presumably amorphous structure would be prepared. As shown in Figure 2.11b, no diffraction patterns were detected for the copolymer, independent of the annealing. This observation also holds for the copolymer made from [2.2]paracyclophanes **11** and **12** in a feed ratio of 2:1. If a large excess of the ketone is used (feed ratio of 5:1), a small diffraction pattern can be detected after annealing, indicating the onset of a semicrystalline structure. Based on the XRD data, we concluded that the CVD copolymerization results in true copolymers with distinct structural properties, rather than layered blends of the individual polymers **14** and **15**.

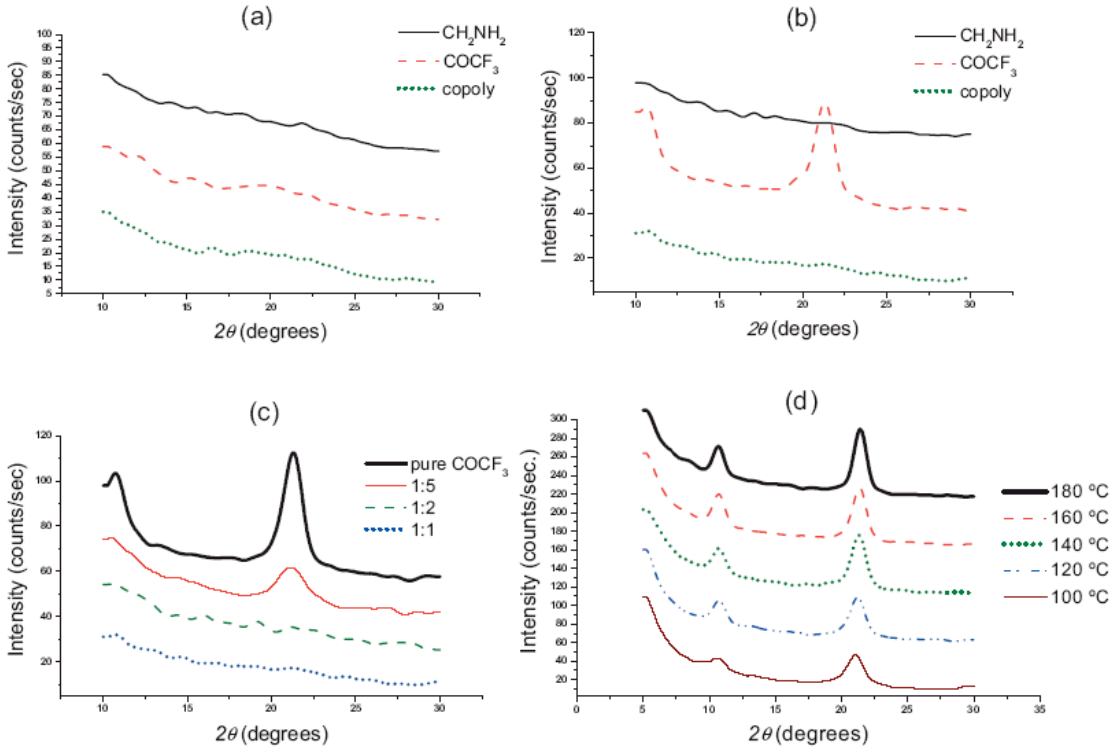

Figure 2.11: XRD patterns of the individual polymers **14** and **15** and the copolymer **13**. (a) before and (b) after annealing at 120 °C. Only polymer **14** exhibits crystallinity after annealing. (c) XRD patterns of copolymers with 100% **11** (black), 1:5 **12:11** (red), 1:2 (green), and 1:1 (blue). (d) XRD patterns of **14** at various annealing temperatures.

The existing CVD polymerization system is equipped with a sample holder that has a built-in temperature control. The platen is equipped with a cooling/heating cycle that can be controlled within +/- 0.5 ºC, spanning a temperature range from -45 ºC to 60 ºC. This study we conducted with the two precursors being used in a 1:1 ratio. As shown in Figure 2.12 samples were placed on defined positions on the sample holders. Tight contact between sample and platen was realized by slightly pressing the sample onto the platen to ensure optimum heat exchange. Although the sample holder is rotatable, this function was turned off during this experiment to evaluate potential spatial differences within the

group. Next, the sample holder was set to a pre-defined temperature varied between -30 ºC and 60 ºC in increments of 15 ºC. Film thickness was determined and was controlled between 60-80 nm for all samples (monitored by using an imaging ellipsometer). In addition, FTIR was conducted with these samples and the peak index was calculated based on the ratio of two FTIR peaks (C=O and C-N), each characteristic for one type of films. The normalized peak ratio for a 1:1 composition was statistically compared in Figure 2.13. As anticipated, homogeneous functionality distribution was discover throughout the temperatures studied, and the normalized result was showing consistent 1:1 functionality ratio on the copolymer film with respect to the 1:1 ratio of the precursors used. On the other hand, results were also averaged throughout the nine positions tested as indicated in Figure 2.12. Samples were systemically placed with a 70 mm distance longitudinally and also a 70 mm distance latitudinally from each other on a sample holder which has a 300 mm diameter. The resulting standard deviation was denoted as the error bars shown in Figure 2.13, which they fluctuate within the margin of error; in other words, the fluctuation of the functionality is independent of the sample positions with respect to the maximum distance of the sample holder in our system. Based on the findings above, we will be able to conclude that the difference of the threshold condensation temperatures of the two precursors used for CVD copolymerization was suppressed and no segregation of the polymer components was discovered; in other words, a homogeneous copolymer with equally distributed functionality was formed by the CVD copolymerzation process.

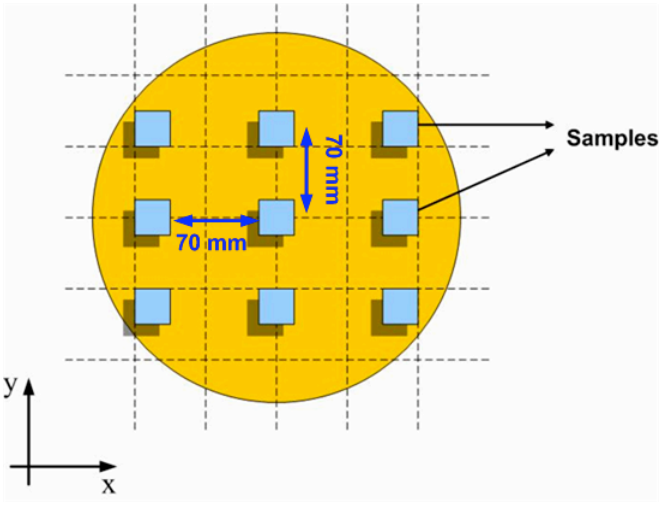

Figure 2.12: Positioning of the samples on the sample holder to evaluate homogenous distribution of polymer components.

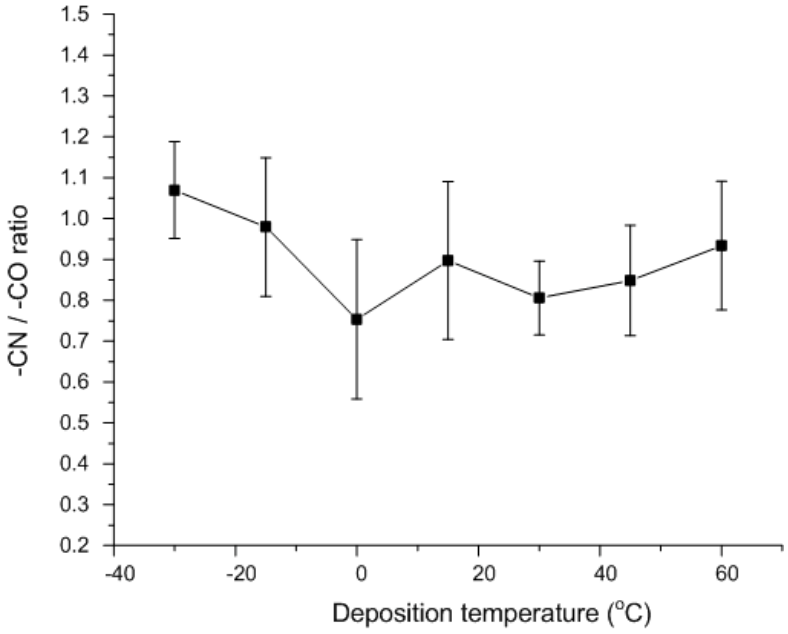

Figure 2.13: Functionality ratio of *C-N*/*C=O* vs. substrate temperature for CVD copolymerization. Data are showing a homogeneous distributed functionality regardless of the change in substrate temperatures. Error bars are showing the standard deviation with respect to sub.

Finally, we verified that both functional groups contained in copolymer **13** are available for further surface modification. The availability of the functional groups for further surface reaction is essential for immobilization of two different types of (bio)molecules. In a proof-of-concept experiment using the approach shown in Figure 2.12, the copolymer surface (**13**) was reacted with two fluorescent ligands that exhibited orthogonal reactivity. The purpose of this experiment was to assess whether or not each functional group remains active and is able to specifically react with the assigned ligands. Fluorescence scanning was used to examine the presence of surfacebound ligands. Figure 2.13 shows the results of the surface reaction of polymer **13** with Atto 655 and biotin-streptavidin. To avoid reaction between the Atto 655 ligand and the amino groups of streptavidin, a consecutive immobilization scheme was employed: The Atto 655 ligand was immobilized first, followed by the biotin ligand. We found Atto 655 to bind strongly to the aminomethylcontaining polymer **15**. In contrast, only negligible amounts of Atto 655 bound to polymer **14**. When reacting the two individual polymers **14** and **15** with the second ligand, a biotin hydrazide derivative, the biotin ligand was found to bind strongly to polymer **14**, but not to **15**. Fluorescence-labeled streptavidin, a specific binding partner of biotin, was used to visualize the biotin ligands and confirmed selective binding to the biotinmodified coating of polymer **14**. In contrast, streptavidin applied to polymer **15**, which was not modified with the biotin ligand, did not give any appreciable fluorescence signal. When performing the same procedure on copolymer **13**, both fluorescence signals were observed simultaneously (Figure 2.13). By varying the feed ratios of [2.2]paracyclophanes **11** and **12** in the CVD copolymerization, the relative ratio of ligands bound to the surface was varied. The relative increase of starting material **12** resulted in surfaces with increased amounts of Atto-labeled ligands (red color), while a relative increase of compound **11** resulted in an increased fluorescence signal indicating more streptavidin–biotin pair bound to the surface. Based on the FTIR spectra (Figure 2.10), these trends can be explained by the controlled variation of binding sites available for the two ligands on the surface, which corresponds to the feed ratio of starting materials used during CVD copolymerization. For the 1:1 ratio, the fluorescence micrographs of different reaction areas are shown in the inset of Figure 2.13. Area 1 shows copolymer **13** treated only with the biotin ligand (green color), while area 2 is

characterized by red fluorescence resulting from surface-immobilization of the Atto-labeled ligand. Where both ligands were allowed to react with the copolymer **13** (area 3), a yellow color is observed, indicating parallel immobilization of the two ligands.

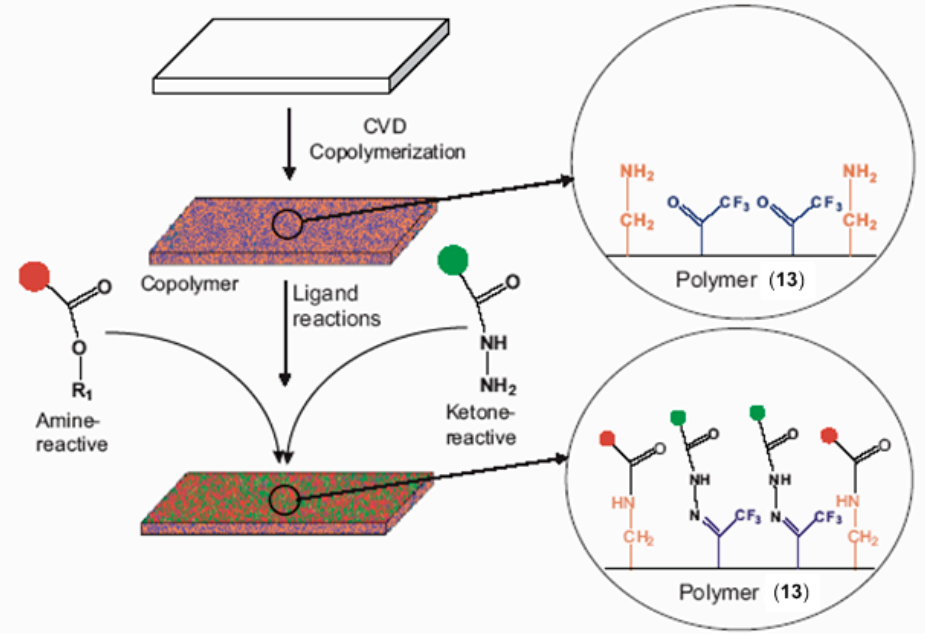

Figure 2.14: Schematic outlining the selective reactivity of the multivalent surface. The activated ester only reacts with the aminomethyl group, while the hydrazide group shows selective reactivity towards ketones.

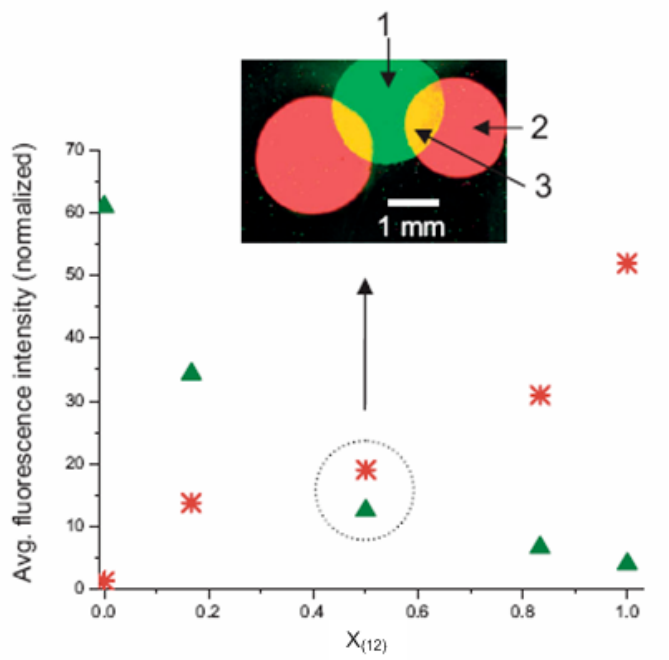

Figure 2.15: Fluorescence intensities detected on the copolymers versus $x_{(12)}$ (the relative feed concentration of [2.2]paracyclophane **12** used for CVD copolymerization). The trends demonstrate ligand immobilization occurs in controlled ratios as a function of increasing relative ratio of the [2.2]paracyclophanes. Inset: Fluorescence micrograph of areas that were reacted with 1) biotin ligand, 2) Atto 655 ligand, or 3) both.

2.4 Conclusions

Future advances in the design of biologically-active interfaces require novel strategies for the robust and specific attachment of biological ligands onto surfaces. The development of bioactive surfaces is an important step towards advanced biomaterials and biointerfaces for applications, such as implantable biomedical devices, bioassays and biosensors.

In this chapter, we reported the synthesis and characterization of a functionalized poly-*p*-xylylene, poly(4-formyl-*p*-xylylene-*co*-*p*-xylylene), using CVD polymerization.

We further demonstrate the usefulness of these polymer coatings for biomimetic surface modifications. The underlying aldehyde-hydrazide coupling chemistry is an attractive bioconjugation approach, because it benefits from (1) the rapid reaction kinetics and (2) the relative inactivity of both, the hydrazide and the carbonyl functionalities towards other biomolecules or biological functionalities, such as amines, acids and thiols. The resulting surfaces may find potential applications for the surface engineering of biomaterials and microfluidic devices.

On the other hand, the alkyne-containing polymer has been found to show a remarkable reactivity towards azides via the chemoselective Huisgen's 1,3-dipolar cycloaddition. In contrast to the di-alkyne containing polymer, mono-alkyne containing polymer showed excellent adhesion and stability. The fact, that spatially controlled cycloadditions can be conducted under mild reaction conditions, will enable the design of topologically differentiated biointerfaces. Further work will be directed towards the elucidation of the CVD polymerization mechanism as well as its scope with respect to different cycloadditions. The key feature of our approach is the use of vapor-based coatings for spatially-controlled orientation of biomolecules. As a flexible bioconjugation platform, this regioselective immobilization strategy could be applicable in the design of biofunctional surfaces for diagnostics (e.g. microarrays), biosensors, and biomedical device coatings.

The herein proposed concept of CVD polymerization of functionalized [2.2]paracyclophanes establishes a general, but simple protocol for preparation of multireactive polymer films. Applicability of the reactive coating to various substrates, such as polymers, metals, or composites, generates a fairly universal platform without relying on broad chemical alteration of the bulk material. Although multipotent biointerfaces could in principle be prepared by simultaneously immobilizing mixtures of two different biomolecules through the same functional groups, the exploration of reactive coatings with two orthogonal functional groups bears several potential advantages: (i) surface ratios can be controlled with high precision, because the ligand immobilization reactions can be conducted independently, (ii) substantially different biomolecules can be co-immobilized, even if their transport to the surface is substantially

different, and (iii) the ability to immobilize biomolecules in sequence allows for combinations of biomolecules that would otherwise cross-react with each other. For applications where substantially different biomolecules need to be immobilized in precisely defined ratios, CVD copolymerization may provide a simple access route. Moreover, this study presents a first step towards the establishment of a modular coating design, where the properties of a coating can simply be dialed in by selecting the right combination of building blocks for CVD copolymerization. Such a modular surface design may be of great value for future biomedical devices, high-throughput screening platforms, microfluidic analysis devices, or diagnostic platforms.

References

[1] Tian, J. D.; Gong, H.; Sheng, N. J.; Zhou, X. C.; Gulari, E.; Gao, X. L.; Church, G., Accurate multiplex gene synthesis from programmable DNA microchips. *Nature* **2004,** 432, (7020), 1050.

[2] Pellois, J. P.; Zhou, X. C.; Srivannavit, O.; Zhou, T. C.; Gulari, E.; Gao, X. L., Individually addressable parallel peptide synthesis on microchips. *Nature Biotechnology* **2002,** 20, (9), 922.

[3] Berg, A.; Olthius, W.; Bergveld, P., *Micro Total Analysis Systems 2000*. 1st ed.; Springer: 2000.

[4] Fu, A. Y.; Spence, C.; Scherer, A.; Arnold, F. H.; Quake, S. R., A microfabricated fluorescence-activated cell sorter. *Nature Biotechnology* **1999,** 17, (11), 1109.

[5] Chen, C. S.; Mrksich, M.; Huang, S.; Whitesides, G. M.; Ingber, D. E., Geometric control of cell life and death. *Science* **1997,** 276, (5317), 1425.

[6] Lucchetta, E. M.; Lee, J. H.; Fu, L. A.; Patel, N. H.; Ismagilov, R. F., Dynamics of Drosophila embryonic patterning network perturbed in space and time using microfluidics. *Nature* **2005,** 434, (7037), 1134.

[7] Khademhosseini, A.; Suh, K. Y.; Jon, S.; Eng, G.; Yeh, J.; Chen, G.-J.; Langer, R., A soft lithographic approach to fabricate patterned microfluidic channels. *Analytical Chemistry* **2004,** 76, (13), 3675.

[8] Lahann, J., Reactive polymer coatings for biomimetic surface engineering. *Chemical Engineering Communications* **2006,** 193, (11), 1457.

[9] Lahann, J., Vapor-based polymer coatings for potential biomedical applications. *Polymer International* **2006,** 55, (12), 1361.

[10] Hermanson, G. T., *Bioconjugate techniques*. Academic Press: San Diego, Calif., **1996**.

[11] Gering, J. P.; Quaroni, L.; Chumanov, G., Immobilization of antibodies on glass surfaces through sugar residues. *Journal of Colloid and Interface Science* **2002,** 252, (1), 50.

[12] Yeo, W. S.; Mrksich, M., Electroactive substrates that reveal aldehyde groups for bio-immobilization. *Advanced Materials* **2004,** 16, (15), 1352.

[13] Lahann, J.; Klee, D.; Hocker, H., Chemical vapour deposition polymerization of substituted [2.2]paracyclophanes. *Macromolecular Rapid Communications* **1998,** 19, (9), 441.

[14] Brink, M., Improved Synthesis of [2,2]Paracyclophane and 4-Formyl-[2,2]Paracyclophane. *Synthesis-Stuttgart* **1975**, (12), 807.

[15]Schurmann, K.; Lahann, J.; Niggemann, P.; Klosterhalfen, B.; Meyer, J.; Kulisch, A.; Klee, D.; Gunther, R. W.; Vorwerk, D., Biologic response to polymer-coated stents: In vitro analysis and results in an iliac artery sheep model. *Radiology* **2004,** 230, (1), 151.

[16] Moothoo, D. N.; Naismith, J. H., A general method for co-crystallization of concanavalin A with carbohydrates. *Acta Crystallographica Section D-Biological Crystallography* **1999,** 55, 353.

[17] Kolb, H. C.; Finn, M. G.; Sharpless, K. B., Click chemistry: Diverse chemical function from a few good reactions. *Angewandte Chemie-International Edition* **2001,** 40, (11), 2004.

[18] Padwa, A., *1,3-dipolar cycloaddition chemistry*. Wiley: New York, 1984; p 2 v.
[19] Kolb, H. C.; Sharpless, K. B., The growing impact of click chemistry on drug discovery. *Drug Discovery Today* **2003,** 8, (24), 1128.
[20] Lewis, W. G.; Green, L. G.; Grynszpan, F.; Radic, Z.; Carlier, P. R.; Taylor, P.; Finn, M. G.; Sharpless, K. B., Click chemistry in situ: Acetylcholinesterase as a reaction vessel for the selective assembly of a femtomolar inhibitor from an array of building blocks. *Angewandte Chemie-International Edition* **2002,** 41, (6), 1053.
[21] Manetsch, R.; Krasinski, A.; Radic, Z.; Raushel, J.; Taylor, P.; Sharpless, K. B.; Kolb, H. C., In situ click chemistry: Enzyme inhibitors made to their own specifications. *Journal of the American Chemical Society* **2004,** 126, (40), 12809.
[22] Lummerstorfer, T.; Hoffmann, H., Click chemistry on surfaces: 1,3-dipolar cycloaddition reactions of azide-terminated monolayers on silica. *Journal of Physical Chemistry B* **2004,** 108, (13), 3963.
[23] Devaraj, N. K.; Miller, G. P.; Ebina, W.; Kakaradov, B.; Collman, J. P.; Kool, E. T.; Chidsey, C. E. D., Chemoselective covalent coupling of oligonucleotide probes to self-assembled monolayers. *Journal of the American Chemical Society* **2005,** 127, (24), 8600.
[24] Collman, J. P.; Devaraj, N. K.; Chidsey, C. E. D., "Clicking" functionality onto electrode surfaces. *Langmuir* **2004,** 20, (4), 1051.
[25] Prescher, J. A.; Bertozzi, C. R., Chemistry in living systems. *Nature Chemical Biology* **2005,** 1, (1), 13.
[26] Nandivada, H.; Chen, H. Y.; Bondarenko, L.; Lahann, J., Reactive polymer coatings that "click"". *Angewandte Chemie-International Edition* **2006,** 45, (20), 3360.
[27] Gajewski, J. J., *Hydrocarbon thermal isomerizations*. 2nd ed.; Elsevier: Amsterdam ; New York, **2004**.
[28] Polzonetti, G.; Cianciusi, A. M.; Furlani, A.; Russo, M. V., Photoelec4ron-Spectroscopy Study of Fecl3 Doped Polyphenylacetyle*e. *Synthetic Metals* **1989,** 28, (3), D413.
[29] Nandivada, H.; Chen, H. Y.; Lahann, J., Vapor-based synthesis of poly [(4-formyl-p-xylylene)-co-(p-xylylene)] and its use for biomimetic surface modifications. *Macromolecular Rapid Communications* **2005,** 26, (22), 1794.
[30] Rostovtsev, V. V.; Green, L. G.; Fokin, V. V.; Sharpless, K. B., A stepwise Huisgen cycloaddition process: copper(I)-catalyzed regioselective \"ligation\" of azides and terminal alkynes. *Angewandte Chemie, International Edition* **2002,** 41, (14), 2596.
[31] Ratner, B. D.; Bryant, S. J., Biomaterials: Where we have been and where we are going. *Annual Review of Biomedical Engineering* **2004,** 6, 41.
[32] Rozenberg, V. I.; Danilova, T. I.; Sergeeva, E. V.; Shouklov, I. A.; Starikova, Z. A.; Hopf, H.; Kuhlein, K., Efficient synthesis of enantiomerically and diastereomerically pure [2.2]paracyclophane-based N,O-ligands. *European Journal of Organic Chemistry* **2003**, (3), 432.
[33] Briggs, D., *Surface analysis of polymers by XPS and static SIMS*. Cambridge University Press: 1998.
[34] Cheng, C. H.; Pearce, E. M., Polymers Containing Fluorinated Ketone Groups .3. Synthesis of Styrene-P-Vinyltrifluoroacetophenone Co-Polymers by Modification of Polystyrene and the Copolymerization of Monomers. *Journal of Polymer Science Part a-Polymer Chemistry* **1980,** 18, (6), 1883.

[35] Cullity, B. D.; Stock, S. R., *Elements of x-ray diffraction*. 3rd ed.; Prentice Hall: Upper Saddle River, NJ, 2001; p xviii.
[36] Isoda, S.; Tsuji, M.; Ohara, M.; Kawaguchi, A.; Katayama, K., Structural-Analysis of Beta-Form Poly(Para-Xylylene) Starting from a High-Resolution Image. *Polymer* **1983,** 24, (9), 1155.
[37] Senkevich, J. J.; Desu, S. B.; Simkovic, V., Temperature studies of optical birefringence and X-ray diffraction with poly(p-xylylene), poly(chloro-p-xylylene) and poly(tetrafluoro-p-xylylene) CVD thin films. *Polymer* **2000,** 41, (7), 2379.
[38] Elkasabi, Y.; Chen, H. Y.; Lahann, J., Multipotent polymer coatings based on chemical vapor deposition copolymerization. *Advanced Materials* **2006,** 18, (12), 1521.

CHAPTER 3

PROTEIN- AND CELL- RESISTANT SURFACE COATINGS

Surfaces resistant to protein adsorption are very desirable for a variety of applications in biomedical engineering and bio-nanotechnology, since protein adsorption is often the first step in a cascade of events leading to systems failure. Initial efforts to create adsorption-resistant surfaces succeeded in reducing the adsorption by 80% compared to untreated surfaces to 100 ng/cm^2 by employing poly(ethylene glycol) coatings.[1] Recently, optimization of brush density and morphology has reduced adsorption to 1 ng/cm^2 or less.[2] These coverages, equal to about one tenth of a percent of a monolayer, represent the detection limit for several measurement techniques, including SPR[2,3] and radiolabeling.[4] Among the numerous strategies developed for preventing non-specific protein adsorption,[5-7] surfaces with PEO or PEO-like structures are often discussed as promising candidates for inhibition of non-specific protein adsorption. Intensive research has thus been focused on the immobilization of such molecules onto surfaces; many methods such as graft polymerization by using plasma treatment,[8] UV/ozone treatment,[9] silanization;[10] or the use of self-assembly monolayers, pre-adsorbed detergents,[11] proteins,[12] and polyelectrolytes[13] have ever since been reported.

In this chapter, we introduce a simple method for protein-resistant modification within microfluidic channels based on vapor deposition of a photodefinable *coating* (PPX-CO-Ph)[14] on the luminal surface of a microfluidic device followed by a photopatterning step. Based on this method, spatially controlled confinement of non-fouling molecules, specifically polyethylene oxides (PEOs), and the selective adsorption of proteins including albumin and fibrinogen within microchannels are demonstrated. Although the focus of this work is on devices made of

polydimethylsiloxane (PDMS), this surface patterning technique can be similarly applied to microfluidic systems fabricated from glass, quartz, metal, or other polymers. On the other hand, an alternative technique *via* vapor-based polymer coatings were used as platforms, and surface-initiated ATRP was applied to prepare poly(ethylene glycol) methyl ether methacrylate (PEGMA) subsequently, resulting in non-fouling surfaces that inhibit protein adsorption and cell adhesion. Kinesin motor proteins and fibrinogen were used as model to study the protein interactions on the according surfaces, while murine fibroblasts (NIH3T3 cells) were used for the cell adhesion study.

3.1 Protein-Resistant Modification via Photoimmobolization on Microfluidic Devices

The materials in this section are adapted from previously reported data in "Fabrication of Discontinuous Surface Patterns within Microfluidic Channels Using Photodefinable Vapor-Based Polymer Coatings, *Analytical Chemistry* (2005)", by H.-Y. Chen, J. Lahann.; and have been slightly modified.

Microfluidic systems are widely used for the separation, detection, and analysis of biochemical reagents.[15] Their miniaturized architecture offers several advantages, such as higher sample throughput and processing rates, low manufacturing costs, advanced system integration, and reduced volumes of samples and analytes.[16,17] The continuously increasing complexity of microfluidic systems will require the development of methods for the precise and stable fabrication of functional surfaces and controlled spatial surface patterns.[8,10,13] Currently employed methods for patterning the luminal surface of microfluidic systems include microfluidic patterning,[18] laminar flow patterning,[2,19,20] robotic spotting[21-23] and jet printing,[24,25] photolithography,[26-30] microcontact printing,[31] and selective plasma etching.[32] Although these methods have been used to pattern cells,[31,33] proteins,[20] and hydrogels[26,30,34] within microfluidic systems, they often are associated with several shortcomings. For instance, patterns generated by laminar flow patterning and microfluidic patterning are limited to a relatively narrow range of continuous patterns, which are mainly determined by the flow

geometry. Photolithography, on the other hand, has mainly been used for the fabrication of three-dimensional elements, because it typically changes both, the surface properties and the device topology.[26,30,34] Microcontact printing, spotting, jetting, and selective plasma etching has to be done prior to device assembly and cannot be applied to previously assembled devices. These pitfalls fuel a great need for generically applicable surface engineering techniques that enable the fabrication of discontinuous features in both, previously assembled and non-assembled devices. In this section, we introduce a surface modification method for the fabrication of discontinuous surface patterns within microfluidic systems. The method is based on chemical vapor deposition (CVD) of a photodefinable coating, poly[4-benzoyl-*p*-xylylene-co-*p*-xylylene], onto the luminal surface of a microfluidic device followed by a photopatterning step to initiate spatially controlled surface binding. During photopatterning, light-reactive groups of the CVD polymer spontaneously react with molecules adjunct to the surface, such as polyethylene oxide. We demonstrate the potential of these reactive polymers for surface modification by preventing non-specific protein adsorption on different substrates including silicon and polydimethylsiloxane as measured by fluorescence microscopy. More importantly, three-dimensional patterns have successfully been created within polymer-based microfluidic channels; establishing spatially controlled, bioinert surfaces. The herein reported surface modification method addresses a challenge with respect to surface engineering of microfluidic devices, namely the fabrication of discontinuous patterns within microchannels.

3.1.1 Methods

Device fabrication. The microfluidic devices were designed using AutoCAD, and the design was printed on high-resolution emulsion transparencies. For fabrication of the master, a layer of photoresist (PR 1813, Hoechst Celanese) was spin-coated at 4000 rpm for 30 s onto a silicon wafer. The wafer was soft-baked at 90°C for 30 min and was then exposed to UV radiation (404.7 nm, 10 mJ/cm^2, 20 sec) to define the desired microstructure from the transparency mask. After removal of the activated photoresist

by developer solution (MF 319, Hoeschst Celanese) for 60 s, the wafer was hard-baked at 110°C for 30 min. The microstructured patterns were formed by deep reactive ion etching. The photoresist was then removed by treatment with a resist stripper (PRS 2000, JT Baker Inc.). The resulting silicon master was placed in a Petri dish and uniformly mixed PDMS prepolymer and curing agent (Sylgard 184, Dow Corning, MI) at a ratio of 10:1 were poured onto the master. The PDMS prepolymer was cured at 70°C for 1 hr. Finally, embossed microchannels were released from the silicon master. Dimensions of the microchannels were typically 50 μm deep and 300 μm wide, but varied in some cases as indicated.

CVD polymerization. 4-Benzoyl[2.2]paracyclophane was synthesized from commercially available [2.2]paracyclophane (Sigma-Aldrich, USA).[67] The starting material was sublimed under vacuum and was converted by pyrolysis into reactive species, which polymerize after condensation to the substrate. Sublimation temperatures were kept at 110-130°C, while pyrolysis temperatures were at 800°C. Subsequently, polymerization occurred on a rotating, cooled sample holder placed inside a stainless steel chamber with a wall temperature of 130°C. The use of a carrier gas was found to be benefical to the film quality and a constant argon flow of 20 sccm was used throughout the CVD polymerization. Under these conditions, the coating pressure was 0.5 mbar. X-ray photoelectron spectroscopy (Perkin Elmer/PHI 5400) and FTIR spectroscopy (Nicolet 6700) were used for characterization of the resulting polymer films. In addition to flat PDMS and PDMS microchannels, flat silicon and platinum-coated silicon were included in this study as reference samples as appropriate.

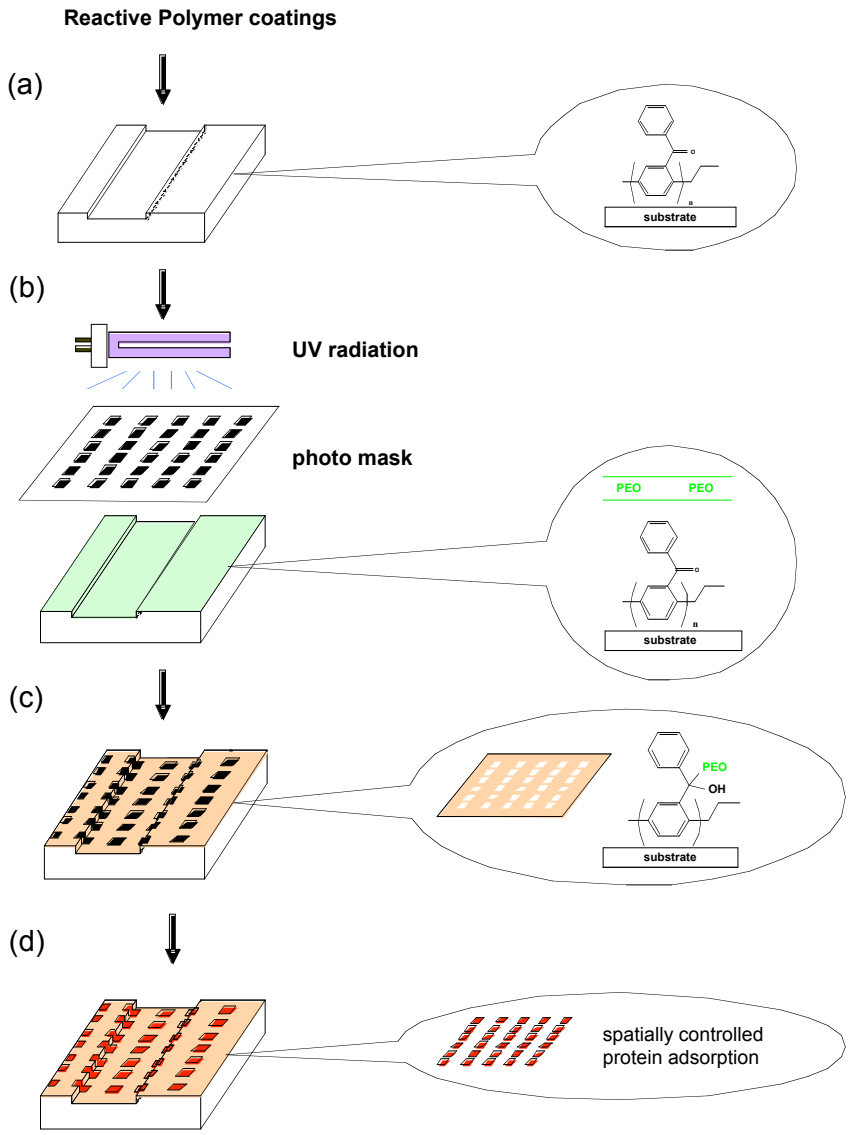

Figure 3.1: Spatially controlled protein adsorption via photopatterning of *reactive coatings* deposited within microchannels. (a) *Reactive coatings* are deposited via CVD polymerization. (b) Photopatterning is conducted using a photomask. (c) After rinsing, PEO is selectively immobilized to areas that were exposed to UV radiation. (d) The entire surface is incubated with protein solutions, but proteins preferentially adsorb to non-modified areas.

TABLE 3.1
CHEMICAL COMPOSITION OF PPX-CO-Ph COATING AS DETERMINED BY XPS

	C-C	C-C=O	C=O	π-π*
BE [eV]	285.0	285.9	286.1	291.5
calcd (%)	87.1	8.6	4.3	-
found (%)	83.3	8.3	4.2	4.2

Photoimmobilization. After surface modification via CVD polymerization, the coated substrates were immersed into the aqueous solutions of selected polyethylene oxides (Figure 3.1). Both hydroxy-terminated, star-PEO (4-arm PEO, 10,000 g/mol, 3 weight-%, Aldrich, WI) and methoxy-terminated, linear PEO (10,000 g/mol, 10 weight-%, Aldrich, WI) were used for comparison. To generate patterns, a photomask was brought in close proximity to the outside surface of the device (the microchannel was 50 μm deep). Samples were then exposed to broad-range UV radiation (Blak-Ray B 100 AP, UVP Inc., CA) of about 320 nm wavelength for 30 min. DI-water was used to rinse off excess PEO. For protein adsorption studies, samples were incubated with protein solutions for 5 min. Alexa Fluor 546-conjugated fibrinogen (Molecular Probes, OR) and rhodamine-conjugated bovine serum albumin (BSA, Molecular Probes, OR) were used at a concentration of 30μg/ml. After incubation, phosphate buffered saline (PBS, pH 7.4, Sigma, MO) and DI-water were used to rinse off loosely adsorbed proteins. Images were captured by fluorescence microscopy (Nikon TE200).

3.1.2 Results and Discussions

A conformal film of PPX-CO-Ph was deposited onto the surfaces of the substrate using CVD polymerization. The reaction leading to the polymer coating followed the previously established mechanism shown in Figure 3.2. The chemical structure of the resulting polymer coatings was verified by grazing-angle FTIR spectroscopy and XPS

spectroscopy. The FTIR spectrum (Figure 3.4) is in accordance with previous findings and reveals characteristic bands of the carbonyl stretches at 1612 and 1665 cm^{-1}. In addition, the spectrum shows characteristic signals at 2962 and 2906 cm^{-1} indicative of aliphatic methylene groups. X-ray photoelectron spectroscopy was used to confirm the results of the FTIR study. The XPS survey spectrum and the high-resolution spectra of oxygen and carbon indicate 95.5 atom-% carbon and 4.5 atom-% oxygen. These values compare well with the theoretical values of 95.8 atom-% for carbon and 4.2 atom-% for oxygen. As shown in Figure 3.3, the high-resolution C_{1s} spectrum further reveals characteristic signals for aliphatic and aromatic carbon (C-C, C-H) normalized to 285.0 eV, carbon in α-position to the carbonyl group (C-C=O) at 285.9 eV, carbonyl carbon (C=O) at 286.1 eV, and a signal indicating π->π* transitions at 291.5 eV. The latter is characteristic for aromatic molecules and has been previously reported for similar poly-*p*-xylylenes.[35] The high resolution O_{1s} spectrum is highly symmetric suggesting a single energy state for all oxygen atoms. The XPS data support the assumption that the synthesized CVD films are in accordance with the structure shown in Figure 3.2. Table 3.1 compares the experimental data obtained by XPS analysis of the PPX-CO-Ph coating with the theoretically obtained values. Undesirable side-reactions, such as decomposition of carbonyl groups, can be largely excluded for polymer films prepared following the conditions used herein for CVD polymerization. The preparation of well-defined interfaces is important for surface engineering applications, where CVD coatings form reactive interfaces for subsequent, often complex immobilization steps.

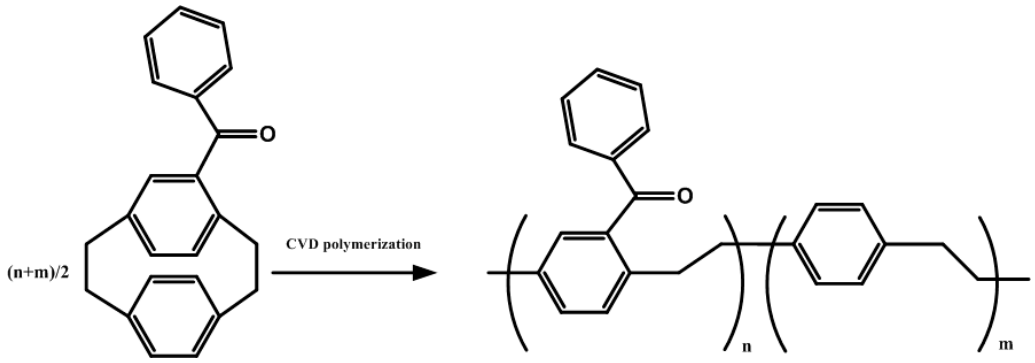

Figure 3.2: CVD polymerization of 4-benzoyl[2.2]paracyclophane. The resulting polymer film establishes a photodefinable coating that is used for further surface modification.

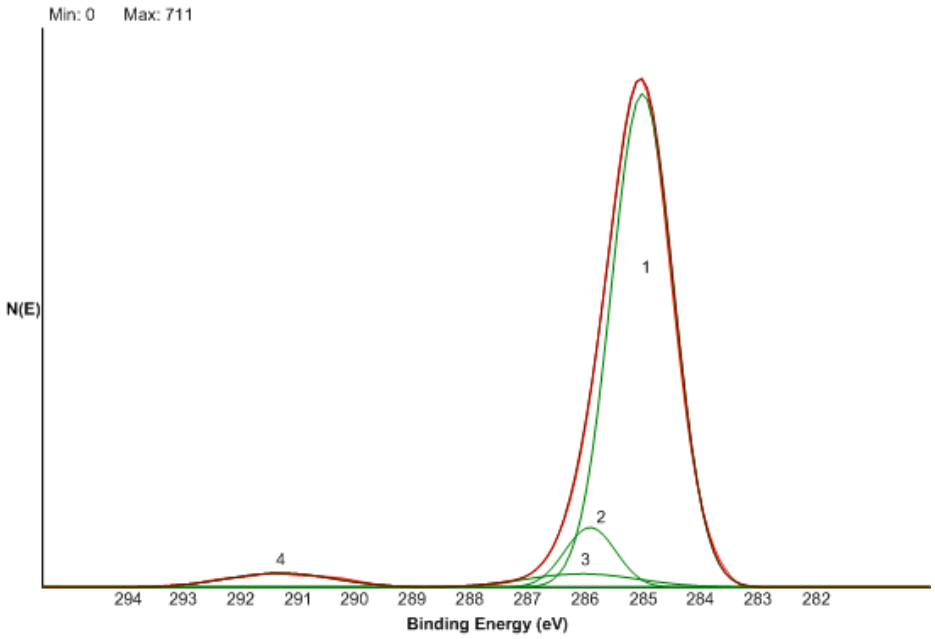

Figure 3.3: High-resolution XPS spectra of C_{1s} and O_{1s} (inlet) for the photodefinable *reactive coating*, PPX-CO-Ph. Individual signals can be assigned as follows: (1) 285.0 eV (C-H, C-C), (2) 285.9 eV (C-C=O), (3) 286.1 eV (C=O), (4) 291.5 eV (π->π* transitions).

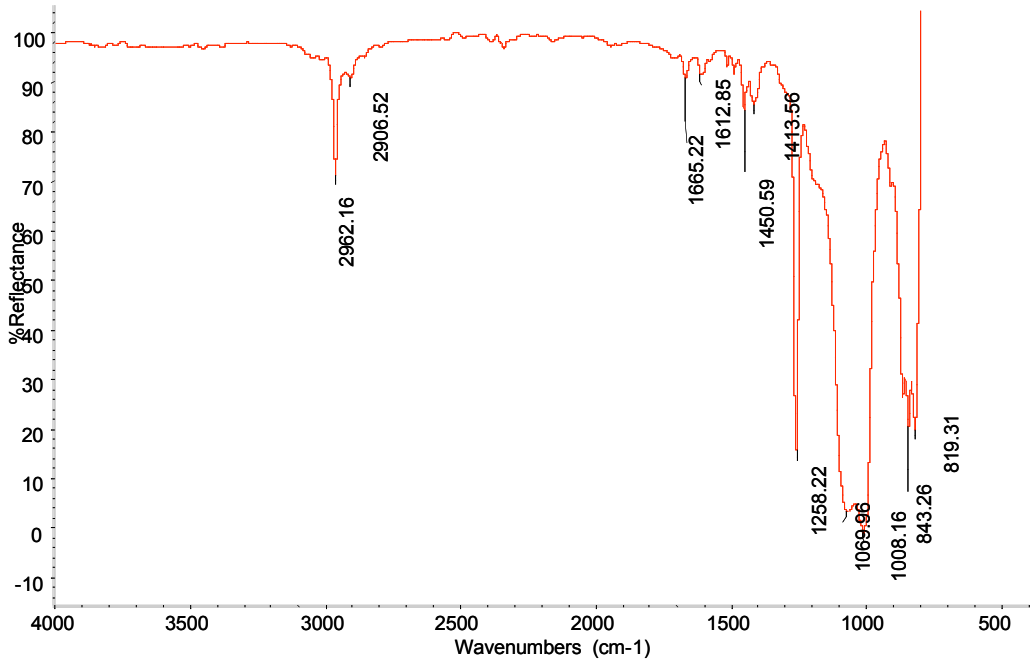

Figure 3.4: ATR-FTIR spectra of a PDMS substrate coated with PPX-COPh. The signals at 1612 and 1665 cm^{-1} indicate the presence of carbonyl stretches.

One of the major shortcomings of PDMS is its tendency to promote non-specific protein adsorption (bio-fouling), which is mainly due to the hydrophobicity of the PDMS. Several methods including graft polymerization,[36-38] plasma treatment,[8] UV/ozone treatment,[12] silanization,[10] adsorption of detergents,[11] proteins, and polyelectrolytes[13] have been used in the past to modify PDMS, but often show hydrophobic recovery and loss of protein-resistance with time. Among the numerous strategies developed for preventing non-specific protein adsorption,[5,6,39,40] surfaces with PEO or PEO-like structures are often discussed as promising candidates for inhibition of non-specific protein adsorption.[5] However, PEO is water-soluble and therefore requires covalent tethering to the PDMS to be effective. With the photoreactive coating technology in place, we now have a straightforward process for covalently tethering PEO polymers onto PDMS surfaces. More importantly, this process does not require any functional

groups on the PEO.

Prior to photopatterning, the luminal surface of the reactive coating is exposed to an aqueous solution of PEO. A photomask is then brought in close proximity to the luminal side of the microchannel and the CVD coating will be illuminated through the mask. The CVD film essentially acts as a reactive photoresist and binds the PEO molecules only in those areas exposed to the light. Due to its structural analogy to benzophenone, the reactive coating provides light-reactive carbonyl groups that are readily activated at wavelengths of about 340 nm. The temporarily generated free radicals spontaneously react with adjunct molecules, mainly via C-H abstraction.[41] Finally, the microchannel is rinsed with PBS buffer to remove non-bound PEO. The resulting microfluidic system is now ready for loading with proteins.

To verify the bioinert properties of the surfaces after covalent tethering of the PEO, we incubated the entire sample surface with fluorescence-labeled model proteins including fibrinogen and albumin. Fibrinogen was used as standard, because it is the prototype of a large protein (Molecular weight: M_W=340 kDa) with strong tendency to adsorb to artificial substrates.[39] Albumin was used because of its abundance in human blood and its strong adhesion tendency (Albumin is routinely used in bioassays to pre-coat consumables). In our study, both, albumin and fibrinogen selectively adsorbed only to areas that corresponded to non-modified surfaces, while areas that were modified with PEO showed very low levels of protein adsorption, as concluded based on the fluorescence micrographs. Figure 3.5 compares different substrate materials coated with PPX-CO-Ph and modified via photopatterning of PEO: Figure 3.5(a) is a fluorescence micrograph of a photo-patterned, bioinert surface after incubation with Alexa Fluor 546-conjugated fibrinogen. Figure 3.5(b) shows an image of a photo-patterned, bioinert surface after incubation with rhodamine-conjugated albumin. In both cases, *reactive coatings* were deposited onto a silicon substrate prior to photoimmobilization of PEO. Figure 3.5(c) shows the photo-patterned, bioinert surface on a PDMS substrate (Alexa Fluor 546-conjugated fibrinogen was used in this experiment). Independent of the substrate, all micrographs reveal the selective adsorption of the proteins to the non-modified surface areas. In our preliminary studies, no

fundamental differences are found for linear PEO and star-PEO. However, further studies are warranted to address this question in details. The photomask used in these experiments has 50 microns features. Nevertheless, it is important to realize, that surface features are not limited to this size range and can be made even smaller if required. On flat substrates, we fabricated hydrogel features as small as 2 microns in the past.[32] With the ability of the technique to fabricate protein-resistant surfaces on flat substrates demonstrated, we than shifted our focus to the spatially controlled modification of the luminal surface of PDMS microchannels.

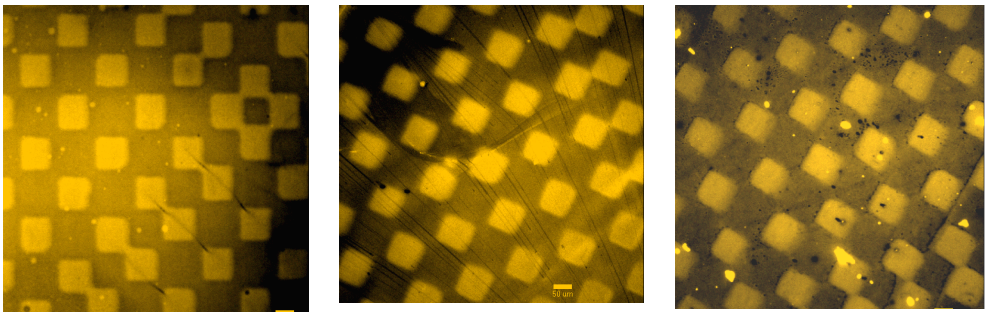

(a) (b) (c)

Figure 3.5: Spatially controlled bioinert surfaces after incubation with model proteins: (a) fibrinogen adsorbed onto CVD/PEO-modified silicon substrate (Linear PEO was used in this example.); (b) bovine serum albumin adsorbed onto CVD/PEO-modified silicon substrate (Star-PEO was used in this example.); (c) fibrinogen adsorbed onto CVD/PEO-modified PDMS substrate (Star-PEO was used in this example.).

The transition from flat substrates to three dimensional microchannels did not require major changes in the protocol. As with the flat PDMS, the microchannel were first coated with the photoreactive coating via CVD polymerization followed by the incubation with an aqueous solution of PEO. For this purpose, the PEO solution was filled into the microchannel and the photomask was placed on bottom side facing the luminal surface of the microchannel. After UV exposure for 30 min, the non-bound PEO was removed and the entire microchannel was incubated with protein solution. Figure 3.6 shows fluorescence micrographs of a microchannel consisting of deep and

shallow areas that was incubated with fluorescence-labeled fibrinogen. Figure 3.6(a) is focused on the shallow part of the microchannel, while Figure 3.6(b) shows the pattern on the deep surface of the microchannel. In both cases, fibrinogen adsorption preferentially occurs on the areas that are not light-activated and thereby modified with PEO. Because fibrinogen is adsorbed only to the PEO-free squares, discontinuous protein pattern can be created within the microchannel. Although the pattern is clearly observable, the features are less sharp on the deeper luminal surface than on the shallow surface. The reduced contrast for the deeper channels is a result of the wider distance of the surface from the mask.

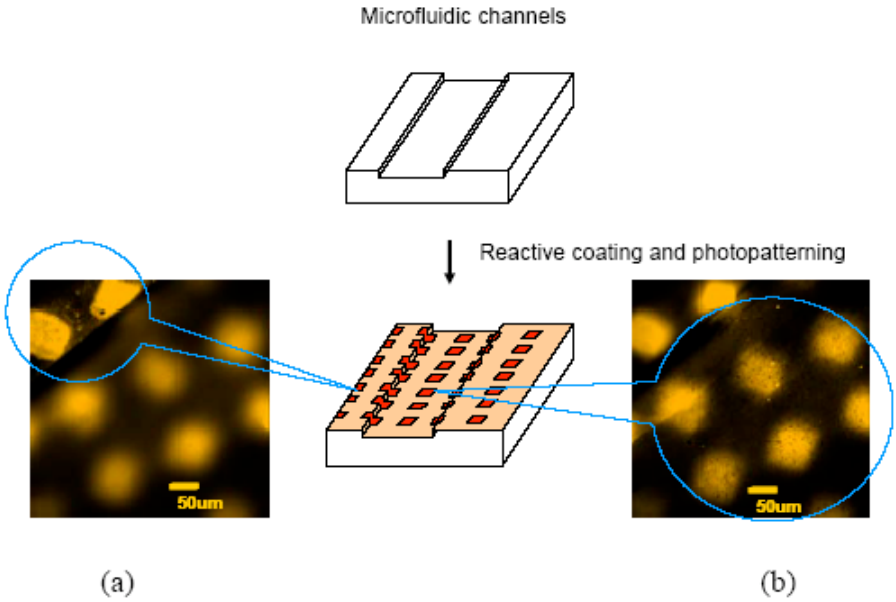

Figure 3.6: Spatially controlled, bioinert coatings created on the luminal surface of a PDMS-based microfluidic channel. Images show shallow (a) and deep (b) parts of the microchannel.

3.2 Ultra-Low Protein Coverages on CVD Modified Surfaces

The materials in this section are adapted from previously reported data in "Quantitative analysis of ultra-low protein coverages on protein-resisting surfaces using surface-bound kinesin motor proteins, *Advanced Materials* (2007) accepted, in press", by

P. Katira, A. Agarwal, T. Fischer, H.-Y. Chen, X. Jiang, J. Lahann, H. Hess; and have been slightly modified.

Non-fouling surfaces are a critical part of hybrid nanodevices, which utilize precisely positioned biomolecules in an artificial environment.[42] For example, controlled adsorption of kinesin,[43-49] myosin[50-52] and F1-ATPase motors[53] has been utilized for the design of molecular shuttles and nanopropellers. Adsorption of motor proteins outside the intended regions at densities down to one motor per square micrometer (0.01 ng/cm^2) can lead to loss of device function, since individual motors can already bind and transport the associated filaments outside their intended tracks.

The binding of associated filaments, such as microtubules or actin filaments, is readily observed by fluorescence microscopy, since these filaments are composed of thousands of protein subunits and carry typically at least a thousand covalently linked fluorophores.[54,55] Howard et al. demonstrated in 1989 that observing the attachment of microtubules from solution to surface-adhered kinesin motors enables the determination of motor densities as low as 2 proteins per μm^2 by measuring the rate of microtubule attachment.[56,57] Attachment rate measurements have subsequently been adapted to the determination of relative kinesin motor activity on different surfaces[45] and to the evaluation of guiding structures for microtubule transport.[49,58] Since kinesins long tail domain evolved to efficiently connect to cargo, we hypothesize that it can serve as a particularly efficient probe for attachment points on the surface.[59,60]

Landing rate measurements enable the measurement of absolute coverages of functional kinesins in the range of 0.003 – 1 ng/cm^2, thus enabling to differentiate the performance of even the best nonfouling surfaces. While landing rate measurements in effect count individual proteins, their complexity is low compared to single molecule fluorescence measurements,[61,62] due to the availability of a kinesin/microtubule kit (Cytoskeleton Inc.) and the high brightness of fluorescent microtubules which can be imaged with a standard fluorescence microscope.

In the following, we demonstrate that the quantification of ultra-low kinesin coverages by landing rate measurements is a valuable tool in determining the

performance of coatings (Figure 3.7) with outstanding resistance to protein adsorption. Specifically, we will describe the adsorption model underlying the method, present experiments which demonstrate the determination of kinesin coverages on fouling and non-fouling surfaces, and discuss the advantages and limitations of the proposed method.

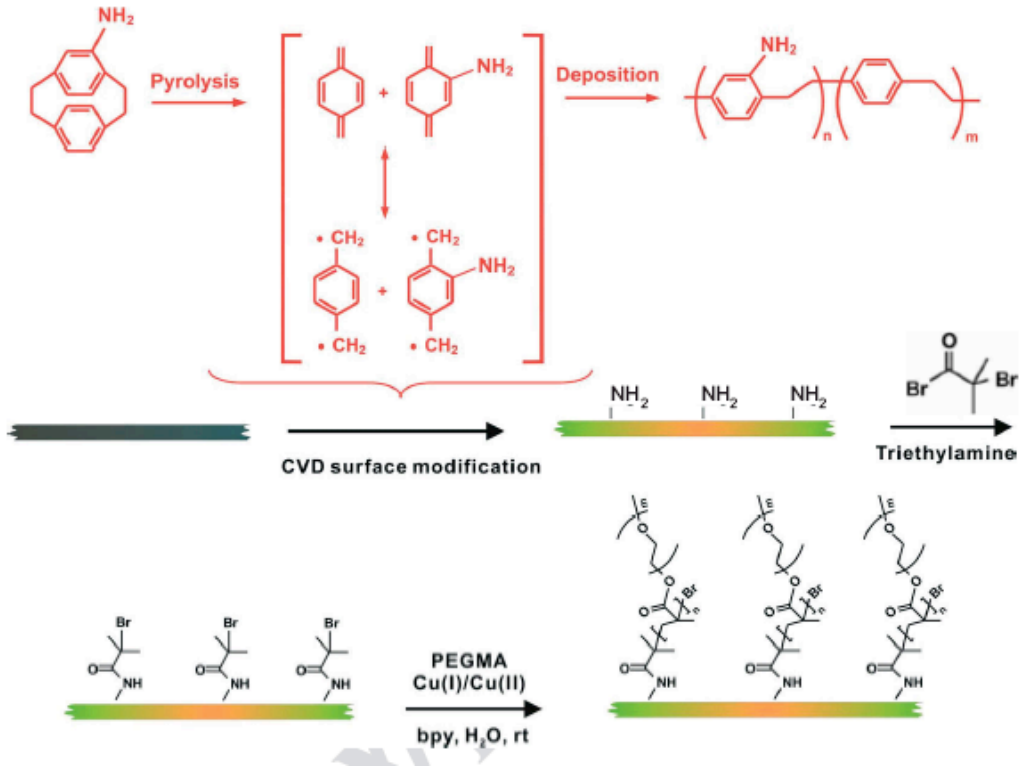

Figure 3.7: Schematic description of the process used to prepared PEGMA-modified glass slides consisting of (i) CVD polymerization, (ii) coupling of the initiator, and (iii) ATRP coating of PEGMA.

It is well-established that direct adsorption of kinesin to fouling (glass) and moderately non-fouling (Pluronic F108 coating) surfaces leads to denaturation and loss of its microtubule-binding ability.[57,63] However, if the surface is covered by either denatured kinesin motors or a blocking protein (e.g. albumin or casein) interstitial binding of kinesin tails to the surface results in high motor functionality. These observations are reproduced in our measurements (Figure 3.9h), which show that direct

absorption of kinesin to glass results in a non-linear increase of the landing rate as the amount of available kinesin is increased. In contrast, pre-coating of the glass, PU and Pluronic surfaces with casein results in an initially linear dependence of microtubule landing rate (Figure 3.10-left) and surface density of active motors (Figure 3.10-right) on the amount of available kinesin.

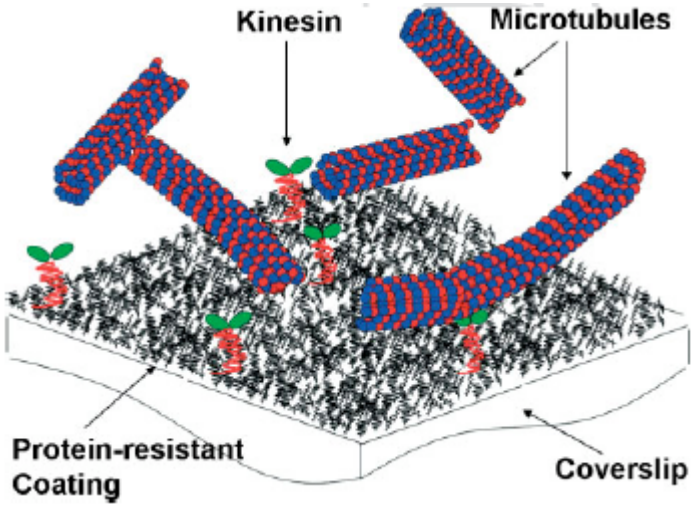

Figure 3.8: Sketch of principle: Adsorption of kinesin motor proteins to a non-fouling surface can be quantified by measuring initial microtubule landing rates. In the first step, kinesin from the solution scans the surface for 'defect sites' and adsorbs to a fraction of available sites. In the second step, the unbound motors in the solution are replaced by a microtubule solution containing AMP-PNP and the landing rate of microtubules on the surface is measured. This along with measurement of the average length of landed microtubules and measurement of the diffusion limited maximum landing rate on a fouling surface provides an estimate of the kinesin surface density of kinesin.

On these surfaces, the diffusion-limited landing rate is reached for moderate (20-fold) dilutions of the kinesin stock solution (Figure 3.9 & 3.10), whose concentration can be calculated as 175 nM (see Methods). This value was used to determine dosage values in Figures 3.10. In all subsequent experiments, the diffusion-limited landing rate Z for a

given microtubule preparation is assumed to be equal to the observed landing rate on a casein-coated glass surfaces exposed to a 17.5 nM kinesin solution (10-fold dilution of stock) for 5 min.

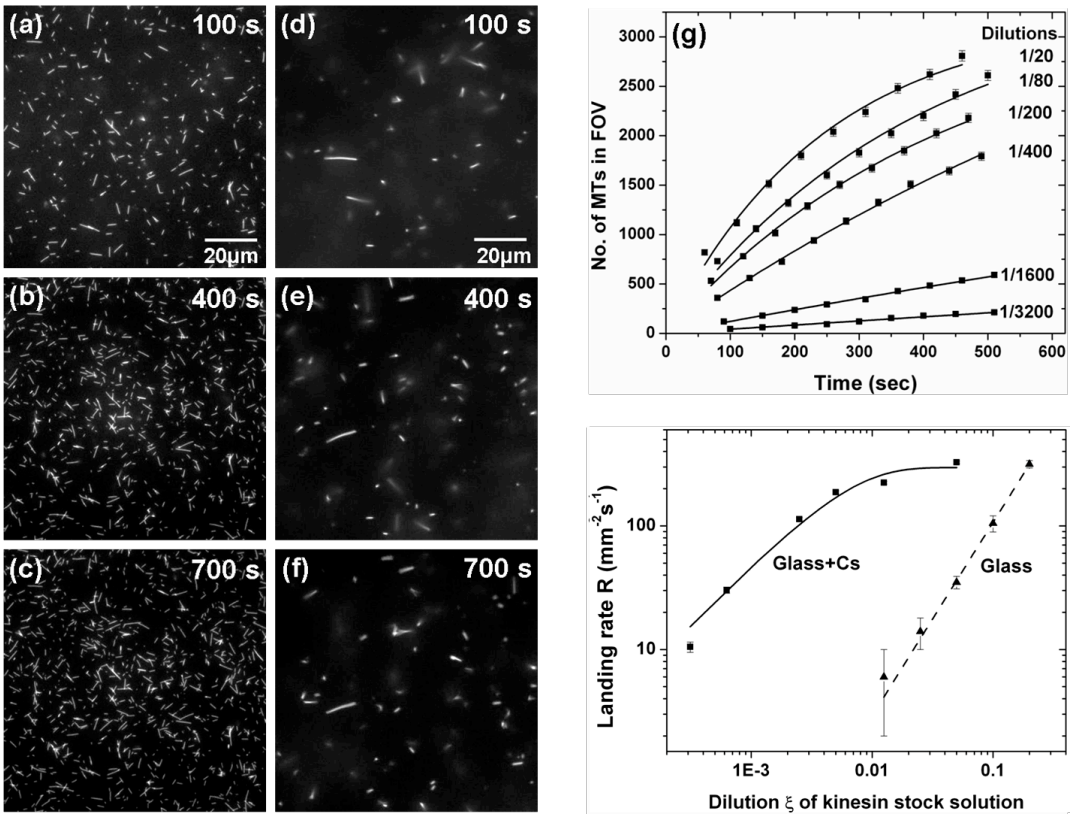

Figure 3.9: Measurement of kinesin surface densities from landing rates of microtubules. (a-c) Microtubules binding 100, 400, and 700 s after microtubule injection to a casein-coated glass surface exposed to kinesin solution twenty-fold diluted from stock (~ 9nM) for 5 min (d-f) Microtubules binding 100, 400, and 700 s after microtubule injection to a PEGMA surface exposed to kinesin solution twenty-fold diluted from stock (~ 9nM) for 5 min. The average length of microtubules for (a-c) is 1.71 ± 0.08μm and for (d-f) is 2.29 ± 0.11μm. The field of view (FOV) was 200 μm x 200 μm but (a-f) are cropped for clarity. (g) The number of microtubules attached to the surface as function of time for the casein-coated glass exposed to kinesin solutions diluted from the stock solution.(h) Landing rates R computed from the data shown in (g) and plotted against the concentration of the kinesin solution for casein-coated glass surfaces (squares) and bare glass surfaces (triangles).

Since physisorbed Pluronic F-108 reduces protein adsorption by ~80%,[64] we interpret the observed four-fold lower density of microtubule-binding motors as a reflection of the reduced adsorption of casein. Kinesin contact to the bare surface will always lead to denaturation, whereas kinesin contact to adsorbed casein will result in a functional motor. Similarly, the density of active motors is 40% lower on PU surfaces compared to glass surfaces at equal kinesin dosages.

With the fundamental principle of the kinesin/microtubule based assay established, we shifted our focus to two types of highly non-fouling surfaces, $(EG)_3OH$-terminated SAMs and polyethylene glycol methacrylate (PEGMA) coated surfaces. To prepare protein-resistant PEGMA coatings, we first introduced functional groups onto the substrates using chemical vapor deposition (CVD) polymerization of 4-amino-[2.2]paracyclophane. CVD polymerization is a vapor-based coating approach that can be used to modify a wide range of different substrate materials and geometries with a series of different chemical groups.[14,65-67] In this case, 50 nm thick films of poly(4-amino-*p*-xylylene-*co*-*p*-xylylene) were CVD deposited on glass substrates to provide free amino groups for further surface modification. The amino-functionalized coating was then reacted with 2-bromoisobutyryl bromide. In the final step, bromoisopropyl groups were used as initiators for surface-initiated atom transfer radical polymerization (ATRP) of poly(ethylene glycol) methyl ether methacrylate (PEGMA). Direct adsorption of kinesin to these surfaces led to low landing rates, which did not increase with increasing kinesin concentration in solution (Figure 3.10). Precoating PEG-SAM surfaces with casein followed by exposure to 17.5 nM of kinesin for 5 min reduced the observed microtubule landing rate from ~ 31 $mm^{-2}s^{-1}$ to ~ 2 $mm^{-2}s^{-1}$, corresponding to a 15-fold reduction in kinesin surface density.

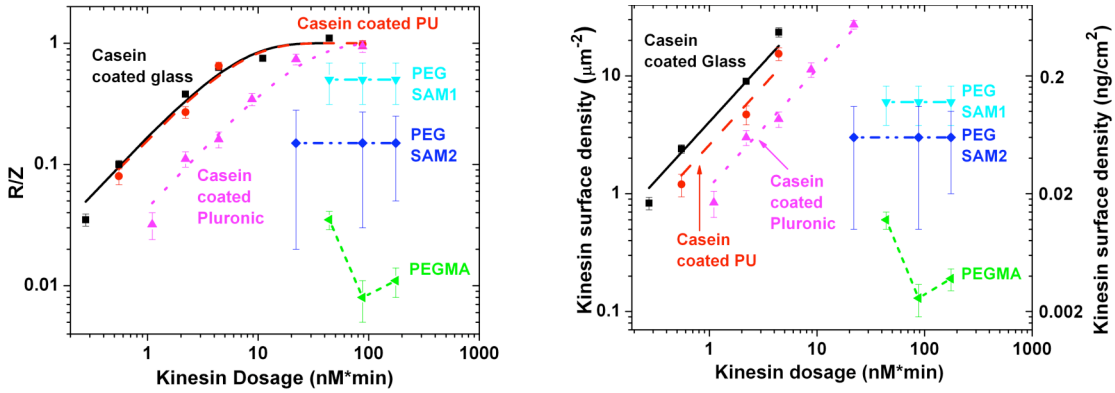

Figure 3.10: Left - The ratio of measured landing rate R to the diffusion-limited landing rate Z as a function of the kinesin dosage for different surfaces. Right - The kinesin surface density as a function of kinesin dosage calculated from the ratio R/Z and the average microtubule length.

Our interpretation of these observations is that the highly non-fouling surface helps conserve kinesin motor function after adsorption, and that casein acts as a competitor for a very limited number of adsorption sites. Furthermore, since the surface density of adsorbed kinesin does not linearly increase with kinesin dosage, the residual kinesin adsorption is not a consequence of kinesins slowly penetrating the coating.[68] Instead, the surface density of adsorbed kinesins is equal to the density of defects in the coating.

$(EG)_3OH$-terminated SAMs, a widely studied model system,[19,69,70] adsorbed an average of 4.5 ± 2.35 μm^{-2} (0.09 ± 0.05 ng/cm^2). This average is derived from two sets of identical surfaces prepared on different days (SAM1, SAM2, and SAM3). In comparison, the values measured using SPR for the adsorption of fibrinogen at hundred- to thousand-fold higher dosages are 0.35 ± 1.75 ng/cm^2 (1 mg/ml adsorbed for 3 min)[71] and 2.8 ± 1.05 ng/cm^2 (1 mg/ml adsorbed for 30 min).[72]

PEGMA surfaces had exceptionally low landing rates as can be seen in Figure 3.9(d-f). The average motor density on these surfaces is 0.16 ± 0.02 μm^{-2} (0.0064 ±

0.0008 ng/cm^2). These data suggest that PEGMA surfaces represent a significant improvement over $(EG)_3OH$-terminated SAM surfaces.

3.3 Protein- and Cell- Resistant Surface Modification by Using Vapor-Based Initiator Coating

The materials in this section are adapted from previously reported data in "Vapor-based initiator coatings for atom transfer radical polymerization, *Advanced Functional Materials* (2007) accepted, in press", by X. Jiang, H.-Y. Chen, G. Galvan, M. Yoshida, J. Lahann; and have been slightly modified.

Based on the chemical vapor deposition of [2.2]paracyclophane-4-methyl 2-bromoisobutyrate, we prepared a novel polymeric initiator coating for surface modification *via* ATRP. This widely applicable approach has been applied to a heterogeneous group of substrates including stainless steel, glass, silicon, poly(dimethylsiloxane), poly(methylmethacrylate), poly(tetratfluoroethylene), and polystyrene. Detailed surface analysis using X-ray photoelectron spectroscopy and Fourier-transformed infrared spectroscopy confirmed the chemical structure of the reactive initiator coatings to be consistent with poly(*p*-xylylene-4-methyl-2-bromoiso-butyrate-*co*-*p*-xylylene). Appropriate reactivity of the bromoisobutyrate side groups was confirmed by surface initiated atom transfer radical polymerization of a oligo(ethylene glycol) methyl ether methacrylate. After solventless deposition of the CVD-based initiator coating, hydrogel films as thick as 300 nm could be conveniently prepared within a 24 hrs timeframe *via* ATRP (Figure 3.11). Moreover, the polymerization showed ATRP-specific reaction kinetics and catalyst concentration dependencies. In addition, spatially controlled deposition of the initiator coatings using vapor-assisted micorstructuring in replica structures resulted in fabrication of spatially confined hydrogel microstructures. Both protein adsorption and cell adhesion was significantly inhibited on areas that were modified by surface-initiated ATRP. The herein described initiator coatings provide a convenient access route to controlled radical polymerization

on a wide range of different materials. While demonstrated only for a representative group of substrate materials including polymers, metals, and semiconductors, this method can be expected to be generically applicable - thereby eliminating the need for cumbersome modification protocols, which so far had to be established for each substrate material independently.

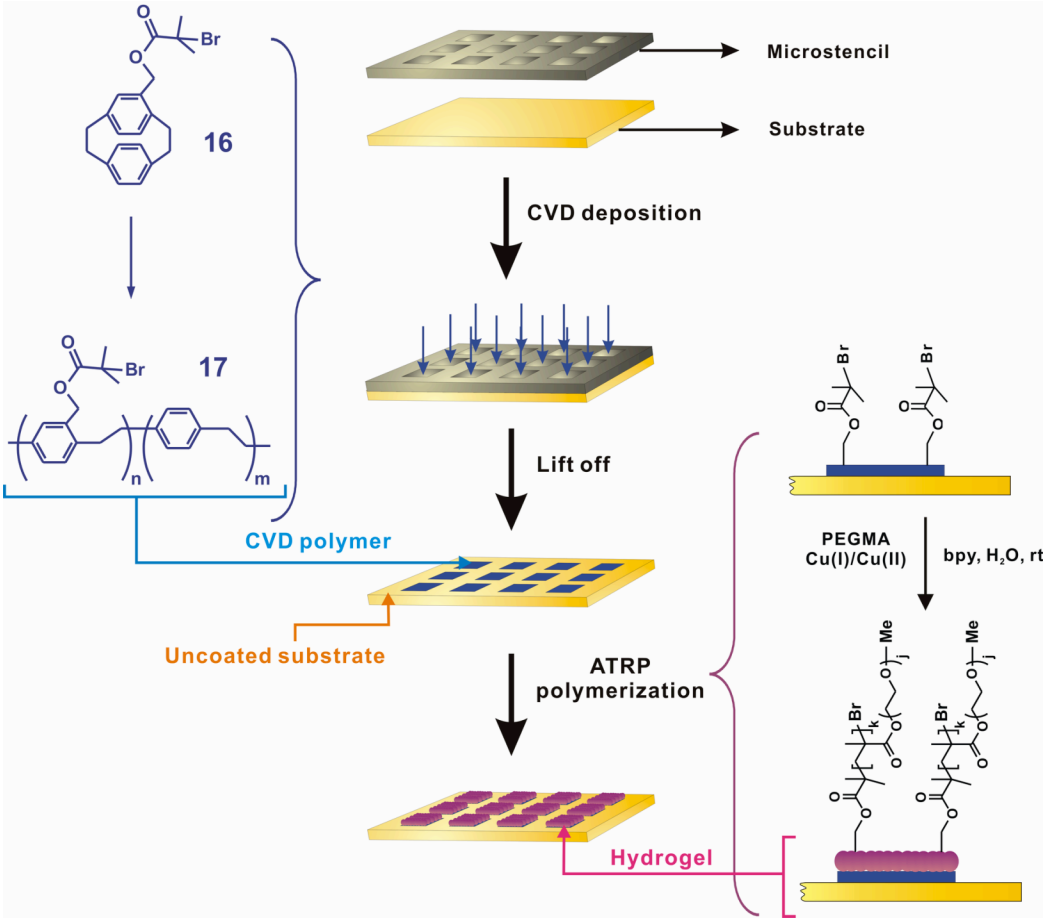

Figure 3.11: CVD polymerization approach to prepare the vapor-based initiator coating **17** for poly(OEGMA) modification *via* ATRP. A microstencil is used during CVD polymerization to direct the reactive initiator coating to defined surface areas only. Using surface-initiated ATRP, a poly(OEGMA) film is then selectively prepared at areas, where the initiator coating **17** has been previously deposited. The result is a microstuctured hydrogel surfaces with potential for protein or cell patterning.

3.3.1 Methods

Materials. Unless otherwise specified, all chemicals were obtained from Aldrich. [2.2]Paracyclopahne (PCS), Titanium (IV) chloride (99.9%), α,α-dichloromethyl methyl ether (98%), lithium aluminium hydride (Acros, 95%), 2-bromoisobutyryl bromide (98%), triethylamine (TEA, 99.5%), Cu(I)Br (99.999%), Cu(II)Br_2 (Fluka, 99%), anhydrous THF (EMD) were used as received. CH_2Cl_2 was distilled over calcium hydride. 2,2'-dipyridyl (bpy, 99%) was sublimed prior to use. Oligo(ethylene glycol) methyl ether methacrylate (OEGMA, average M_n: *ca.* 475) was passed through a 20 cm column of inhibitor remover and subsequently stored at -20 °C in the dark.

Preparation of [2.2]paracyclophane-4-methyl 2-bromoisobutyrate (16). Under nitrogen, Titanium (IV) chloride (9.0 mL, 82 mmol) was added dropwise over 20 min to an ice-cooled 1 L round bottom flask charged with anhydrous CH_2Cl_2 (400 mL) and [2.2]paracyclophane (10.0 g, 48 mmol). After the addition, the mixture was stirred for 20 min, followed by dropwise addition of α,α-dichloromethyl methyl ether (7.0 mL, 77 mmol). The reaction mixture was stirred at 0 °C for 90 min and was subsequently poured into ice water (300 mL). The organic layer was washed with 3M HCl (2 x 300 mL), water (2 x 300 mL), and saturated aqueous sodium bicarbonate (2 x 300 mL), and dried over Na_2SO_4. After filtration and removal of the solvent, the crude product was dissolved in anhydrous THF (100 mL). To this THF solution, LAH (3.7 g, 96 mmol) was carefully added and the mixture was stirred at room temperature for 36 hrs. The excess LAH was then decomposed by careful addition of ethyl acetate. The solution was then diluted by diethyl ether (200 mL), washed with 3 M HCl (3 x 200 mL) and water (2 x 200 mL), and dried over Na_2SO_4. The crude product was isolated and purified on silica gel using hexane/ethyl acetate (4/1) as eluent to yield 4-(hydroxymethyl)[2.2]paracyclophane as white crystals (8.1 g, 71%). Next, 4-(hydroxymethyl)[2.2]paracyclophane (5.0 g, 21 mmol) and 2-bromoisobutyryl bromide (5.2 mL, 42 mmol) were dissolved in anhydrous THF (100 mL) and cooled at 0 °C under nitrogen. To this stirred solution, TEA (14.6 mL, 105 mmol) was added dropwise over 30 min and the solution was stirred for two hours at 0 °C . The solution was then diluted with diethyl ether (200 mL), washed with 3 M HCl

(3 x 200 mL) and water (2 x 200 mL), and dried over Na_2SO_4. The isolated, crude product was purified on silica gel using hexane/ethyl acetate (85/15) to yield [2.2]paracyclophane-4-methyl 2-bromoisobutyrate as off-white crystals (7.0 g, 86%). ^{1}H NMR δ 6.64 (m, 1H), 6.50 (m, 4H), 6.40 (m, 2H), 5.15 (d, 1H), 4.96 (d, 1H), 3.35 (m, 1H), 3.07 (br m, 6H), 2.89 (m, 1H), 1.94 (d, 6H). ^{13}C NMR δ 171.63, 140.12, 139.50, 139.12, 138.06, 135.03, 133.94, 133.27, 133.15, 133.14, 132.88, 132.27, 129.40, 66.95, 55.78, 35.23, 34.97, 34.32, 32.84, 30.74, 30.72. IR: 3008 (w), 2926 (m), 2852 (m), 1730 (vs), 1269 (s), 1160 (s), 1104 (s). MS (m/z) 387.2 (M+1).

Polymerization of OEGMA from initiator coating (17). For kinetic studies, an aqueous solution of OEGMA (OEGMA/H_2O, 2:1, v:v), 2,2'-bipyridine (bpy), and $CuBr_2$ was stirred in a Schlenk flask at room temperature. The homogeneous solution was degassed using three freeze-pump-thaw cycles. Next, CuBr was added under nitrogen purge to the frozen solution and the molar ratio of CuBr/$CuBr_2$/bpy was set to be 1/0.3/2.5. The mixture was warmed up to room temperature and was stirred until a homogeneous dark brown solution was formed. The solution was then transferred into a nitrogen-purged glovebag, and split into 20 mL scintillation vials containing one CVD-coated substrate per vial. The polymerizations proceeded at room temperature for a set reaction time. Samples were analyzed in triplicate. To prepare samples for protein adsorption and cell adhesion studies, the CuBr concentration was 10 mM and polymerizations proceeded for three hours at room temperature.

Fabrication of Microstencils. Micropatterns were designed using AutoCAD, and the design was printed on high-resolution emulsion transparencies (40640 DPI, Photoplot Store). For fabrication of the master, a layer of photoresist (SU-8 100, MicroChem Co.) was spin-coated at 1000 rpm for 30 s onto a silicon wafer. The wafer was soft-baked at 65 °C for 30 min followed by 95 °C for 90 min, and then exposed to UV radiation (404.7 nm, 10 mJ/cm^2) for 4 min to define the desired microstructure from the transparency mask. Post-exposure bake was performed at 65 °C for 1 min followed by 95 °C for 20 min. After removal of the activated photoresist by exposing to a SU-8 developer solution (MicroChem Co.) for 20min with agitation, the resulting SU-8 master was cleaned with isopropyl alcohol (IPA). Uniformly mixed PDMS prepolymer and curing agent

(Sylgard 184, Dow Corning) were combined at a ratio of 10:1 and were spin-coated at 1200 rpm for 30 s onto the SU-8 master, and resulted in a 150 μm thick layer. The PDMS prepolymer was cured at 70 °C for 1 hr. Finally, a microstencil with embossed microgeometries was released from the SU-8 master. The fabricated PDMS microstencils were 150 μm high, and had square-shaped columns of 500 μm x 500 μm. The replicated PDMS microstencil was brought into intimate contact with the substrate and the sample was placed onto the sample holder located in the deposition chamber for further modification by CVD polymerization.

CVD Polymerization. Poly(*p*-xylylene-4-methyl-2-bromoisobutyrate-*co*-*p*-xylylene) (**17**) was prepared via CVD polymerization in a custom-made CVD polymerization system.[44] The starting material, [2.2]paracyclophane-4-methyl 2-bromoisobutyrate (**16**), was sublimed under vacuum and converted by pyrolysis into the corresponding quinodimethanes, which spontaneously polymerized upon condensation to the cooled substrate surface, which was maintained at 15 ^{o}C. Throughout CVD polymerization, a constant argon flow of 20 sccm and a working pressure of 0.5 mbar were maintained. The pyrolysis temperature was set to be 550 ^{o}C and sublimation temperatures were between 115-125 ^{o}C under these conditions. CVD Polymerization spontaneously occurred on samples placed on a rotating, cooled sample holder. In cases, where patterned substrates were required, the PDMS microstencils were sealed to the substrates during CVD polymerization.

Surface Analysis. X-ray photoelectron spectroscopy (XPS) data were recorded on an Axis Ultra X-ray photoelectron spectrometer (Kratos Analyticals, UK) equipped with a monochromatized Al Kα X-ray source. XPS spectra were recorded with an X-ray power of 150 kW. Pass energies were 160.0 eV and 20.0 eV for survey spectra and high-resolution elemental spectra, respectively. Surface morphology data were obtained with a Nanoscope IIIa scanning probe microscopy (Digital Instruments/Veeco, USA) using a JV type scanner (150 μm x 150 μm maximum scan size). NSC 16 cantilevers (MikroMasch, USA) with spring constants between 25 N/m and 60 N/m, and resonance frequencies of 150 - 170 kHz were used as AFM tips. Scanning size for the images shown herein was 5 μm x 5 μm at a scan rate of 0.8 Hz. Film thicknesses were measured

using a multi-wavelength rotating analyzer ellipsometer (M-44, J. A. Woollam) at an incident angle of 75°. The data were analyzed using WVASE32 software, and thickness determinations were performed on at least three spots that were at least 3 mm away from each other. Thickness measurements were recorded by fitting the ellipsometric psi and delta data with fixed An (1.46) and Bn (0.01) values using a Cauchy model and software module integrated with the system. For thickness imaging, data were recorded at an angle of incident of 65^{o} using an EP^{3}-SW imaging ellipsometer (Nanofilm Technologie GmbH, Germany) equipped with a 532 nm solid state laser operated at 15 mW. Measurements were performed by an imaging scanner with a lateral resolution of 1 μm at a field of view of about 100 μm x 500 μm. The images were captured using a CCD camera with a maximum resolution of 768 x 572 pixels. Infrared spectroscopy was performed using a Thermo/Nicolet 6700 spectrometer utilizing the grazing angle accessory (Smart SAGA) at a grazing angle of 85^{o}.

Protein Adsorption Studies. Alexa Fluor 546-conjugated fibrinogen (Molecular Probes Inc.) was used as model protein to study the fouling property of surface-modified substrates. Protein solutions were prepared at a concentration of 60 μg/ml according to manufacturer's manual. Samples were incubated with the protein solution for 10 min. After incubation, phosphate buffered saline (PBS) and DI-water were used to rinse off excess adsorbed proteins. The resulting samples were then examined by fluorescence microscopy (TE 200, Nikon).

Cell Adhesion Studies. Cryopreserved murine fibroblasts (NIH3T3) were purchased from ATCC (Manassas, VA) and cultured in DMEM containing 10% fetal calf serum (FCS). For cell adhesion, PMMA was used as the substrate. ATRP/poly(OEGMA) modified surfaces were rinsed in EtOH, dried, and coated with 25 mg/ml fibronectin for 20 min at 37°C. These surfaces were then rinsed with PBS, and briefly maintained in Dulbecco's Modified Eagle Medium (DMEM) (ATCC, Manassas, VA) FCS (Invitrogen, Carlsbad, CA) until cells were ready to be seeded. Cells were re-suspended in DMEM without FCS, and added to the wells containing the modified surfaces. They were then allowed to adhere onto the substrates for 2 hrs at 37°C in DMEM without serum, and analyzed by phase contrast microscopy. Alternatively, a sub-group of samples was

rinsed with DMEM after this initial 2h adhesion, and the media was exchanged to FCS-containing DMEM. The substrates were then incubated for additional 24 hrs and analyzed by phase contrast microscopy without washing.

3.3.2 Results and Discussions

Prior to CVD polymerization, synthesis of the starting material [2.2]paracyclophane-4-methyl 2-bromoisobutyrate (**16**) was established. Starting from the commercially available [2.2]paracyclophane (**18**), Rieche formylation with α,α-dichloromethyl methyl ether under the influence of titanium chloride and subsequent reduction with lithium aluminum hydride resulted in 4-hydroxymethyl[2.2]paracyclophane (**19**) with 71% yields (Figure 3.12). Compound **19** was converted into paracyclophane (**16**) by reaction with 2-bromoisobutyryl bromide under basic conditions. After careful purification, paracyclophane **16** was used as starting material for CVD polymerization. The overall yield of the three-step synthesis was 61 %.

Optimized CVD polymerization conditions included sublimation of paracyclophane **16** (100 mg, 0.26 mmol) at 115-125 ºC under reduced pressure (0.5 mbar) and subsequent transfer into the pyrolysis zone, which was maintained at 550 ºC. Deposition of the polymer onto the substrate occurred on a temperature-controlled sample holder at 15 ºC. Substrates were either homogenously coated or microstructured using a recently developed masking technology, which will be discussed in chapter 6 section 6.4. Under these conditions, deposition rate of the polymer coating was 1 Å/s, as determined by quartz crystal microbalance. Film thickness depended on the amount of starting material **16** used during CVD polymerization and was 50-70 nm under the conditions stated above. After CVD polymerization, the resulting polymer **17** was stable in aqueous solutions and certain non-halogenated organic solvents, such as ethanol, toluene and THF. To evaluate the adhesion properties of the initiator coating **17,** the scotch tape test[73] was performed on polymer coated samples including glass, silicon, quartz, PDMS, PMMA, polystyrene, and gold. On all substrates, the deposited polymer films showed excellent adhesion.

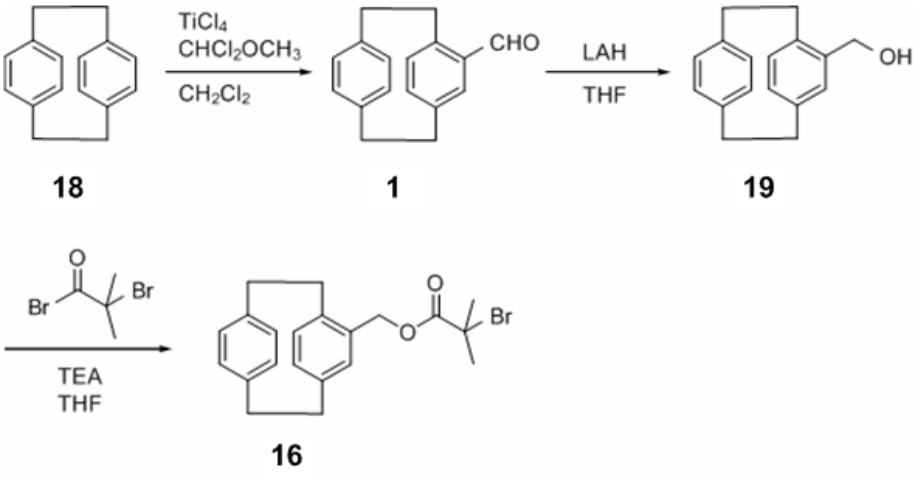

Figure 3.12: Synthetic route towards [2.2]paracyclophane-4-methyl 2-bromoisobutyrate (**16**).

Furthermore, reactive polymer coating **17** was studied using a combination of surface-sensitive methods, including XPS, grazing angle Fourier-transformed infrared reflection adsorption spectroscopy (IRRAS) and imaging ellipsometry. The XPS survey spectrum of polymer **17** is shown in Figure 3.13a and revealed C_{1s}, O_{1s}, and Br_{3p} signals (red curve). Quantitative composition data are summarized in Table 1. A typical initiator coating consisted of 87.5 atom-% of carbon, 9.8 atom-% of oxygen, and 2.7 atom-% of bromine. Within the margins of error of XPS, these values compare well with the theoretical values of 87.5 atom-% for carbon, 8.3 atom-% for oxygen, and 4.2 atom-% for bromine. As shown in Figure 3.13b, the high-resolution C_{1s} spectrum of polymer **17** provides further insight into the chemical composition of polymer **17**. The spectrum reveals a characteristic signal at 285.0 eV, which has an intensity of 82.8 atom-% and can be assigned to aliphatic and aromatic carbons (*C-C, C-H*). This signal compares well to the theoretical aliphatic and aromatic carbon concentration of 85.6 atom-%. Moreover, the C_{1s} spectrum shows characteristic signals for ether bonds (*C-O*) at 286.6 eV as well as ester bonds (*O-C=O*) at 287.0 eV (both 5.3 atom-%). Both signals are in good agreement with the expected theoretical values of 4.8 atom-% each, as summarized in Table 3.2. In addition, a characteristic signal at 289.2 eV with 4.5 atom-% can be assigned to

bromine-bound carbon (*C*-*Br*). This signal is in good agreement with the theoretically expected value of 4.8 atom-%. A smaller signal centered at 291.2 eV can be attributed to π-π^* shake-up signal characteristic of aromatic π electrons and has been previously reported for similar poly-*p*-xylylenes.[74]

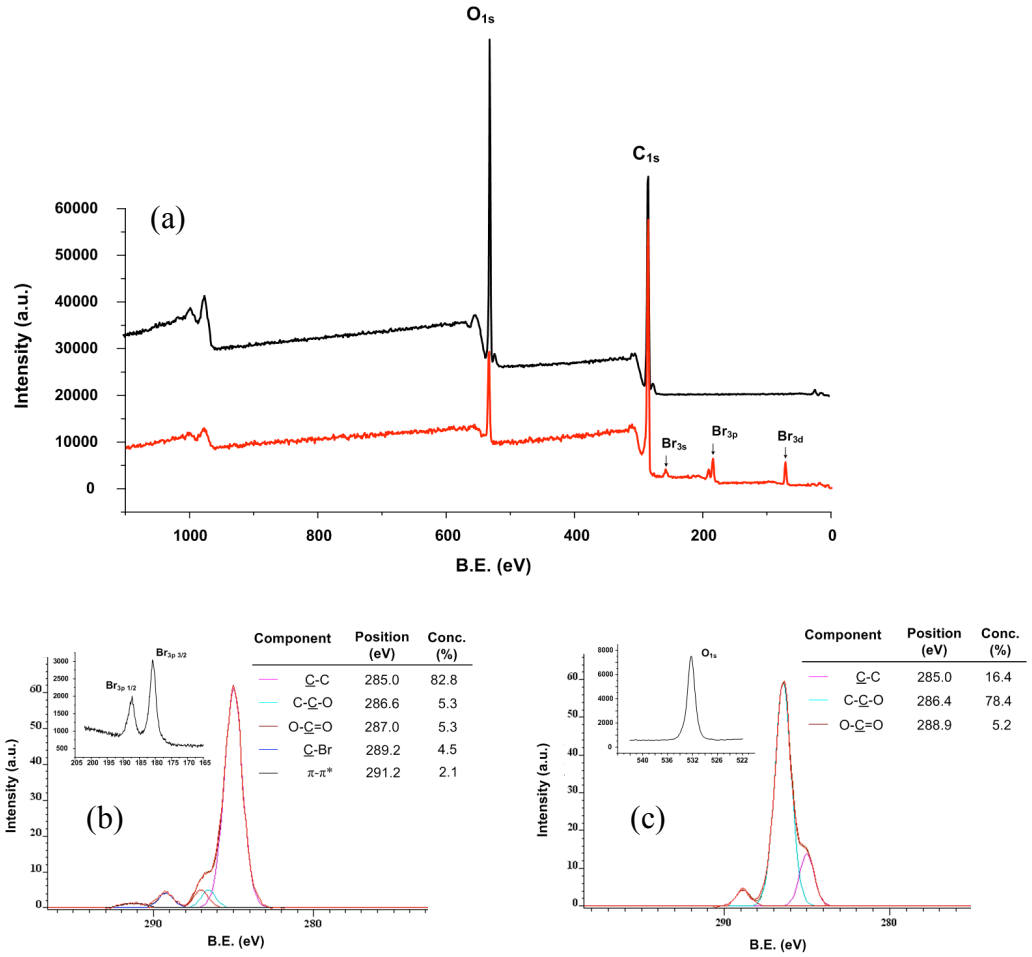

Figure 3.13: XPS analysis of a poly(*p*-xylylene-4-methyl-2-bromoisobutyrate-*co*-*p*-xylylene) film with a thickness of 25 nm as well as a 15 nm-thick poly(OEGMA) film grafted onto the initiator coating **17** via ATRP. (a) Survey spectra of poly(*p*-xylylene-4-methyl-2-bromoisobutyrate-*co*-*p*-xylylene) before (black line) and after (red line) ATRP reaction. (b) High-resolution XPS spectra of carbon and bromine recorded for coating **17**. (c) High-resolution XPS spectra of carbon and oxygen after ATRP of OEGMA from initiator coating **17**.

TABLE 3.2
XPS ANALYSIS OF POLY(*P*-XYLYLENE-4-METHYL-2-BROMOISOBUTYRATE-*CO*-*P*-XYLYLENE) BEFORE AND AFTER SURFACE-INITIATED ATRP OF OEGMA.

		C_{1s}	O_{1s}	Br_{3p}
Binding Energy (eV)		285.0	532.0	184.0
initiator coating **17**	calcd. (%)	87.5	8.3	4.2
	found (%)	87.5	9.8	2.7
poly(OEGMA) modified	calcd. (%)	67.7	32.3	-
	found (%)	69.5	30.5	-

The correct structure of CVD coating **17** was further confirmed by IRRAS. Figure 3.14(a) shows the FT-IR spectrum of reactive polymer coating **17** on a gold-coated silicon substrate. Characteristic functional groups of polymer **17** can be associated with absorption bands at 3004, 2934 and 2860 cm^{-1} due to *C-H* symmetric and asymmetric stretching bands, a strong, sharp band at 1730 cm^{-1} indicative of the *C=O* bond of the ester group, and a strong band at 1160 cm^{-1}, which is due to *C-O-C* stretches of the ester group.

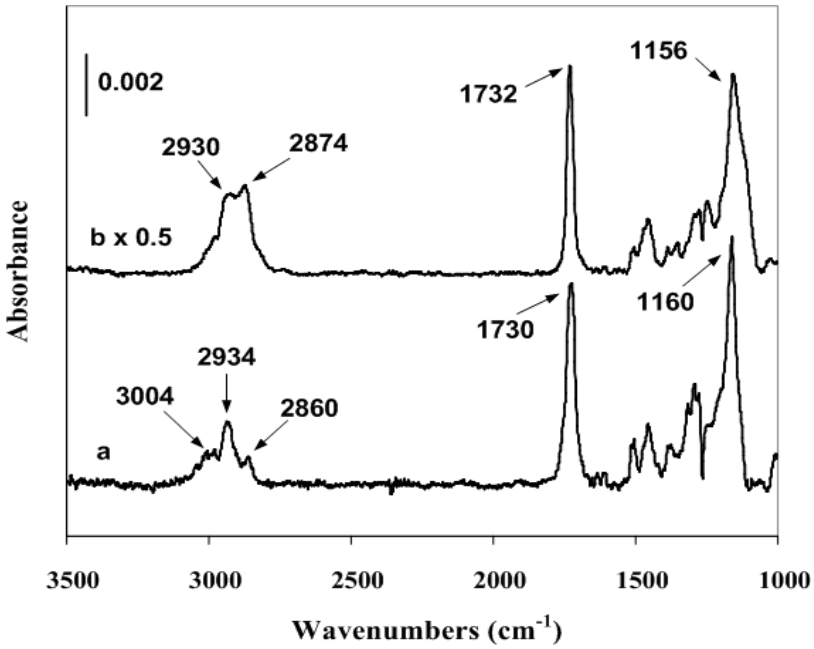

Figure 3.14: IRRAS spectra of poly(*p*-xylylene-4-methyl-2-bromoisobutyrate-*co*-*p*-xylylene) (**a**) deposited as a film with a thickness of 25 nm, and of a 15 nm-thick poly(OEGMA) film grafted onto the initiator coating **17** via surface-initiated ATRP (**b**).

Surface-initiated ATRP from the vapor-based initiator coating. After confirming the successful synthesis of poly(*p*-xylylene-4-methyl-2-bromoisobutyrate-*co*-*p*-xylylene), we conducted a series of experiments to assess the ability of these coatings to initiate ATRP. Gold substrates modified with the initiator coating **17** were incubated under inert conditions with aqueous solution of oligo(ethylene glycol) methyl ether methacrylate (OEGMA, average M_n *ca.* 475), which contained CuBr/$CuBr_2$/bpy as the catalyst. After ATRP, the polymer thickness of the poly(OEGMA) layer was ~15 nm, as determined by multiwavelength ellipsometry. Figure 3.14shows the FTIR spectra of the initiator coating **17** before (Figure 3.14a) and after ATRP (Figure 3.14b). After ATRP, the strong absorption bands at 2874 and 2930 cm^{-1} due to *C-H* stretching, a sharp band at 1732 cm^{-1} from *C=O* stretch in the ester group, and a strong band at 1156 cm^{-1} due to *C-O-C* stretch can be clearly resolved and indicate the presence of poly(OEGMA).

To further support these data, we also analyzed ATRP-modified surfaces by XPS and compared the data to the bare initiator coating **17**. Figure 3.13a (black curve) displays

XPS survey spectrum of a substrate after surface-initiated ATRP. As summarized in Table 3.2, chemical composition of 69.5 atom-% carbon and 30.5 atom-% oxygen was observed. These data correspond well with the theoretical composition of a poly(OEGMA) film with carbon and oxygen compositions of 67.7 atom-% and 32.3 atom-%, respectively. Accordingly, the oxygen/carbon ratio increased from 0.11 for coating **17** to 0.48 after ATRP polymerization, which compares well with the theoretically expected ratio of 0.44. The presence of bromine was no longer detected. Furthermore, high-resolution XPS spectral analysis of carbon is shown in Figure 3.13c and confirmed the presence of poly(OEGMA) as indicated by aliphatic (*C*-*C, C*-*H*), ether-bound (*C*-*O*), and ester-bound (*O*-*C*=*O*) carbon atoms corresponding to binding energies at 285.0 eV, 286.4 eV, and 288.9 eV, respectively. The aliphatic (*C*-*C, C*-*H*) component of 13.6 atom-% compared well with the theoretical value of 16.4 atom-%. A significant ether (*C*-*O*) component was detected (78.4 atom-%), which compared well with the theoretical value of 81.8 atom-%. In addition, characteristic ester (*O*-*C*=*O*) atoms were detected at 5.2 atom-%, which compares to a theoretical value of 4.6 atom-%.

Reaction kinetics of the surface-initiated ATRP of OEGMA using the vapor-based initiator coating. ATRP is often considered a controlled/living radical polymerization, because the irreversible termination reactions, such as radical coupling, are suppressed due to the very low free radical concentration.[75] As such, ATRP should follow a linear relationship between film thickness and polymerization time. However, irreversible chain termination reactions and loss of catalyst activity cannot be entirely excluded in reality. Baker, Bruening, and co-workers' study of kinetics of surface-initiated ATRP of methyl methacrylate and methyl acrylate with a Cu/tris[2-(dimethylamino)ethyl]amine catalyst system suggested that the controllability of a given surface-initiated ATRP is directly related to the catalyst concentration.[76] In our case, $CuBr/CuBr_2$/bpy was used as the catalyst system and the molar ratio was set to be 1/0.3/2.5. In order to assess if considerable film thicknesses and sufficient polymerization controllability can be achieved by surface-initiated ATRP from reactive coating **17**, a range of different catalyst concentrations was examined (Figure 3.15). As expected, lower catalyst concentrations lead to slower polymerization rates and increased process controllability. When a catalyst concentration of 5.0 mM was employed, the film

growth rate was relatively constant over a 26-h period, but only a ~15 nm thick film was generated after 26 hrs. In contrast, when a catalyst concentration of 15 mM was used, a more than 100 nm thick polymer film was formed within 5 hours. Under the same conditions, up to ~300 nm thick films were prepared, when surface-initiated ATRP was allowed to proceed for 24 hours. For a wide range of experimental conditions, surface-initiated ATRP of OEGMA from initiator coating **17** showed excellent controllability over a period of at least five hours and was in agreement with previously reported surface-initiated ARTP reactions in aqueous media.[77]

Spatial homogeneity of the polymer coatings was further studied using a combination of imaging ellipsometry and scanning probe microscopy. Figure 3.15 shows the ellipsometric image of a 350 x 650 μm^2 area of a polymer square that consists of a two layers: (i) a 66 nm thick layer of the initiator coating **17** and (ii) a 68 nm thick top layer of poly(OEGMA). The films were deposited on PMMA using vapor-assisted micropatterning in replica structures as described in the chapter 6 section 6.4. The image indicates homogeneous deposition throughout the coated area. Moreover, the deposited film shows sharp boundaries suggesting that patterns can be prepared with exquisite spatial control. Further AFM analysis of modified and unmodified surface areas suggests a substantial smoothening effect due to the deposited polymer films (Figure 3.16). In spite of the fact that the overall thickness of the polymer film was only 134 nm, the root mean square roughness, recorded in the dry state, decreased from initially 1.44 nm for PMMA (Figure 3.16a) to 0.64 nm after surface modification (Figure 3.16b). All values are recorded for a 5 x 5 μm^2 area. The significant decrease in surface roughness indicates that the surface modification not only changes the physico-chemical properties of the surface, but also have a leveling effect on surface roughness.

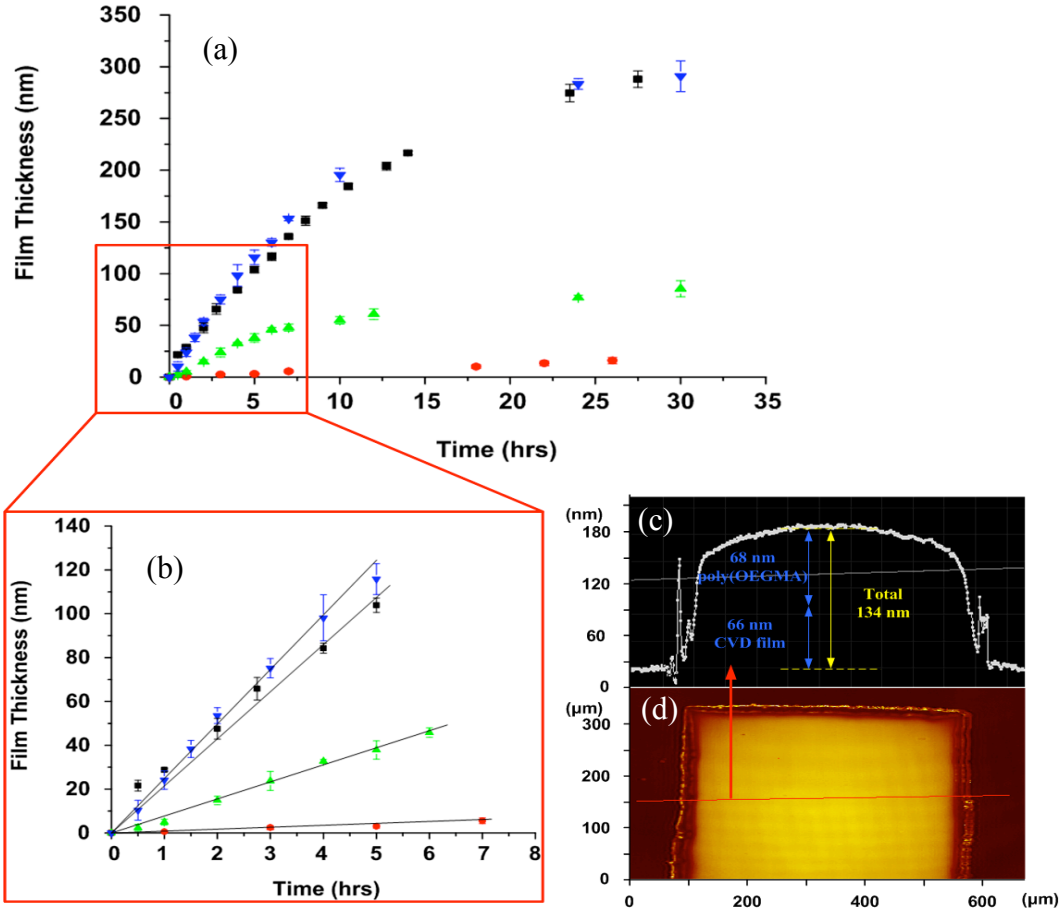

Figure 3.15: (a) Dependence of poly(OEGMA) film thickness on polymerization time for ATRP of aqueous OEGMA (OEGMA/water, 2:1, v:v) at room temperature with different concentrations of CuBr/$CuBr_2$/bpy as catalyst system (CuBr:$CuBr_2$:bpy = 1:0.3:2.5, molar ratio). (▼) [CuBr] = 5 mM, (▲) [CuBr] = 7.5 mM, (●) [CuBr] = 10 mM, (■) [CuBr] = 15 mM; n=3. Inset (b) shows an enlarged view of the plot shown in (a) clarifying the linear relationship between reaction time and thickness for a 5hrs period independent of the catalyst concentration. Cross-section thickness profile (c) and thickness map (d) were acquired by using imaging ellipsometry. In this example, the thickness was found to be 66 nm for reactive coating **17**, and 68 nm for poly(OEGMA) resulting in a total thickness of 134 nm.

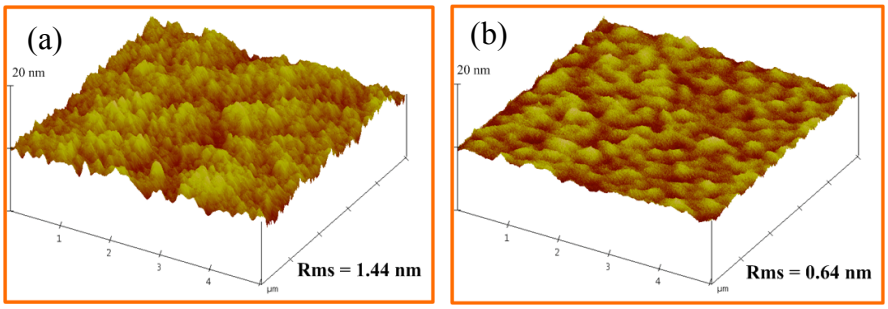

Figure 3.16: Surface roughness analysis by using SPM of (**a**) PMMA background with a surface roughness of R_{ms} = 1.44 and (b) the same substrate after CVD deposition of coating **17** and subsequent surface-initiated ATRP (R_{ms} = 0.64).

Assessment of non-fouling properties after surface-initiated ATRP. Finally, we verified that the resulting poly(OEGMA) coatings exhibit expected biological properties, such as protein- and cell-resistance. To confirm the protein-resistant property of PMMA surfaces modified *via* CVD polymerization in conjunction with ATRP, we incubated the entire sample surface consisting of a poly(OEGMA)-coated background and unmodified PMMA squares with an aqueous buffer solution of fluorescence-labeled fibrinogen. Fibrinogen was used as a model protein, because it is the prototype of a large protein (M_W=340 kDa) with strong tendency to adsorb to artificial substrates.[39] As shown in Figures 3.17a and 3.17b, fibrinogen selectively adsorbed only to areas that corresponded to non-modified surfaces, *i.e.,* surface areas without initiator coating **17**. In contrast, areas that were modified with the reactive initiator coating **17** during CVD polymerization and, as such, were able to support surface-initiated ATRP polymerization of OEGMA, showed consistently low levels of protein adsorption. Image analysis revealed high contrast between surface-modified areas and background (Figures 3.17a and b) and unambiguously demonstrates the effectiveness of the CVD-based initiator coating in supporting ATRP polymerization. The ability to create surfaces that can support low levels of non-specific protein adsorption is an important feature of any biomedical coating technology that these coatings could be instrumental in preventing non-specific

adsorption of proteins in several applications, such as biosensors or microfluidic devices.

To further complement the protein adsorption study, we investigated the adhesion of murine fibroblasts (NIH3T3 cells) to poly(OEGMA)-modified surfaces. The samples were coated with fibronectin prior to cell seeding. NIH3T3 cells were re-suspended in DMEM without FCS, and were added to wells containing the surface-modified samples. Cells were allowed to adhere onto the substrates for 2 hrs at 37°C in serum-free DMEM. Samples were then evaluated via phase contrast microscopy without further washing or fixation steps. The rationale for eliminating washing steps was to ensure that the direct contact properties of these surfaces with cells were evaluated, which may be altered during subsequent washing. As shown in Figure 3.17c, even without further washing, a clear contrast was observed between areas that were surface modified and the bare PMMA substrates. In fact, in the areas modified via CVD polymerization and ATRP, essentially no cells were found to be adherent. After this initial 2h adhesion, a subset of samples was rinsed with DMEM. The samples were then incubated with FCS-containing DMEM for additional 24 hrs and analyzed using phase contrast microscopy (Figure 3.17d). Again, no washing steps were employed prior to analysis. Interestingly, even after prolonged exposure to serum-containing media, cell adhesion to poly(OEGMA)-modified surface areas was still negligible. Cell adhesion data corroborate protein adsorption data and suggest that the herein proposed method can result in remarkably protein-resistant surfaces coatings.

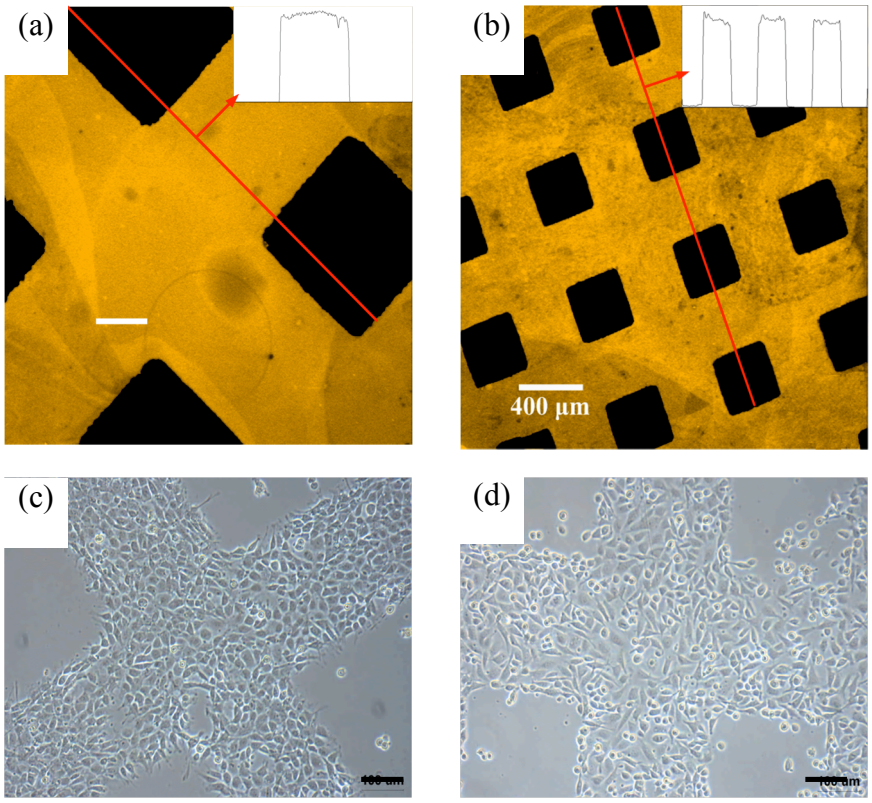

Figure 3.17: Biological properties of patterned surfaces. Regular (a) and large-area (b) view of a microstructured surface after exposure to an aqueous solution of fluorescence-labeled fibrinogen. The surfaces were prepared by spatially controlled deposition of the initiator coating **17** *via* vapor-assisted micropatterning in replica structures and subsequent ATRP. The histogram at the upper right corner of each image shows the line profile of the fluorescence intensity. (c) and (d): NIH3T3 cells on surface-modified PMMA substrates that were exposed to serum-free (c) and serum-containing (d) media. The images have been acquired without employing any washing step. Scale bars are 100 µm (a, c-d) and 400 µm (b), respectively.

3.4 Conclusions

Discontinuous patterns have been fabricated within microfluidic devices following a two-step surface modification process. The reported surface modification method consists of CVD polymerization of the photodefinable coating, and photopatterning and has several characteristic features: (1) The method establishes a generic surface engineering

protocol that is widely applicable to a range of materials and even hybrid structures, because of the substrate independence of the CVD coating step. (2) This approach enables the fabrication of spatially controlled bioinert surfaces for patterning within microchannels. (3) The method further allows to fully leveraging the potential of CVD coatings towards microfluidic applications by providing access to bioinert CVD coatings with minimal, non-specific protein adsorption. (4) The light-induced formation of radicals from the benzoyl groups enables immobilization of PEO polymers onto PDMS surfaces without the necessity of functional groups on the PEO itself. Although end-group modified PEO polymers with a range of reactive end groups are commercially available, the ability to use unmodified PEO polymers will be simpler and more cost-effective than methods that must rely on specialized PEO polymers. Due to the precise control of surface properties, such as non-specific protein adsorption, and the ease, with which patterns can be created on flat substrates as well as within microchannels, we foresee the technology to be useful for the fabrication of cell-based screening devices, BioMEMS applications, and diagnostic bioassays.[78]

Kinesin protein adsorption followed by microtubule landing rate measurements enables the determination of active protein coverages between 0.1 and 30 μm^{-2} (0.004 – 1 ng/cm^2). This detection range extends the lower end of the detection range of established methods. In essence, microtubule landing rate measurements afford single molecule sensitivity by exploiting the thousand-fold amplification of fluorescence signal afforded by labeled microtubules. The detection limit can be further reduced by increasing the observable number of microtubule landing events (increasing the field of view, observation time, or microtubule solution concentration). It is possible, that the ability of kinesin to bind microtubules is reduced after adsorption to the highly non-fouling surfaces. However, this reduced activity affects primarily the absolute protein coverage calculated from the data, and not the relative performance of two highly non-fouling surfaces. While the method does not determine the performance of non-fouling surfaces in blood serum or solutions of blood proteins, the reduced detection limit enables the quantification of adsorption events which would be invisible to established techniques. As a result, the performance of highly non-fouling surfaces can be determinated and optimized. For example, the adsorption of kinesin to PEGMA surfaces is fifteen-fold

reduced compared to $(EG)_3OH$-terminated SAM surfaces. We hope that the low technical requirements (fluorescence microscope with camera) and the commercial availability of a kinesin motility kit (Cytoskeleton Inc.) make this method widely accessible. In the context of hybrid devices integrating motor proteins, the measurements demonstrate that newly developed coatings can achieve the extreme degree of adsorption resistance desirable for the reliable placement of kinesin motors. Similar to such hybrid devices, biosensors utilizing nanowires or other nanostructures as transducing elements require highly adsorption resistant surfaces to maintain their performance advantages on the system level. These are only two examples of the diverse applications of high performance protein-resistant coatings in biotechnology.

Non-fouling surface coatings have been created on a representative range of different substrates using a two-step surface modification protocol. This method consists of CVD polymerization of a novel reactive initiator coating, poly(*p*-xylylene-4-methyl-2-bromo-isobutyrate-*co*-*p*-xylylene), which effectively supported surface-initiated ATRP. Because of the substrate independence of the CVD coating step, this approach establishes a generic surface engineering protocol that is widely applicable to a range of materials and even hybrid structures consisting of two or more materials in close proximity to each other. Moreover, the method establishes a versatile avenue to highly controlled surfaces with distinct materials features, such as the ability to support fabrication of spatially controlled bioinert surfaces for protein or cell patterning. Finally, this study manifests an important demonstration of the versatility of the CVD polymerization technology by providing a simple access route towards bioinert surfaces. In this sense, this work effectively leverages the potential of *reactive coatings* for biological applications by minimizing the non-specific protein adsorption and cell adhesion. Given that the essential step, the CVD polymerization of the initiator coating is equally applicable to a wide range of different substrates, we foresee the technology to be useful for the fabrication of cell-based screening devices, BioMEMS applications, and diagnostic bioassays.

References

[1] Xiao, D. Q.; Zhang, H.; Wirth, M., Chemical modification of the surface of poly(dimethylsiloxane) by atom-transfer radical polymerization of acrylamide. *Langmuir* **2002,** 18, (25), 9971.

[2] Regenberg, B.; Kruehne, U.; Beyer, M.; Pedersen, L. H.; Simon, M.; Thomas, O. R. T.; Nielsen, J.; Ahl, T., Use of laminar flow patterning for miniaturised biochemical assays. *Lab on a Chip* **2004,** 4, (6), 654.

[3] Cao, L.; Chang, M.; Lee, C. Y.; Castnet, D. G.; Sukavaneshvar, S.; Ratner, B. D.; Horbett, T. A., Plasma-deposited tetraglyme surfaces greatly reduce total blood protein adsorption, contact activation, platelet adhesion, platelet procoagulant activity, and in vitro thrombus deposition. *Journal of Biomedical Materials Research Part A* **2007,** 81A, (4), 827.

[4] Archambault, J. G.; Brash, J. L., Protein repellent polyurethane-urea surfaces by chemical grafting of hydroxyl-terminated poly(ethylene oxide): effects of protein size and charge. *Colloids and Surfaces B-Biointerfaces* **2004,** 33, (2), 111.

[5] Castner, D. G.; Ratner, B. D., Biomedical surface science: Foundations to frontiers. *Surface Science* **2002,** 500, (1-3), 28.

[6] Irvine, D. J.; Mayes, A. M.; Satija, S. K.; Barker, J. G.; Sofia-Allgor, S. J.; Griffith, L. G., Comparison of tethered star and linear poly(ethylene oxide) for control of biomaterials surface properties. *Journal of Biomedical Materials Research* **1998,** 40, (3), 498.

[7] Ratner, B. D., *Biomaterials science : an introduction to materials in medicine*. 2nd ed.; Elsevier Academic Press: Amsterdam ; Boston, 2004.

[8] Duffy, D. C.; McDonald, J. C.; Schueller, O. J. A.; Whitesides, G. M., Rapid Prototyping of Microfluidic Systems in Poly(dimethylsiloxane). *Analytical Chemistry* **1998,** 70, (23), 4974.

[9] Berdichevsky, Y.; Khandurina, J.; Guttman, A.; Lo, Y. H., UV/ozone modification of poly(dimethylsiloxane) microfluidic channels. *Sensors and Actuators B-Chemical* **2004,** 97, (2-3), 402.

[10] Grzybowski, B. A.; Haag, R.; Bowden, N.; Whitesides, G. M., Generation of Micrometer-Sized Patterns for Microanalytical Applications Using a Laser Direct-Write Method and Microcontact Printing. *Analytical Chemistry* **1998,** 70, (22), 4645.

[11] Ocvirk, G.; Munroe, M.; Tang, T.; Oleschuk, R.; Westra, K.; Harrison, D. J., Electrokinetic control of fluid flow in native poly(dimethylsiloxane) capillary electrophoresis devices. *Electrophoresis* **2000,** 21, (1), 107.

[12] Yang, T. L.; Jung, S. Y.; Mao, H. B.; Cremer, P. S., Fabrication of phospholipid bilayer-coated microchannels for on-chip immunoassays. *Analytical Chemistry* **2001,** 73, (2), 165.

[13] Barker, S. L. R.; Tarlov, M. J.; Canavan, H.; Hickman, J. J.; Locascio, L. E., Plastic Microfluidic Devices Modified with Polyelectrolyte Multilayers. *Analytical Chemistry* **2000,** 72, (20), 4899.

[14] Chen, H. Y.; Lahann, J., Fabrication of discontinuous surface patterns within microfluidic channels using photodefinable vapor-based polymer coatings. *Analytical Chemistry* **2005,** 77, (21), 6909.

[15] Burns, M. A.; Johnson, B. N.; Brahmasandra, S. N.; Handique, K.; Webster, J. R.; Krishnan, M.; Sammarco, T. S.; Man, P. M.; Jones, D.; Heldsinger, D.; Mastrangelo, C. H.; Burke, D. T., An integrated nanoliter DNA analysis device. *Science* **1998,** 282, (5388), 484.
[16] Lion, N.; Rohner, T. C.; Dayon, L.; Arnaud, I. L.; Damoc, E.; Youhnovski, N.; Wu, Z.-y.; Roussel, C.; Josserand, J.; Jensen, H.; Rossier, J. S.; Przybylski, M.; Girault, H. H., Microfluidic systems in proteomics. *Electrophoresis* **2003,** 24, (21), 3533.
[17] Qu, H.; Wang, H.; Huang, Y.; Zhong, W.; Lu, H.; Kong, J.; Yang, P.; Liu, B., Stable Microstructured Network for Protein Patterning on a Plastic Microfluidic Channel: Strategy and Characterization of On-Chip Enzyme Microreactors. *Analytical Chemistry* **2004,** 76, (21), 6426.
[18] Delamarche, E.; Bernard, A.; Schmid, H.; Bietsch, A.; Michel, B.; Biebuyck, H., Microfluidic Networks for Chemical Patterning of Substrates: Design and Application to Bioassays. *Journal of the American Chemical Society* **1998,** 120, (3), 500.
[19] Takayama, S.; Ostuni, E.; LeDuc, P.; Naruse, K.; Ingber, D. E.; Whitesides, G. M., Subcellular positioning of small molecules. *Nature* **2001,** 411, (6841), 1016.
[20] Takayama, S.; McDonald, J. C.; Ostuni, E.; Liang, M. N.; Kenis, P. J. A.; Ismagilov, R. F.; Whitesides, G. M., Patterning cells and their environments using multiple laminar fluid flows in capillary networks. *Proceedings of the National Academy of Sciences of the United States of America* **1999,** 96, (10), 5545.
[21] Heller, R. A.; Schena, M.; Chai, A.; Shalon, D.; Bedilion, T.; Gilmore, J.; Woolley, D. E.; Davis, R. W., Discovery and analysis of inflammatory disease-related genes using cDNA microarrays. *Proceedings of the National Academy of Sciences of the United States of America* **1997,** 94, (6), 2150.
[22] Schena, M.; Shalon, D.; Davis, R. W.; Brown, P. O., Quantitative monitoring of gene expression patterns with a complementary DNA microarray. *Science* **1995,** 270, (5235), 467.
[23] Shalon, D.; Smith, S. J.; Brown, P. O., A DNA microarray system for analyzing complex DNA samples using two-color fluorescent probe hybridization. *Genome research* **1996,** 6, (7), 639.
[24] Lopez, M. F.; Pluskal, M. G., Protein micro- and macroarrays: Digitizing the proteome. *Journal of Chromatography, B: Analytical Technologies in the Biomedical and Life Sciences* **2003,** 787, (1), 19.
[25] Roda, A.; Guardigli, M.; Russo, C.; Pasini, P.; Baraldini, M., Protein microdeposition using a conventional ink-jet printer. *BioTechniques* **2000,** 28, (3), 492.
[26] Heo, J.; Thomas, K. J.; Seong, G. H.; Crooks, R. M., A microfluidic bioreactor based on hydrogel-entrapped E. coli: Cell viability, lysis, and intracellular enzyme reactions. *Analytical Chemistry* **2003,** 75, (1), 22.
[27] Holden, M. A.; Jung, S.-Y.; Cremer, P. S., Patterning Enzymes Inside Microfluidic Channels via Photoattachment Chemistry. *Analytical Chemistry* **2004,** 76, (7), 1838.
[28] Koh, W.-G.; Itle, L. J.; Pishko, M. V., Molding of hydrogel microstructures to create multiphenotype cell microarrays. *Analytical Chemistry* **2003,** 75, (21), 5783.
[29] Koh, W.-G.; Revzin, A.; Pishko, M. V., Poly(ethylene glycol) hydrogel microstructures encapsulating living cells. *Langmuir* **2002,** 18, (7), 2459.

[30] Zhan, W.; Seong, G. H.; Crooks, R. M., Hydrogel-based microreactors as a functional component of microfluidic systems. *Analytical Chemistry* **2002,** 74, (18), 4647.
[31] Sigal, G. B.; Mrksich, M.; Whitesides, G. M., Effect of surface wettability on the adsorption of proteins and detergents. *Journal of the American Chemical Society* **1998,** 120, (14), 3464.
[32] Khademhosseini, A.; Suh, K. Y.; Jon, S.; Eng, G.; Yeh, J.; Chen, G.-J.; Langer, R., A soft lithographic approach to fabricate patterned microfluidic channels. *Analytical Chemistry* **2004,** 76, (13), 3675.
[33] Rhee, S. W.; Taylor, A. M.; Tu, C. H.; Cribbs, D. H.; Cotman, C. W.; Jeon, N. L., Patterned cell culture inside microfluidic devices. *Lab on a Chip* **2005,** 5, (1), 102.
[34] Beebe, D. J.; Moore, J. S.; Bauer, J. M.; Yu, Q.; Liu, R. H.; Devadoss, C.; Jo, B.-H., Functional hydrogel structures for autonomous flow control inside microfluidic channels. *Nature* **2000,** 404, (6778), 588.
[35] Lahann, J.; Langer, R., Novel Poly(p-xylylenes): Thin Films with Tailored Chemical and Optical Properties. *Macromolecules* **2002,** 35, (11), 4380.
[36] Hu, S.; Ren, X.; Bachman, M.; Sims, C. E.; Li, G. P.; Allbritton, N., Surface Modification of Poly(dimethylsiloxane) Microfluidic Devices by Ultraviolet Polymer Grafting. *Analytical Chemistry* **2002,** 74, (16), 4117.
[37] Hu, S.; Ren, X.; Bachman, M.; Sims, C. E.; Li, G. P.; Allbritton, N. L., Surface-Directed, Graft Polymerization within Microfluidic Channels. *Analytical Chemistry* **2004,** 76, (7), 1865.
[38] Hu, S.; Ren, X.; Bachman, M.; Sims, C. E.; Li, G. P.; Allbritton, N. L., Tailoring the Surface Properties of Poly(dimethylsiloxane) Microfluidic Devices. *Langmuir* **2004,** 20, (13), 5569.
[39] Ratner, B. D.; Bryant, S. J., Biomaterials: Where we have been and where we are going. *Annual Review of Biomedical Engineering* **2004,** 6, 41.
[40] Irvine, D. J.; Mayes, A. M.; GriffithCima, L., Self-consistent field analysis of grafted star polymers. *Macromolecules* **1996,** 29, (18), 6037.
[41] Shen, W. W.; Boxer, S. G.; Knoll, W.; Frank, C. W., Polymer-supported lipid bilayers on benzophenone-modified substrates. *Biomacromolecules* **2001,** 2, (1), 70.
[42] Katira, P.; Agarwal, A.; Fischer, T.; Chen, H. Y.; Jiang, X.; Lahann, J.; Hess, H., Quantitative analysis of ultra-low protein coverages on protein-resisting surfaces using surface-bound kinesin motor proteins. *Advanced Materials* **2007**, accepted.
[43] van den Heuvel, M. G. L.; Butcher, C. T.; Smeets, R. M. M.; Diez, S.; Dekker, C., High rectifying efficiencies of microtubule motility on kinesin-coated gold nanostructures. *Nano Letters* **2005,** 5, (6), 1117.
[44] Reuther, C.; Hajdo, L.; Tucker, R.; Kasprzak, A. A.; Diez, S., Biotemplated nanopatterning of planar surfaces with molecular motors. *Nano Letters* **2006,** 6, (10), 2177.
[45] Moorjani, S. G.; Jia, L.; Jackson, T. N.; Hancock, W. O., Lithographically patterned channels spatially segregate kinesin motor activity and effectively guide microtubule movements. *Nano Letters* **2003,** 3, (5), 633.
[46] Ionov, L.; Stamm, M.; Diez, S., Size sorting of protein assemblies using polymeric gradient surfaces. *Nano Letters* **2005,** 5, (10), 1910.

[47] Hiratsuka, Y.; Tada, T.; Oiwa, K.; Kanayama, T.; Uyeda, T. Q. P., Controlling the direction of kinesin-driven microtubule movements along microlithographic tracks. *Biophysical Journal* **2001,** 81, (3), 1555.
[48] Clemmens, J.; Hess, H.; Lipscomb, R.; Hanein, Y.; Bohringer, K. F.; Matzke, C. M.; Bachand, G. D.; Bunker, B. C.; Vogel, V., Mechanisms of microtubule guiding on microfabricated kinesin-coated surfaces: Chemical and topographic surface patterns. *Langmuir* **2003,** 19, (26), 10967.
[49] Qian, J.; Liu, Y.; Liu, H.; Yu, T.; Deng, J., Immobilization of horseradish peroxidase with a regenerated silk fibroin membrane and its application to a tetrathiafulvalene-mediating H2O2 sensor. *Biosensors & Bioelectronics* **1997,** 12, (12), 1213.
[50] Nicolau, D. V.; Suzuki, H.; Mashiko, S.; Taguchi, T.; Yoshikawa, S., Actin motion on microlithographically functionalized myosin surfaces and tracks. *Biophysical Journal* **1999,** 77, (2), 1126.
[51] Mahanivong, C.; Wright, J. P.; Kekic, M.; Pham, D. K.; dos Remedios, C.; Nicolau, D. V., Manipulation of the motility of protein molecular motors on microfabricated substrates. *Biomedical Microdevices* **2002,** 4, (2), 111.
[52] Sundberg, M.; Balaz, M.; Bunk, R.; Rosengren-Holmberg, J. P.; Montelius, L.; Nicholls, I. A.; Omling, P.; Tagerud, S.; Mansson, A., Selective spatial localization of actomyosin motor function by chemical surface patterning. *Langmuir* **2006,** 22, (17), 7302.
[53] Bachand, G. D.; Soong, R. K.; Neves, H. P.; Olkhovets, A.; Craighead, H. G.; Montemagno, C. D., Precision attachment of individual F-1-ATPase biomolecular motors on nanofabricated substrates. *Nano Letters* **2001,** 1, (1), 42.
[54] Yajima, J.; Alonso, M. C.; Cross, R. A.; Toyoshima, Y. Y., Direct long-term observation of kinesin processivity at low load. *Current Biology* **2002,** 12, (4), 301.
[55] Diez, S.; Schief, W. R.; Howard, J., Molecular motors: Single-molecule recordings made easy. *Current Biology* **2002,** 12, (6), R203.
[56] Howard, J.; Hunt, A.; Baek, S., Assay of Microtubule Movement Driven by Single Kinesin Molecules. In *Methods in Cell Biology, Vol 39*, 1993; Vol. 39, pp 137.
[57] Howard, J.; Hudspeth, A. J.; Vale, R. D., Movement of microtubules by single kinesin molecules. *Nature* **1989,** 342, 154.
[58] Lin, H. H.; Kim, J.; Sun, L.; Crooks, R. M., Replication of DNA microarrays from zip code masters. *Journal of the American Chemical Society* **2006,** 128, (10), 3268.
[59] Schliwa, M.; Woehlke, G., Molecular motors. *Nature* **2003,** 422, (6933), 759.
[60] Kerssemakers, J.; Howard, J.; Hess, H.; Diez, S., The distance that kinesin-1 holds its cargo from the microtubule surface measured by fluorescence interference contrast microscopy. *Proceedings of the National Academy of Sciences of the United States of America* **2006,** 103, (43), 15812.
[61] Wirth, M. J.; Swinton, D. J.; Ludes, M. D., Adsorption and diffusion of single molecules at chromatographic interfaces. *Journal of Physical Chemistry B* **2003,** 107, (26), 6258.
[62] Xu, C.; Barnes, S. E.; Wu, T.; Fischer, D. A.; DeLongchamp, D. M.; Batteas, J. D.; Beers, K. L., Solution and surface composition gradients via microfluidic confinement: fabrication of a statistical-copolymer-brush composition gradient. *Advanced Materials* **2006,** 18, (11), 1427.

[63] deCastro, M. J.; Ho, C. H.; Stewart, R. J., Motility of dimeric ncd on a metal-chelating surfactant: Evidence that ncd is not processive. *Biochemistry* **1999,** 38, (16), 5076.
[64] O'Connor, S. M.; DeAnglis, A. P.; Gehrke, S. H.; Retzinger, G. S., Adsorption of plasma proteins on to poly(ethylene oxide)/poly(propylene oxide) triblock copolymer films: a focus on fibrinogen. *Biotechnology and Applied Biochemistry* **2000,** 31, 185.
[65] Elkasabi, Y.; Chen, H. Y.; Lahann, J., Multipotent polymer coatings based on chemical vapor deposition copolymerization. *Advanced Materials* **2006,** 18, (12), 1521.
[66] Lahann, J., Vapor-based polymer coatings for potential biomedical applications. *Polymer International* **2006,** 55, (12), 1361.
[67] Suh, K. Y.; Kim, Y. S.; Lee, H. H., Capillary force lithography. *Advanced Materials* **2001,** 13, (18), 1386.
[68] Satulovsky, J.; Carignano, M. A.; Szleifer, I., Kinetic and thermodynamic control of protein adsorption. *Proceedings of the National Academy of Sciences of the United States of America* **2000,** 97, (16), 9037.
[69] Prime, K. L.; Whitesides, G. M., Self-Assembled Organic Monolayers - Model Systems for Studying Adsorption of Proteins at Surfaces. *Science* **1991,** 252, (5009), 1164.
[70] Herrwerth, S.; Eck, W.; Reinhardt, S.; Grunze, M., Factors that determine the protein resistance of oligoether self-assembled monolayers - Internal hydrophilicity, terminal hydrophilicity, and lateral packing density. *Journal of the American Chemical Society* **2003,** 125, (31), 9359.
[71] Chapman, R. G.; Ostuni, E.; Yan, L.; Whitesides, G. M., Preparation of mixed self-assembled monolayers (SAMs) that resist adsorption of proteins using the reaction of amines with a SAM that presents interchain carboxylic anhydride groups. *Langmuir* **2000,** 16, (17), 6927.
[72] Siegers, C.; Biesalski, M.; Haag, R., Self-assembled monolayers of dendritic polyglycerol derivatives on gold that resist the adsorption of proteins. *Chemistry-a European Journal* **2004,** 10, (11), 2831.
[73] Nandivada, H.; Chen, H. Y.; Lahann, J., Vapor-based synthesis of poly [(4-formyl-p-xylylene)-co-(p-xylylene)] and its use for biomimetic surface modifications. *Macromolecular Rapid Communications* **2005,** 26, (22), 1794.
[74]Schurmann, K.; Lahann, J.; Niggemann, P.; Klosterhalfen, B.; Meyer, J.; Kulisch, A.; Klee, D.; Gunther, R. W.; Vorwerk, D., Biologic response to polymer-coated stents: In vitro analysis and results in an iliac artery sheep model. *Radiology* **2004,** 230, (1), 151.
[75] Matyjaszewski, K.; Xia, J. H., Atom transfer radical polymerization. *Chemical Reviews* **2001,** 101, (9), 2921.
[76] Kim, J. B.; Huang, W. X.; Miller, M. D.; Baker, G. L.; Bruening, M. L., Kinetics of surface-initiated atom transfer radical polymerization. *Journal of Polymer Science Part a-Polymer Chemistry* **2003,** 41, (3), 386.
[77] Chen, P. J.; Rodger, D. C.; Humayun, M. S.; Tai, Y. C., Unpowered spiral-tube parylene pressure sensor for intraocular pressure sensing. *Sensors and Actuators a-Physical* **2006,** 127, (2), 276.

[78] Vilkner, T.; Janasek, D.; Manz, A., Micro Total Analysis Systems. Recent Developments. *Analytical Chemistry* **2004,** 76, (12), 3373.
[79] Katira, P.; Agarwal, A.; Fischer, T.; Chen, H. Y.; Jiang, X.; Lahann, J.; Hess, H., Quantitative analysis of ultra-low protein coverages on protein-resisting surfaces using surface-bound kinesin motor proteins. *Advanced Materials* **2007**, accepted.
[80] Jiang, X.; Chen, H. Y.; Galvan, G.; Yoshida, M.; Lahann, J., Vapor-based initiator coatings for atom transfer radical polymerization. *Advanced Functional Materials* **2007**, accepted.

CHAPTER 4

SURFACE MODIFICATION OF CONFINED MICROGEOMETRIES VIA VAPOR-DEPOSITED POLYMER COATINGS

The materials in this chapter are adapted from previously reported data in "Surface Modification of Confined Microgeometries via Vapor-Deposited Polymer Coatings, *Journal of the American Chemical Society* (2006) 128, 1, 374", by H.-Y. Chen, Y. Elkasabi, J. Lahann; and have been slightly modified.

The development of generally applicable protocols for the surface modification of complex substrates has emerged as one of the key challenges in biotechnology. The use of vapor-deposited polymer coatings may provide an appealing alternative to the currently employed arsenal of surface modification methods consisting mainly of wet-chemical approaches. Herein, we demonstrate the usefulness of chemical vapor deposition polymerization for surface modification in confined microgeometries with both, non-functionalized and functionalized poly(*p*-xylylenes). For a diverse group of polymer coatings, homogenous surface coverage of different microgeometries are demonstrated based on optical microscopy and imaging X-ray photoelectron spectroscopy. In addition, height profiles of deposited polymer footprints were obtained by atomic force microscopy, and imaging ellipsometry indicating continuous transport and deposition throughout the entire microchannels. Finally, the ability of reactive coatings to support chemical binding of biological ligands, when deposited in previously assembled microchannels, is demonstrated, verifying the usefulness of the CVD coatings for applications in micro/nano-fluidics, where surface modifications with stable and designable biointerfaces are essential. The fact that reactive coatings can be deposited within confined microenvironments exhibits an important step towards new device architectures with potential relevance to bioanalytical, medical, or "BioMEMS" applications.

4.1 Background and Motivations

Defined and stable surface properties along with the capability to immobilize active biomolecules onto a surface are key features for the development of miniaturized biodevices, such as micro total analysis systems (μTAS),[1] microfabricated cell sorters,[2] microseparators for DNA[3,4] and proteins,[5-7] cell-based assays,[8] and embryonic patterning networks.[9] In such miniaturized high-tech systems, very large surface-to-volume ratios are typically encountered creating a situation where slight inhomogeneities in the surface chemistry will cause device malfunction.[10] The development of advanced surface modification protocols that are equally applicable to flat and three-dimensional surfaces has accordingly emerged as one of the critical challenges for many biotechnology applications. From a device design perspective, polydimethylsiloxane (PDMS) is often discussed as the prime candidate material for microfluidic systems because of its favorable mechanical properties[11,12] and its straightforward manufacturing by rapid prototyping.[13] However, PDMS is a very hydrophobic polymer, has undefined surface properties, and promotes non-specific protein adhesion.[14] In addition, the absence of functional groups at the PDMS surface prevents covalent immobilization of proteins, enzymes or antibodies. To reduce these adverse properties of PDMS, several methods including graft polymerization,[15,16] plasma treatment,[13] UV/ozone treatment,[17] silanization,[18] adsorption of detergents,[14] proteins,[19] and polyelectrolytes[20] have been used to modify PDMS, but often show hydrophobic recovery of PDMS and loss of protein-resistance with time hampering their use for long-term applications.[21]

Deposition of thin polymer films to establish chemically defined interfaces offers a unique way to overcome these limitations. Recently, we reported a widely applicable surface modification approach based on chemical vapor deposition (CVD) polymerization to deposit *reactive coatings* on the luminal surface of open PDMS-based microchannels.[22] In addition to being compatible with the requirements of biological assays, these coatings provide a designable interlayer that is stable under the conditions

of bioassays.[22,23] The *reactive coatings* are based on polymers known as functionalized poly(*p*-xylylenes), which establish interfaces equipped with chemically reactive groups that can be selected from a variety of different chemical species, including amines, alcohols, aldehydes, activated carboxylic acids, and anhydrides.[24,25] *Reactive coatings* have been useful for immobilization of biomolecules,[26,27] planar cell and protein patterning,[28] and for patterning of polymer brushes[29,30] on freely accessible substrates. However, the appropriate question of whether the concept of CVD polymerization is expandable to the coating of complex microgeometries with high aspect ratios or only applicable to cases, where the individual pieces are modified prior to assembly, remains open.[16] If CVD polymerization indeed could be applied to previously assembled devices, the scope of practical use could be significantly widened. In this report, we will demonstrate - for the first time - that CVD polymerization can be used to deposit a white range of functionalized poly(*p*-xylylenes) within confined microgeometries (Figure 4.1).

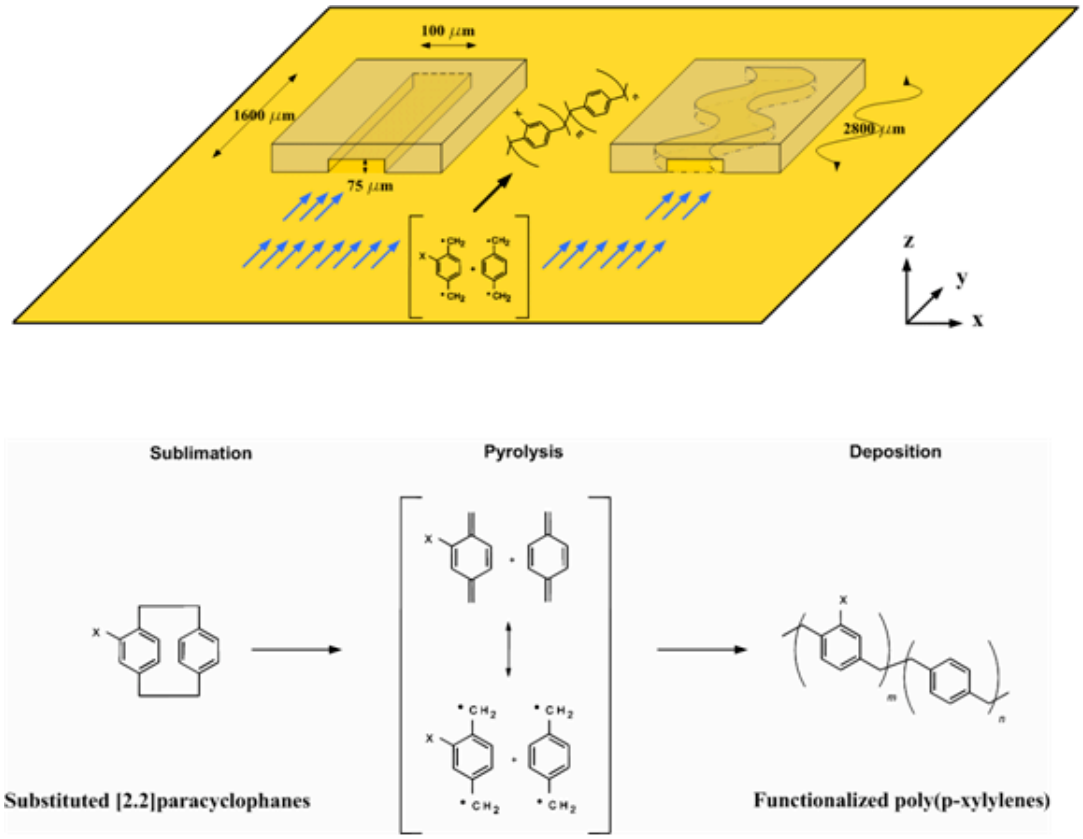

functionalized poly(*p*-xylylenes)	20	14	21	22	23	24	25
X =	—NH_2	O, CF_3	O, C_2F_5	C_6F_5, O, O	O, C_6H_5	—Cl	—H

Figure 4.1: (a) Chemical vapor deposition polymerization within confined geometries of straight and meandering channels. (b) Functionalized poly(*p*-xylylenes) prepared via chemical vapor deposition polymerization used in this study.

4.2 Methods

Device fabrication. The microfluidic devices were designed using AutoCAD, and the design was printed on high-resolution emulsion transparencies. For fabrication of the master, a layer of photoresist (PR 1813, Hoechst Celanese) was spin-coated at 4000 rpm for 30 s onto a silicon wafer. The wafer was soft-baked at 90 °C for 30 min and was then exposed to UV radiation (404.7 nm, 10 mJ/cm^2, 20 sec) to define the desired microstructure from the transparency mask. After removal of the activated photoresist by exposition to a developer solution (MF 319, Hoeschst Celanese) for 60 s, the wafer was hard-baked at 110 °C for 30 min. The microstructured patterns were formed by deep reactive ion etching. The photoresist was then removed by treatment with a resist stripper (PRS 2000, JT Baker Inc.). The resulting silicon master was placed in a Petri dish and uniformly mixed PDMS prepolymer and curing agent (Sylgard 184, Dow Corning) at a ratio of 10:1 were poured onto the master. The PDMS prepolymer was cured at 70 °C for 1 hr. Finally, embossed microchannels were released from the silicon master. Dimensions of the microchannels were typically 75 μm deep and 100 μm wide, but varied in some cases as indicated. The replicated PDMS molds were used to assemble devices with silicon and glass substrates. Devices were prepared with both removable and sealed PDMS molds. The sealing process was done by UV/ozone oxidation on both PDMS and glasses for 10 min. PDMS mold and glass substrate were brought into contact immediately (<1 min) after oxidation. Finally, the sealed devices were baked at 70 °C.

CVD polymerization of poly(*p*-xylylenes). Functionalized poly(*p*-xylylenes) were synthesized via CVD polymerization. The starting material (functionalized [2.2]paracyclophanes) was sublimed under vacuum and converted by pyrolysis into the corresponding quinodimethanes, which spontaneously polymerized upon condensation to the substrate surface. A constant argon flow of 20 sccm was used as the carrier. Sublimation temperatures were kept at 70-105 °C followed by pyrolysis at 670-700 °C depending on the type of [2.2]paracyclophane and the pressure used. Subsequently, polymerization occurred on a rotating, cooled sample holder placed inside a stainless

steel chamber with a wall temperature of 130 °C. The coating pressure was 0.5 mbar or below. The exit of the chamber was connected via a cooling trap to a mechanical pump. Polymerization parameters are summarized in Table 4.1. For CVD polymerization, PDMS molds were sealed reversibly or irreversibly to a silicon wafer, which was placed onto the sample holder.

TABLE 4.1
REPRESENTATIVE PARAMETERS USED FOR CVD POLYMERIZATION OF [2.2]PARACYCLOPHANES

polymer	sublimation temp (℃)	pyrolysis temp (℃)	substrate temp (℃)	system pressure (mbar)	argon mass flow (sccm)
20	85	700	15	0.5	20
14	70	670	15	0.5	20
21	70	670	15	0.09	5
22	120	800	15	0.09	5
23	100	680	15	0.5	20
24	105	670	15	0.5	20
25	95	670	15	0.5	20

Surface characterization. X-ray photoelectron spectroscopy (XPS) data were recorded on an Axis Ultra X-ray photoelectron spectrometer (Kratos Analyticals, UK) equipped with a monochromatized Al Kα X-ray source. In these experiments, the lens mode was in hybrid, pass energy was set to 160.0 eV, and the aperture was 600 μm x 600 μm for all imaging acquisitions. Silicon (Si_{2p}) mapping was performed at 99.0 eV with an X-ray power of 150 kW. Height analysis data on microchannels for polymers **14**, **20**, **21**, **24**, **25** were obtained with a Nanoscope IIIa scanning probe microscopy (Digital Instruments/Veeco, USA). Scanning size was 30 μm x 30 μm with scan rate of 0.8 Hz, using a JV type scanner (150 μm x 150 μm maximum scan size). NSC 16 cantilevers (MikroMasch, USA) with spring constants between 25 N/m and 60 N/m, and resonance frequencies of 150–170 kHz were used as AFM tips. Height analysis data on

microchannels for polymer **22** and **23** were recorded at a wavelength of 532 nm using an EP^3-SW imaging ellipsometry (Nanofilm Technologie GmbH, Germany). Both, nulling (four zones) and mapping experiments were performed at an angle of incident of 60^o, and an anisotropic Cauchy model was used to model the ellipsometric parameters psi and delta. For the mapping mode, data were recorded by an imaging scanner with a lateral resolution of 1 μm at a field of view of about 100 μm x 500 μm. The images were captured using a CCD camera (768 x 572 pixels).

Immobilization of biomolecules. As shown in Scheme S1, reaction with biotin ligands followed by binding to streptavidin was used to visualize the reactive coatings. Based on this procedure, coatings **14** and **20** were modified via immobilization of biotin and streptavidin. For this purpose, devices coated with polymer **20** were incubated in Petri dishes with PFP-biotin ((+)-biotin pentafluorophenyl ester, 10 mM, Pierce) in dimethyl formamide (DMF) and phosphate buffered saline (PBS, pH 7.4) for 60 min. The surface was then rinsed several times with DMF and PBS. After rinsing, devices were incubated with rhodamine (TRITC) conjugated streptavidin (10 μg/ml, Pierce) in PBS containing 0.1% (w/v) bovine albumin and Tween 20 (0.02% (v/v)) for 60 min. The surface was rinsed several times with PBS containing 0.1% (w/v) bovine albumin and Tween 20 (0.02% (v/v)). Devices coated with polymer **14** were incubated in Petri dishes with biotin-hydrazide (10 mM, Pierce) in phosphate buffered saline (PBS, pH 7.4) for 5 min. The surface was then rinsed several times with PBS. After rinsing, devices were incubated with rhodamine (TRITC) conjugated streptavidin (10 μg/ml, Pierce) in PBS containing 0.1% (w/v) bovine albumin and Tween 20 (0.02% (v/v)) for 60 min. The surface was rinsed several times with PBS containing 0.1% (w/v) bovine albumin and Tween 20 (0.02% (v/v)). The resulting samples were then examined by fluorescence microscopy (TE 200, Nikon) and optical microscopy (BX 60, Olympus).

4.3 CVD Polymerization in Enclosed Microchannels

To create a general understanding of the phenomenon of CVD polymerization within

confined microgeometries, seven different poly(*p*-xylylenes) were deposited via CVD polymerization within both, removable and sealed microchannels. A sub-group of five poly(*p*-xylylenes), polymers **14**, **15**, **21**, **22**, **23**, had reactive side group (so-called reactive coatings), while two commercially available poly(*p*-xylylenes) were included as non-functionalized references (polymers **24** and **25**). The CVD polymerization process used for coating of the microfluidic channels with both, reactive coatings and non-functionalized coatings, is an adaptation of the commercially exploited Gorham process, routinely practiced for the deposition of polymer coatings marketed as parylenes. As shown in Figure 4.1, functionalized [2.2]paracyclophanes are first sublimed and the resulting vapor is transferred into the pyrolysis zone. Through control of the polymerization parameters, such as sublimation and pyrolysis temperatures, pressure, and mass flow, selective cleavage of C-C bonds can be obtained.[31] While quantitative conversion into the corresponding *p*-quinodimethanes is critical for CVD polymerization,[24] care must be taken to avoid decomposition of the functional groups under the conditions of thermal activation. The selection of process parameters must account for this balance between activation, i.e. the opening of the aliphatic bridges of the [2.2]paracyclophanes, and the avoidance of thermally induced side reactions. The PDMS microchannels used in this study were open at both ends and had the following dimensions: 75 μm high and 100 μm wide, and both straight (1600 μm long) and meandering channel (2800 μm long) layouts were studied. After removal of the PDMS molds, the footprint of the deposited films remained on the silicon substrates as confirmed by optical microscopy. In Figures 4.2a and 2b, optical micrographs of a silicon substrate coated with polymer **25** are shown for both, straight and meandering microchannels. While the deposited polymer films were thicker in the inlet and outlet region of the microchannels than in the center, the micrographs clearly indicate homogeneous deposition of polymer **25** throughout the entire microchannel. To verify that the contrast in the micrographs is indeed due to the vapor-deposited coating, we examined the footprints of polymer **25** on the silicon substrate using XPS in the imaging mode. This technique enables spatially resolved mapping of the elemental distribution of reporter atoms on a surface. Figure 4.2c shows the elemental composition map of silicon recorded for a 600 x 600 μm^2 area of a meandering channel coated with polymer

25. Silicon is a characteristic atom of the substrate used in this study, a silicon wafer, and is not present in polymer coating **25**. As anticipated, the composition map confirms that silicon is only detectable for areas that were masked during CVD polymerization, while the entire microchannel footprint is devoid any detectable amounts of silicon. Based on this finding we concluded that the entire microchannel is covered with a homogeneous film of polymer **25**, which must be thicker than the information depth of XPS (about 10 nm).[37] Correspondingly, a homogeneous distribution of carbon was detected throughout the entire footprint of the microchannel, but not for the areas masked during CVD polymerization (See supporting information). Taken together, the data obtained by optical microscopy and imaging XPS suggest that CVD polymerization can be used to deposit homogeneous polymer films within confined geometries, such as the straight and meandering microchannels used in this study.

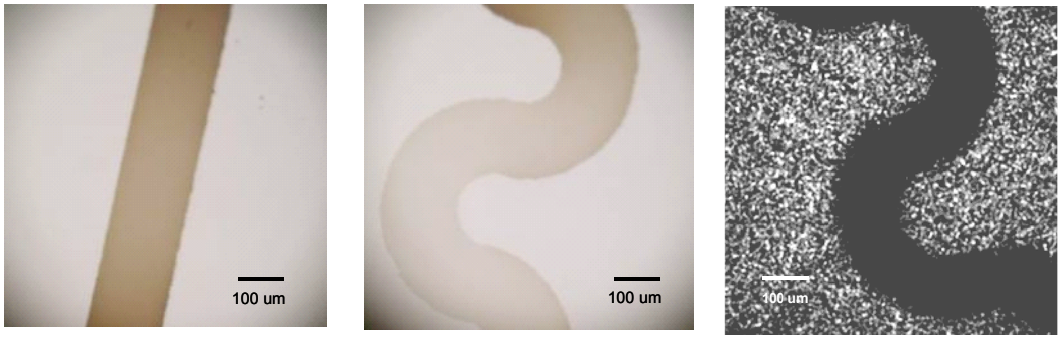

(a) (b) (c)

Figure 4.2: (a, b) Optical micrographs showing poly-*p*-xylylene (**25**) films deposited within microchannels. (c) XPS mapping (Si_{2p}, 99.0 eV) of poly-*p*-xylylene films deposited within microchannels. All images were taken after CVD coating in a confined microgeometry and removal of the PDMS molds for imaging purposes.

4.4 Deposition of Reactive Coatings in Enclosed Microchannels

Once the fundamental feasibility of CVD polymerization within previously assembled microdevices was demonstrated for the non-functionalized poly(*p*-xylylene)

25, we extended our study to reactive CVD coatings **14**, **20**, **21**, **22**, **23**. For comparison, CVD polymerization was again conducted in straight and meandering microchannel geometries and film thicknesses were quantified with atomic force microscopy (AFM) and/or ellipsometry. In all cases, the CVD polymerization of [2.2]paracyclophanes resulted in transparent and topologically uniform polymer films. Moreover, the footprints of the reactive coatings deposited within the microchannels were typically detectable by optical microscopy. The ability to visualize the footprints of the coatings enabled us to extract height profiles at the interface between polymer coating using AFM in the tapping mode (Figure 4.3). The AFM study revealed height profiles for polymers **14**, **20**, **21**, **24,** and **25** (Table 4.2). In case of polymers **22** and **23** however, the deposited films were substantially thinner and the boundary between film and substrate was no longer observable by light microscopy making it difficult to use AFM for height profiling. In these cases, we used imaging ellipsometry to unambiguously confirm the presence of the polymer films throughout the microchannel footprint. Figure 4.4 shows ellipsometric thickness maps recorded for polymer **22** on both, straight and meandering microchannels. A clearly observable contrast between areas coated with the polymer film and the Si substrate is revealed by imaging ellipsometry. Quantitative height profiles were obtained from the ellipsometric data shown in Figure 4.4 indicating a thickness of 6 nm for the straight microchannel and 5 nm for the meandering microchannel, respectively. Prior to this experiment, the usefulness of imaging ellipsometry for thickness determination of ultra-thin polymer films was validated by comparing the thickness of the same sample of polymer **20** measured by AFM and imaging ellipsometry. Within the margins of error, the thicknesses measured by AFM and imaging ellipsometry were identical demonstrating the usefulness of imaging ellipsometry for surface analysis of ultrathin CVD films. Throughout this series of experiments, film thicknesses measured at the center of the microchannel footprints were compared to film thicknesses measured for unconfined substrates, that is, open surfaces distant to the microchannels. Table 1 summarizes the complete set of thickness data for all polymers tested. Under the conditions of CVD polymerization, substantially different thicknesses were observed ranging from 38 nm measured for polymer **25** to 524 nm for polymer **23**. The film thickness was mainly determined by the amount of a given

[2.2]paracyclophane used for CVD polymerization. Based on the thickness data, we were able to extract the degree of deposition for each polymer; being defined as the ratio of film thicknesses measured at the center of the microchannel and at the open substrate. In essence, this ratio indicates, how effective a CVD coating can be deposited in the confined geometry. The deposition degree will be 100% for a coating that is not limited by the confinement imposed by a microchannel geometry. Although we intuitively expected the deposition degree to be independent from the film thickness, we verified this relationship by depositing films of polymer **20** with various thicknesses and measured the corresponding degrees of deposition. We were able to compare polymer coatings with substantially different deposition degrees (Table 4.2). Polymers **20**, **22**, and **23** showed relative low deposition degrees, ranging from 1 % to 16 % for straight microchannels and from 0.4 % to 9 % for meandering channels. In contrast, polymers **14**, **21**, **24**, and **25** had deposition degrees higher than 80% for the straight microchannel geometry, and above 40% for the meandering microchannel geometry. The differences between both layouts may be explained with (i) the curved layout of the microchannels, and (ii) the 1.75 times longer pathway of the meandering microchannels as compared to the straight microchannels (meandering channels have aspect ration of 37 compared to 21 for straight channels). It is important to note that the actual thickness of the deposited reactive coatings is less critical to a given surface modification applications, as long as the deposition of the polymer film occurs homogeneously throughout the microchannel and the resulting coatings still provide functional groups for further modification. With the homogeneous deposition of functionalized and non-functionalized poly(*p*-xylylenes) in confined geometries unambiguously confirmed, we therefore moved our focus towards the assessment of the ability of reactive coatings to support subsequent surface reactions, when deposited in complex microgeometries. In principle, the polymer coatings can then provide anchoring groups on the channel walls for the linkage of biomolecules.

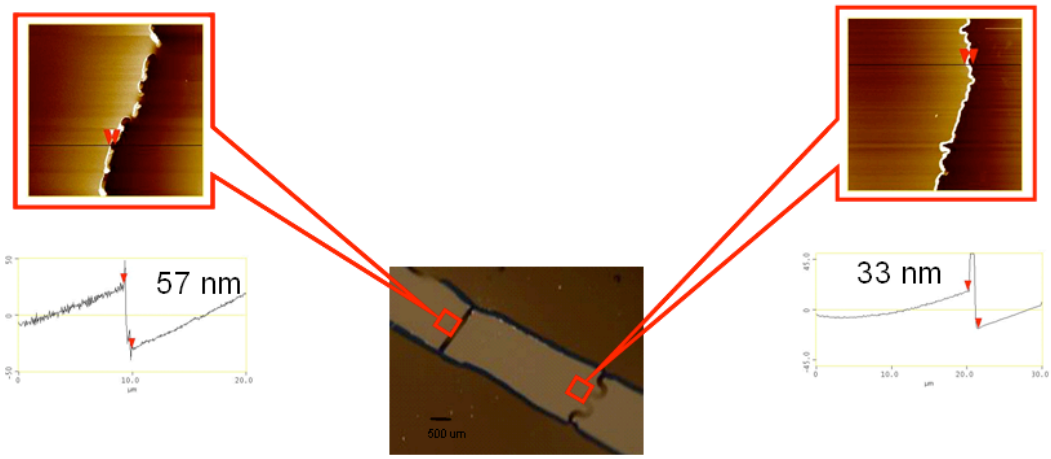

Figure 4.3: AFM cross-section height analysis of (a) straight and (b) meandering channels of a substrate coated with CVD polymer **21**. The scanning size is 20 μm by 20 μm. (c, d) Corresponding height profiles revealing 57 nm film thickness for the straight channel and 33 nm for the meandering channel; (e) matching photograph taken by a digital camera.

TABLE 4.2
FILM THICKNESS CHARACTERIZATION

polymer	film thickness (h_0)[a] outside the channels (nm)	film thickness (h_1)[b] at straight channels (nm)	degree of deposition[d] at straight channels (%)	film thickness (h_2)[b] at meandering channels (nm)	degree of deposition at meandering channels (%)
20	103	16	(16%)	9	(9%)
14	127	113	(89%)	74	(58%)
21	70	57	(81%)	33	(47%)
22	437	6[c]	(1.4 %)	5[c]	(1.1%)
23	524	5[c]	(1.0 %)	2[c]	(0.4%)
24	59	46	(80%)	24	(41%)
25	38	33	(86%)	16	(42%)

[a]Based on ellipsometry

[b]If indicated, otherwise the reported values are based on AFM

[c]Based on ellipsometry

[d]Degree of deposition (%) $= \frac{h_1 (or h_2)}{h_0} \times 100\%$

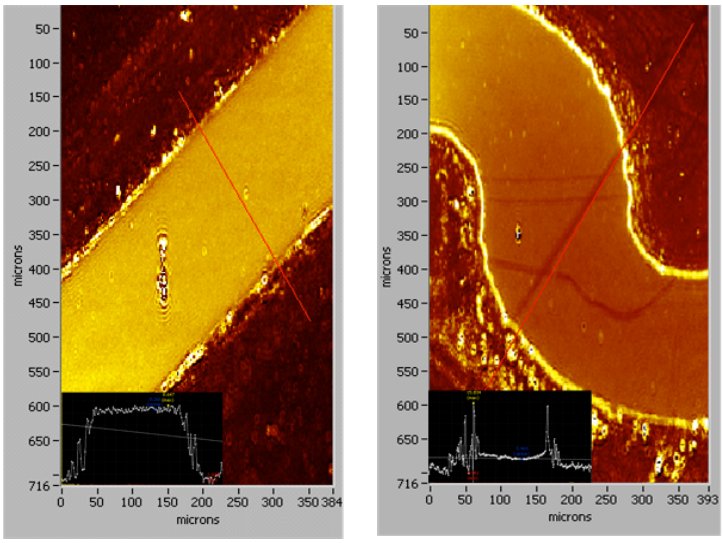

Figure 4.4: Cross-section height analysis by imaging ellipsometry at straight and meandering channels coated with CVD polymer **22** is shown as an example.

4.5 Chemical and Biological Activity of Reactive Coatings Deposited onto the Luminal Surface of Enclosed Microchannels

To address the question of whether polymer films deposited within micorchannels still maintain their typical reactivity towards corresponding binding partners, we conducted a series of immobilization studies with permanently sealed PDMS devices after CVD polymerization. The microchannels were coated with polymers **14** or **20** prior to immobilization. While polymer **20** provides primary amino groups for coupling with activated carboxyl groups (amide formation), polymer **14** has keto groups that can react with hydrazines or hydrazides. To assess the chemical activity of both reactive coatings, PFP-derived biotin ligands and hydrazide-derived biotin ligands were used.[21] These ligands were chosen because they undergo nearly quantitative conversion with amines or ketones, respectively. Moreover, the interactions between biotin and streptavidin result in tight confinement of streptavidin on the biotin-modified surface, which can be exploited for visualization of ligand binding. Figure 4.5 illustrates the surface modification approach used in this study based on the example of reactive coating

14. For all ligand immobilization, aqueous solutions of the corresponding biotin derivative were filled into the sealed microchannels of either meandering or straight geometry. After incubation for 60 min (5 min for hydrazide-derived biotin ligands), non-reacted ligands were washed away.

To examine the immobilization of biotin ligands within the microchannels, we allowed rhodamine (TRITC) conjugated streptavidin to bind to the biotin-modified surfaces. After thourough rinsing with buffer, the surfaces were visualized by fluorescence microscopy. Figure 4.6 shows microchannels that were coated with polymer **20** and then subjected to the biotin/strepdavidin protocol. Homogenous distribution throughout the entire microchannel was observed, indicating that amino groups were available throughout the entire coating area. Similarly, the biotin ligands bound homogenously to polymer **14**, as shown in Figure 4.7. Similar to the situation observed for polymer **20**, this finding indicates homogenous reactivity of the deposited polymer films, which appears to be independent from the observed thickness differences. This phenomenon appears to be independent of the observed thickness, because reactive coating **22** had one of the lowest degrees of deposition of all polymers included in this study (Figure 4.8). The ability to deposit polymer coating with relative homogenous distribution of reactive binding sides throughout the microchannel will be a critical feature when using reactive coatings to tailor surface properties of microchannels towards the needs of specific biological applications. While CVD polymerization of monomers other than [2.2]paracyclophanes has been used to coated PDMS microchannels,[32] the herein described deposition of poly(*p*-xylylenes) presents a promising alternative due to the unuasually low sticking coefficients encountered during CVD polymerization promising homogeneous deposition in confined geometries.[33,34]

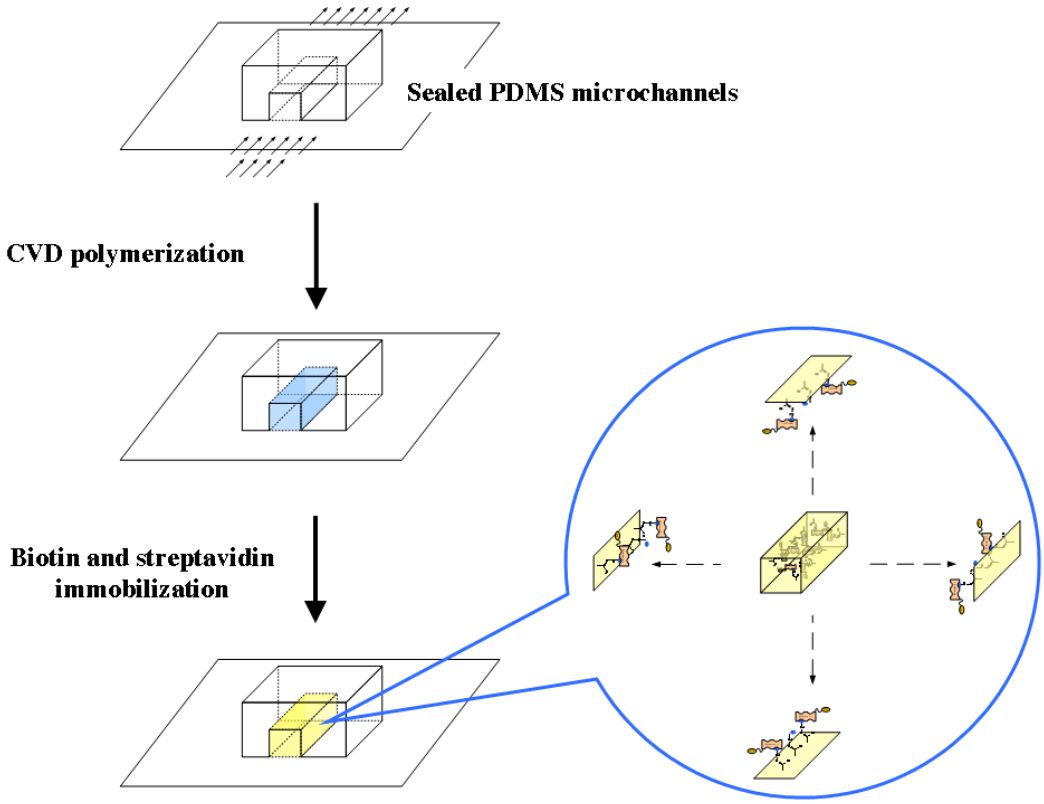

Figure 4.5: Three-dimensional immobilization protocol used for the surface modification of the luminal surface area of the microchannels, as shown for the example of reactive coating **14**.

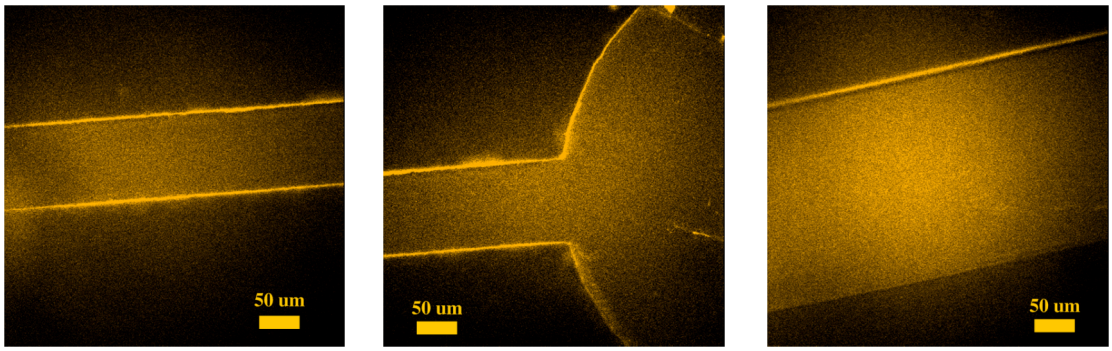

Figure 4.6: Fluorescence micrographs of sealed devices coated with reactive coating **20** after immobilization of PFP-biotin and self-assembly of TRITC-conjugated streptavidin. Examples are shown in different geometries with 75 μm depth and 100 - 300 μm width or 500 μm diameter.

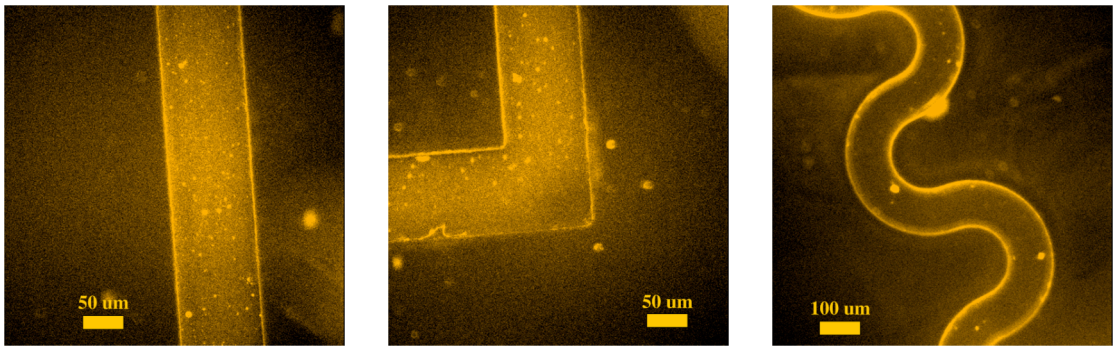

Figure 4.7: Fluorescence micrographs of sealed devices coated with reactive coating **14** after immobilization of hydrazide-biotin and self-assembly of TRITC-conjugated streptavidin. Examples are shown in different channel geometries of 75 μm depth and 100 μm width.

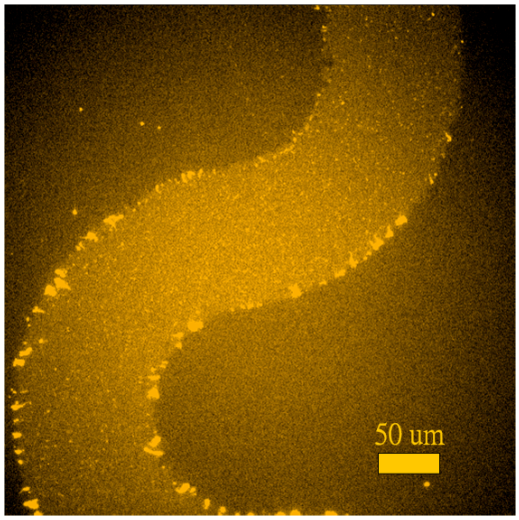

Figure 4.8: Fluorescence micrographs of reactive coating **22** after immobilization of amine-biotin and self-assembly of TRITC-conjugated streptavidin.

4.6 Deposition of Reactive Coatings in Vascular Grafts

Based on the technology discovered in previous sections in this chapter, we further investigate the accessibility of preparing these *reactive polymers* within a polytetrafluoroethylene (PTFE) based vascular grafts. Poly[4-trifluoroacetyl-*p*-xylylene-*co*-*p*xylylene] (**4**) was used as model polymer in this study. PTFE vascular grafts were obtained from commercially available products (GORE-TEX®, Gore & Associates Inc.) as shown in Figure 4.9 and were used as received for CVD coating. The graft is 700 mm long and 4 mm in diameter. Figure 4.10 is showing the XPS survey and high-resolution C_{1s} spectra of the resulting PTFE grafts after CVD modification. Samples at different section of the graft were examined including entrance, center, end, and control experiment (without CVD coating). For the control experiment (Figure 4.10a), it is clearly shown that the detected carbon in XPS survey spectrum is only contributed from the symmetric C-F binding (291.9 eV) recorded consistently from C_{1s} high-resolution acquisition. As anticipated, samples (Figure 4.10b-d) which were modified with CVD polymer are showing additional C-C, C=O binding energy states at 285.0 eV and 288.0±1.0 eV respectively, which are characteristic components of the

poly[4-trifluoroacetyl-*p*-xylylene-*co*-*p*xylylene] (**4**) used in this study. Similar evidence can be obtained from the fact that oxygen signal (533.0 eV) was only detected on the CVD modified samples but not on the pristine PTFE samples by comparing the XPS survey spectra.

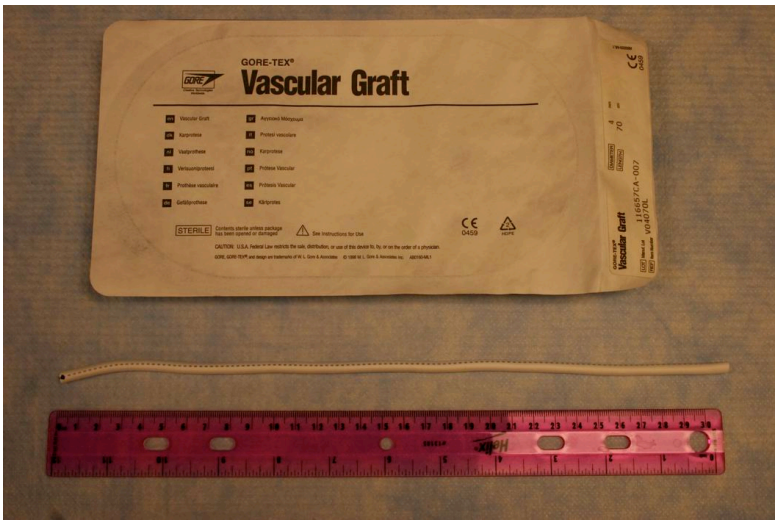

Figure 4.9: Photograph of a PTFE vascular graft used in this study. Received graft was 700 mm long and 4 mm in diameter. Picture is showing the 300 mm long graft after cutting.

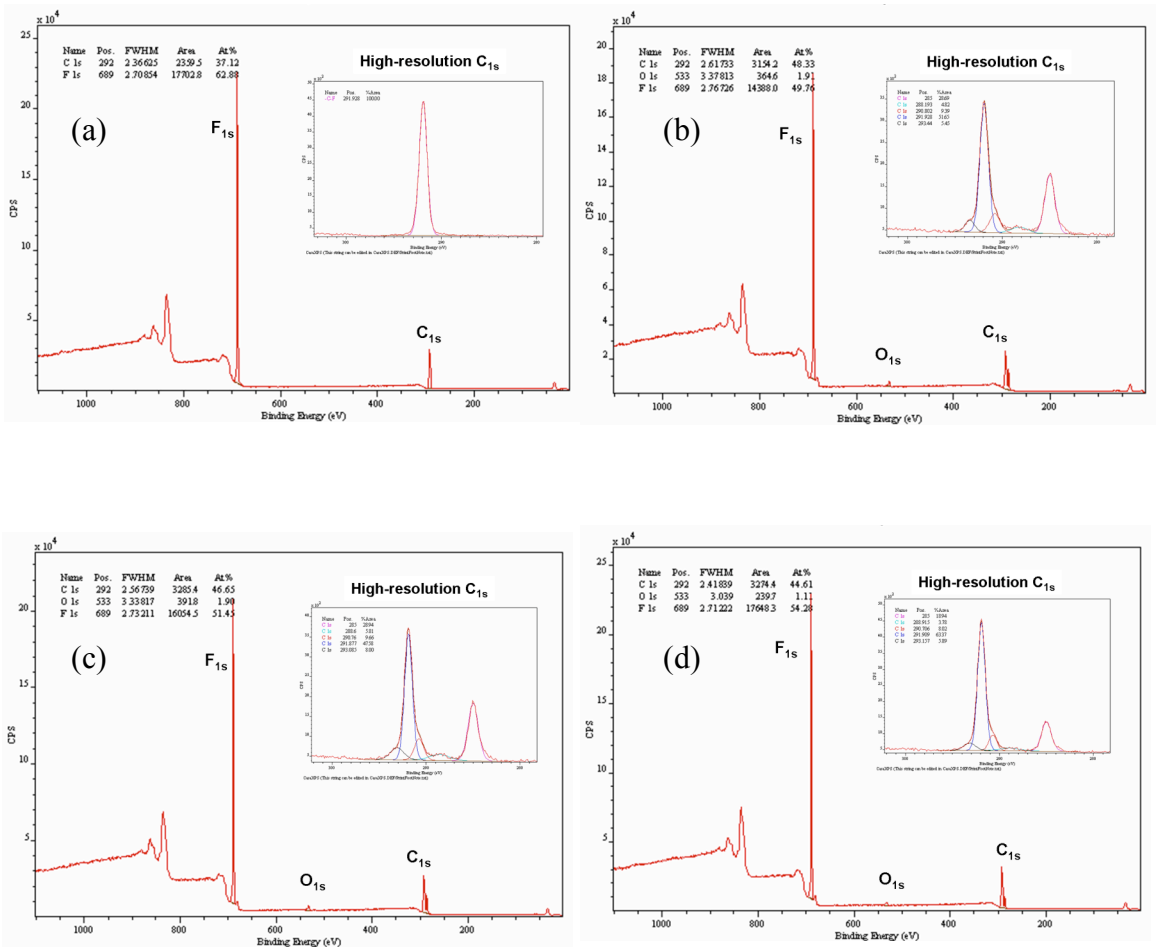

Figure 4.10: XPS survey and high-resolution C1s (inserts on the upper right corner) spectra of the PTFE vascular graft modified with CVD polymer. (a) Control experiment conducted on pristine PTFE showing only fluorine and carbon peaks in survey spectrum, and only characteristic C-F (291.9 eV) binding energy from PTFE was detected in high resolution C1s spectrum. (b) Data recorded at the entrance of the graft, showing additional oxygen peak (533.0 eV) in survey spectrum and additional binding energies in high resolution C1s spectrum corresponding to C-C (285.0 eV) and C=O (288.2 eV) detected from CVD polymer (**14**). (c) Data recorded at the center of the graft, showing additional oxygen peak (533.0 eV) in survey spectrum and additional binding energies in high resolution C1s spectrum corresponding to C-C (285.0 eV) and C=O (288.6 eV) detected from CVD polymer (**14**). (d) Data recorded at the end of the graft, showing additional oxygen peak (533.0 eV) in survey spectrum and additional binding energies in high resolution C1s spectrum corresponding to C-C (285.0 eV) and C=O (288.9 eV) detected from CVD polymer (**14**).

To address the question of whether polymer films deposited within grafts still maintain their typical reactivity towards corresponding binding sites, we conducted a series of immobilization studies with the grafts after CVD polymerization. The grafts were coated with polymers **14** prior to immobilization. While polymer **14** has keto groups that can react with hydrazides. To assess the chemical activity of the coating, hydrazide-derived biotin ligand was used. This ligand was chosen because it undergoes nearly quantitative conversion with ketone group. Moreover, the interactions between biotin and streptavidin result in tight confinement of streptavidin on the biotin-modified surface, which can be exploited for visualization of ligand binding. For immobilization, aqueous solutions of the corresponding biotin derivative were filled into the entire graft. After incubation for 5 min, non-reacted ligands were washed away.

To examine the immobilization of biotin ligand within the grafts, we allowed rhodamine (TRITC) conjugated streptavidin to bind to the biotin-modified surfaces. After thorough rinsing with buffer, the surfaces were visualized by using confocal laser scanning microscopy (CLSM). Figure 4.11 shows the resulting grafts that were coated with polymer **14** and then subjected to the biotin/strepdavidin protocol. Binding experiment on control sample with no CVD coating was also performed by the same biotin/strepdavidin protocol for comparison. As shown in Figure 4.11, fluorescence signals were detected by CLSM on all the samples coated with polymer **14**, but not on the control sample, which indicates homogenous reactivity of the deposited polymer films on the entire graft. The ability to deposit polymer coating with relative homogenous distribution of reactive binding sides throughout the vascular grafts will be a critical feature when using reactive coatings to tailor surface properties of grafts towards the needs of specific biological applications. While CVD polymerization of monomers other than [2.2]paracyclophanes has been used to modify confined microchannels, the herein described deposition of poly(*p*-xylylenes) presents promising results on tubular grafts, which demonstrate the potential applicability of utilizing these reactive polymers on a wide range of different geometries and materials.

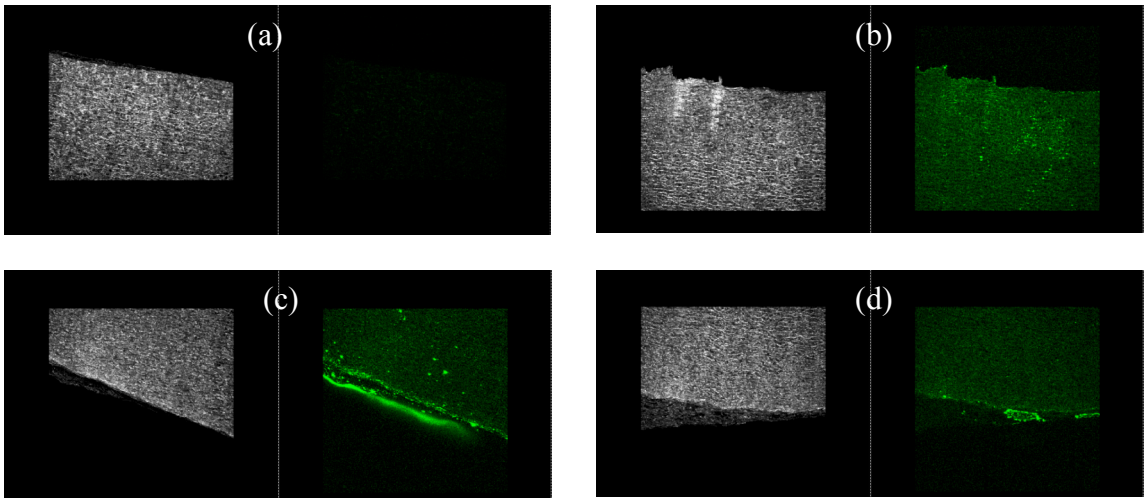

Figure 4.11: CLSM micrographs showing control and CVD modified PTFE vascular graft. (a) Pristine PTFE vascular after biotin and subsequent TRITC-streptavidin immobilizations. Phase contrast image (left) is showing the surface of the graft, while fluorescence image (right) is showing low fluorescence signal detected. (b) Entrance part of the graft. Phase contrast image (left) is showing the surface of the graft, while fluorescence image (right) is showing significant fluorescence signal detected. (c) Center part of the graft. Phase contrast image (left) is showing the surface of the graft, while fluorescence image (right) is showing significant fluorescence signal detected. (d) End part of the graft. Phase contrast image (left) is showing the surface of the graft, while fluorescence image (right) is showing significant fluorescence signal detected. (a) is shown as control experiment in this study.

4.7 Conclusions

CVD polymerization of functionalized [2.2]paracyclophanes establishes a simple, but general protocol for preparation of ultrathin polymer coatings (smaller than 100 nm). The resulting reactive coatings provide a designable interface useful for a wide range of surface modifications: Active ester groups allow for immobilization of proteins; amino- or carboxylic acid groups may control surface charges and electro-osmotic flows; and alkyl groups may provide hydrophobic interfaces for electrochromatographic applications.

In this study, we have used a combination of surface-analytical methods including

optical and fluorescence microscopy, imaging elipsometry, atomic force microscopy, and imaging XPS to unambiguously establish the applicability of CVD coatings to the coating of confined microgeometries. Based on this study, we suggest that (1) CVD polymerization can be applied to microdevices and results in homogenous polymer films, which can be made of either reactive or non-reactive coatings; (2) a decrease of film thicknesses occurs towards the center of the microchannels suggesting the existence of an upper limit in the aspect ratio of the microdevices that can be coated; (3) polymer deposition is applicable to both, straight and curved microchannels; (4) reactive coatings deposited within confined microgeometries provide functional groups that can sustain chemical conversion yielding in homogenous deposition of biomolecules; and (5) preparation of these reactive polymers is applicable within a wide range of different materials and geometries, e.g., PTFE vascular grafts. The fact that we have – for the first time - confirmed the deposition of reactive CVD coatings within confined microgeometries bridges a critical technological gap towards surface-modified microfluidic and nanofluidic devices with use for biosensor and "BioMEMS" applications, bioseparation, the design of high-throughput screening platforms, or the development of novel tissue constructs for regenerative medicine applications.

References

[1] Berg, A.; Olthius, W.; Bergveld, P., *Micro Total Analysis Systems 2000*. 1st ed.; Springer: 2000.

[2] Fu, A. Y.; Spence, C.; Scherer, A.; Arnold, F. H.; Quake, S. R., A microfabricated fluorescence-activated cell sorter. *Nature Biotechnology* **1999,** 17, (11), 1109.

[3] Burns, M. A.; Johnson, B. N.; Brahmasandra, S. N.; Handique, K.; Webster, J. R.; Krishnan, M.; Sammarco, T. S.; Man, P. M.; Jones, D.; Heldsinger, D.; Mastrangelo, C. H.; Burke, D. T., An integrated nanoliter DNA analysis device. *Science* **1998,** 282, (5388), 484.

[4] Effenhauser, C. S.; Bruin, G. J. M.; Paulus, A.; Ehrat, M., Integrated Capillary Electrophoresis on Flexible Silicone Microdevices: Analysis of DNA Restriction Fragments and Detection of Single DNA Molecules on Microchips. *Analytical Chemistry* **1997,** 69, (17), 3451.

[5] Chen, S. H.; Sung, W. C.; Lee, G. B.; Lin, Z. Y.; Chen, P. W.; Liao, P. C., A disposable poly(methylmethacrylate)-based microfluidic module for protein identification by nanoelectrospray ionization-tandem mass spectrometry. *Electrophoresis* **2001,** 22, (18), 3972.

[6] Huber, D. L.; Manginell, R. P.; Samara, M. A.; Kim, B.-I.; Bunker, B. C., Programmed adsorption and release of proteins in a microfluidic device. *Science* **2003,** 301, (5631), 352.

[7] Mao, H.; Yang, T.; Cremer, P. S., Design and characterization of immobilized enzymes in microfluidic systems. *Analytical Chemistry* **2002,** 74, (2), 379.

[8] Li, P. C.; Harrison, D. J., Transport, manipulation, and reaction of biological cells on-chip using electrokinetic effects. *Analytical chemistry* **1997,** 69, (8), 1564.

[9] Lucchetta, E. M.; Lee, J. H.; Fu, L. A.; Patel, N. H.; Ismagilov, R. F., Dynamics of Drosophila embryonic patterning network perturbed in space and time using microfluidics. *Nature* **2005,** 434, (7037), 1134.

[10] Li, Y.; Pfohl, T.; Kim, J. H.; Yasa, M.; Wen, Z.; Kim, M. W.; Safinya, C. R., Selective surface modification in silicon microfluidic channels for micromanipulation of biological macromolecules. *Biomedical Microdevices* **2001,** 3, (3), 239.

[11] Quake, S. R.; Scherer, A., From micro- to nanofabrication with soft materials. *Science* **2000,** 290, (5496), 1536.

[12] Johnson, T. J.; Ross, D.; Gaitan, M.; Locascio, L. E., Laser Modification of Preformed Polymer Microchannels: Application To Reduce Band Broadening around Turns Subject to Electrokinetic Flow. *Analytical Chemistry* **2001,** 73, (15), 3656.

[13] Duffy, D. C.; McDonald, J. C.; Schueller, O. J. A.; Whitesides, G. M., Rapid Prototyping of Microfluidic Systems in Poly(dimethylsiloxane). *Analytical Chemistry* **1998,** 70, (23), 4974.

[14] Linder, V.; Verpoorte, E.; Thormann, W.; de Rooij, N. F.; Sigrist, H., Surface biopassivation of replicated poly(dimethylsiloxane) microfluidic channels and application to heterogeneous immunoreaction with on-chip fluorescence detection. *Analytical Chemistry* **2001,** 73, (17), 4181.

[15] Hu, S.; Ren, X.; Bachman, M.; Sims, C. E.; Li, G. P.; Allbritton, N., Surface Modification of Poly(dimethylsiloxane) Microfluidic Devices by Ultraviolet Polymer Grafting. *Analytical Chemistry* **2002,** 74, (16), 4117.
[16] Hu, S.; Ren, X.; Bachman, M.; Sims, C. E.; Li, G. P.; Allbritton, N. L., Surface-Directed, Graft Polymerization within Microfluidic Channels. *Analytical Chemistry* **2004,** 76, (7), 1865.
[17] Berdichevsky, Y.; Khandurina, J.; Guttman, A.; Lo, Y. H., UV/ozone modification of poly(dimethylsiloxane) microfluidic channels. *Sensors and Actuators B-Chemical* **2004,** 97, (2-3), 402.
[18] Grzybowski, B. A.; Haag, R.; Bowden, N.; Whitesides, G. M., Generation of Micrometer-Sized Patterns for Microanalytical Applications Using a Laser Direct-Write Method and Microcontact Printing. *Analytical Chemistry* **1998,** 70, (22), 4645.
[19] Yang, T. L.; Jung, S. Y.; Mao, H. B.; Cremer, P. S., Fabrication of phospholipid bilayer-coated microchannels for on-chip immunoassays. *Analytical Chemistry* **2001,** 73, (2), 165.
[20] Barker, S. L. R.; Tarlov, M. J.; Canavan, H.; Hickman, J. J.; Locascio, L. E., Plastic Microfluidic Devices Modified with Polyelectrolyte Multilayers. *Analytical Chemistry* **2000,** 72, (20), 4899.
[21] Makamba, H.; Kim, J. H.; Lim, K.; Park, N.; Hahn, J. H., Surface modification of poly(dimethylsiloxane) microchannels. *Electrophoresis* **2003,** 24, (21), 3607.
[22] Lahann, J.; Balcells, M.; Lu, H.; Rodon, T.; Jensen, K. F.; Langer, R., Reactive polymer coatings: A first step toward surface engineering of microfluidic devices. *Analytical Chemistry* **2003,** 75, (9), 2117.
[23] Chen, H. Y.; Lahann, J., Fabrication of discontinuous surface patterns within microfluidic channels using photodefinable vapor-based polymer coatings. *Analytical Chemistry* **2005,** 77, (21), 6909.
[24] Lahann, J.; Langer, R., Novel Poly(p-xylylenes): Thin Films with Tailored Chemical and Optical Properties. *Macromolecules* **2002,** 35, (11), 4380.
[25] Nandivada, H.; Chen, H. Y.; Lahann, J., Vapor-based synthesis of poly [(4-formyl-p-xylylene)-co-(p-xylylene)] and its use for biomimetic surface modifications. *Macromolecular Rapid Communications* **2005,** 26, (22), 1794.
[26] Lahann, J.; Klee, D.; Pluester, W.; Hoecker, H., Bioactive immobilization of r-hirudin on CVD-coated metallic implant devices. *Biomaterials* **2001,** 22, (8), 817.
[27] Lahann, J.; Pluster, W.; Rodon, T.; Fabry, M.; Klee, D.; Gattner, H.-G.; Hocker, H., Universal approach towards r-hirudin derivatives with high anti-thrombin activity based on chemical differentiation of primary amino groups. *Macromolecular Bioscience* **2002,** 2, (2), 82.
[28] Lahann, J.; Balcells, M.; Rodon, T.; Lee, J.; Choi, I. S.; Jensen, K. F.; Langer, R., Reactive polymer coatings: A platform for patterning proteins and mammalian cells onto a broad range of materials. *Langmuir* **2002,** 18, (9), 3632.
[29] Lahann, J.; Choi, I. S.; Lee, J.; Jensen, K. F.; Langer, R., A new method toward microengineered surfaces based on reactive coating. *Angewandte Chemie, International Edition* **2001,** 40, (17), 3166.

[30] Lahann, J.; Langer, R., Surface-initiated ring-opening polymerization of e-caprolactone from a patterned poly(hydroxymethyl-p-xylylene). *Macromolecular Rapid Communications* **2001,** 22, (12), 968.
[31] Greiner, A.; Mang, S.; Schaefer, O.; Simon, P., Poly(p-xylene)s. Synthesis, polymer analogous reactions, and perspectives on structure-property relationships. *Acta Polymerica* **1997,** 48, (1/2), 1.
[32] Gu, H.; Xu, C.; Weng, L.-T.; Xu, B., Solventless Polymerization: Spatial Migration of a Catalyst To Form Polymeric Thin Films in Microchannels. *Journal of the American Chemical Society* **2003,** 125, (31), 9256.
[33]Tolstopyatov, E. M., Thickness uniformity of gas-phase coatings in narrow channels: I. Long channels. *Journal of Physics D-Applied Physics* **2002,** 35, (13), 1516.
[34] Tolstopyatov, E. M.; Yang, S. H.; Kim, M. C., Thickness uniformity of gas-phase coatings in narrow channels: II. One-side confined channels. *Journal of Physics D-Applied Physics* **2002,** 35, (21), 2723.

CHAPTER 5

DRY ADHESIVE BONDING BY USING REACTIVE POLYMER COATINGS

Bonding of substrates has continuously been an important technical challenge in a range of electronic and biotechnological applications, such as the fabrication microelectromechanical systems (MEMS) or elastomeric microanalytical devices. Several bonding technologies including direct bonding, adhesive bonding, anodic bonding, solder or eutectic bonding, as well as thermo-compression bonding have been established, but these methods are often limited to a specific substrates or involve the application of additional bonding chemicals or require harsh process conditions.[1] For instance, bonding of poly(dimethylsiloxane) (PDMS), widely used in biotechnological applications, typically requires oxidative pretreatment, such as oxygen plasma[2-4] or UV/ozone[5] activation. Upon exposure to highly oxidative environments, silanol groups (Si-OH) are created, which can result in strong intermolecular bonding.[2] However, the effects of oxidative activation are only temporary due to hydrophobic recovery and must be done immediately prior to bonding. In addition, these approaches are limited to a small group of substrates, such as PDMS, silicon, or glass, impeding the use for hybrid devices, which may consist of a multiple different materials.

We herein propose an alternate strategy for bonding, solventless adhesive bonding (SAB) process, which is applicable to a wide range of materials, including, but not limited to PDMS. As shown in Figure 5.1, bonding is instead achieved through reactions between two vapor-deposited polymer coatings with complementary functional groups, *i.e.*, amino and aldehyde groups. The ultra-thin adhesion layers are conformally applied to the substrates using a reactive coating technology recently developed in our group.[6,7] The CVD-based polymer films form well-adherent coatings on a range of different substrate materials including polymers, glass, silicon, metals, paper and can be stored for

extended periods prior to bonding without loosing the bonding capability.[8] In fact, reactive coatings used herein, poly(4-methanamine-*p*-xylylene-co-*p*-xylylene)[9,10] (**15**) and poly(4-formyl-*p*-xylylene-*co*-*p*-xylylene)[11] (**2**), are stable under try conditions until brought in contact at elevated temperatures. Prior to mechanical testing, the chemical structures of all polymer films were confirmed by X-ray photoelectron spectroscopy (XPS). Film thicknesses were in the range of 40 - 80 nm as measured by ellipsometry. Because this novel approach uses solventless polymer coatings, it eliminates the need for solvent-based adhesives as well as pretreatment steps that need to be applied immediately prior to bonding.

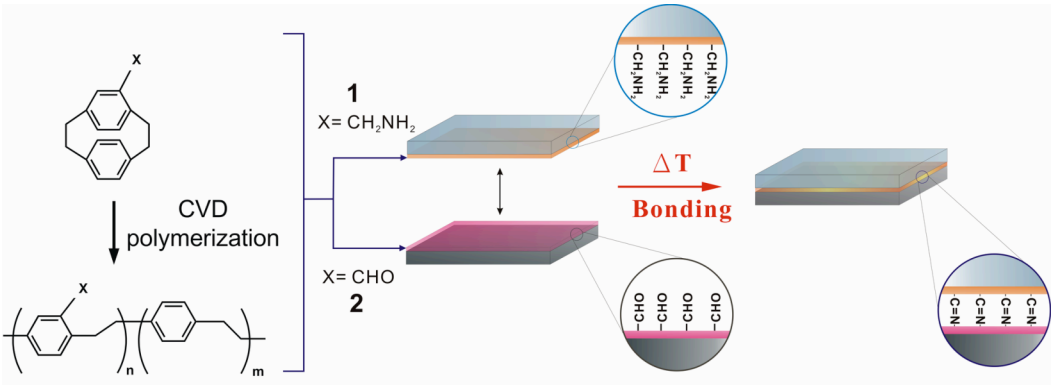

Figure 5.1: Schematic illustration of the solventless adhesive bonding (SAB) process. During SAB, formation of a strong adhesion layer is achieved by bonding of two complementary CVD reactive coatings **2** and **15**.

5.1 Methods

Materials. PDMS samples were prepared by uniformly mixed PDMS prepolymer and curing agent (Sylgard 184, Dow Corning) at a ratio of 10:1 and were cured at 70 ºC for 1 hr. Glass slide (Fisher), PTFE film (0.01 mm, Goodfellow), and stainless steel (AISI 316L - Fe/Cr18/Ni10/Mo3, annealed, 0.1 mm, Goodfellow) were used as received. Gold samples were prepared on silicon wafers (Silicon Valley Microelectronics, Inc.) by e-beam deposition, with 3 nm of titanium followed by 80 nm of gold.

CVD polymerization. Poly(4-methanamine-*p*-xylylene)-co-(*p*-xylylene) (**15**) and poly(4-formyl-*p*-xylylene-*co*-*p*-xylylene) (**2**) were synthesized via CVD polymerization in a custom-made CVD polymerization system. The starting material, 4-aminomethyl[2.2]paracyclophane and 4-formyl[2,2]paracyclophane, were sublimed under vacuum and converted by pyrolysis into the corresponding quinodimethanes, which spontaneously polymerized upon condensation to the cooled substrate surface, which was maintained at 15 ^{o}C. Throughout CVD polymerization, a constant argon flow of 20 sccm and a working pressure of 0.5 mbar were maintained. The pyrolysis temperature was set to be 700 ^{o}C and sublimation temperatures were between 90-110 ^{o}C under these conditions. CVD polymerization spontaneously occurred on samples placed on a rotating, cooled sample holder.

Surface characterizations. Film thicknesses were measured using a multi-wavelength rotating analyzer ellipsometer (M-44, J. A. Woollam) at an incident angle of 75°. The data were analyzed using WVASE32 software. Thickness measurements were recorded by fitting the ellipsometric psi and delta data with An = 1.65, Bn = 0.01 for polymer **15** and An = 1.76 and Bn = 0.01 for polymer **2** using a Cauchy model and software module integrated with the system. SFG spectra were recorded by using a pulsed visible laser beam and a tunable pulsed infrared beam that are overlapped spatially and temporally on sample surfaces at incident angles of 60^{o} and 45^{o}, with pulse energies of ~200 and ~100 μJ, respectively. Unless otherwise specified, all SFG spectra were recorded by ssp (*s*-polarized sum frequency output, *s*-polarized visible input, and *p*-polarized IR input) polarization combination and were normalized by the intensities of input visible and IR beams. The details of SFG setup and experimental geometry were detailed elsewhere.[12,13]

Curing process and tensile stress test. SAB process was performed by first coating substrates with polymer **1** and **2.** After coating, samples were brought into contact, and then were placed in oven at 140 ^{o}C for 3 hr. Resulting samples were tested and stored at room temperature (20 ^{o}C). UV/ozone bonding was performed by using a UVO-cleaner (model 342, Jelight Co.) treating the substrates for 30 min. The resulting samples were then cured at 120 ^{o}C for 20 min. Oxygen plasma bonding was performed

by using a plasma etcher (SPI Plasma-Prep II, SPI Supplies/Structure Probe, Inc.). Treatment was done by using 10 W energetic oxygen plasma under 200 - 300 mTorr pressure for 30 sec. The plasma-treated samples were then cured at 60 ^{o}C for 10 min or 120 ^{o}C for 10 min. For all samples, tensile stress was tested using a Bionix 100 mechanical tester (MTS, Co.) equipped with a 10N load sensor. Samples were prepared in a cross-section area of 10 mm x 10 mm, and the measurement was recorded at a displacement rate of 0.05 mm/min.

5.2 Mechanical Test and SFG Characterizations

In a typical bonding experiment, polymers **15** and **2** have been deposited via CVD polymerization on different substrates and adhesion was measured using a standard tensile stress experiment (Table 5.1). For bonding, a substrate coated with either polymer **15** and a substrate coated with polymer **2** were brought into conformal contact without applying additional pressure. The contacting samples were then placed in a 140°C oven for at least 3hr and adhesion was tested using a Bionix 100 mechanical tester (MTS, Co.) equipped with a 10N load sensor. For many of the tested substrate combinations, very high bonding strengths were measured. When bonding two PDMS substrates coated with either polymer **15** or **2**, tensile stresses as high as 2.44±0.15 MPa were measured, which is identical to the fracture strengths of PDMS. Accordingly, rupture consistently occurred within one of the PDMS substrates and not at the bonding interface. Similar results were obtained, when PDMS was bonded to stainless steel, silicon, or glass. When using the dry bonding approach to seal PDMS to polytetrafluoethylene (PTFE, Teflon), bonding strengths averaged 1.21±0.35 MPa, which is lower than the values obtained for the earlier discussed samples, but still higher than bonding data obtained without reactive coatings or UV/ozone activated bonding, which was included in the study as gold standard.

TABLE 5.1
EXPERIMENTAL TENSILE STRESS DATA

Method	Material	Bonding Strength (MPa)
SAB[a]	PDMS - PDMS	> 2.44±0.15[b]
SAB[a]	PDMS - PTFE	1.21±0.35
SAB[a]	PDMS - Stainless Steel	> 2.44±0.15
SAB[a]	PDMS - Silicon Wafer	> 2.44±0.15
SAB[a]	PDMS - Glass	> 2.44±0.15
SAB[a]	PDMS - Gold	> 2.44±0.15
Physical contact	PDMS - PDMS	0.02±0.11
Heat (140 ^{o}C)	PDMS - PDMS	0.19±0.09
UV/Ozone	PDMS - PDMS	0.78±0.08
Oxygen Plasma (cured at 120 ^{o}C)	PDMS - PDMS	2.34±0.27
Oxygen Plasma (cured at 60 ^{o}C)	PDMS - PDMS	1.15±0.18

[a] CVD coatings of **15** and **2** were used as examples.
[b] Fracture strength of PDMS was 2.44±0.15 MPa compared to 2.24 MPa reported in *Polymer Data Handbook* (by James E. Mark, **1999**)

Based on a series of control experiments with CVD coatings that had different side groups, we attributed the high bonding strengths to covalent binding *via* imine bonds formed between CHO and CH_2NH_2 groups of the polymer coatings To further elucidate the underlying mechanism of the bonding process further, we used sum frequency generation (SFG) spectroscopy. SFG provides details about the interface between two polymers and is well suited for investigating the adhesion layer formed between the two substrates. When a PDMS substrate coated with polymer **15** is initially brought in contact with a quartz substrate coated with polymer **2**, characteristic signals of the primary amino groups of polymer **15** at 1637 and 3330 cm^{-1} (Figure 5.2a and 5.2b) as well as

characteristic C=O stretches (Figure 5.2c) of the aldehyde groups of polymer **2** were detected. Prior to exposure to elevated temperatures, the complementary chemical groups continue to co-exist. After the substrate temperature is raised to 140 ºC, however, both amines and aldehyde groups are simultaneously consumed as indicated by the disappearance of the characteristic signals at 1637 cm^{-1}, 3330 cm^{-1} (C-N and C-H stretches of polymer **15**) and 1725 cm^{-1} (C=O stretch of polymer **2**). Interestingly, these effects were not observed, when the substrates were brought in contact without heating (Figure 5.2a) or when one coating alone was heated (Figure 5.2c) suggesting that the observed changes in the SFG spectra indeed cause the bonding results. Because SFG can further provide information about the relative orientation of interfacial chemical groups, we attempted to verify that the functional groups essential for bonding are indeed available in optimal configuration at the surface. For this reason, we recorded SFG spectra of polymer **15** by using ssp, ppp, and sps polarization combinations. All spectra were analyzed before bonding. As shown in Figure 5.2d, the spectra confirm the presence of characteristic NH signals at 3330 cm^{-1} and 3385 cm^{-1}. The signal intensity reaches a maximum for the case of ppp polarization combination, suggesting that the majority of NH groups are oriented normal to the substrate surface. This orientation is optimal for bonding.

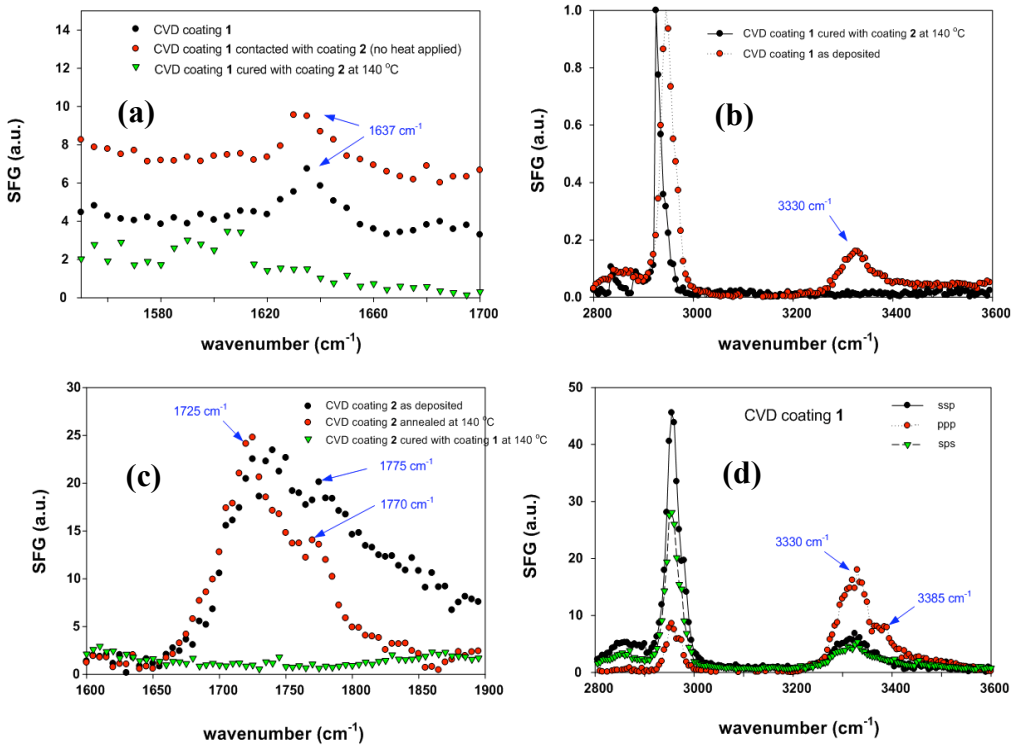

Figure 5.2: SFG characterizations on polymer **15** and **2** before and after bonding. (a) SFG spectra of polymer **15** showing presence of the characteristic C-N peak at 1637 cm^{-1} before bonding, which disappears after bonding. (b) SFG spectra of polymer **15** showing presence of the characteristic -N-H peak at 3330 cm^{-1} before bonding. The signal disappears after bonding. (c) SFG spectra of polymer **2** showing the presence of characteristic C=O peak before bonding. The signal disappears after bonding. (d) SFG spectra by using ssp, ppp, and sps polarization combinations of polymer **15** analyzed before bonding.

5.3 Chemical and Biological Activity of Reactive Coatings within luminal surface of Enclosed Microchannels after Curing Process

To address the question of whether polymer films deposited within microchannels still maintain their typical reactivity after curing process, we conducted a series of immobilization studies. PDMS based microchannels were fabricated using standard procesure described previously.[14] Poly(4-formyl-*p*-xylylene-*co*-*p*-xylylene) (**2**) was deposited onto the resulting PDMS microchannels *via* CVD polymerization process. Commercially available glass cover slips were used as received, and were coated with

poly(4-methanamine-*p*-xylylene-co-*p*-xylylene) (**15**) also *via* CVD polymerization process. After CVD modification, the PDMS microchannels and glass cove slips were brought in intimate contact and were cured by the procedure described in section 5.1 and 5.2. The microchannels were coated with polymers **15** or **2** and were cured in order to seal the mocrochannels prior to immobilization (Figure 5.3). While polymer **2** provides primary amino groups for coupling with activated carboxyl groups (amide formation), polymer **15** has keto groups that can react with hydrazines or hydrazides. To assess the chemical activity of the coating, hydrazide-derived biotin ligand was used in this study. This ligand was chosen because it undergoes nearly quantitative conversion with ketone group. Moreover, the interactions between biotin and streptavidin result in tight confinement of streptavidin on the biotin-modified surface, which can be exploited for visualization of ligand binding. For immobilization, aqueous solutions of the corresponding biotin derivative were filled into the resulting sealed mirochannels. After incubation for 5 min, non-reacted ligands were washed away.

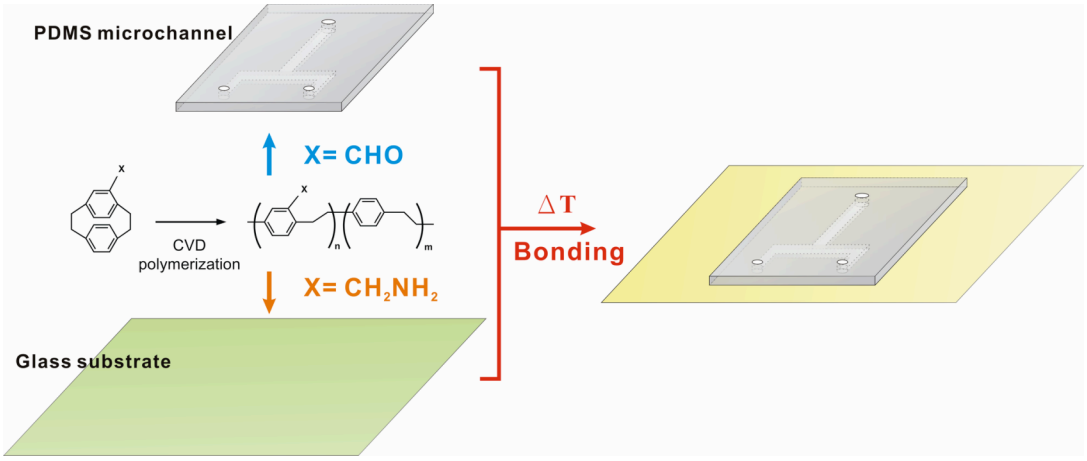

Figure 5.3: Process of dry adhesive bonding on microchannels by using CVD reactive coatings.

To examine the immobilization of biotin ligand within the microchannels, we allowed rhodamine (TRITC) conjugated streptavidin to bind to the biotin-modified surfaces. After thorough rinsing with buffer, the surfaces were visualized by

fluorescence microscopy. Figure 5.4 shows the resulting microchannels that were coated with polymer **2** (on three PDMS luminal surfaces) and polymer **15** (on the bottom glass substrate), and then subjected to the biotin/strepdavidin protocol. Homogenous distribution throughout the entire microchannel was observed, indicating that aldehyde groups were available throughout the entire coating area. In theory, the binding should only occurred on three PDMS luminal surfaces that were modified with polymer **2** but not on the polymer **15** modified glass substrate; however, due to the limits of fluorescence microscopy, one can only access to two dimensional information of the analyzed sample, and only single focal plan can be researched. The limits will prevent us from knowing whether the binding of biotin/streptavidin is specifically occurring on the PDMS luminal surfaces (modified with polymer **2**) or whether the tendency of non-specific streptavindin adsorption would occur on polymer **15** coated glass substrate. In order to address this issue, we further performed a routine that involved two consecutive immobilization cycles, which we incubated the microchannels with atto-655-NHS ester in the first step, allowing covalent amide formation with polymer 15 modified surface (glass substrate, bottom). After thorough rinse with buffer solution, subsequent biotin/streptavidin immobilization was performed according to the previously described procedure. Confocal laser scanning microscopy (CLSM) was used to examine the resulting microchannels in details. As shown in Figure 5.5, three surfaces colored in green were comprised of TRITC-labeled streptavidin, which was immobilized accordingly to the biotin-hydrazide presented on polymer **2** modified surfaces. The red surface in the bottom was formed by covalent immobilization of a red-fluorescent atto-655-NHS ester on the amino groups presented on the bottom surface that was modified by polymer **15**. The CLSM image is showing two clearly distinguishable colors on the luminal surfaces. Based on their characteristic emission wavelengths, the layers could clearly be attributed to the strepdavidin (green color) and atto-ester (red color), respectively. In spite of the additional complexity stemming from the presence of two different surface layers (molecules) immobilized, excellent homogeneity throughout the entire channel, minimal non-specific adsorption between different molecules (or proteins), and excellent bonding strength avoiding any solution leakage during the incubation process. This method lends itself to a simple, dry and clean

process with excellent bonding strength applicable to a wide range of materials, substrates, and geometries. In addition, the deposited reactive polymers contain different functional groups as anchoring sites, providing a multiple, biologically distinct binding platform. This technology may find applications in biosensors, bioassays, microfluidics, and bioMEMS.

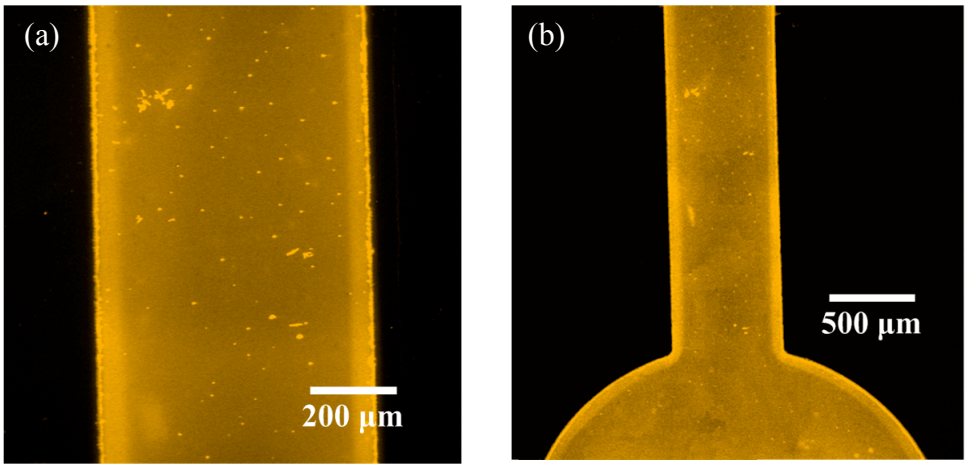

Figure 5.4: Fluorescence micrographs showing the reactivity of CVD polymers **2** on sealed microchannels after dry adhesive bonding process. (a) and (b) are showing different geometries.

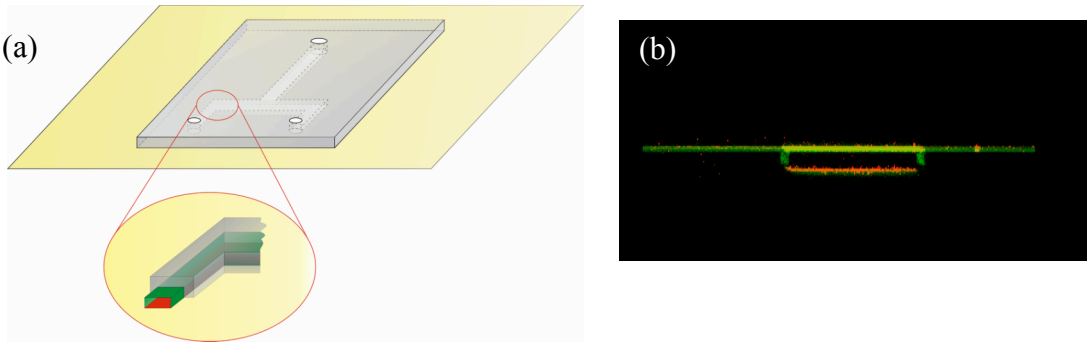

Figure 5.5: (a) Illustrative picture showing the distribution of fluorescence signals according the ligands and dye used in this experiment. Green color comprises of TRITC-labeled streptavidin, which was immobilized accordingly to the biotin-hydrazide presented on polymer **2** modified surfaces. The red surface in the bottom was formed by covalent immobilization of a red-fluorescent atto-655-NHS ester on the amino groups presented on the bottom surface that was modified by polymer **15**. (b) Confocal micrographs is showing according fluorescence image of the sealed microchannel. Image was recorded by using image collection in z-direction.

5.4 Conclusions

We report a novel, solventless bonding approach that relies on a well-defined chemical reaction between two reactive coatings with complementary chemical groups. An important aspect of the dry adhesion technology is that substrates can be stored for extended times prior to bonding eliminating the need for pre-activation immediately prior to bonding (e.g. plasma or UV/ozone treatment). Moreover, bonding results in excellent adhesion of PDMS to a wide range of substrates including PDMS, glass, silicon, stainless steel and PTFE with tensile strengths being higher than those measured for substrates bonded with plasma or UV/ozone treatment. Because this dry adhesion process is (i) essentially independent of the chemical composition of the substrate, (ii) well-defined with respect to the bonding chemistry, (iii) can be controlled on demand, and (iv) can provide a multiple and biologically distinct binding platform, it may have important technological implications for miniaturized bio-analytical systems as well as MEMS

technology, where a substantial diversification of process materials is currently observed.

References

[1] Niklaus, F.; Stemme, G.; Lu, J. Q.; Gutmann, R. J., Adhesive wafer bonding. *Journal of Applied Physics* **2006,** 99, (3).

[2] Bhattacharya, S.; Datta, A.; Berg, J. M.; Gangopadhyay, S., Studies on surface wettability of poly(dimethyl) siloxane (PDMS) and glass under oxygen-plasma treatment and correlation with bond strength. *Journal of Microelectromechanical Systems* **2005,** 14, (3), 590.

[3] Duffy, D. C.; McDonald, J. C.; Schueller, O. J. A.; Whitesides, G. M., Rapid Prototyping of Microfluidic Systems in Poly(dimethylsiloxane). *Analytical Chemistry* **1998,** 70, (23), 4974.

[4] McDonald, J. C.; Duffy, D. C.; Anderson, J. R.; Chiu, D. T.; Wu, H. K.; Schueller, O. J. A.; Whitesides, G. M., Fabrication of microfluidic systems in poly(dimethylsiloxane). *Electrophoresis* **2000,** 21, (1), 27.

[5] McDonald, J. C.; Whitesides, G. M., Poly(dimethylsiloxane) as a Material for Fabricating Microfluidic Devices. *Accounts of Chemical Research* **2002,** 35, (7), 491.

[6] Lahann, J., Reactive polymer coatings for biomimetic surface engineering. *Chemical Engineering Communications* **2006,** 193, (11), 1457.

[7] Lahann, J.; Langer, R., Novel Poly(p-xylylenes): Thin Films with Tailored Chemical and Optical Properties. *Macromolecules* **2002,** 35, (11), 4380.

[8] Lahann, J.; Balcells, M.; Lu, H.; Rodon, T.; Jensen, K. F.; Langer, R., Reactive polymer coatings: A first step toward surface engineering of microfluidic devices. *Analytical Chemistry* 75, (9), 2117.

[9] Elkasabi, Y.; Chen, H. Y.; Lahann, J., Multipotent polymer coatings based on chemical vapor deposition copolymerization. *Advanced Materials* **2006,** 18, (12), 1521.

[10] Rozenberg, V. I.; Danilova, T. I.; Sergeeva, E. V.; Shouklov, I. A.; Starikova, Z. A.; Hopf, H.; Kuhlein, K., Efficient synthesis of enantiomerically and diastereomerically pure [2.2]paracyclophane-based N,O-ligands. *European Journal of Organic Chemistry* **2003**, (3), 432.

[11] Nandivada, H.; Chen, H. Y.; Lahann, J., Vapor-based synthesis of poly [(4-formyl-p-xylylene)-co-(p-xylylene)] and its use for biomimetic surface modifications. *Macromolecular Rapid Communications* **2005,** 26, (22), 1794.

[12] Chen, C.-y.; Even, M. A.; Wang, J.; Chen, Z., Sum Frequency Generation Vibrational Spectroscopy Studies on Molecular Conformation of Liquid Polymers Poly(ethylene glycol) and Poly(propylene glycol) at Different Interfaces. *Macromolecules* **2002,** 35, (24), 9130.

[13] Wang, J.; Chen, C.; Buck, S. M.; Chen, Z., Molecular Chemical Structure on Poly(methyl methacrylate) (PMMA) Surface Studied by Sum Frequency Generation (SFG) Vibrational Spectroscopy. *Journal of Physical Chemistry B* **2001,** 105, (48), 12118.

[14] Chen, H. Y.; Elkasabi, Y.; Lahann, J., Surface modification of confined microgeometries via vapor-deposited polymer coatings. *Journal of the American Chemical Society* **2006,** 128, (1), 374.

CHAPTER 6

DESIGNABLE SURFACE PATTERNS BY USING REACTIVE POLYMER COATINGS

Methods for creating micro- or nanostructured surfaces are of fundamental importance to a range of applications including electronics and biotechnology.[1] For instance, bioanalytical diagnostic devices, such as DNA or protein arrays,[2,3] artificial substrates to mitigate cell-growth regulation,[4] or next-generation micro/nanofluidic systems[5-7] will require precisely structured surfaces.[8,9] It can be expected that further progress in these and other areas of biotechnology will continue to fuel the need for simple and scalable surface structuring methods that result in both, topologically and chemically defined surfaces. Over the past decade, extensive efforts have been made to create topological surface patterns using either lithographical methods on the basis of light,[10] electron[11] and ion beams,[12] X-rays,[13] or atoms[14] as well as printing methods, such as dip/pen lithography,[15] patterning via scanning probes,[16] imprinting lithographies,[17,18] or soft lithography.[19,20] The latter comprises an arsenal of methods, such as microcontact printing,[21] replica moulding,[22] microtransfer moulding,[23] micromoulding in capillaries,[24] solvent-assisted micromoulding,[25] capillary force lithography,[26] which all rely on the use of elastomeric stamps or replica structures to transfer material from a solution onto a surface. Patterned substrates created using shadow masks included a range of different materials, such as semiconductors,[27-29] organic metals,[30] polymers,[31] biomaterials[9] or cells.[32-34]

In the past, we used chemical vapor deposition (CVD) polymerization to deposit *reactive coatings* on the luminal surface of PDMS-based microchannels.[35] In addition to being compatible with the requirements of biological assays, these coatings provide a designable interlayer that is stable under the conditions of bioassays.[35] The *reactive coatings* are based on polymers known as functionalized poly-*p*-xylylenes, which

establish interfaces equipped with chemically reactive groups that can be selected from a variety of different chemical species, including amines, alcohols, activated carboxylic acids, and anhydrides. *Reactive coatings* have been useful for immobilization of biomolecules,[36,37] planar cell and protein patterning,[38] and for patterning of polymer brushes.[39,40] More recently, a photodefinable polymer, poly[4-benzoyl-*p*-xylylene-co-*p*-xylylene] (PPX-CO-Ph), was prepared by CVD polymerization and was used for confinement of hydrogel elements[41] and protein patterns.[42] This polymer has the potential to enable light-induced crosslinking of molecules in close proximity to the photoreactive surface. Although spatially controlled surface modification of CVD coatings via microcontact printing has been demonstrated in the past, patterning in complex geometries, such as three dimensional, curved surfaces, remains and yet unsolved challenge. This technological gap exists because the spin-coating technology used in traditional photolithographic processes is not applicable to the curved surfaces of spherical objects. In this chapter, we address this challenge by replacing the spin-coated photoresist with a vapor-deposited, photodefinable polymer coating. To prove this concept, we fabricated microstructured colloids with a wealth of surface patterns - including asymmetric and chiral surface structures - that so far were exclusively limited to flat substrates. For instance, this high-throughput method can yield surface-structured colloidal particles at a rate of about 10^7 to 10^8 particles per operator per 1 day.[43] Equipped with spatially defined binding pockets, colloids can engage in programmable interactions leading to directed self-assembly. The ability to create a wide range of colloids with both, simple and complex surface patterns may contribute to the genesis of previously unknown colloidal super-structures and may have important technological implications in a range of different areas including photonic and phononic materials or chemical sensors.

The second method studied in this chapter, the supramolecular nanostamping, (SuNS), is base on previously reported technology[85,86] developed in Stellacci's research group in MIT. It is comprised of three steps: an original master consisting of a patterned monolayer of single-stranded DNA (ssDNA) molecules is immersed in a solution of complementary DNA sequences (cDNA) suitably 5' modified so to terminate with chemical groups that can bind to a surface. After hybridization the master is brought

into contact with another substrate (secondary substrate). The functionalized cDNA's end binds to the secondary substrate. Upon heating the two substrates, the DNA dehybridizes allowing the two substrates to come apart. The master and secondary substrate obtained contain the same DNA pattern of complementary chemical structure. Crooks' group used force to separate the two substrates[44-46] and has recently shown that cDNA can be synthesized directly on the master.[44] Being a chemical-bond based contact printing method, SuNS has the major disadvantage of needing a new immobilization protocol every time a new secondary substrate/ binding group combination is needed. This is in stark contrast with its overall versatility and robustness. In section 6.2, we will address this challenge by using CVD reactive coatings to provide a general protocol for tethering cDNA onto a wide range of substrates. Poly(4-formyl-*p*-xylylene-*co*-*p*-xylylene) (**1**) is used as a model polymer to prove the concept and is discussed in detail in the according section. This simple, one-step surface modification, in addition to being substrate-independent, offers accurate control of the chemical composition and the architecture of the films, and an excellent adhesion.

On the other hand, based on of our preliminary results[47] as well as results obtained by others,[30,48,49] we hypothesize that chemical and topological surface microstructures can be obtained by masking certain areas of the substrate during chemical vapor deposition polymerization and then depositing the *reactive coatings* only within the exposed areas. Such an approach towards microstructures surfaces, although of intriguing conceptual simplicity, comes with a series of challenges: (1) In CVD polymerization, the deposition of polymers is transport-limited and it is unclear whether the polymer can be deposited within replica structures with micron-scale capillaries. (2) Even though polymer films may be deposited with sufficient homogeneity, reactive groups may not be freely accessible at the interface for further surface modification. (3) The range of available microstructures may be limited to discontinuous, low-coverage features obtainable by conventional shadow masking approaches.[28,50] (4) Even in these low coverage patterns, the deposition of discontinuous polymer films could interfere with substrate encapsulation by the CVD-deposited polymer film thereby negatively affecting the adhesion between reactive coating and substrate. (5) Potential defects during polymer deposition or lift-off may further contribute to decreased pattern fidelity.[51-53] These

challenges are also discussed and addressed in detail in this chapter.

6.1 Photopatterning Process towards 3-D Surfaces by Using Photodefinable CVD Polymer

The materials in this section are adapted from previously reported data in "Colloids with High-Definition Surface Structures, *Proceedings of the National Academies of Science of the USA* (2007) 104, 27, 11173", by H.-Y. Chen, J.-M. Rouillard, E. Gulari, J. Lahann; and have been slightly modified.

Complex colloidal structures have been a major focus of fundamental and applied research because of their potential applications in photonic[54-59] or phononic[60] band gap materials, chemical sensors,[61] or data storage devices.[62] Many of these applications will require colloids to be organized in non-trivial colloidal crystal structures with exquisite lattice periodicity, such as the diamond lattice. In principle, co-crystallization of binary mixtures of oppositely charged particles can form a range of unusual colloidal crystals.[63-67] An alternate approach relies on the use of colloids that have spatially defined binding patches to encode and ultimately direct lattice organization.[68] Although the potential merits of such an approach, *e.g.*, homogenous colloidal assemblies and potentially superior optical properties, have been widely recognized,[68,69] successful experimental implementation has been hampered by the limited availability of suitable surface modification protocols for colloidal particles.[19,32,70-72] This stands in clear contrast to the sizable number of patterning processes that have been developed for flat surfaces,[73] contributing to major technological breakthroughs in electronics and biotechnology.[74]

Recently, chemical vapor deposition (CVD) polymerization, a solventless coating process, which relies on the deposition of reactive coatings made of functionalized poly-*p*-xylylenes, has been developed as a flexible surface modification approach.[75] Reactive coatings have been used to prepare polymer films with a wide range of functional groups including photoreactive groups on various substrate materials and

geometries.[42,47,75,76] Most importantly, the CVD technology is not intrinsically limited to flat substrates, but can – at least in principle – be equally applied to curved surfaces.

To generate microstructures colloidal particles we pursued a route that uses solventless deposition of a photoreactive polymer coating onto colloidal particles followed by light-directed surface modification. As shown in Figure 6.1, microstructured colloidal particles were fabricated by a two-step procedure: (*i*) Coating of the colloids with a photodefinable polymer, poly[4-benzoyl-*p*-xylylene- *co*-*p*-xylylene], *via* chemical vapor deposition polymerization;[41,42] and (*ii*) spatially controlled surface reaction of the photoreactive coatings using a highly parallel projection lithographic patterning step. The rationale for selecting poly[4-benzoyl-*p*- xylylene-*co*-*p*-xylylene] as base coating was that this CVD-based reactive polymer coating forms homogeneous interlayers on curved surfaces while providing photo-reactive chemical groups for further surface modification.[41,42]

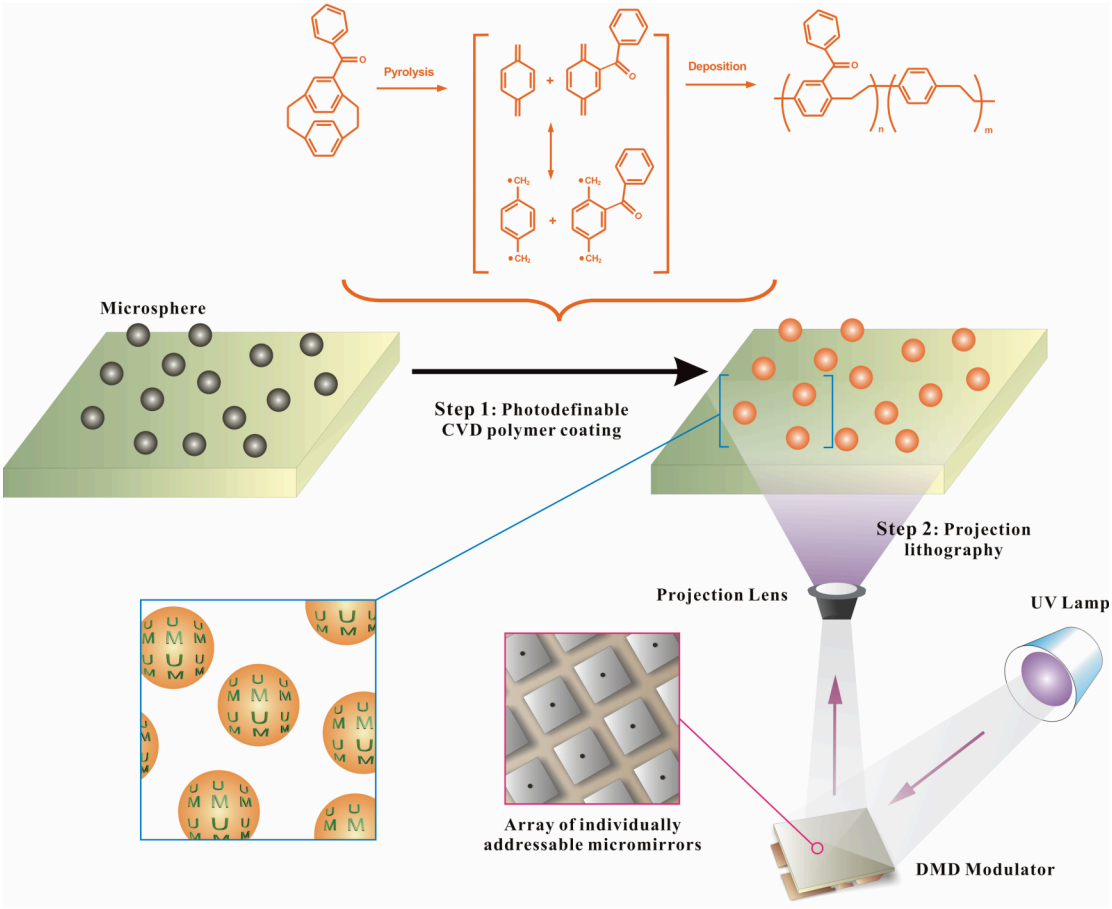

Figure 6.1: Schematic description of the 3D microstructuring technique. The method comprises two process steps: deposition of the photodefinable CVD coating (step 1) and subsequent projection lithographic rendering (step 2).

6.1.1 Methods

CVD Polymerization. Poly[4-benzoyl-*p*-xylylene-co-*p*-xylylene] was synthesized via CVD polymerization.[41,42] The starting material, 4-benzoyl[2.2]paracyclophane, was sublimed under vacuum and converted by pyrolysis into the corresponding quinodimethanes, which spontaneously polymerized upon condensation to the substrate surface. A HPR-30 mass spectrometer (Hiden Analytical, U.K.) was connected to the

deposition chamber for in situ analysis. Mass spectra were recorded at 1000 μA emission and 70.0 V electron energy using a faraday detector scanning from 100 g/mol to 500 g/mol. A constant argon flow of 20 sccm was used as the carrier. Sublimation temperatures were kept at 120 °C followed by pyrolysis at 800 °C. Subsequently, polymerization occurred on a rotating, cooled sample holder placed inside a stainless steel chamber with a wall temperature of 120 °C. The coating pressure was 0.2 mbar or below. The exit of the chamber was connected via a cooling trap to a mechanical pump. Both polystyrene and glass microspheres (Polysciences, Inc.) were used in this study as spherical substrates, which were surface modified via CVD polymerization to deposit the photodefinable CVD polymer (poly[4-benzoyl-*p*- xylylene-co-*p*-xylylene]). Sphere radii ranged from 50 μm to 200 μm. To generate contrast during microscopy, some microspheres were coated with a 80 nm thick gold layer.

Projection Lithography. Microstructure blueprints were generated by a custom made projection system (Figure 6.1) consisting of a 1024 x 768 pixels digital micromirror device (DMD, TI-Instruments, TX, USA), a high-pressure mercury light source (350 nm - 450 nm), and a downstream focus lens system (Brilliant Technologies, TX, USA). The projected pixel size is 27.5 μm x 27.5 μm. Microspheres were modified with photodefinable CVD polymer and then were aligned on a glass substrate. Subsequently, the resulting sample was immersed into a ligand solution followed by exposure to a pre-designed pattern (UM, 247.5 μm x 137.5 μm). De-ionized water was used after projection to wash away unreacted ligands.

Self-Organization Experiments. Two pairs of polystyrene microspheres with radii between 50 μm and 60 μm were used to study self-organization. One pair was coated with gold (80 nm thickness, yellow in color) in order to distinguish from a second pair (bare polystyrene, gray in color). After CVD modification, both groups were subsequently immersed into 10 mM biotin-hydrazide/PBS (pH 7.4) solution followed by exposure to a predesigned pattern (square, 55 μm x 55 μm). Subsequent incubation with streptavidin (10 μg/ml, Pierce Biotechnology, Inc) for 90 min was preformed on

gold-coated microspheres only. Finally, both groups were mixed/incubated in PBS (pH 7.4) solution for 90 min. Self-organized colloidal structures were observed by optical microscopy (BX 60, Olympus). In a parallel control experiment, self-assembly of particles without streptavidin was examined.

Multi-Functional Modifications. 355 μm - 425 μm spheres were modified with photodefinable CVD polymer. After CVD coating, samples were exposed to predesigned pattern within 20 mM biotin-PEO dimer solution (Pierce Biotechnology, Inc.) in the first step. De-ionized water was carefully used to wash away unreacted biotin-PEO dimer after projection. The resulting samples were then exposed to a second pre-designed pattern within 2% (w/v) 4-arm poly(ethylene oxide) solution (amine terminated, Aldrich). De-ionized water was used to wash away unreacted poly(ethylene oxide) after projection. For bioconjugation, samples were first incubated with atto-655 NHS ester (50 μg/ml, Fluka) in PBS containing 0.1% (w/v) bovine albumin and Tween 20 (0.02% (v/v)) for 120 min and subsequently rinsed several times with PBS containing 0.1% (w/v) bovine albumin and Tween 20 (0.02% (v/v)). Secondly, the rinsed samples were incubated with incubated with rhodamine (TRITC) conjugated streptavidin (50 μg/ml, Pierce) in PBS containing 0.1% (w/v) bovine albumin and Tween 20 (0.02% (v/v)) for 90 min. Finally, samples were thoroughly rinsed with PBS containing 0.1% (w/v) bovine albumin and Tween 20 (0.02% (v/v)).

Confocal Microscopy. Samples were analyzed by confocal laser scanning microscopy (CLSM) (TCS SP2, Leica Microsystems, USA) on an inverted microscope (DMIRE2, Leica Microsystems, USA). An GreNe laser (wavelength 543 nm) and a HeNe laser (wavelength 633 nm) were used to excite TRITC-labeled streptavidin and atto-655 NHS ester respectively. The emission was confined to 560-595 nm for TRITC-labeled streptavidin and 650-700 nm for atto-655 NHS ester upon observation. Confocal z-stack imaging scanning was performed using a 2.5 μm pixel resolution in z direction.

6.1.2 Results and Discussions

In step 1, *i.e.,* the deposition of a thin photoreactive coating on the surface of the colloids, the starting material, 4-benzoyl[2.2]paracyclophane, is polymerized without the need of solvent, initiator, or any additional additives. In a series of initial experiments, reaction conditions were adjusted to ensure the polymerization shown in Figure 6.1 to proceed with a growth rate of about 0.5 Å/s, as estimated based on *in situ* quartz crystal microbalancing (QCM) analysis. Ellipsometric analysis revealed that polymer films with thicknesses of 60 – 80 nm were deposited under these conditions. With respect to subsequent modification steps, it was important that the photoreactive coatings are chemically well defined and can be deposited without significant loss of functionality. The chemical structure of the deposited polymer films was examined with a combination of adsorption/reflection Fourier transformed infrared (FTIR) and X-ray photoelectron (XPS) spectroscopy and was found to be in accordance with the predicted polymer structure of poly[4-benzoyl-*p*-xylylene-co- *p*-xylylene] as shown in Figure 6.1. Specifically, the FTIR spectra revealed the characteristic carbonyl stretches at 1604 and 1663 cm^{-1}, while XPS survey spectra indicated an average chemical composition of 95.5 atom-% carbon and 4.5 atom-% oxygen, which is in close agreement with the theoretically obtained values of 95.8 atom-% for carbon and 4.2 atom-% for oxygen.[41,42] The high-resolution C_{1s} XPS spectrum of the polymer film can provide further information regarding the chemical fine-structure of the polymer films. The C_{1s}-spectrum shows characteristic signals of aliphatic and aromatic carbon atoms (C-C, C-H, 285.0 eV), carbon atoms in α-position to the carbonyl group (C-C=O, 285.9 eV), carbonyl carbon (C=O, 286.1 eV), as well as a π->π* satellite signal at 291.5 eV, which is characteristic for aromatic poly-*p*-xylylene polymers.[77] It is known from similar systems that the photoactivated carbonyl groups of the polymer are metastable and rapidly react *via* insertion into CH- or NH-bonds.[78] This insertion reaction can be exploited for covalent immobilization of adjunct molecules onto illuminated surface areas.

Once the deposition of the photoreactive coatings on colloidal particles was demonstrated, spatially directed microstructuring became achievable on curved surfaces.

To obtain spatially controlled surface patches on colloids, we selectively illuminated certain areas of previously coated colloids with light at 365 nm using a high-throughput projection technique that has been previously used for *in situ* synthesis of peptides and DNA on microarrays.[2,3,79] Programmable patterns were created using a 1024 pixel x 768 pixel digital micromirror device (DMD, Figure 6.1). While the entire colloids were coated with the photoreactive coating during CVD polymerization, only the areas illuminated with the DMD underwent photochemical conversion of the carbon-oxygen double bond from the singlet ground state into the corresponding triplet state.[80] To obtain the patterned colloids shown in Figure 6.2, a biotin derivative was used as a model molecule because of its established relevance as a biomolecular linker for subsequent biological modification and its high binding affinity towards strepdavidin.[81] To immobilize the biotin-based linker, photoreactive colloids were immersed into an aqueous biotin solution during the photopatterning step. The colloids were then selectively activated via spatially directed illumination with the DMD; resulting in selective immobilization to the exposed surface areas. To visualize the micropatterns, the surface modified colloids were further incubated with TRITC-labeled strepdavidin, which has been shown to selectively bind to surface areas that present biotin ligands.[39] Figure 6.2 shows typical examples of colloids coated with photoreactive CVD coating and modified via projection lithography. Both, the "UM" patterns shown in Figure 6.2a and 6.2b as well as the stripe patterns (Figure 6.2c), demonstrate high selectivity of strepdavidin towards active binding patches, *i.e.*, the illuminated areas. The 3-D confocal laser scanning microscopy (CLSM) images further reveal high contrast as indicated by precise contour lines between pattern and unmodified areas, even for the smallest colloids with a radius of 50 μm.

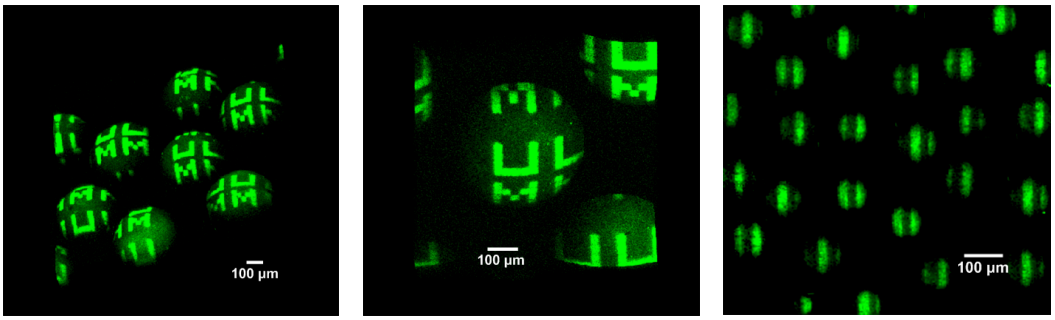

(a) (b) (c)

Figure 6.2: High-precision microstructuring of colloids. 3-D CLSM micrographs of designer colloids obtained by spatially controlled photoimobilization of biotin and subsequent binding of TRITC-strepdavidin. (a) and (b) are showing "UM" patterns with different magnification polystyrene microspheres with radii of 200 µm. (c) Stripe patterns on polystyrene microspheres with 50 µm radii. (All scale bars are 100 µm.)

Based on these findings, several aspects of these results are noteworthy. (*i*) High pattern fidelity and excellent contrast are observed suggesting efficient conversion of the photoactive groups in the exposed areas only. (*ii*) A range of different patterns has been created demonstrating that patterns can be arbitrarily chosen. This is in clear contrast to the currently existing methods for patterning of colloids, which are all subject to constrains imposed by the patterning technique itself. (*iii*) High-resolution patterns can be created on spheres with different radii. Particle radii of the examples shown in the Figure 6.2 range from 50 to 200 µm. Because CVD coatings can be conformally deposited on sub-micron features without loss of topological information,[82] the lower resolution of the 3D printing process is not limited by the CVD step, but is defined by the photopatterning process, and more specifically, by the maximum resolution of the DMD. In this study, a DMD with a maximum resolution of 27.5 x 27.5 μm^2 pixels was used. It is important to recognize that this is not a fundamental limit but rather a limit imposed by the available optics in our laboratories. Commercially available projection lithography instrumentation can result in pixel sizes as small as a few microns square;[83,84] suggesting that the proposed approach will have significant potential for covering a major size range

of colloidal particle science ranging from hundreds of microns down to the single-digit microns regime.

With the selective modification of colloidal surfaces demonstrated, the focus of our study shifted towards fabrication of colloids with controlled binding sites, which can act as precisely designed binding pockets for programmable self-assembly. If colloids were indeed equipped with sticky binding pockets, this could manifest an important step towards the design of building blocks for programmable colloidal self-assembly. For proof-of concept, we selected one of the simplest geometries for the binding patch: a 55 x 55 μm^2 square pattern consisting of either biotin or strepdavidin. Two visually distinct groups of equally sized colloids, *i.e.*, polystyrene microspheres (dark) and gold-coated polystyrene microspheres (light), were surface modified using our colloidal patterning technique. Prior to photopatterning, all colloids were coated with a 60 nm thick film of the photoreactive CVD coating. Subsequently, dark colloids were modified with a 55 x 55 μm^2 square patterns of biotin, whereas light colloids were surface-modified to present strepdavidin (Figure 6.3a). Prior to self-assembly, the presence of the binding patches was confirmed by incubating biotin-modified colloids with TRITC-strepdavidin. As shown in Figure 6.3b, well-defined, isolated squares can be observed on the surface of the colloids confirming the successful introduction of the binding patches. Moreover, in accordance with the microstructured colloids shown in Figure 6.2, excellent contrast between modified and unmodified areas was observed.

For the self-assembly experiments, an equivalent number of colloidal particles from both groups was simultaneously suspended in phosphate buffered saline (PBS, pH 7.4) solution for 90 min. During the course of each experiment, the colloids precipitated and self-oriented into a range of different shapes. Based on light microscopy, a total of 123 colloidal aggregates from three independent runs were statistically analyzed. A range of different configurations was identified and colloidal assemblies were categorized in 9 sub-groups as shown in Figure 6.3c. As anticipated, the by far largest fraction of colloidal assemblies comprised the “heterozygote” AB couples consisting of a single biotin-modified polystyrene colloid (A) and a single strepdavidin-modified gold colloid (B). The large abundance of the AB configuration suggests the dominance of specific

interactions between the complementary biotin and strepdavidin binding patches. The AB fraction was more than twice as large as the next largest fraction consisting of AA couples. In addition to AA assemblies, a number of aggregated structures were also observed during the experiment, which may be attributed to non-specific interactions. We further confirmed these results with a control experiment, in which colloids that were modified with the photoreactive polymer plus biotin, but lacked strepdavidin, were allowed to self-assemble in the same fashion. *S*pecific biotin/strepadvidin interactions were excluded in this experiment. In the control experiment, the AB configurations were not significantly different from AA configurations indicating the absence of the specific biotin/strepdavidin interactions. Overall, the predominance of AB assemblies was highly significant for the encoded self-assembly as compared to the control group.

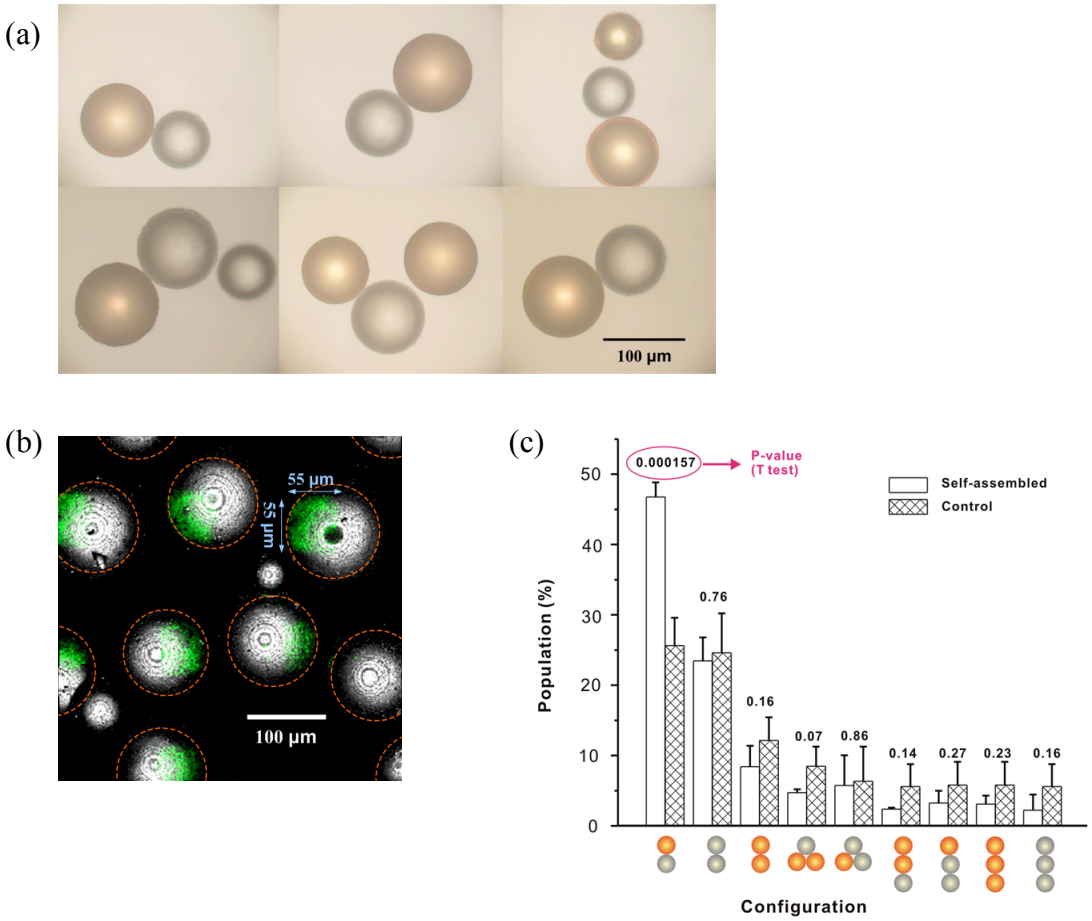

Figure 6.3: Self-organization of microspheres. (a) Micrographs showing self assembly of gold coated microspheres (light, streptavidin modified) with polystyrene microspheres (dark, biotin modified). (b) Patterns used for studying self assembly. Green areas denote fluorescence signal detected by CLSM. (c) Configuration distribution of self-assembled microspheres; the number on top denotes the P-value from T test, showing the self-assembled pairs (first configuration) is significantly different (P-value of 0.000157) than its control group. (In (b) orange dot lines are drawn to guide the eye; all scale bars are 100 µm.)

While simpler patterns, such as the line pattern shown in Figure 6.2c, are, at least in principle, also obtainable by other techniques,[19,32,71,72] we wanted to demonstrate the applicability of our 3D photopatterning technique to more complex patterns. To further extend the repertoire of surface structures that can be created on curved colloidal surfaces, structures consisting of two different patterns, each made of a different type of

biomolecule were designed. As shown in Figure 6.4a, we approached this challenge with a routine that involved two consecutive photopatterning cycles. After CVD of the photoreactive coating onto the colloidal surfaces, an initial photopatterning step resulted in a 110 μm x 137.5 μm green U pattern. These patterns were comprised of TRITC-labeled streptavidin, which was immobilized according to the previously described protocol. In a subsequent step, the red M pattern (110 μm x 137.5 μm) was formed by light-directed photoimmobilization of an amino-terminated *star*-polyethylene glycol. The resulting amino-functionalized surface areas supported covalent immobilization of a red-fluorescent atto-655-NHS ester. Confocal laser scanning microscopy (CLSM) was used to examine the resulting colloids in details. As shown in Figure 6.4b, two independent microstructures were clearly distinguishable on the colloidal surfaces. Based on their characteristic emission wavelengths, the structures could clearly be attributed to the strepdavidin (green color) and atto-ester (red color), respectively. In spite of the additional complexity stemming from the presence of two different surface patches, excellent pattern fidelity, minimal cross-talk between different dyes, and excellent particle-to-particle reproduction were observed. To the best of our knowledge, this type of multifunctional colloids has never been observed before. Based on a relatively simple cascade of process steps, we were able to demonstrate not only the accessibility of precisely controlled, complex surface patches, but to establish a simple access route to multifunctional colloids. This method lends itself to the simple fabrication of colloids with unusual surface patterns, including asymmetric particles. In fact, the particles shown in Figure 6.4b do not have an axis of symmetry and are therefore chiral.

In addition to the controlled fabrication of a series of identical colloids with multiple, biologically distinct binding patches, parallel fabrication of multiple types of distinct colloids is of specific interest to a range of different applications, such as biosensors. Using our 3D patterning approach, a large number of individually customized colloids could, in principle, be prepared simultaneously. However, individual addressability of each single colloid becomes imperative. Using a protocol similar to the one established for multifunctional colloids (Figure 6.4a), we created an array of colloids with two distinct structures: a red square and a green cross (both 137.5 μm x 137.5 μm in size). Figure 6.4c shows a 3 x 3 array of colloids. In this array, four colloids were modified

with a red square, while four other colloids were surface-structured with green crosses. The colloid located in the upper right corner was intentionally not modified to demonstrate independent addressability and designability. The resulting 3x3 array has resemblance with a miniaturized game board. To generate the colloidal assembly shown in the confocal micrograph of Figure 6.4c, only two consecutive photopatterning cycles were needed. Again, both pattern fidelity and reproduction were superb and were not compromised by the use of multiple photopatterning and washing steps.

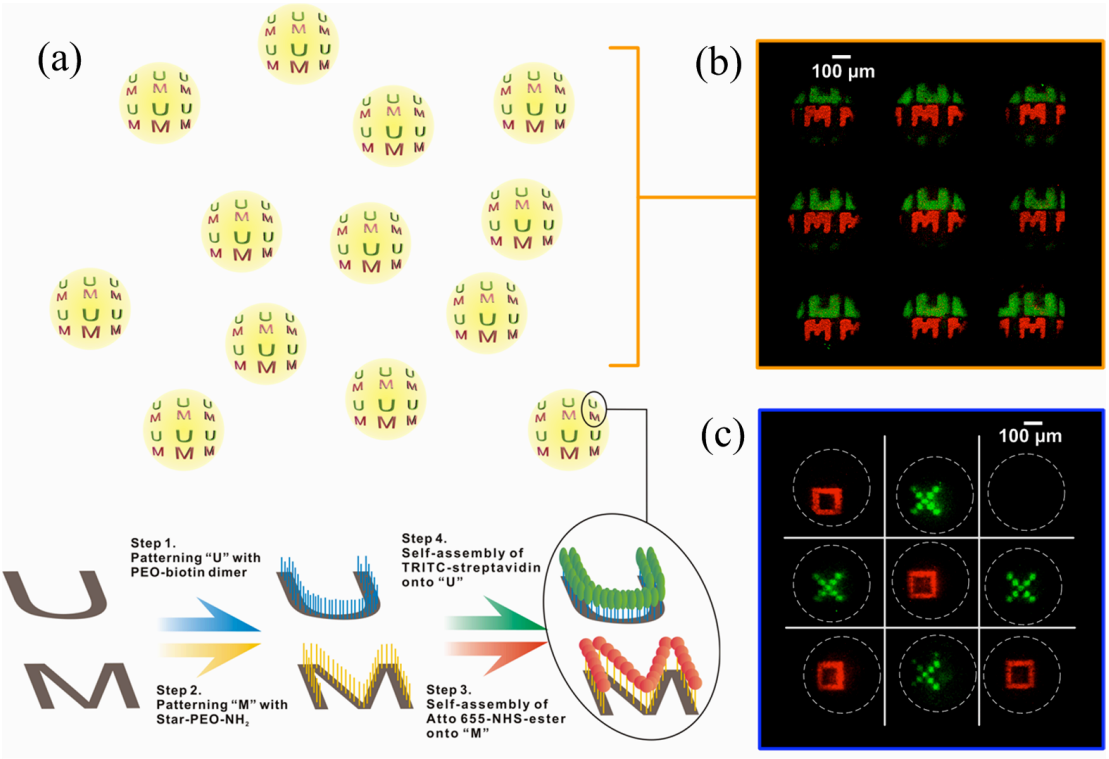

Figure 6.4: The 3-D microstructuring technique can result in colloids with multi-functional surfaces. (a) Experimental approach used for immobilization of multiple (bio-)molecules to create two specific patterns. ("green U" and "red M"). (b) 3-D CLSM micrograph of close to identical colloids modified with two different proteins according to the process described in (a). (c) 3-D CLSM micrograph of 9 colloids with distinct surface modifications fabricated through parallel processing using two process cycles; lines are drawn to guide the eye. (All scale bars are 100µm.)

While significant attention has been given in the past to controlling sizes and shapes of colloids, much less is known about the precise engineering of colloidal surfaces. It was our intent to design colloids with microstructured surfaces that rival their flat substrates with respect to pattern precision and quality. Because traditional spin-coating technology used during photolithographic processing is intrinsically limited to flat substrates, we replaced the spin-coated photoresist with a vapor-deposited, photodefinable polymer coating. These coatings were applied as ultra-thin, homogeneous films on curved surfaces and supported high-precision microstructuring of colloidal particles with radii between 50 and 200 microns. These findings mark an important progress, because well-established lithographic processes, such as projection lithography used in this study, can now be extended to the curved surfaces of spherical objects. With the concept of colloidal surface patterning demonstrated, future research may need to be directed towards fine-tuning binding affinities and patch geometries to yield optimal interactions during self-organization and towards extending the operative particle size ranges from tens and hundreds of microns down to the sub-micron regime.

Compared to the limited range of surface-structured colloids available prior to this study, this approach establishes a shift in paradigm with respect to ease of fabrication as well as variability and complexity of available surface motifs. Finally, the technology relies on flexible surface chemistries for surface modification and is therefore compatible with a wide range of different surface markers. This feature may provide access to colloids with delicate balances between repulsive and attractive surface interactions, which are believed to play an essential role in programmed self-assembly of next-generation optoelectronic materials.[68]

6.2 Supramolecular Nanostamping (SuNS) Process by Using Formyl Functionalized CVD Polymer

The materials in this section are adapted from previously reported data in "A generic approach towards nanostructured surfaces based on supramolecular nanostamping on reactive polymer coatings, *Advanced Materials* (2007) accepted, in press", S. Thévenet, H.-Y. Chen, J. Lahann, F. Stellacci; and have been slightly modified.

The previously reported method, Supramolecular NanoStamping (SuNS),[85,86] comprised of three steps, shown in Fugure 6.5. An original master consisting of a patterned monolayer of single-stranded DNA (ssDNA) molecules is immersed in a solution of complementary DNA sequences (cDNA) suitably 5' modified so to terminate with chemical groups that can bind to a surface. After hybridization the master is brought into contact with another substrate (replica). The functionalized cDNA's end binds to the replica. Upon heating the two substrates, the DNA dehybridizes, allowing the two substrates to come apart. The master and replica obtained contain the same DNA pattern of complementary chemical structure. Crooks' group used force to separate the two substrates[44-46] and has recently shown that cDNA can be synthesized directly on the master.[44]

Being a chemical-bond based contact printing method, SuNS has the major disadvantage of needing a new immobilization protocol every time a new secondary substrate/binding group combination is selected. This is in stark contrast with the overall versatility and robustness of the process. In this section, we report a new approach to generalize a substrate-independent stamping technique by using supramolecular nanostamping (SuNS) process. It relies on functionalizing surfaces with reactive polymer coatings *via* chemical vapor deposition (CVD) polymerization used to modify a wide range of different substrates with a series of different functional groups, including amines, active esters, anhydrides, alkines, aldehydes, or ketones. Using a modified Gorham process, the CVD polymerization uses substituted [2.2]paracyclophanes as starting

materials and results in ultra-thin, conformal polymer coatings. CVD modified substrates have been used for immobilization of proteins or sugars and have been spatially modified by μCP as well as photolithographic methods in the past. This simple, one-step surface modification, in addition to being substrate-independent, offers accurate control of the chemical composition and the architecture of the films, and an excellent adhesion. Because the reactive coatings can exhibit a variety of chemically reactive groups, cDNA can be tethered to the surface in a variety of manners. In the scope of this article we focused on one chemistry for the attachment of DNA, using poly(4-formyl-*p*-xylylene-*co*-*p*-xylylene) that links to 5' amine modified cDNA by forming an imine bond. The aldehydefunctionalized coating was deposited on glass, silicon, poly(dimethylsiloxane) (PDMS), poly(methylmethacrylate) (PMMA), and polystyrene (PS), as previously reported.[86]

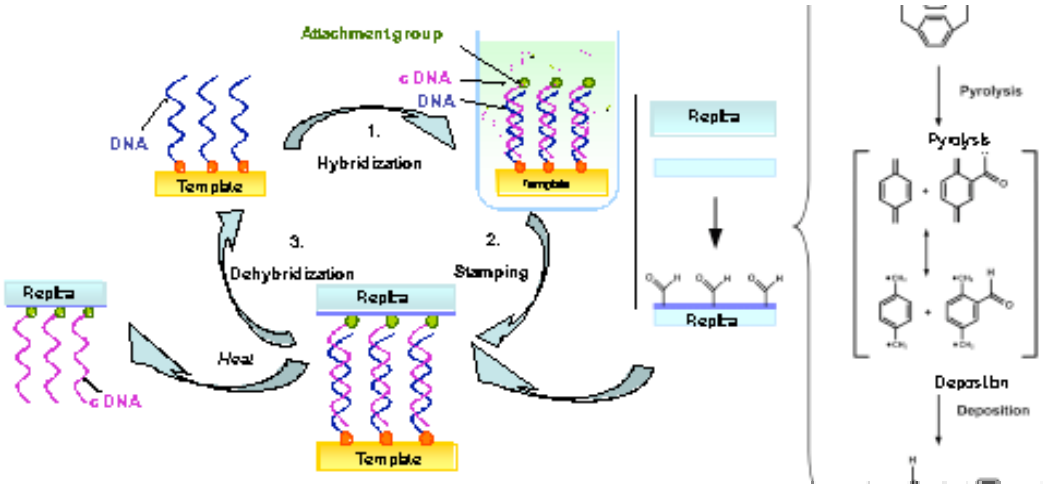

Figure 6.5: Schematic drawing showing SuNS's working principle. The right scheme shows the approach used in this paper to achieve a substrate-independent stamping technique.

The chemical structure of the polymer coating has been confirmed by X-ray photoelectron spectroscopy (XPS) and grazing angle Fourier transformed infrared spectroscopy (FTIR) to be (i) independent of the substrate used and (ii) in agreement with the previously reported data.[87] Specifically, the presence of aldehyde groups was confirmed by FTIR stretches at 1688 and 2734 cm^{-1} and a signal at 287.9 eV in the high-resolution C_{1s} spectrum. The poly(4-formyl-*p*-xylylene-*co*-*p*-xylylene) coatings were 50 – 70 nm thick, as determined by ellipsometry.

To prove that different substrates coated with the same polymer could be stamped on with the same approach we prepared masters consisting of evenly spaced ssDNA lines. The masters were prepared starting from a silicon substrate made using either interference lithography or achromatic interference lithography. In the former case the line pitch was 740 nm with 370 nm thick silicon oxide lines. In the latter case the pattern pitch was 100 nm with 50 nm silicon oxide lines. The top part of the lines was gold coated through shadow evaporation (see experimental). A ssDNA (5'modified with hexyl-thiol) monolayer was assembled on the gold layer by placing the master in a 4 µM DNA solution for 4 days. Throughout this paper DNA strands composed of 50 bases

were used. These masters were used to stamp onto silicon, quartz, PS, PMMA, and PDMS, all coated with a layer of poly(4-formyl-*p*-xylylene-*co*-*p*-xylylene). Typical results are shown in Figure 6.6. Briefly our stamping procedure consisted of placing a drop of 1 μM 5' hexylamine modified cDNA solution onto the master in a humid chamber for at least two hours. After this period, the master was cleaned and dried and the polymer coated replica, without any additional pretreatment, was brought into contact with the master. A slight pressure was applied and maintained overnight to the substrates, which were kept in a vacuum desiccator. The two substrates were then heated at 90°C to dehybridize the DNA strands, and separated. Detailed procedures are described in the Experimental Section. The printed substrates were imaged using atomic force microscopy (AFM) in tapping mode (Figure 6.6), parallel lines with the correct pitch and with thicknesses varying from 100 nm to 390 nm and from 25 nm to 75 nm were found when printing from the 740 nm-pitch and the 100 nm-pitch masters, respectively. Thickness seemed to vary because of printing conditions (mostly pressure applied) but not because of the substrate used. The printed DNA lines had a height comprised between 3 and 10 nm, showing that the printed DNA lines are made of monolayers not dense enough to force the DNA to stand (in that case the lines would be ~20 nm tall) but also not sparse enough to cause DNA to lay on the substrate. Again, the height of the DNA strands appeared to be independent of the substrate material.

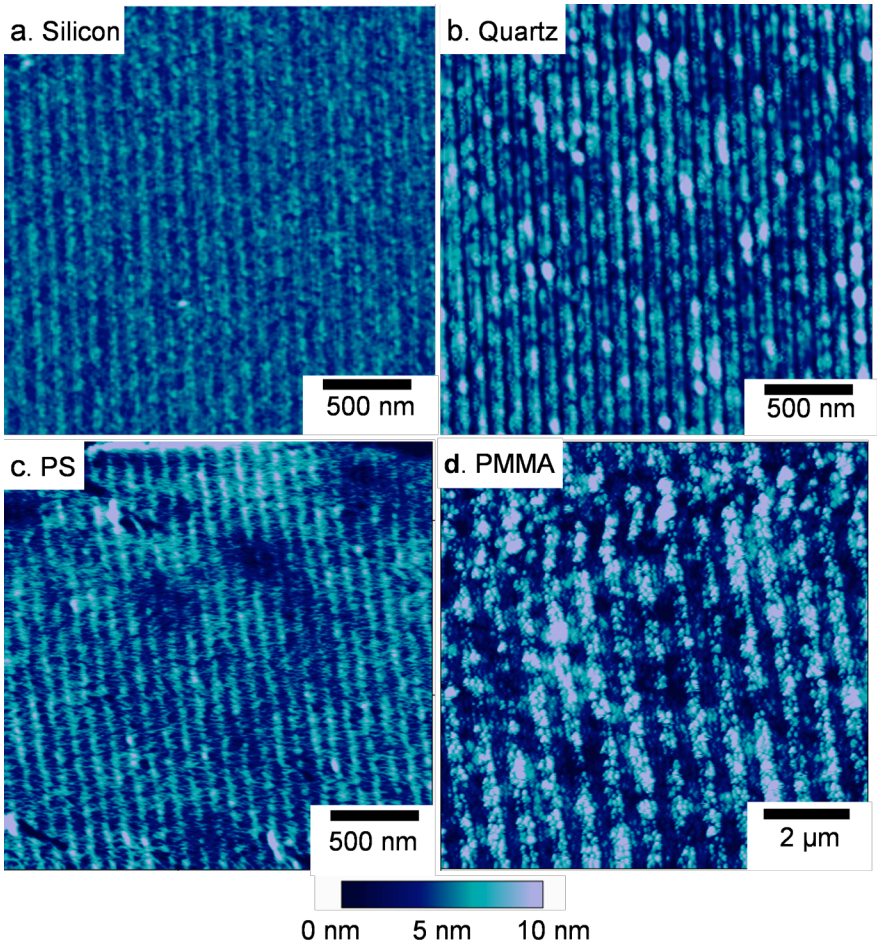

Figure 6.6: Tapping mode AFM images of DNA lines stamped on a variety of substrates. (a) Silicon; (b) Quartz; (c) Polystyrene; (d) Acrylic. The masters used for these printings are gold coated silicon grating patterns with a 100 nm pitch (a-c) and a 700 nm pitch (d). For this set of experiments masters have been used to stamp successively on as many as 7 different substrates.

In order to prove that the lines observed in the AFM images were actually made of ssDNA of a sequence complementary to the original one, we employed a unique characteristic (and advantage) of SuNS: the possibility of reusing a printed replica as master. Only if the stamping process has worked correctly, the printed substrate can be 'inked' with DNA of the original sequence (suitably 5' modified) and reused as master. Specifically we used one of the printed silicon substrates to print onto poly(4-formyl-*p*-xylylene-*co*-*p*-xylylene)-coated PS using the procedure described above.

The results are shown in Figure 6.7. The high pattern fidelity observed in Figure 6.7 corroborates our model, in that the stamped pattern consists of DNA strands of the expected sequence in a conformation that retains binding activity.

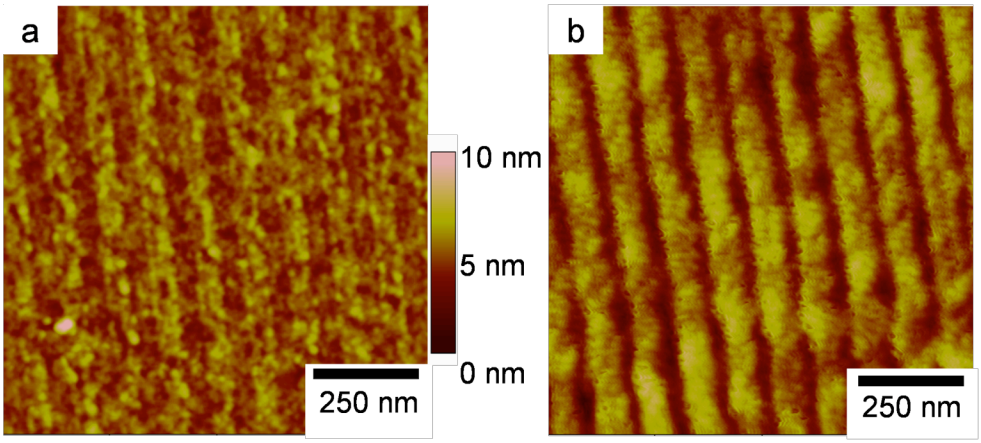

Figure 6.7: Second generation printing. (a) Tapping mode AFM image of a DNA-printed poly(4-formyl-*p*-xylylene-*co*-*p*-xylylene)-coated silicon substrate used as a master (b) Tapping mode AFM image of a polystyrene substrate reprinted from the printed silicon substrate shown in (a).

Further control experiments aiming at demonstrating that the observed AFM patterns were made of ssDNA of the correct sequence were performed using fluorescence microscopy. The masters used in these experiments were silicon substrates photolithographically patterned with 1 μm large gold squares, on which a monolayer of thiolated ssDNA was assembled. These masters were used to print onto poly(4-formyl-*p*-xylylene-*co*-*p*-xylylene)-coated PS and PDMS substrates using the above-mentioned protocol. The stamped substrates were placed in a solution of fluorescently labelled DNA strands of the same sequence as the one present on the master. The hybridized substrates were then imaged with a fluorescence microscope. As shown in Figure 6.8a-b, the correct pattern of squares could be imaged using fluorescence microscopy. Furthermore, the same sample was re-imaged after a dehybridization step, in which the substrate was immersed and cleaned in a hot water solution. The line plot in Figure 6.8b shows that the contrast along one imaging line disappeared after this process.

To further prove that the DNA present on the square was of the correct sequence we placed the printed substrate in a 1 μM solution of fluorescently labelled ssDNA of a sequence that was not complementary to the one originally stamped. As expected in this case, no contrast was observed on the imaged (see Figure 6.8c green line). These experiments clearly prove that only ssDNA of the programmed sequence was printed on the poly(4-formyl-*p*-xylylene-*co*-*p*-xylylene)-modified substrates.

Because the binding chemistry was the same for all the substrates, SuNS's protocols were nearly identical for all the substrates. The only difference was the method used to provide contact between the master and the secondary substrate during the stamping step itself. Substrate's mechanical properties (mainly rigidity) drastically change the way pressure is transferred into good surface-to-surface contact. Hard substrates like silicon and quartz were stamped simply using a mechanical vise adapted with soft PDMS plates. This sometimes leads to overall contact areas limited by the presence of macroscopic roughness or dust particles. Polymeric substrates offer the unique property of allowing for softening with the consequent improvement of conformity to the substrate they are pushed onto. Hence at the beginning of the stamping step we elevated the temperature to 60°C, enabling the secondary polymeric substrate to conform better to the intrinsic roughness of the master's surface, thus increasing the printed area. As for a soft material like PDMS, we gently applied uniform pressure by inflating a balloon placed between the substrate and the upper part of our mechanical vice. As it is inflated, the balloon applies a growing pressure on the substrates starting from the center of the substrates, therefore avoiding the trapping of air bubbles between the samples.

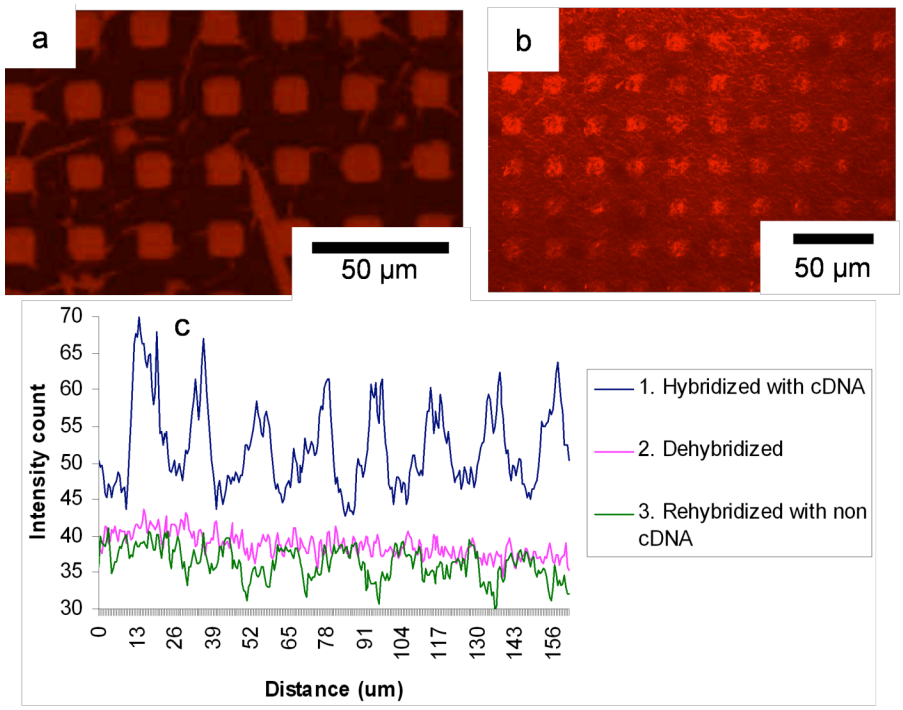

Figure 6.8: Fluorescence microscopy image of a printed polystyrene substrate.

To further demonstrate the versatility of this novel approach, we extended the technique to pre-patterned substrates. Because of the excellent conformal coatings obtained with chemical vapor deposition, reactive coatings can be deposited within confined geometries.[47] In the context of this study, combination with a secondary SuNS printing step can be used to generate hierarchical structures on different length scales. To prove this point, we printed 100 nm-pitch DNA lines onto an array of 200 µm squares spaced 200 µm, obtaining a superimposition of the two patterns as shown in Figure 6.9. PS substrates were coated with poly(4-formyl-*p*-xylylene-*co*-*p*-xylylene) as a square array with a periodicity of 400 µm. Such pre-patterned surface was used as a replica surface for SuNS starting with a 100 nm pitch grating. The stamped surface was hybridized with its fluorescent modified complement. Fluorescence microscopy enabled us to check that the DNA was transferred only in the coated squares (Figure 6.9a), while using atomic force microscopy we could observe the printed patterns in the coated squares (Figure 6.9b) and verify the absence of nanopatterns outside the coated squares.

These data also clearly eliminate the possibility of imprinting (mechanical deformation)[88] as the cause of pattern formation.

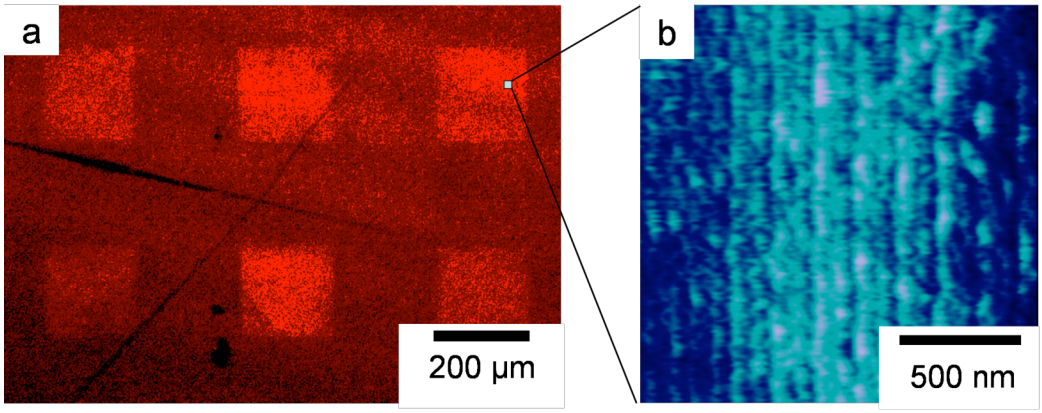

Figure 6.9: Hierarchical printing. (a) Fluorescence microscope image of a printed pre-patterned polystyrene substrate. (b) Atomic force microscope image of the printed pattern inside a square.

6.3 Vapor-Assisted Micropatterning in Replica Structures (VAMPIR) Process

The materials in this section are adapted from previously reported data in "Vapor-Assisted Micropatterning in Replica Structures: A Solventless Approach towards Topologically and Chemically Designable Surfaces, *Advanced Materials* (2007) accepted, in press", by H.-Y. Chen, J. Lahann; and have been slightly modified.

Throughout this study, we have focused on a specific *reactive coating*, poly(4-pentafluoropropionyl-*p*-xylylene-*co*-*p*-xylylene) **21** deposited *via* chemical vapor deposition (CVD) polymerization to proof the concept of vapor-assisted micropatterning in replica structures (VAMPIR, Figure 6.10). However, the same principles should hold for other previously established functionalized poly-*p*-xylylenes containing a wide range of different functional groups, such as amines,[89] aldehydes,[87] anhydrides, active

esters,[38] or alkynes.[90] Prior to CVD polymerization, polydimethylsiloxane (PDMS) based replica structures or stencils designed to generate a desired surface pattern were reversibly sealed onto the substrate. The masked substrate was then placed onto a temperature-controlled stage (15 ºC) inside of the CVD polymerization chamber. Using an adaptation of the commercially exploited Gorham process (Scheme 1b), 4-pentafluoropropionyl[2.2]paracyclophane (**26**) was first sublimed and the resulting vapor was transferred into the pyrolysis zone. Starting materials **26** was synthesized from commercially available [2.2]paracyclophane via one-step synthesis adapting previously established synthesis conditions.[91]

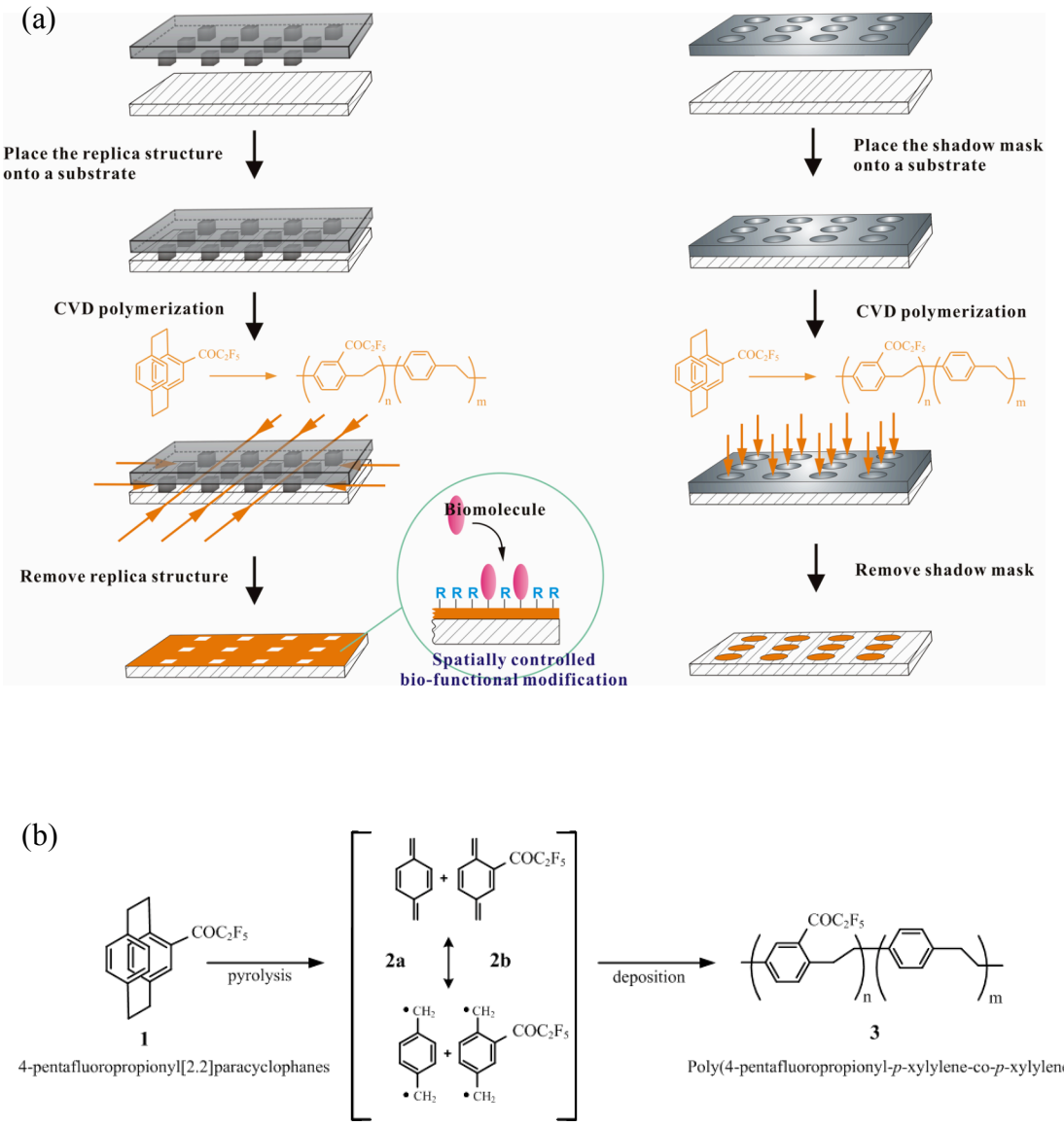

Figure 6.10: (a) Process of vapor-assisted micropatterning using replica structures (left column) as well as shadow masks (right column) during CVD polymerization. (b) Chemical vapor deposition (CVD) polymerization reaction used to deposit poly(4-pentafluoropropionyl-*p*-xylylene-*co*-*p*-xylylene).

6.3.1 Methods

Device fabrication. The replica structures were designed using AutoCAD, and the design was printed on high-resolution emulsion transparencies (40,640 DPI, Photoplot Store). For fabrication of the master, a layer of photoresist (SU-8 2050, MicroChem Co.) was spin-coated at 2000 rpm for 30 s onto a silicon wafer. The wafer was soft-baked at 65 °C for 3 min followed by 95 °C for 9 min, and the wafer was then exposed to UV radiation (404.7 nm, 10 mJ/cm^2) for 4 min to define the desired microstructure from the transparency mask. Post exposure bake was preformed at 65 °C for 1 min followed by 95 °C for 7 min. After removal of the activated photoresist by exposition to a SU-8 developer solution (MicroChem Co.) for 7min with agitation the resulting SU-8 master was cleaned with isopropyl alcohol (IPA), and then was dried with compressed air. The resulting silicon master was placed in a Petri dish and uniformly mixed PDMS prepolymer and curing agent (Sylgard 184, Dow Corning) at a ratio of 10:1 were poured onto the SU-8 master. The PDMS prepolymer was cured at 70 °C for 1 hr. Finally, embossed microgeometries were released from the SU-8 master. The replicated PDMS molds and silicon substrates were brought into contact and the resulting devices were placed onto the sample chamber for CVD polymerization. The fabricated PDMS molds were 75 μm high, 4000 μm long in y direction, and has different width dimension of 150 μm, 100 μm, 50 μm, and 25 μm.

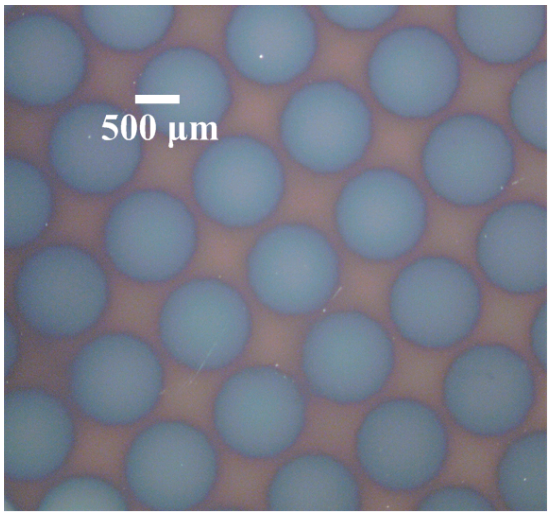

Figure 6.11: Optical image of microstructured surface patterns by using a shadow mask. The image shows a circular pattern of a CVD polymerized poly(4-pentafluoropropionyl-*p*-xylylene-co-*p*-xylylene) on a silicon substrate.

CVD Polymerization. Poly(4-pentafluoropropionyl-*p*-xylylene-co-*p*-xylylene) (**21**) was synthesized via CVD polymerization (Figure 6.10). The starting material, 4-pentafluoropropionyl [2.2]paracyclophane (**26**), was sublimed under vacuum and converted by pyrolysis into the corresponding quinodimethanes **27a** and **27b**, which spontaneously polymerized upon condensation to the substrate surface. A HPR-30 mass spectrometer (Hiden Analytical, U.K.) was connected to the deposition chamber for in situ analysis. Mass spectra were recorded at 1000 µA emission and 70.0 V electron energy using a faraday detector scanning from 100 g/mol to 500 g/mol. A constant argon flow of 20 sccm was used as the carrier. Sublimation temperatures were kept at 70 °C followed by pyrolysis at 670 °C. Subsequently, polymerization occurred on a rotating, cooled sample holder placed inside a stainless steel chamber with a wall temperature of 120 °C. The coating pressure was 0.12 Torr or below. The exit of the chamber was connected via a cooling trap to a mechanical pump. For CVD polymerization, PDMS molds were sealed reversibly to a silicon wafer, which was placed onto the sample holder.

Poly(4-pentafluoropropionyl-*p*-xylylene-co-*p*-xylylene) (**21**): IR (grazing angle of 85°): $\tilde{\nu}$ = 832, 943, 1066, 1140, 1165, 1191, 1232, 1351, 1453, 1497, 1566, 1610, 1714, 2867, 2941, 3039 cm^{-1}; XPS survey: C, 73.6% (76.0% calcd.); O, 5.2% (4.0% calcd.); F, 21.2% (20.0% calcd.); XPS high resolution C_{1s}: -C-H at 285.0 eV 83.0% (84.1% calcd.); -C=O at 288.4 eV, 5.1% (5.3% calcd.); -C-F_2 at 290.9 eV, 5.0% (5.3% calcd.); -C-F_3 at 293.4 eV, 4.7% (5.3% calcd.); π-π* at 291.8 eV, 2.2%.

Surface Characterizations. X-ray photoelectron spectroscopy (XPS) data were recorded on an Axis Ultra X-ray photoelectron spectrometer (Kratos Analyticals, UK) equipped with a monochromatized Al Kα X-ray source. In these experiments, the lens mode was in hybrid, pass energy was set to 160.0 eV, and the aperture was 600 μm x 600 μm for all imaging acquisitions. Elemental maps of fluorine (F_{1s}) and silicon (Si_{2s}) were performed at 689.9 and 150.0 eV respectively with an X-ray power of 150 kW. Thickness profile analysis data were recorded using an single wavelength (532 nm) EP^3-SW imaging ellipsometry (Nanofilm Technologie GmbH, Germany). Both, nulling (four zones) and mapping experiments were performed at an angle of incident of 65°, and a constant n (refractive index) and k (extinction coefficient) value model was used to model the ellipsometric parameters psi and delta. For the mapping mode, data were recorded by an imaging scanner with a lateral resolution of 1 μm at a field of view of about 200 μm x 600 μm. The images were captured using a CCD camera (768 x 572 pixels).

Bio-Functional Modifications. Reaction with biotin ligands followed by binding to streptavidin was used to visualize the resulting patterns. Based on this procedure, samples were incubated in Petri dishes with biotin-hydrazide (10 mM, Pierce) in phosphate buffered saline (PBS, pH 7.4) for 5 min. The surface was then rinsed several times with PBS. After rinsing, devices were incubated with rhodamine (TRITC) conjugated streptavidin (10 μg/ml, Pierce) in PBS containing 0.1% (w/v) bovine albumin and Tween 20 (0.02% (v/v)) for 60 min. On the other hand, streptavidin-conjugated quantum dots (CdSe) (1μM Qdot® 525, Quantum Dot Co.) was also incubated as another set of experiment in order to prove the concept. Both surfaces were rinsed several times with PBS containing 0.1% (w/v) bovine albumin and Tween 20 (0.02% (v/v)). The

resulting samples were then examined by fluorescence microscopy (TE 200, Nikon).

6.3.2 Results and Discussions

During CVD polymerization, polymer growth rates on freely accessible surfaces were estimated to be about 1.0 Å/s based on *in situ* quarz microbalance analysis. The CVD process was further monitored using *in situ* mass spectrometry. Under the conditions reported for CVD polymerization, mass peaks at 104 g/mol and 250 g/mol corresponding to the quinodimethanes **27a** and **27b** were detected. In contrast, no signal was found at 354 g/mol excluding the presence of uncleaved paracyclophane **26**. The latter suggests that the selected process conditions indeed yield quantitative cleavage of the starting material **26**. After completion of the CVD polymerization and subsequent removal of the PDMS molds, a chemically and topologically structured surface was created. Surface features were defined by the deposited polymer footprints (Figure 6.11). Initially, we masked the substrate with a PDMS membrane, which had circular 500 microns openings. Subsequent CVD polymerization resulted in localized islands of ultra-thin polymer films. Similar shadow masks or stencils were previously applied for area-selective deposition using both rigid and elastomeric materials.[30,48,51] While many of these pattern processes are limited to hydrophilic polymers soluble in polar solvents - apolar solvents will swell elastomeric masks -, the solvent-free process described here can be used for both hydrophilic and hydrophobic coatings.

Chemical analysis of the as-deposited polymer films using a combination of X-ray photoelectron spectroscopy (XPS) and FTIR spectroscopy confirmed the proposed structure of poly(4-pentafluoropropionyl-*p*-xylylene-*co*-*p*-xylylene) (**21**). To characterize the resulting polymer films, we utilized infrared reflection absorption spectroscopy (IRAS). The data reveal characteristic bands of the carbonyl stretches at 1714 cm^{-1} and C-F stretches at 1165, 1191, 1232 cm^{-1}. In addition, signals at 2867, 2941, and 3039 cm^{-1} indicative of aliphatic methylene groups (C-H) were also detected.[77] A XPS survey spectrum was acquired for quantitative evaluation of F_{1s}, O_{1s}, and C_{1s}, and the data

indicate 73.6 atom-% carbon, 5.2 atom-% oxygen, and 21.2 atom-% fluorine. These values compare well with the theoretical values of 76.0 atom-% for carbon, 4.0 atom-% for oxygen, and 20.0 atom-% for fluorine. The high-resolution C_{1s} spectrum after curve fitting of the C_{1s} envelope further reveals characteristic signals for aliphatic and aromatic carbon (C-C, C-H) normalized to 285.0 eV at 83.0 % atomic concentration, which compares well with the theoretical concentration of 84.1%. Similarly, carbonyl carbon (C=O, 288.4 eV) at 5.1 % atomic concentration, C-F_2 at 290.9 eV with 5.0 % atomic concentration, and C-F_3 at 293.4 eV with 4.7 % atomic concentration are all in good accordance with the theoretical values. A signal indicating π->π* transitions at 291.8 eV was also found, which is characteristic for aromatic molecules and has been previously reported for similar poly-*p*-xylylenes.[77,92] These findings are in accordance with our earlier work regarding the CVD polymerization of substituted [2.2]paracyclophanes, which typically showed close to theoretical compositions of the resulting functionalized poly-*p*-xylylenes.[77] As shown in Figure 6.11, the spatially controlled CVD polymerization results in homogenous polymer patterns with little variation with respect to shape of individual elements over large surface areas (3 x 3 cm^2). Moreover, pattern fidelity does not appear to be compromised by the lift-off of the PDMS membrane, as indicated by the rather sharp contour lines between masked and unmasked areas. The thickness of the polymer elements can be controlled by the amount of starting material used for CVD polymerization. Typical thicknesses are in the range of 40 to 400 nm. The thickness of the polymer structures shown in Figure 6.11 is 90 nm as determined by imaging ellipsometry.

Next, we examined the stability of the polymer patterns by immersing them in a range of different solvents, including methanol, ethanol, acetone, and chloroform; and studying their chemical structure via IRAS. For all solvents investigated in this study, the polymers were stable and the FTIR spectra before and after solvent exposure were close to identical within the margins of error. Moreover, by using a tape test in conjugation with a visual inspection,[87] we assessed stability of a 50 nm thick patterned polymer film. Again, the patterns showed remarkable stability. Finally, the availability of the pentafluoropropionyl groups was assessed by probing reactivity based on immobilization of fluorescence-labeled model proteins followed by fluorescence imaging. For this reason,

we conducted a series of reaction steps that initially involved the covalent binding of a biotin hydrazide followed by the surface-directed self-assembly of rhodamine-labeled strepdavidin. The fluorescence images reveal high contrast between polymer-coated and masked (uncoated) areas suggesting effective reactivity of the deposited polymer islands. Based on these experiments we concluded that (i) a simple masking of the substrate via PDMS membranes can result in large-scale structuring of surfaces with discontinuous features; and (ii) the technology is equally applicable to a wide range of substrates including silicon, glass, gold, PDMS, or polystyrene. While this simple masking approach may provide a promising access route to spatially confined polymer patterns, the use of membrane-type stencils is still restricted to rather uncomplicated, discontinuous patterns. For larger, continuous features however, the applicability of shadow masks is inherently impractical.[50]

With the feasibility of selective polymer deposition and the stability of the resulting discontinuous polymer thin films demonstrated, we continued our studies by extending the CVD technology to large-coverage replica structures with interconnected topological features, such as more complicated, continuous patterns (Figure 6.10). Replica structures used in this approach are made of PDMS and are fabricated with microcapillaries as topological features. During the first step, the elastomeric replica structure has to be brought in intimate contact with the substrate surface. In the subsequent CVD polymerization step, the vapor-based monomers enter the replica structures and polymerize on vacant surface areas. Figure 6.12 shows results of imaging X-ray photoelectron spectroscopy and imaging ellipsometry for a silicon substrate modified by a continuous 100 x 100 μm^2 grid of *reactive coating* **21**. The polymer patterns were further characterized using FTIR and XPS analysis and were again in accordance with the expected structure of poly(4-pentafluoropropionyl-*p*-xylylene-*co*-*p*-xylylene) (**21**, chemical structure shown in Figure 6.10). The XPS imaging analysis reveals spatially confined distribution of fluorine as indicated by the F_{1s} signal at 689.9 eV. Fluorine is a reporter atom for reactive coating **21**, which contains about 21% fluorine due to its side group functionalization. As seen in Figure 6.12, the fluorine-containing areas unambiguously correspond to substrate regions not masked during CVD polymerization. In contrast, no fluorine was detected on the areas masked during CVD polymerization. A

rather sharp contour line between masked and unmasked areas can be observed resulting in high pattern fidelity. In accordance with these data, only areas that were covered with the PDMS replica structure during CVD polymerization showed detectable amounts of silicon as indicated by the distribution of the Si_{2p} signal at 150.0 eV (Silicon is an indicator of the substrate, but is not present in the reactive coating). Moreover, imaging ellipsometry unambiguously revealed selective deposition in the unmasked areas. As shown in Figures 6.12c and 6.12d, substantial thickness differences, 41 nm in the example of Figure 6.12, can be observed between coated polymer areas and the silicon background. Moreover, the thickness map revealed high pattern fidelity over large-scale surface areas confirming the results obtained by imaging XPS.

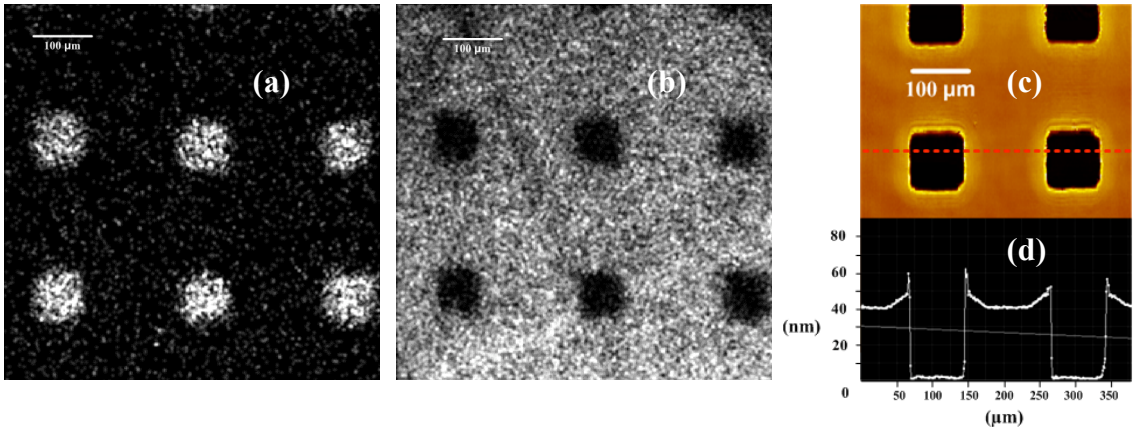

Figure 6.12: Surface patterns of poly(4-pentafluoropropionyl-*p*-xylylene-co-*p*-xylylene) **21** prepared by VAMPIR process. (a) Imaging XPS Si_{2s} elemental map at 150.0 eV. (b) Imaging XPS F_{1s} elemental map at 689.9 eV. (c) Imaging ellipsometry thickness map. (d) A cross-section thickness profile representing thickness data along the red-dot line shown in (c). The replica structure used in this experiment had the following dimensions: 100 µm x 100 µm x 75 µm posts with 150 µm spacing between posts.

To address the question of whether polymer films deposited within micorchannels still maintain their typical reactivity towards corresponding binding partners, we complimented the physico-chemical analysis with a series of immobilization studies. Reactive coating **21** has keto groups that can react with hydrazines or hydrazides in high

yields.[93] We used a model ligand, hydrazide-derived biotin, for immobilization onto the functionalized polymer films. In a subsequent step, the well-known interactions between biotin and streptavidin are used for visualization of surface-immobilized biotin. To examine the immobilization of biotin ligands within the patterns, we allowed both rhodamine (TRITC) conjugated streptavidin and CdSe quantum dots (Qdot® 525) conjugated streptavidin to bind to the biotin-modified surfaces. As anticipated, after biotin immobilization, the subsequently self-assembled strepdavidin was resolved into a range of different pre-designed patterns in Figure 6.13.

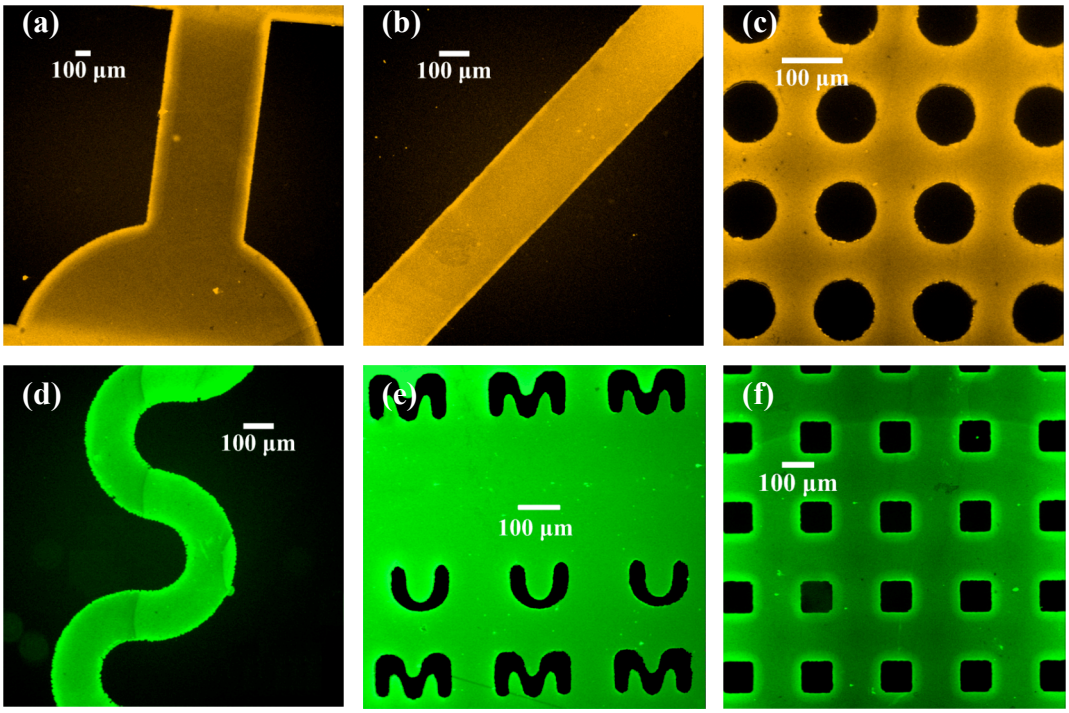

Figure 6.13: Fluorescence micrographs of a range of different surface patterns created through the VAMPIR process followed by immobilization of hydrazide-biotin and self-assembled strpetavidin. (a) (b) (c) are showing TRITC conjugated streptavidin self-assembly on VAMPIR structures. (d) (e) (f) are showing CdSe quantum dots conjugated streptavidin self-assembled onto also VAMPIR structures.

Once the fabrication of microstructured surfaces using CVD polymerization in replica structures was demonstrated, the lower limit of feature sizes accessible with

VAMPIR could be evaluated. We therefore prepared a PDMS replica structure with varying distances between posts resulting in feature sizes of 150 μm, 100 μm, 50 μm, and 25 μm, respectively. The rationale for the choice of dimension was based on the previously reported result that CVD polymers can penetrate 100 μm wide microchannels.[47] Figure 6.14 shows a substrate after VAMPIR-modification analyzed by a combination of imaging XPS, imaging ellispometry, and fluorescence microscopy. The composition map from imaging XPS confirms that silicon (Si_{2s}, 150.0 eV) is only detectable for areas that were masked during CVD polymerization, while the entire polymer footprint is devoid any detectable amounts of silicon as shown in Figure 6.14a. This holds for the entire range of feature sizes from 150 to 25 μm. Correspondingly, fluorine, a representative element for reactive coating **21** was detected only on areas not masked during CVD polymerization. The XPS results were further confirmed by imaging ellipsometry. Thicknesses of the deposited polymer coatings were measured in the center of each region. As expected, the thickness decreased from 49.6 nm measured for the area with 150 μm feature sizes, over 42 nm (100 μm) and 28.7 nm (50 μm), to 7.3 nm measured for the areas with 25 μm wide features. The coating thickness distribution for different feature sizes can be expressed in a relative co-ordinate system.[94,95] Rearrangement of the thickness data in terms of dimensionless thicknesses $\delta(x)/\delta_0$ and width (x/b) - where $\delta(x)/\delta_0$ denotes the ratio of the absolute film thickness at the given point x to that at the open surface, and x/b is the ratio of depth over width of the feature – reveals an uniform behavior. As indicated in Figure 6.15, the dimensionless thicknesses measured for feature sizes ranging from 25 μm to 200 μm, are falling onto a single trend line. This behavior suggests process parameters, but not feature size, to be dominating. This behavior is in accordance with the theoretical studies by Tolstopyatov *et al.*, who found universal thickness distributions for the deposition of unfunctionalized poly-*p*-xylylene in microchannels.[94,95]

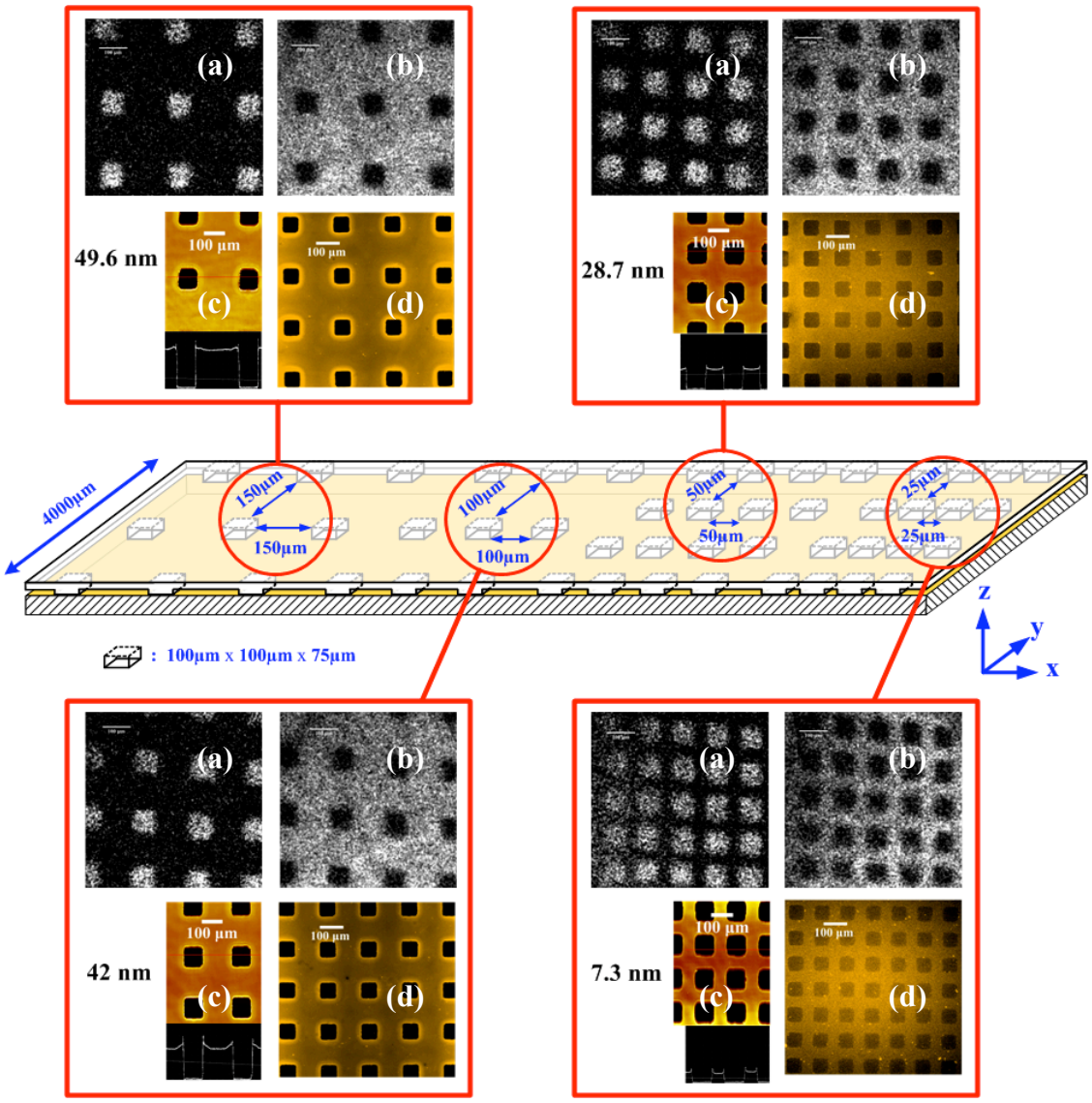

Figure 6.14: Influence of structure diameter on polymer depth during VAMPIR process. (a) Imaging XPS Si_{2s} (150.0eV) elemental map. (b) Imaging XPS F_{1s} (689.9eV) elemental map. (c) Imaging ellipsometry thickness map. (d) Fluorescence micrograph showing biotin/TRITC-streptavidin modification. All the scale bars denote 100 µm.

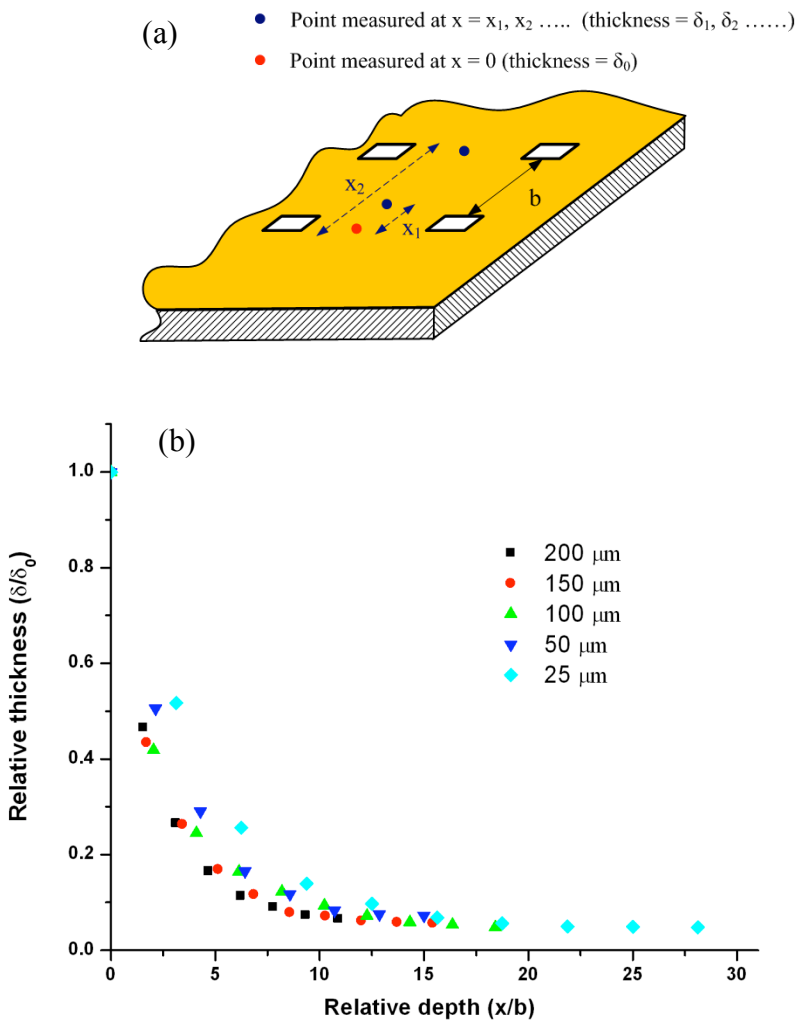

Figure 6.15: (a) Illustration of the thickness measurement conducted. b is the feature size studied (25 μm, 50 μm, 100 μm, 150 μm, and 200 μm), while δ_0 is the absolute thickness measured at an open areas (x = 0) for each case. Data points were measured at x = x_1, x_2, etc., and the corresponding thicknessδ_1, δ_2 ,etc., were recorded. (b) Plot of dimensionless thicknesses $\delta(x)/\delta_0$ vs. dimensionless width (x/b), where δ_0 is film thickness (nm) on an open area for an according dimension recorded by using imaging ellipsometry; b is the width (μm) of the dimension studied ranging from 25 μm to 200 μm accordingly. Results show a universal distribution in dimensionless coordinate consistantly compared to the theoretical expectation.

While the results obtained by imaging ellipsometry suggest a lower feature size of about 25 μm, a more functional evaluation is needed in order to ensure that these coatings can still support effective immobilization. To address this question, we conducted

immobilization studies with a model ligand, hydrazide-derived biotin, on the microstructures surfaces (experiments were conducted for 150 μm, 100 μm, 50 μm, 25 μm). Figure 6.14d shows the corresponding polymer patterns after biotin immobilization and subsequent self-assembly of strepdavidin. Interestingly, similar reactivity was found independent of the thickness of the deposited polymer film suggesting that even for features sizes of 25 μm, effective surface immobilization is obtained. To further elucidate this matter, we investigated the quality of features in the centre areas of the replica structure; i.e. areas farthest away from the inlets were monomers had to travel longest distances prior to deposition. By virtue of the process, these areas are most prone to film defects because of the inherently transport-limited character of the VAMPIR process. For this reason, imaging XPS element mapping was examined on the smallest 25 μm regions in more details (Figure 6.16). Three areas at or around the centre of the sample were compared. Region 1 (Figure 6.16a, denotes as red colour) examined the area farthest away from the centre, and both F_{1s} and Si_{2s} element maps are clearly resolved. For regions 2 and 3, XPS imaging still reveals high contrast and excellent resolution for fluorine originating from the reactive coating, but reduced contrast for silicon. These data may imply that the polymer films are approaching thicknesses below 10 nm in the center region, which is the excepted sampling depth of XPS for polymer coatings.[96] This is also in accordance with the earlier discussed thickness values obtained by imaging ellipsometry as well as the homogeneous surface coverage obtained by subsequent chemical modification. The fact that homogeneous surface structures with feature sizes as small as 25 μm can be obtained may have important implications when developing robust tools for tailoring surface properties.

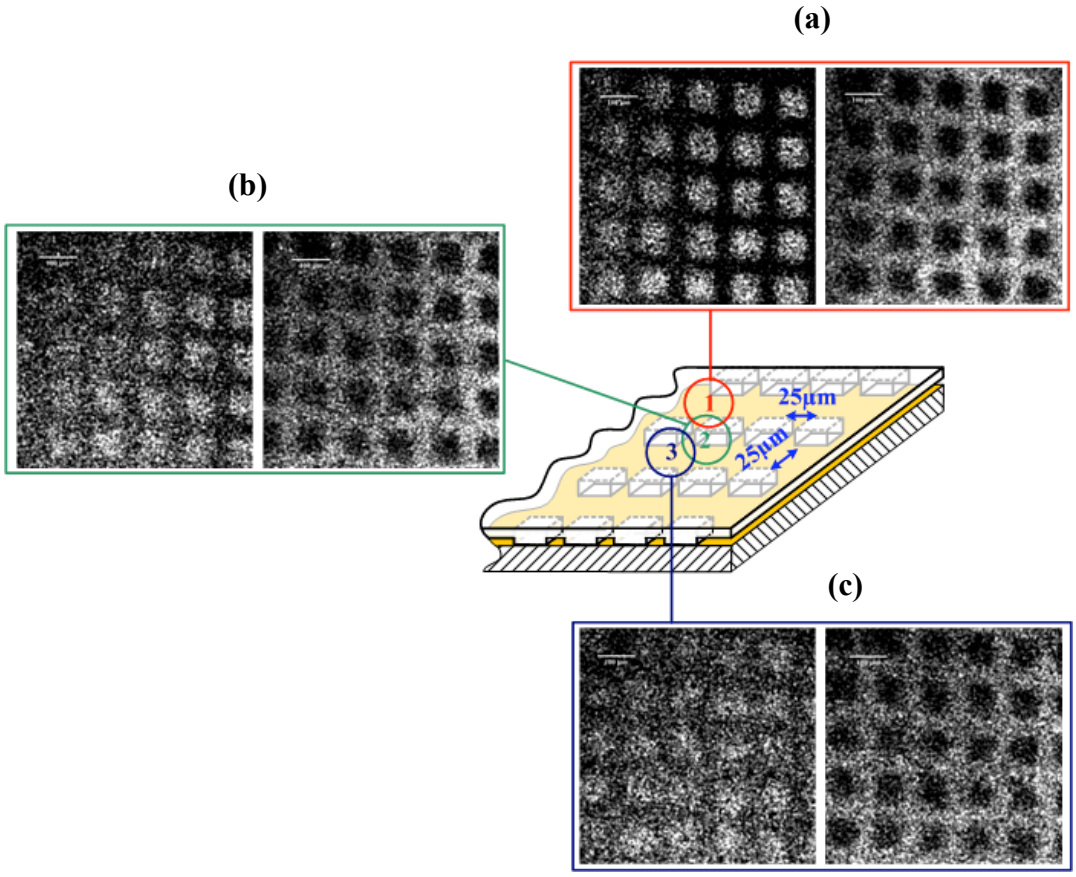

Figure 6.16: High resolution imaging XPS elemental map in the centre region of 25 µm structures. (a) Region 1 (red) examined the area farthest away from the centre area. Both F_{1s} and Si_{2s} elemental maps were clearly resolved. (b) Region 2 (green) examined intermidiate area between region 1 and region 3. Si_{2s} signal shows reduced contrast while F_{1s} signal is still well resolved. (3) Region 3 (dark blue) examined the center area. Si_{2s} signal shows vague contrast while F_{1s} signal keeps well-resolved contrast. Scale bar denotes 100 µm.

6.4 Conclusions

While significant attention has been given in the past to controlling sizes and shapes of colloids, much less is known about the precise engineering of colloidal surfaces. It was our intent to design colloids with microstructured surfaces that rival their flat substrates with respect to pattern precision and quality. Because traditional spin-coating technology

used during photolithographic processing is intrinsically limited to flat substrates, we replaced the spin-coated photoresist with a vapor-deposited, photodefinable polymer coating. These coatings were applied as ultra-thin, homogeneous films on curved surfaces and supported high-precision microstructuring of colloidal particles with radii between 50 and 200 microns. These findings mark an important progress, because well-established lithographic processes, such as projection lithography used in this study, can now be extended to the curved surfaces of spherical objects. With the concept of colloidal surface patterning demonstrated, future research may need to be directed towards fine-tuning binding affinities and patch geometries to yield optimal interactions during self-organization and towards extending the operative particle size ranges from tens and hundreds of microns down to the sub-micron regime. Compared to the limited range of surface-structured colloids available prior to this study, this approach establishes a shift in paradigm with respect to ease of fabrication as well as variability and complexity of available surface motifs. Finally, the technology relies on flexible surface chemistries for surface modification and is therefore compatible with a wide range of different surface markers. This feature may provide access to colloids with delicate balances between repulsive and attractive surface interactions, which are believed to play an essential role in programmed self-assembly of next-generation optoelectronic materials.[68]

We have also shown that various surfaces can successfully be coated with reactive polymer coatings and then modified with DNA features using SuNS. This approach represents an important step forward, because it essentially renders SuNS a substrate-independent method. Indeed, it enabled us to print with the same protocol onto five very different materials: silicon, quartz, polystyrene, acrylic and PDMS. Future work may include the extension of this method to reactive coatings with different functional groups or the employment of multi-functional coatings that offer two or more functional groups in defined surface ratios.[92] With its potential for mass-production, this new approach could benefit to a broad spectrum of applications in the field of bio- and nanodevices, where the development of inexpensive, consumable platforms that, at the same time, offer high information densities might have a profound impact.

Vapor-assisted micropatterning in replica structures (VAMPIR) establishes a simple

technique to create both, chemical and topological surface patterns. The process is essentially independent of the (solid) substrate material and relies solely on masking certain areas of the substrate during chemical vapor deposition polymerization and then depositing the reactive coatings only within the exposed areas. Our study further reveals that this process is applicable to a range of different structures, including both continuous and discontinuous features with feature sizes as small as 25 μm. For all features examined in this study, the adhesion between reactive coating and substrate was excellent and was not affected by exposure to standard solvents. Similarly, excellent pattern fidelity was observed within the entire feature range and no negative impact due to lift-off of the replica structures was observed. Most importantly, reactive side groups present in the polymer can serve as anchoring sites for subsequent surface modifications. Therefore, the resulting reactive surface patterns could provide a precisely confined microenvironment for biological applications, and may create an essential tool for the precise control towards effective bio-functional modifications. In future, surface properties can be further tailored by changing the type of *reactive coating* used during the VAMPIR process. This will provide a wide range of choices to ensure use of functional groups most optimally suited for a specific application.[76,77,97]

References

[1] Burns, M. A.; Johnson, B. N.; Brahmasandra, S. N.; Handique, K.; Webster, J. R.; Krishnan, M.; Sammarco, T. S.; Man, P. M.; Jones, D.; Heldsinger, D.; Mastrangelo, C. H.; Burke, D. T., An integrated nanoliter DNA analysis device. *Science* **1998,** 282, (5388), 484.

[2] Pellois, J. P.; Zhou, X. C.; Srivannavit, O.; Zhou, T. C.; Gulari, E.; Gao, X. L., Individually addressable parallel peptide synthesis on microchips. *Nature Biotechnology* **2002,** 20, (9), 922.

[3] Tian, J. D.; Gong, H.; Sheng, N. J.; Zhou, X. C.; Gulari, E.; Gao, X. L.; Church, G., Accurate multiplex gene synthesis from programmable DNA microchips. *Nature* **2004,** 432, (7020), 1050.

[4] Chen, C. S.; Mrksich, M.; Huang, S.; Whitesides, G. M.; Ingber, D. E., Geometric control of cell life and death. *Science* **1997,** 276, (5317), 1425.

[5] Lucchetta, E. M.; Lee, J. H.; Fu, L. A.; Patel, N. H.; Ismagilov, R. F., Dynamics of Drosophila embryonic patterning network perturbed in space and time using microfluidics. *Nature* **2005,** 434, (7037), 1134.

[6] Takayama, S.; McDonald, J. C.; Ostuni, E.; Liang, M. N.; Kenis, P. J. A.; Ismagilov, R. F.; Whitesides, G. M., Patterning cells and their environments using multiple laminar fluid flows in capillary networks. *Proceedings of the National Academy of Sciences of the United States of America* **1999,** 96, (10), 5545.

[7] Thorsen, T.; Maerkl, S. J.; Quake, S. R., Microfluidic large-scale integration. *Science* **2002,** 298, (5593), 580.

[8] Mack, N. H.; Dong, R.; Nuzzo, R. G., Quantitative Imaging of Protein Adsorption on Patterned Organic Thin-Film Arrays Using Secondary Electron Emission. *Journal of the American Chemical Society* **2006,** 128, (24), 7871.

[9] Ringeisen, B. R.; Callahan, J.; Wu, P. K.; Pique, A.; Spargo, B.; McGill, R. A.; Bucaro, M.; Kim, H.; Bubb, D. M.; Chrisey, D. B., Novel laser-based deposition of active protein thin films. *Langmuir* **2001,** 17, (11), 3472.

[10] Rai-Choudhury, P., *Handbook of Microlithography, Micromachining, and Microfabrication. Volume 1: Microlithography*. SPIE-The International Society for Optical Engineering: 1997.

[11] Yao, N.; Wang, Z. L., *Handbook of Microscopy for Nanotechnology*. Springer: 2005.

[12] Tseng, A. A., Recent developments in nanofabrication using ion projection lithography. *Small* **2005,** 1, (6), 594.

[13] Cerrina, F., X-ray imaging: applications to patterning and lithography. *Journal of Physics D: Applied Physics* **2000,** 33, (12), R103.

[14] Meschede, D.; Metcalf, H., Atomic nanofabrication: Atomic deposition and lithography by laser and magnetic forces. *Journal of Physics D: Applied Physics* **2003,** 36, (3), R17.

[15] Ginger, D. S.; Zhang, H.; Mirkin, C. A., The evolution of dip-pen nanolithography. *Angewandte Chemie, International Edition* **2004,** 43, (1), 30.

[16] Kraemer, S.; Fuierer, R. R.; Gorman, C. B., Scanning Probe Lithography Using Self-Assembled Monolayers. *Chemical Reviews (Washington, DC, United States)* **2003,** 103, (11), 4367.

[17] Chou, S. Y.; Krauss, P. R.; Renstrom, P. J., Imprint of Sub-25 Nm Vias and Trenches in Polymers. *Applied Physics Letters* **1995,** 67, (21), 3114.
[18] Chou, S. Y.; Krauss, P. R.; Renstrom, P. J., Imprint lithography with 25-nanometer resolution. *Science* **1996,** 272, (5258), 85.
[19] Xia, Y. N.; Whitesides, G. M., Soft lithography. *Annual Review of Materials Science* **1998,** 28, 153.
[20] Kumar, A.; Whitesides, G. M., Features of Gold Having Micrometer to Centimeter Dimensions Can Be Formed through a Combination of Stamping with an Elastomeric Stamp and an Alkanethiol Ink Followed by Chemical Etching. *Applied Physics Letters* **1993,** 63, (14), 2002.
[21] Wilbur, J. L.; Kumar, A.; Kim, E.; Whitesides, G. M., Microfabrication by microcontact printing of self-assembled monolayers. *Advanced Materials* **1994,** 6, (7/8), 600.
[22] Xia, Y. N.; Kim, E.; Zhao, X. M.; Rogers, J. A.; Prentiss, M.; Whitesides, G. M., Complex optical surfaces formed by replica molding against elastomeric masters. *Science* **1996,** 273, (5273), 347.
[23] Zhao, X. M.; Xia, Y. N.; Whitesides, G. M., Fabrication of three-dimensional micro-structures: Microtransfer molding. *Advanced Materials* **1996,** 8, (10), 837.
[24] Kim, E.; Xia, Y. N.; Whitesides, G. M., Polymer Microstructures Formed by Molding in Capillaries. *Nature* **1995,** 376, (6541), 581.
[25] Kim, E.; Xia, Y. N.; Zhao, X. M.; Whitesides, G. M., Solvent-assisted microcontact molding: A convenient method for fabricating three-dimensional structures on surfaces of polymers. *Advanced Materials* **1997,** 9, (8), 651.
[26] Suh, K. Y.; Kim, Y. S.; Lee, H. H., Capillary force lithography. *Advanced Materials* **2001,** 13, (18), 1386.
[27] De Vusser, S.; Steudel, S.; Myny, K.; Genoe, J.; Heremans, P., Integrated shadow mask method for patterning small molecule organic semiconductors. *Applied Physics Letters* **2006,** 88, (10).
[28] Schallenberg, T.; Schumacher, C.; Gundel, S.; Faschinger, W., Shadow mask technology. *Thin Solid Films* **2002,** 412, (1-2), 24.
[29] Tsang, W. T.; Cho, A. Y., Molecular-Beam Epitaxial Writing of Patterned Gaas Epilayer Structures. *Applied Physics Letters* **1978,** 32, (8), 491.
[30] Duffy, D. C.; Jackman, R. J.; Vaeth, K. M.; Jensen, K. F.; Whitesides, G. M., Patterning electroluminescent materials with feature sizes as small as 5 mu m using elastomeric membranes as masks for dry lift-off. *Advanced Materials* **1999,** 11, (7), 546.
[31] Takano, N.; Doeswijk, L. M.; van den Boogaart, M. A. F.; Auerswald, J.; Knapp, H. F.; Dubochet, O.; Hessler, T.; Brugger, J., Fabrication of metallic patterns by microstencil lithography on polymer surfaces suitable as microelectrodes in integrated microfluidic systems. *Journal of Micromechanics and Microengineering* **2006,** 16, (8), 1606.
[32] Ostuni, E.; Kane, R.; Chen, C. S.; Ingber, D. E.; Whitesides, G. M., Patterning mammalian cells using elastomeric membranes. *Langmuir* **2000,** 16, (20), 7811.
[33] Pal, R.; Sung, K. E.; Burns, M. A., Microstencils for the patterning of nontraditional materials. *Langmuir* **2006,** 22, (12), 5392.

[34] Castner, D. G.; Ratner, B. D., Biomedical surface science: Foundations to frontiers. *Surface Science* **2002,** 500, (1-3), 28.
[35] Lahann, J.; Balcells, M.; Lu, H.; Rodon, T.; Jensen, K. F.; Langer, R., Reactive polymer coatings: A first step toward surface engineering of microfluidic devices. *Analytical Chemistry* **2003,** 75, (9), 2117.
[36] Lahann, J.; Klee, D.; Pluester, W.; Hoecker, H., Bioactive immobilization of r-hirudin on CVD-coated metallic implant devices. *Biomaterials* **2001,** 22, (8), 817.
[37] Lahann, J.; Pluster, W.; Rodon, T.; Fabry, M.; Klee, D.; Gattner, H.-G.; Hocker, H., Universal approach towards r-hirudin derivatives with high anti-thrombin activity based on chemical differentiation of primary amino groups. *Macromolecular Bioscience* **2002,** 2, (2), 82.
[38] Lahann, J.; Balcells, M.; Rodon, T.; Lee, J.; Choi, I. S.; Jensen, K. F.; Langer, R., Reactive polymer coatings: A platform for patterning proteins and mammalian cells onto a broad range of materials. *Langmuir* **2002,** 18, (9), 3632.
[39] Lahann, J.; Choi, I. S.; Lee, J.; Jensen, K. F.; Langer, R., A new method toward microengineered surfaces based on reactive coating. *Angewandte Chemie, International Edition* **2001,** 40, (17), 3166.
[40] Lahann, J.; Hocker, H.; Langer, R., Synthesis of amino[2.2]paracyclophanes-beneficial monomers for bioactive coating of medical implant materials. *Angewandte Chemie, International Edition* **2001,** 40, (4), 726.
[41] Suh, K. Y.; Langer, R.; Lahann, J., A novel photoderinable reactive polymer coating and its use for microfabrication of hydrogel elements. *Advanced Materials* **2004,** 16, (16), 1401.
[42] Chen, H. Y.; Lahann, J., Fabrication of discontinuous surface patterns within microfluidic channels using photodefinable vapor-based polymer coatings. *Analytical Chemistry* **2005,** 77, (21), 6909.
[43] Chen, H. Y.; Rouillard, J. M.; Gulari, E.; Lahann, J., Colloids with high-definition surface structures. *Proceedings of the National Academy of Sciences of the United States of America* **2007,** 104, (27), 11173.
[44] Kim, J.; Crooks, R. M., Transfer of surface polymerase reaction products to a secondary platform with conservation of spatial registration. *Journal of the American Chemical Society* **2006,** 128, (37), 12076.
[45] Lin, H. H.; Kim, J.; Sun, L.; Crooks, R. M., Replication of DNA microarrays from zip code masters. *Journal of the American Chemical Society* **2006,** 128, (10), 3268.
[46] Lin, H. H.; Sun, L.; Crooks, R. M., Replication of a DNA microarray. *Journal of the American Chemical Society* **2005,** 127, (32), 11210.
[47] Chen, H. Y.; Elkasabi, Y.; Lahann, J., Surface modification of confined microgeometries via vapor-deposited polymer coatings. *Journal of the American Chemical Society* **2006,** 128, (1), 374.
[48] Gu, H. W.; Zheng, R. K.; Zhang, X. X.; Xu, B., Using soft lithography to pattern highly oriented polyacetylene (HOPA) films via solventless polymerization. *Advanced Materials* **2004,** 16, (15), 1356.
[49] Jackman, R. J.; Duffy, D. C.; Cherniavskaya, O.; Whitesides, G. M., Using elastomeric membranes as dry resists and for dry lift-off. *Langmuir* **1999,** 15, (8), 2973.

[50] Tixier, A.; Mita, Y.; Gouy, J. P.; Fujita, H., A silicon shadow mask for deposition on isolated areas. *Journal of Micromechanics and Microengineering* **2000,** 10, (2), 157.
[51] Graff, M.; Mohanty, S. K.; Moss, E.; Frazier, A. B., Microstenciling: A generic technology for microscale patterning of vapor deposited materials. *Journal of Microelectromechanical Systems* **2004,** 13, (6), 956.
[52] Kim, G. M.; van den Boogaart, M. A. F.; Brugger, J., Fabrication and application of a full wafer size micro/nanostencil for multiple length-scale surface patterning. *Microelectronic Engineering* **2003,** 67-8, 609.
[53] Zhou, Y. X.; Johnson, A. T., Simple fabrication of molecular circuits by shadow mask evaporation. *Nano Letters* **2003,** 3, (10), 1371.
[54] Wijnhoven, J. E. G. J.; Vos, W. L., Preparation of photonic crystals made of air spheres in Titania. *Science* **1998,** 281, (5378), 802.
[55] Mezzenga, R.; Ruokolainen, J.; Fredrickson, G. H.; Kramer, E. J.; Moses, D.; Heeger, A. J.; Ikkala, O., Templating organic semiconductors via self-assembly of polymer colloids. *Science* **2003,** 299, (5614), 1872.
[56] Meseguer, F.; Fenollosa, R., Non-close packed colloidal crystals. *Journal of Materials Chemistry* **2005,** 15, (43), 4577.
[57] Maldovan, M.; Thomas, E. L., Diamond-structured photonic crystals. *Nature Materials* **2004,** 3, (9), 593.
[58] Braun, P. V.; Wiltzius, P., Microporous materials: Electrochemically grown photonic crystals. *Nature* **1999,** 402, (6762), 603.
[59] Blanco, A.; Chomski, E.; Grabtchak, S.; Ibisate, M.; John, S.; Leonardo, S. W.; Lopez, C.; Meseguer, F.; Miguez, H.; Mondia, J. P.; Ozin, G. A.; Toader, O.; Van Driel, H. M., Large-scale synthesis of a silicon photonic crystal with a complete 3-dimensional bandgap near 1.5 micrometres. *Nature* **2000,** 405, (6785), 437.
[60] Cheng, C. H.; Pearce, E. M., Polymers Containing Fluorinated Ketone Groups .3. Synthesis of Styrene-P-Vinyltrifluoroacetophenone Co-Polymers by Modification of Polystyrene and the Copolymerization of Monomers. *Journal of Polymer Science Part a-Polymer Chemistry* **1980,** 18, (6), 1883.
[61] Holtz, J. H.; Asher, S. A., Polymerized colloidal crystal hydrogel films as intelligent chemical sensing materials. *Nature* **1997,** 389, (6653), 829.
[62] Kitaev, V.; Ozin, G. A., Self-assembled surface patterns of binary colloidal crystals. *Advanced Materials* **2003,** 15, (1), 75.
[63] Qian, J.; Liu, Y.; Liu, H.; Yu, T.; Deng, J., Immobilization of horseradish peroxidase with a regenerated silk fibroin membrane and its application to a tetrathiafulvalene-mediating H2O2 sensor. *Biosensors & Bioelectronics* **1997,** 12, (12), 1213.
[64] Shevchenko, E. V.; Talapin, D. V.; Kotov, N. A.; O'Brien, S.; Murray, C. B., Structural diversity in binary nanoparticle superlattices. *Nature* **2006,** 439, (7072), 55.
[65] Leunissen, M. E.; Christova, C. G.; Hynninen, A. P.; Royall, C. P.; Campbell, A. I.; Imhof, A.; Dijkstra, M.; van Roij, R.; van Blaaderen, A., Ionic colloidal crystals of oppositely charged particles. *Nature* **2005,** 437, (7056), 235.
[66] Kalsin, A. M.; Fialkowski, M.; Paszewski, M.; Smoukov, S. K.; Bishop, K. J. M.; Grzybowski, B. A., Electrostatic self-assembly of binary nanoparticle crystals with a diamond-like lattice. *Science* **2006,** 312, (5772), 420.

[67] Cho, Y. S.; Yi, G. R.; Lim, J. M.; Kim, S. H.; Manoharan, V. N.; Pine, D. J.; Yang, S. M., Self-organization of bidisperse colloids in water droplets. *Journal of the American Chemical Society* **2005,** 127, (45), 15968.
[68] Velev, O. D., Self-assembly of unusual nanoparticle crystals. *Science* **2006,** 312, (5772), 376.
[69] Zhang, Z. L.; Keys, A. S.; Chen, T.; Glotzer, S. C., Self-assembly of patchy particles into diamond structures through molecular mimicry. *Langmuir* **2005,** 21, (25), 11547.
[70] Zhang, G.; Wang, D. Y.; Mohwald, H., Patterning microsphere surfaces by templating colloidal crystals. *Nano Letters* **2005,** 5, (1), 143.
[71] Nagle, L.; Fitzmaurice, D., Templated nanowire assembly on the surface of a patterned nanosphere. *Advanced Materials* **2003,** 15, (11), 933.
[72] Arden, W. M., The International Technology Roadmap for Semiconductors - Perspectives and challenges for the next 15 years. *Current Opinion in Solid State & Materials Science* **2002,** 6, (5), 371.
[73] Pregibon, D. C.; Toner, M.; Doyle, P. S., Multifunctional Encoded Particles for High-Throughput Biomolecule Analysis. *Science* **2007,** 315, (5817), 1393.
[74] Zhang, G.; Wang, D. Y.; Moehwald, H., Nanoembossment of Au patterns on microspheres. *Chemistry of Materials* **2006,** 18, (17), 3985.
[75] Lahann, J., Vapor-based polymer coatings for potential biomedical applications. *Polymer International* **2006,** 55, (12), 1361.
[76] Lahann, J., Reactive polymer coatings for biomimetic surface engineering. *Chemical Engineering Communications* **2006,** 193, (11), 1457.
[77] Lahann, J.; Langer, R., Novel Poly(p-xylylenes): Thin Films with Tailored Chemical and Optical Properties. *Macromolecules* **2002,** 35, (11), 4380.
[78] Shen, W. W.; Boxer, S. G.; Knoll, W.; Frank, C. W., Polymer-supported lipid bilayers on benzophenone-modified substrates. *Biomacromolecules* **2001,** 2, (1), 70.
[79] Gao, X. L.; Zhou, X. C.; Gulari, E., Light directed massively parallel on-chip synthesis of peptide arrays with t-Boc chemistry. *Proteomics* **2003,** 3, (11), 2135.
[80] Taton, K. S.; Guire, P. E., Photoreactive self-assembling polyethers for biomedical coatings. *Colloids and Surfaces B-Biointerfaces* **2002,** 24, (2), 123.
[81] Lahiri, J.; Ostuni, E.; Whitesides, G. M., Patterning ligands on reactive SAMs by microcontact printing. *Langmuir* **1999,** 15, (6), 2055.
[82] Suh, K. Y.; Langer, R.; Lahann, J., Fabrication of elastomeric stamps with polymer-reinforced sidewalls via chemically selective vapor deposition polymerization of poly(p-xylylene). *Applied Physics Letters* **2003,** 83, (20), 4250.
[83] Gao, Y. Q.; Shen, T. Z.; Chen, J. S.; Luo, N. N.; Qi, X. M.; Jin, Q., Research on high-quality projecting reduction lithography system based on digital mask technique. *Optik* **2005,** 116, (7), 303.
[84] Lu, B.; Xie, J.; Lu, C.; Wu, C.; Wei, Y., Oriented Immobilization of Fab' Fragments on Silica Surfaces. *Analytical Chemistry* **1995,** 67, (1), 83.
[85] Yu, A. A.; Savas, T.; Cabrini, S.; diFabrizio, E.; Smith, H. I.; Stellacci, F., High resolution printing of DNA feature on poly(methyl methacrylate) substrates using supramolecular nano-stamping. *Journal of the American Chemical Society* **2005,** 127, (48), 16774.

[86] Yu, A. A.; Savas, T. A.; Taylor, G. S.; Guiseppe-Elie, A.; Smith, H. I.; Stellacci, F., Supramolecular nanostamping: Using DNA as movable type. *Nano Letters* **2005,** 5, (6), 1061.
[87] Nandivada, H.; Chen, H. Y.; Lahann, J., Vapor-based synthesis of poly [(4-formyl-p-xylylene)-co-(p-xylylene)] and its use for biomimetic surface modifications. *Macromolecular Rapid Communications* **2005,** 26, (22), 1794.
[88] Chou, S. Y.; Krauss, P. R.; Zhang, W.; Guo, L. J.; Zhuang, L., Sub-10 nm imprint lithography and applications. *Journal of Vacuum Science & Technology B* **1997,** 15, (6), 2897.
[89]Schurmann, K.; Lahann, J.; Niggemann, P.; Klosterhalfen, B.; Meyer, J.; Kulisch, A.; Klee, D.; Gunther, R. W.; Vorwerk, D., Biologic response to polymer-coated stents: In vitro analysis and results in an iliac artery sheep model. *Radiology* **2004,** 230, (1), 151.
[90] Nandivada, H.; Chen, H. Y.; Bondarenko, L.; Lahann, J., Reactive polymer coatings that "click"". *Angewandte Chemie-International Edition* **2006,** 45, (20), 3360.
[91] Lahann, J.; Klee, D.; Hocker, H., Chemical vapour deposition polymerization of substituted [2.2]paracyclophanes. *Macromolecular Rapid Communications* **1998,** 19, (9), 441.
[92] Elkasabi, Y.; Chen, H. Y.; Lahann, J., Multipotent polymer coatings based on chemical vapor deposition copolymerization. *Advanced Materials* **2006,** 18, (12), 1521.
[93] Hermanson, G. T., *Bioconjugate techniques*. Academic Press: San Diego, Calif., 1996.
[94] Tolstopyatov, E. M.; Yang, S. H.; Kim, M. C., Thickness uniformity of gas-phase coatings in narrow channels: II. One-side confined channels. *Journal of Physics D-Applied Physics* **2002,** 35, (21), 2723.
[95]Tolstopyatov, E. M., Thickness uniformity of gas-phase coatings in narrow channels: I. Long channels. *Journal of Physics D-Applied Physics* **2002,** 35, (13), 1516.
[96] Briggs, D., *Surface analysis of polymers by XPS and static SIMS*. Cambridge University Press: 1998.
[97] Yoshida, M.; Langer, R.; Lendlein, A.; Lahann, J., From advanced biomedical coatings to multi-functionalized biomaterials. *Polymer Reviews* **2006,** 46, (4), 347.

CHAPTER 7

CONCLUSIONS

CVD polymerization of functionalized [2.2]paracyclophanes establishes a general but simple protocol for the preparation of reactive polymers. The resulting reactive coatings contain anchoring groups with reactivity patterns that enable controlled binding of biomolecules for tailoring surface properties in precision. Aldehyde, anhydride, or active ester groups allow for immobilization of proteins; amino or carboxylic acid groups may be used to control surface charges and electro-osmotic flow; while alkyl and fluoroalkyl groups may provide hydrophobic interfaces for electrochromatographic applications. In addition, multipotent biointerfaces could in principle be prepared by using CVD copolymerized multipotent and modular coatings enabling simultaneous presentation of multiple biomolecules in controllable ratios. Applicability of the reactive coating to various substrates, such as polymers, metals, or composites, generates a general platform without relying on broad chemical alteration of the bulk material. This eliminates contaminations and guarantees a biocompatible process being free of harmful solvents, initiators, or accelerators. Reactive polymer coatings can improve the interfacial biocompatibility of implant surfaces or can be compatible with complex biological features as they represent a designable interlayer; stable under the conditions of the bioassay. Recent advances have exploited these coatings to prepare surfaces with excellent degree of adsorption resistance towards proteins and cells. On the other hand, accessibility of reactive CVD coatings within confined microgeometries has been systematically studied, and the preparation of homogeneous polymer thin films within the inner surface of microchannels has been demonstrated. More recent work has also applied these advanced coatings to develop dry adhesion process which is (i) essentially independent of the chemical composition of the substrate, (ii) well-defined with respect

to the bonding chemistry, (iii) can be controlled on demand, and (iv) can provide a multiple and biologically distinct binding platform. These process-flexible properties bridge a critical technological gap towards surface-modified microfluidic and nanofluidic devices with use for biosensor and "BioMEMS". Significant attention has been given on preparing surface microstructures and surface patterns through photopatterning, projection lithography, supramolecular nanostamping (SuNS), and vapor-assisted micropatterning in replica structures (VAMPIR) processes. These techniques complimentarily provide access to precisely confined microenvironment on flat and curved geometries for biological applications, and may create an essential tool for the precise control towards effective bio-functional modifications.

7.1 Future Directions

7.1.1 Selective CVD Polymerization

Vaeth and Jensen have reported that the deposition of poly-*p*-xylylenes and poly(*p*-phenylene vinylene) (PPV) can be inhibited by iron and iron salts,[1] allowing the integration of selective CVD polymer growth into complex device structure. They further claim that the modified layer can be processed into a wide range of patterns and surfaces to achieve the desired spatial definition. This highlights the flexibility in substrate choice with the iron growth inhibition method. Another study done by the same research group showed that several transitional metals, metal salts, and organometallic complexes can also be used to inhibit the growth of the CVD polymers. A possible mechanism suggested is that the polymer molecule did not adsorb on the metal surface or if the polymer interacts with the metal in such a way that it is deactivated while adsorbed.[2] However, the exact mechanism of selective CVD polymerization still remains unclear. Suh et al. recently applied this technique and selectively grew poly-*p*-xylylene films on the sidewalls of PDMS (polydimethylsiloxane) channels, resulting in a reinforced PDMS

stamp for microcontact printing (μCP) with extremely high resolution (180nm lines). This approach addresses the mechanical shortcomings of PDMS stamps in the submicron range.[3]

Our reliminary results compared well with the literature data and is summaried in Figure 7.3, but showing no selective behavior on most of the functionalized poly-*p*-xylylenes listed. Fortunately, recent discovery has shown that the growth of vinyl functionalized poly-*p*-xylylene can be inhibited by titanium (Ti) as shown is Figure 7.4.

Based on the findings described above, this selective CVD polymerization process provides substrate-dependent platform for surface modification, which the metal inhibitors first block certain areas to be polymer-free regions followed by selective deposition of polymers on the rest of the areas via CVD process (selective CVD) in the second step. By designing the topology of the metal inhibitor in advance, spatial deposition of the polymers can be achieved; in addition, the equipped functional groups served as anchoring groups that provide further surface modification in facile. However the exact mechanism is still unclear, and only non-functionalized poly-*p*-xylylene (parylene N and parylene C) were shown to undergo selective deposition so far.[2]

Future research direction will be to systematically exploit these methodologies onto more functionalized poly-*p*-xylylenes in order to (i) study the exact mechanism of selective CVD polymerization on different substrates, (ii) integrate this substrate-dependent modification technology with other fabrication processes, e.g., electropolymerization to achieve sophisticated surface engineering on hybrid composites. We foresee the potential uses in biosensors and electrophoresis devices.

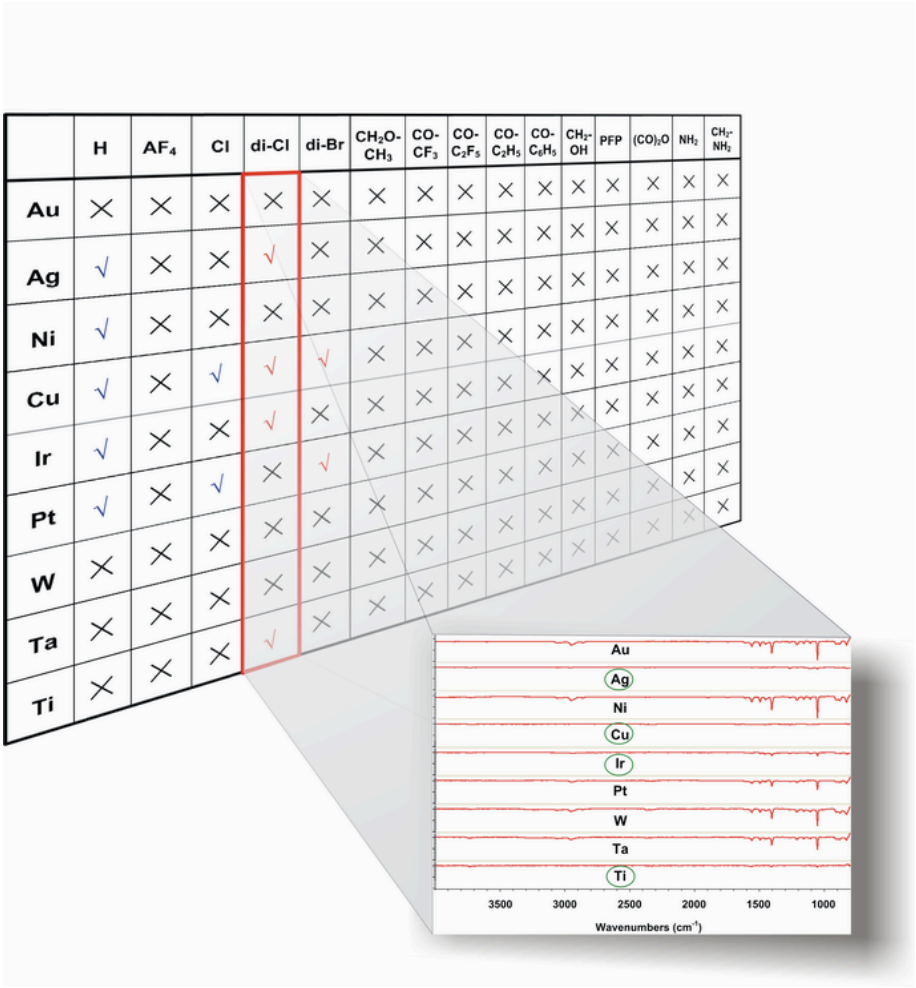

Figure 7.1: Summary of preparing non-functionalized and functionlized poly-*p*-xylylenes on different metal substrates. Data is determined by using FTIR to detect the presence of polymers on according metals. Example is showing the FTIR spectra of di-cholorinated poly-*p*-xylylene (parylene-D) grown on different metal substrates, and its growth can be inhibited by silver (Ag), copper (Cu), iridium (Ir), and titanium (Ti).

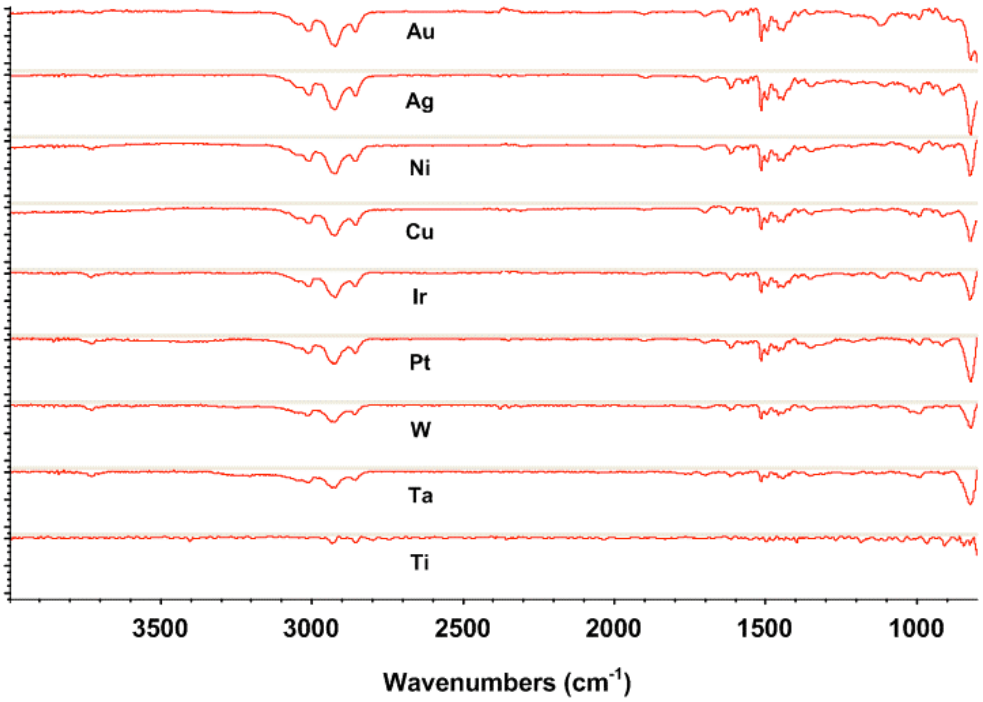

Figure 7.2: FTIR spectra of vinyl functionalized poly-*p*-xylylene grown on different metal subsrates via CVD polymerization. Data is showing the growth of vinyl functionalized poly-*p*-xylylene can be inhibited by titanium (Ti).

7.1.2 Biodegradable Polymer Coatings by CVD Polymerization

From the beginnings of the material sciences, the development of highly stable materials has been a major research challenge. Today, many polymers are available that are virtually nondestructible in biological systems, e.g., Teflon, Kevlar, or poly(ester ether ketone) (PEEK).[4] On the other hand, the development of degradable biomaterials is a relatively new area of research. The variety of available, degradable biomaterials is still too limited to cover a wide enough range of diverse material properties. Thus, the design and synthesis of new biomaterials that can provide predetermined and controlled cellular response is a critically needed component of most practical applications.[5] For instance, an implantable drug delivery device is by necessity a temporary device, as the

device will eventually runt out of drug or the need for the delivery of a specific drug is eliminated once the disease is treated.[6] One can expect that the future acceptance of implantable drug delivery devices by physicians and patients alike will depend on the availability of degradable systems that do not have to be explanted surgically.

Over the past decade, dozens of hydrolytically unstable polymers have been suggested as degradable biomaterials; however, in most cases, no attempts have been made to develop these new materials for specific medical application. Thus, detailed toxicological studies *in vivo*, investigations of degradation rate and mechanism, and careful evolutions of the phyicomechanical properties have so far been published for only a very small fraction of those polymers;[4] an even smaller number of synthesis, degradable polymers have so far been used in medical implants and devices that gained approval by the Food and Drug Administration (FDA) for use in patients. Note that the FDA does not approve polymers of materials by itself, but only specific devices or implants.[4] As of 2004, only five distinct synthetic, degradable polymers have been approved for use in a narrow range of clinical applications. There polymers are poly(lactic acid), poly(glycolic acid), polydioxanone, polycaprolactone, and poly(PCPP-SA anhydride).[4,7] A variety of other synthetic, degradable biomaterials currently in clinical use are blends or copolymers of these base materials such as a wide range of copolymers of lactic and glycolic acid.[7] Recent research has led to a number of well-established investigational polymers that may find practical applications as degradable implants within the next decade. Research in developing synthetic, degradable polymer thin films, however, is still in its infancy, and does have an essential need to explore in order to fulfill the gap needed for investigating the interface between biomaterials and biological systems.

Our preliminary results exploited hydrolytically unstable diazo-moiety into poly(*p*-xylylenes)' backbone, and was hypothesized to undergo degradation process in optimized hydrolytic conditions. Diazo-containing compound and [2.2]paracyclophane mixtures were used as starting materials for CVD copolymerization. After CVD polymerization, the homopolymer (control experiment) and the copolymers were incubated within PBS buffer solution (pH 7.4) at 37 ^{o}C. Resulting samples were

examined by using infrared reflection absorption spectroscopy (IRAS), and surface morphologies of the resulting samples were observed by using atomic force microscopy (AFM). Thickness measurement was recorded by using a multi-wavelength. As shown in Figure 7.3, FTIR spectra were used to study the degradation process from 0 hr to 210 hr for both homopolymer and copolymer. From this preliminary result, the characteristic peaks of *C-O* at 1604 and 1674 cm^{-1} from diazo moiety were showing decreasing dependency according to incubation time, showing possible hydrolysis process occurred for both cases. In addition, the increasing *COOH* peak at 1735 cm^{-1} in both homopolymer and copolymer is also showing the evidence of occurring hydrolytic reaction. From the surface morphology point of view, the AFM images indicate the pinhole formation increases with time also for both systems studied as shown in Figure 7.4. These isotropically formed pinholes may also associated with the degradation process. Film thickness was also monitored according to time during the hydrolysis process in this preliminary study. As indicated in Figure 7.5, both systems are showing a exponentially decayed tendency with respect to the time studied. As anticipated, a more rapid decay was found in the system of homopolymer due to it contains a greater number of diazo moieties than the copolymer, which can undergo a more rapid hydrolytic reaction.

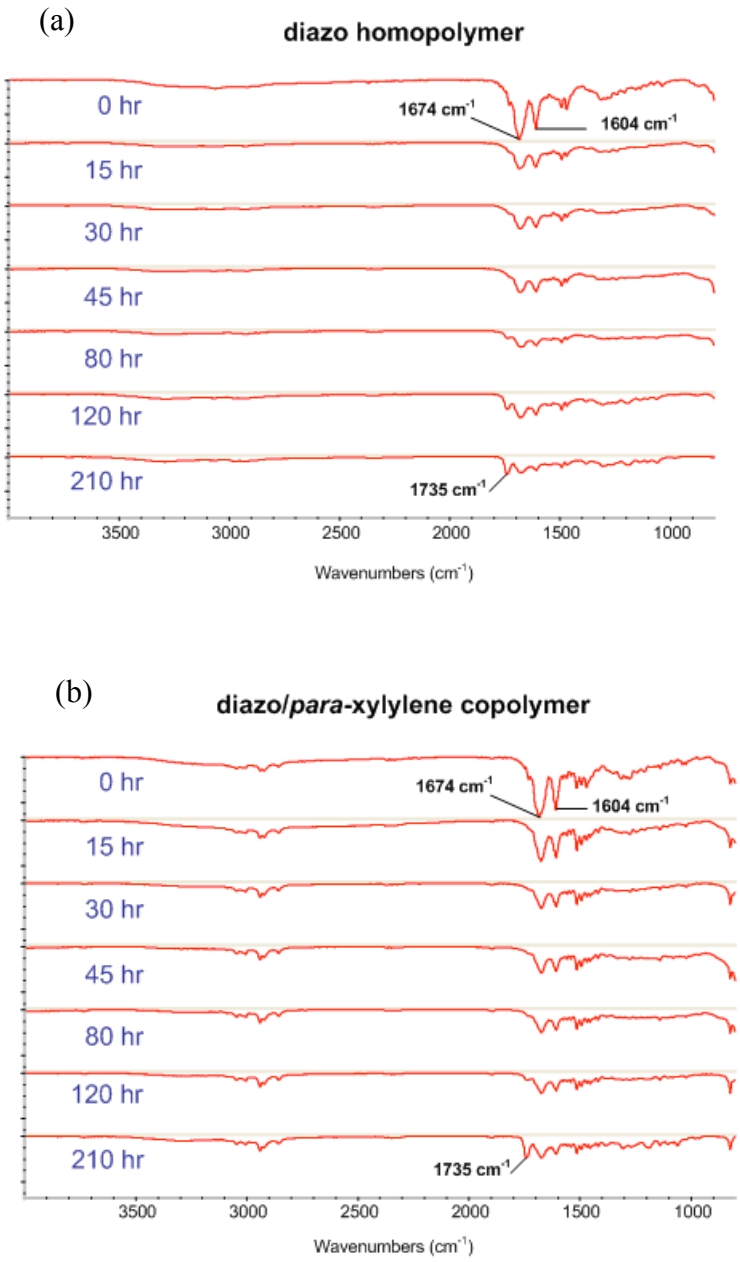

Figure 7.3: FTIR spectra of (a) diazo containing homopolymer and (b) azo/*para*-xylylene copolymer showing the decreasing *C-O* peaks at 1604 and 1674 cm^{-1}, and increasing *COOH* peak at 1735 cm^{-1} during degradation process. Samples were incubated at PBS buffer solution (pH 7.4) at 37 ^{o}C, and the data were recorded according to time from 0 hr to 210 hr.

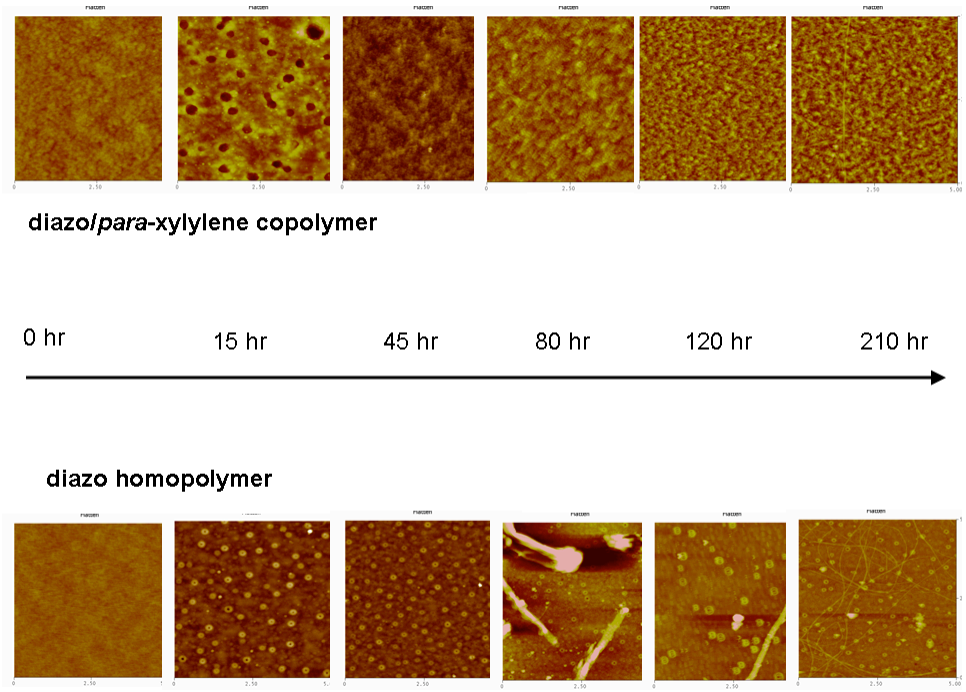

Figure 7.4: Surface morphology of diazo containing homopolymer and azo/*para*-xylylene copolymer recorded by AFM. Samples were incubated at PBS buffer solution (pH 7.4) at 37 ^{o}C, and the data were recorded according to time from 0 hr to 210 hr.

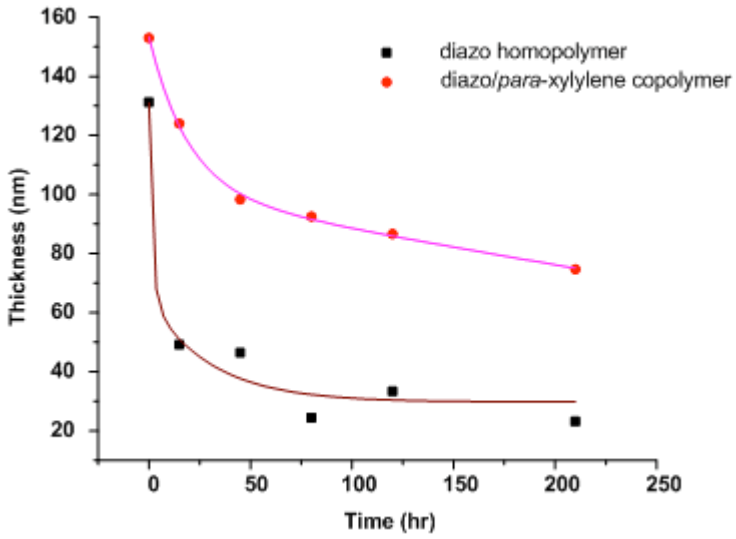

Figure 7.5: Thickness measurement of diazo containing homopolymer and azo/*para*-xylylene copolymer by using a multi-wavelength ellipsometer. Exponential decay was found for both systems.

Future direction on degradable polymer thin film will be conducted by using CVD copolymerization process to deposit a functional poly-*p*-xylylene based copolymer with hydrolytical moiety imbedded within the polymer backbone. These copolymers can be prepared with general protocols by using CVD copolymerization on various substrates and devices as conformal coatings. In addition, the equipped anchoring groups can be used as reactive sites for tailoring the surface properties. Future works on developing these degradable polymer thin films will be to conduct systemic study of these films with respect to their biocompatibility, toxicity, protein and cell response *in vitro* and *in vivo*. We foresee the applications in drug delivery and biosensors.

7.2 Concluding Remarks

Reactive polymer coatings can improve the interfacial biocompatibility of biomedical surfaces or can be compatible with complex biological features as they represent a designable interlayer; stable under the conditions of the bioassay. Many key features of exploiting the reactive coatings for biological applications have been demonstrated during the past few years. Recently, some advances such as the uses in microfluidic devices, fabrication of non-fouling surfaces, precise surface modification 3-D curved surfaces, as well as chemically and biologically defined surface microstructures have also been demonstrated and were discussed in this thesis. These advanced coatings provide a technology platform that will improve active long-term control and improved mimicry of biological systems. In addition, they will enable rendering surfaces dynamic with potential for achieving a degree of remodeling that may – at some point in the future – rival the properties of naturally occurring biological substrates and surfaces. Development of these technologies will hold promise for enabling study and control of cell/cell, cell/protein, and protein/surface interactions with applications in biosensors, extracellular matrix substitutes, and microfluidics. We foresee the use of these advanced polymer coatings in efforts to revolutionize the current trend of surface engineering which has been largely focused on two-dimensional modifications. This will be accomplished by advancing the coating technology into

three-dimensional geometries, down to micro- or even nano- scale, and by providing high-precision modifications using combinatorial approach for high throughput screening and production of new biomimetic materials.

References

[1] Vaeth, K. M.; Jensen, K. F., Selective growth of poly(p-phenylene vinylene) prepared bg chemical vapor deposition. *Advanced Materials* **1999,** 11, (10), 814.

[2] Vaeth, K. M.; Jensen, K. F., Transition metals for selective chemical vapor deposition of parylene-based polymers. *Chemistry of Materials* **2000,** 12, (5), 1305.

[3] Suh, K. Y.; Langer, R.; Lahann, J., Fabrication of elastomeric stamps with polymer-reinforced sidewalls via chemically selective vapor deposition polymerization of poly(p-xylylene). *Applied Physics Letters* **2003,** 83, (20), 4250.

[4] Ratner, B. D., *Biomaterials science : an introduction to materials in medicine*. 2nd ed.; Elsevier Academic Press: Amsterdam ; Boston, 2004.

[5] James, K.; Kohn, J., Applications of pseudo-poly(amino acid) biomaterials. *Trends in Polymer Science* **1996,** 4, (12), 394.

[6] Langer, R., New Methods of Drug Delivery. *Science* **1990,** 249, (4976), 1527.

[7] Hollinger, J. O., *Biomedical applications of synthetic biodegradable polymers*. CRC Press: Boca Raton, 1995.